The Dynamics of Allochthonous Terranes in the Pangean Suture Zone of Southern Iberia

by

James A. Braid

Submitted in partial fulfillment of the requirements
For the degree of Doctor of Philosophy

at
Dalhousie University
Halifax, Nova Scotia
December 2010

DALHOUSIE UNIVERSITY

DEPARTMENT OF EARTH SCIENCES

The undersigned hereby certify that they have read and recommend to the Faculty of Graduate Studies for acceptance a thesis entitled "The Dynamics of Allochthonous Terranes in the Pangean Suture Zone of Southern Iberia" by James A. Braid in partial fulfillment of the requirements for the degree of Doctor of Philosophy.

Dated: December 2nd, 2010

External Examiner: _____

Research Supervision: _____

Examining Committee _____

_____

_____

_____

Departmental representative_____

DALHOUSIE UNIVERSITY

DATE: December 2nd, 2010

AUTHOR: James A. Braid

TITLE: The Dynamics of Allochthonous Terranes in the Pangean Suture Zone of Southern Iberia

DEPARTMENT OR SCHOOL: Department of Earth Sciences

DEGREE: Ph.D CONVOCATION: May YEAR: 2011

Permission is herewith granted to Dalhousie University to circulate and to have copied for non-commercial purposes, at its discretion, the above title upon the request of individuals or institutions.

_____
Signature of Author

DEDICATION

To Olivia and Lyla for reminding me every day the importance of imagination.

TABLE OF CONTENTS

LIST OF FIGURES

LIST OF TABLES

ABSTRACT

Most researchers contend that the destruction of the Rheic Ocean culminated in the formation of the supercontinent Pangea. However, despite the importance of this ocean, there are major uncertainties in the identification of its margins, mechanisms and timing of its formation, and the geodynamics of its closure. Rocks recording the evolution of the Rheic are excellently preserved in the southern Iberian peninsula of Western Europe. Here, the Ossa Morena (OMZ) is separated from theSouth Portuguese (SPZ) zone by a sequence of polydeformed rocks know as the Pulo do lobo Zone (PDLZ). The PDLZ isinterpreted as a late Paleozoic accretionary prism, which contains potential vestiges of the ancient Rheic Ocean (ophiolites). The objective of this study is to better understand the processes associated with the formation of Pangea by determining the lithotectonic histories of both the PDLZ and SPZ. New field, geochronological and geochemical data are used to test and further constrain current models for the evolution of Pangea as recorded in the Variscan orogen.Fieldwork and geochronological data indicate that the PDLZ was derived from neither the OMZ (Gondwana) nor the SPZ suggesting that if the PDLZ is an accretionary prism it was not derived from the upper or lower plate. This apparent conundrum can be reconciled by a model involving excision of a crustal fragment during collision between an Iberian indenter (Gondwana) with Laurussia during the formation of Pangea. Geochronological and Geochemical data from the SPZ indicate that the lower crust isnot compositionally similar to the overlying Devonian-Carboniferous continental detritus. This unusual relationship is similar to the relationship between the relatively juvenile basement and ancient upper crust documented in the exposed portion of the Meguma terrane in the northern Appalachians, which paleogeographic reconstructions show was immediately outboard of southern Iberia in the Late Devonian. Taken together with the suggested complex tectonic history of the PDLZ the results of this thesis provide important insight into the geometry and timing of the formation of Pangea and indicate that re-interpretation may be required for what is known concerning the tectonic evolution of both the Variscan and Appalachian orogens.

LIST OF ABBREVIATIONS USED

BAO = Beja Acebuches Ophiolite

BCSZ = Badajoz Cordoba Shear Zone

BFZ = Bristol Fault Zone

CAA = Cantabrian Asturias Arc

CHUR = Chondritc Uniforn Reservoir

εNd = Epsilon Neodymium

HREE = Heavy Rare Earth Elements

IPB = Iberian Pyrite Belt

IAA = Iberian Armorican Arc

LA-ICPMS = Laser Ablation Inductively Coupled Mass Spectrometry

LREE = Light Rare Earth Elements

OMZ = Ossa Morena Zone

PCIGR = Pacific Centre for Isotopic and Geochemical Research

PDL = Pulo do Lobo Formation

PDLZ = Pulo do Lobo Zone

RDL = Ribeira de Limas Formation

REE = Rare Earth Elements

T_{DM} = Depleted Mantle Model Age

SIF= Santa Iria Flysch

SISZ = South Iberian Shear Zone

Sm-Nd = Samarium- Neodymium

SNB = Sierra Norte Batholith

SPZ = South Portuguese Zone

U/Pb = Uranium / Lead

VSC = Volcano Sedimentary Complex

ACKNOWLEDGEMENTS

I am grateful to my primary supervisor Brendan Murphy for his guidance, support and generosity not only throughout this endeavor but also throughout my entire tenure as an undergraduate and graduate student. I am also grateful to Nick Culshaw Rebecca Jamieson and John Gosse for their support throughout this thesis work.Cecilio Quesada is thanked for his wisdom and guidance with fieldwork in Spain and writing of the thesis. Rafael López-Guijarro helped me immensely with fieldwork and logistics in Spain. I thank him greatly for his practical help and also his friendship. I also thank my other Spanish friends, Javier Fernandez-Suarez, Gabriel Gutierrez-Alonso and Maider Armendáriz for their generosity and help. James Mortensen at the Pacific Center for Geochemical and Isotopic Research at the University of British Columbia provided invaluable assistance with the geochronological analyses and is also thanked for taking time to discuss the process and results. Luke Bickerton and Elizabeth Walsh helped prepare figures, tables and maps. Stephen Johnston from the University of Victoria is thanked for inspiring discussions and comments.I also thank my friends Jonathan Taylor, Curran Jensen and Ben Theuerkauf for their support and timely distractions. Last but not least I am grateful to my wife Cori and the rest of my family for giving me support, inspiration and the necessary time to complete this thesis. Much of this work was funded by and Natural Sciences and Engineering Research Council of Canada (NSERC) post-graduate (CGS-M and PGS-D) scholarships, as well as a Dalhousie Killam scholarship. Fieldwork and most of the analytical work was supported by an NSERC discovery grant to Brendan Murphy.

CHAPTER 1

GENERAL INTRODUCTION

1.1. Introduction

Pangea formed in the late Paleozoic as the result of the closure of the Rheic Ocean and the terminal collision between Gondwana and Laurussia (Fig. 1.1). These events gave rise to the Alleghenian orogen in eastern North America and the Variscan orogen of Western Europe. Aside from shaping the planet geologically, the formation of Pangea and its dispersal had a fundamental impact on paleobiology, ecology and climate, which is echoed in our modern understanding and interpretation of many of these systems (Poulsen et al., 2007;Veevers, 1990; Hoffman et al., 1998;Worsley et al., 1984). However, despite the fact that Pangea is a foundation for understanding many modern earth systems, its geometry, timing of formation and processes that contributed to its formation, remain poorly understood.

The investigation of suture zones are of fundamental importance to the understanding of processes involved in collisional orogenesis because these zones link pieces of autochthonous continental crust that were once separated by an intervening oceanic basin. As a result, these suture zones potentially record in their lithological,geochemical and structural

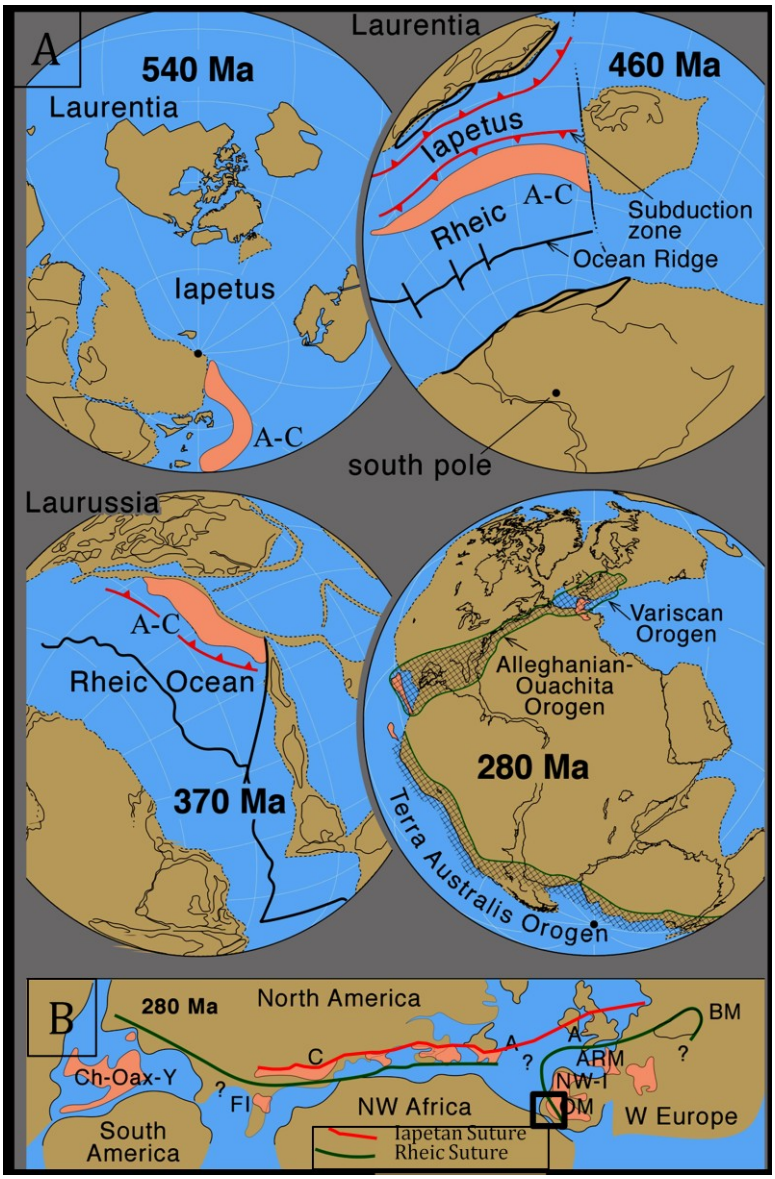

Fig. 1.1 (a)Paleozoic reconstructions showing the location of peri-Gondwananterranes along the Gondwanan margin at ca. 500 Ma, the opening of the Rheic Ocean by separation and northward drift of these terranes from Gondwana by 460 Ma, their ca. 440 Ma accretion to Baltica, followed by accretion to Laurentia, leading to the closure of the Iapetus Ocean. Subsequent northwesterly-directed subduction beneath the Laurussian margin leading to closure of the Rheic Ocean and the beginning of the amalgamation of Pangea by ca. 350 Ma). (b)Late Paleozoic reconstruction showing approximate locations of Iapetan and Rheic suture zones. Ac-Oax, Acatlán-Oaxaquia; Fl, Florida; C, Carolinia; A, Avalonia; OM Ossa Morena; NW-I, Northwest Iberia; Arm, Armorica; BM, Bohemian massif, MC Massif Central(from Murphy et al., 2006) (modified from Stampfli et al., 2002).

makeup the main events that contributed to supercontinent amalgamation. In terms of late Paleozoic geologic events, a complete picture of Pangean orogenesis is hampered by (i) limited exposure of late Paleozoic suture zones which potentially record these processes, and (ii) the lack of continuity of the Variscan and Appalachian belts which were sundered in the Early Mesozoic by the opening of the Atlantic Ocean. As a result many of the suture zones that marked the late Paleozoic stitching between Gondwana and Laurussia, particularly those that formed by consumption of the Rheic Ocean, were either destroyed, hidden beneath the Atlantic continental shelves or are covered by post-Pangean rocks. Therefore, understanding the processes, which led to the formation of Pangea requires the targeting of specific regions and sequences, which escaped post-Pangean destruction.

In the Variscan orogen of southern Iberia, a rare exposure of a Pangean suture zone is potentially preserved (Fig. 1.2). Here, the Gondwanan parautochthon is separated from a sliver allochthonous crust known as the South Portuguese Zone (SPZ) by a sequence of Late Devonian mélange, metasediments and mafic complexes known as the Pulo do lobo Zone (PDLZ). As a result this region of southern Iberia provides an excellent opportunity to document first order geologic events associated with convergence and collision of Gondwana with Laurussia.

The PDLZ is classically considered an accretionary complex, developed during the subduction of the Rheic Ocean beneath Gondwana and deformed during collision between Gondwana and the SPZ (e.g. Eden, 1991; Onézime et al., 2003). Although the SPZ is widely considered allochthonous with respect to the Gondwana para-autochthon,

its oldest exposed units are Late Devonian. Therefore determining its pre-Pangean affinity requires determination of (i) its late Paleozoic relationships to the PDLZ and (ii) the composition and geologic history of the unexposed SPZ basement.

This thesis reports the results of two field seasons in southern Iberia including detailed field mapping of a portion of the PDLZ and geochronological, isotopic and geochemical investigations of the PDLZ and the SPZ. Based on this work, new models for the tectonic evolution of the SPZ and PDLZ are proposed. These models have implicationsfor the timing of formation of Pangea and processes that contributed to its formation, as well as the paleogeography within and adjacent to the suture zone.

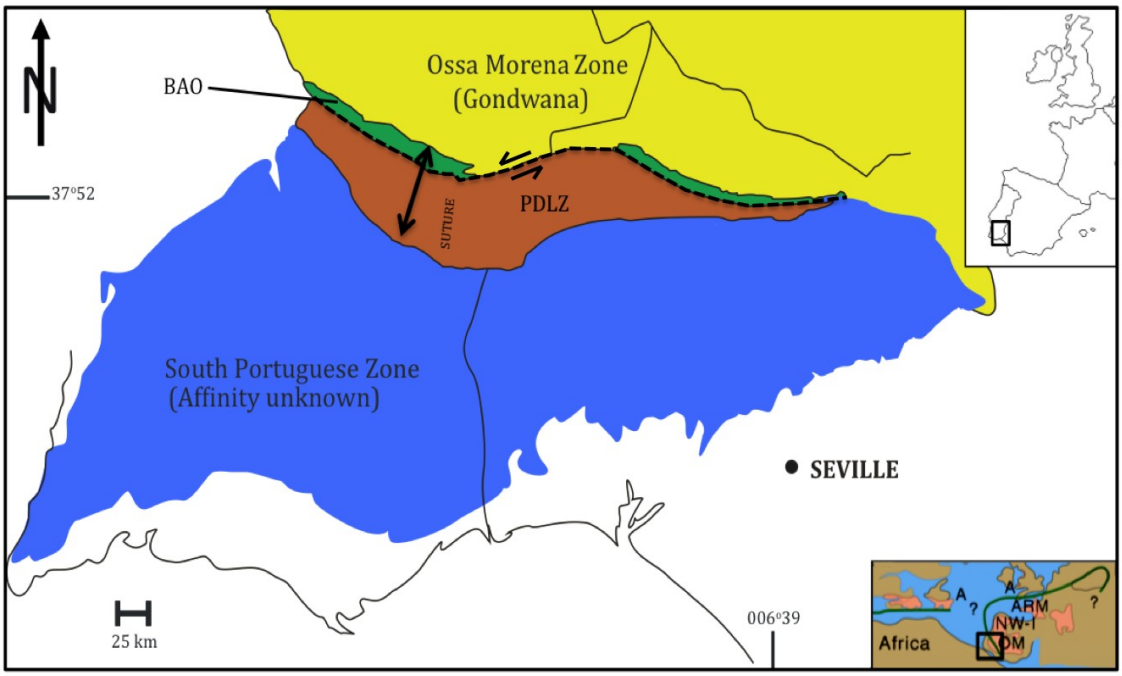

Fig. 1.2 Zonal subdivisions of Southern Iberia outlining a potential Rheic suture (inset). In terms of late Paleozoic geodynamics The Ossa Morena Zone = Gondwana; the Pulo do Lobo Zone (PDLZ) and Beja Acebuches Ophiolite (BAO) = Pangean suture zone; The South Portuguese Zone = exotic terrane; Dashed line = The South Iberian Shear Zone

1.2. Geologic Background

1.2.1. The Formation of Pangea

Paleogeographic reconstructions show that Pangea was formed by the sequential closure of the Iapetus and Rheic oceans (e.g. Scotese, 2003) (Fig. 1.1a). The Iapetus Ocean formed from ca. 610 to 530 Ma (Cawood et al., 2001) and was closed by ca. 420 Ma. The closure is marked by the collision between peri-Gondwanan terranes (e.g. Ganderia, Avalonia, Meguma) Baltica and Laurentia (e.g. van Staal et al., 1998; van Staal

et al., 2009). These collisions were responsible for several orogenic events in the northern Appalachians and the British Caledonides and are delineated by well-defined suture zones. Vestiges of the Iapetus Ocean are preserved along this suture zone as ophiolites in central and western Newfoundland, Canada (e.g. Jamieson, 1981; Williams and Hatcher, 1982; Williams et al., 1987; Kurth et al., 1998) (Fig 1.1b).

The Rheic Ocean, opened by the Early Ordovician with the separation of the peri-Gondwanan terranes from the margin of northern Gondwana (e.g., Avalonia, Ganderia, Carolinia, Meguma). Therefore Gondwana and the eastern margin of peri-Gondwana (Meguma terrane) flanked the Rheic throughout its evolution. The Rheic Ocean reached its greatest width (~ 4000 km) in the Silurian by which time Laurentia had collided with Baltica to the north and with Avalonia–Carolinia to the south, subsequently closing the Iapetus (e.g. Stampfli et al., 2002; Scotese, 2003). Closure of the Rheic Ocean began in the Early Devonian and it generally accepted that this closure was accommodated by northward subduction beneath the Laurussian margin, where arc magmatism developed on the previously accreted peri-Gondwanan terranes (e.g.,), Vestiges of the Early Ordovician–Carboniferous Rheic Ocean are preserved in several ophiolitic complexes in western Europe (e.g. the Lizard Complex of Britain (Davies, 1984) (Fig 1.1b). Terminal collision between Gondwana and Laurussia was complete by the Late Carboniferous and gave rise to the Alleghenian orogeny of North America and the Variscan orogeny of Western Europe.

1.2.2. Peri-Gondwanan Terranes

Peri-Gondwanan terranes are arc-related terranes that formed along the periphery of western Gondwana in the Neoproterozoic (e.g. Avalonia, Carolinia, Ganderia, Meguma). During the Cambrian - Ordovician opening of the Rheic Ocean these terranes separated from the Gondwanan margin. Peri-Gondwanan type rocks are exposed throughout the Appalachian orogen from the United States through Atlantic Canada, with correlatives in Ireland and Britain (e.g. Landing, 1996). Most late Paleozoic reconstructions indicate that the Avalon and Meguma terranes formed the easternmost margin of Laurussia and were roughly along strike of Iberia during the amalgamation of Pangea (e.g. Scotese, 2003; Woodcock et al., 2007).

Avalonia is the largest suspect terrane in the northern Appalachian orogen. It occupies much of the southern flank of the Appalachians and also occurs in the basement rocks of Ireland, southern Britain, and adjacent parts of continental Europe (O'Brien et al., 1983; Johnson and Van der Voo 1986, Nance and Murphy, 1989;Nance and Murphy, 1994; Keppie et al. 1996, Murphy et al. 1997) (Fig 1.1a).In the northern Appalachians the terrane contains abundant late Neoproterozoic voluminous volcanic rocks (ca. 570–680 Ma). Geochemistry of these volcanic rocks indicates that they were erupted in a volcanic arc environment (Keppie et al., 1991).

On the other hand, the Meguma terrane, which is the most outboard of the Appalachian terranes, is exposed only in southeastern Nova Scotia (Maritime Canada), however samples from offshore wells and geophysical data show that the Meguma

terrane forms the basement of Mesozoic–Cenozoic sedimentary basins as far as 200 km offshore Nova Scotia (Pe-Piper and Jansa, 1999). The Avalon terrane and the Meguma terrane collectively comprise the present day geology of Nova Scotia (northern Appalachians). The Meguma terrane is principally characterized by a thick (>10 km) succession of Cambrian to Ordovician turbiditic meta-sandstones and slates (the Meguma Supergroup) overlain by thinner Silurian to Devonian volcanics and shelf sediments (e.g. Schenk, 1997). Although the basement to the Meguma terrane is not exposed, the isotope geochemistry of (i) ca. 440 Ma within plate volcanics (White Rock formation), (ii) Late Devonian Meguma granitoid rocks (Clarke et al. 1988) and (iii) lower crustal xenoliths (Owen et al. 1988; Owen and Greenough 1991; Eberz et al. 1991; Greenough et al., 1999) suggest the Meguma terrane is underlain by comparatively juvenile peri-Gondwanan (Avalonian?) basement. Conversely, geochemistry of granitoid rocks offshore on the continental shelf indicates a relatively ancient basement signature consistent with the West African craton (Pe-Piper and Jansa, 1999).

1.2.3. Iberian-Armorican Arc

The Iberian-Armorican arc is defined as a curvilinear macrostructure that dominates the late Paleozoic Variscan orogenic belt of Iberia and France (Fig. 1.3) (Matte and Ribeiro, 1975;Franke, 1989, 2000; Onézime et al., 2003; Van Der Voo, 2004). This macrostructure includes two lines of sutures parallel to the orogenic belt that separate

three distinct tectono-stratigraphic zones that are correlated along the length of the macrostructure. These zones are, from the core to the outer arc: (1) the Moldanubian-Central and South Armorican-Central Iberian, (2) the Saxothuringian and Barrandian-North Armorican-Ossa Morena (3) the Rheno-Hercynian-Southwest England-South Portuguese zones (Franke, 2000; Onézime et al., 2003). The Rheno-Hercynian-Southwest England-South Portuguese Zone is characterized by synorogenic flysch deposits and by local occurrences of oceanic terranes delineating potential Variscan sutures between the Gondwanan autochthon and allochthonous terranes (ribbon continents, exotic terranes?) accreted during the late Paleozoic closure of the Rheic Ocean (Matte, 1986; Ribeiro, 1995; Lefort, 1999; Franke, 2000) (Fig. 1.3). Although the existence of these relationships and geometric associations was recognized in the 1920's, both the genesis of this macrostructure and the lateral continuity of the suture zones remain controversial (e.g. Franke, 2000;Simancas et al., 2005).

It has been suggested that the Iberian-Armorican arc is a direct result of continent-continent collision between an Iberian-Aquitanian indenter (Western Gondwana) and a northern continent (Laurussia) (Brun and Burg, 1982; Matte, 1986; Burg et al., 1987; Ribeiro et al., 1990; Quesada, 1991; Quesada et al., 1991; Dias and Ribeiro, 1996). This indenter model proposes that collision produced crustal imbrication in northern Iberia related to continent-continent collision, and explains the kinematic evidence for coeval left-lateral transpression in southern Iberia and right-lateral transpression in Armorica. Alternatively, the arcuate shape is attributed to oroclinal bending of an originally linear

belt accompanied by lithospheric thinning and delamination (Weil et al., 2001; Van der Voo, 2004; Gutiérrez-Alonso et al., 2008). This latter model requires late-to-post-orogenic bending of the lithosphere around a vertical axis accommodated in the upper crust either by tangential longitudinal strain (Gutiérrez-Alonso et al., 1999) or by flexural movement along existing shear zones (ribbon continent sutures) (Van der Voo, 2004).

The southern branch of the Iberian-Armorican arccrops out in the western part of the Iberian Peninsula (Fig 1.3). The Iberian Peninsula is classically divided into six distinct tectono-stratigraphic zones (Fig. 1): the Cantabrian, West Asturian-Leonese, Galicia-Tras-os-Montes, Central Iberian, OMZ and SPZ (Lotze 1945; Julivert et al., 1974; Franke, 1989; Ribeiro et al., 1990). The Cantabrian, West Asturian-Leonese and Central Iberian zones occur in the core of the Iberian-Armorican arc and are correlated with the Moldanubian domain. The Galicia-Tras-os-Montes and OMZ are correlated with the internal segment (Armorican-Barrandian) and the SPZ is commonly correlated with the outer domain (Rheno-Hercynian) (Fig. 1.3) (Julivert et al., 1974; Ribeiro et al., 1991; Quesada et al., 1991; Ribeiro and Sanderson, 1996). In the late Paleozoic, the OMZ is therefore considered para-autochthonous with respect to Gondwana, the SPZ allochthonous (underlain by peri-Gondwanan basement (e.g. De la Rosa et al., 2001)) and the PDLZ, an oceanic terrane that potentially records the docking of the SPZ to the OMZ during the formation of Pangea (Fig. 1.4) (Quesada, 1991; Ribeiro et al., 1990; Quesada et al., 1991).

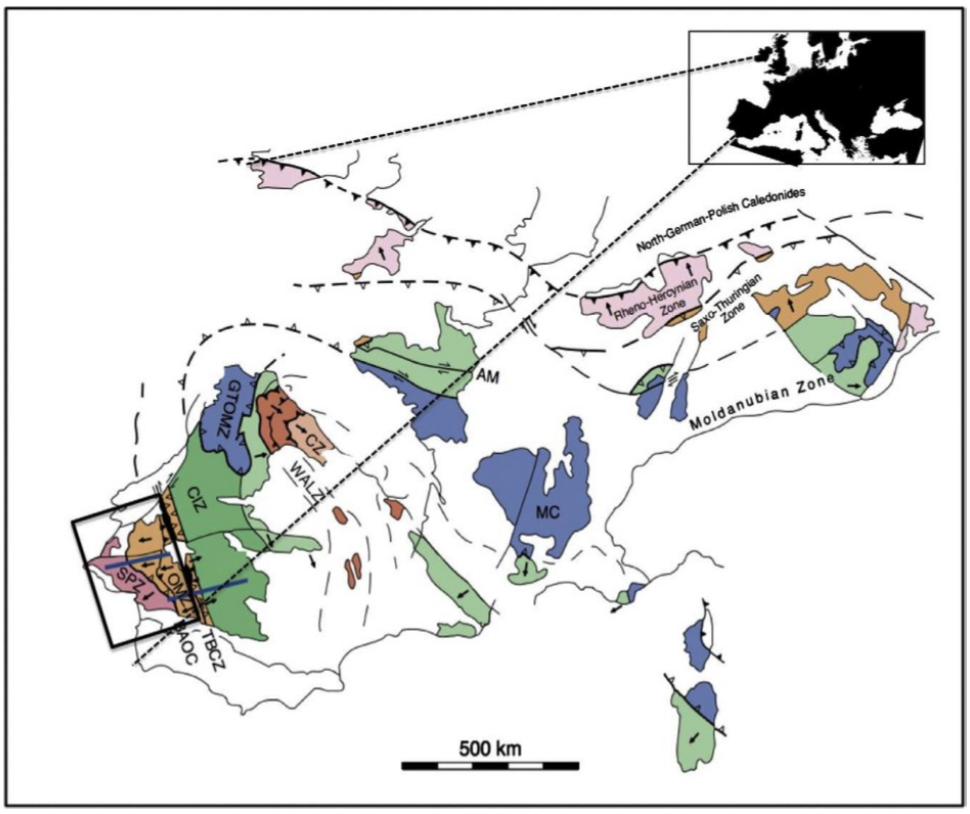

Fig. 1.3 Tectonostratigraphic zonation of the Variscan orogen in Europe showing the Iberian-Armorican arc (after Franke 2000; Martínez Catalán et al. 2007). SPZ, South Portuguese Zone; PDL, Pulo de Lobo Zone; CIZ, Central Iberian Zone; RHZ, Rheno-Hercynian zone; ST Saxothuringian Zone; M, Moldanubian.

1.2.4. Ossa Morena Zone

The OMZ has been interpreted as a composite terrane accreted to the Central Iberian Zone (CIZ) during the Cadomian orogeny (Quesada et al., 1991; Quesada et al., 2006) (Fig 1.2). The suture separating these zones is considered cryptic within the Badajoz-Córdoba shear zone (Quesada, 1990,1997). Prior to the onset of the Variscan orogeny, the stratigraphy in both the OMZ and CIZ includes Ediacaran and Paleozoic rocks that are interpreted to record the Neoproterozoic to Early Cambrian accretion of the OMZ to the CIZ and the subsequent opening of the Rheic Ocean (Quesada, 1991;

Quesada et al., 1991, 2006; Sánchez-García et al., 2003, 2008; López-Guijarro et al., 2008). The inferred sequence of events includes:

(a) a deposition of an Ediacaran pre-Cadomian sedimentary succession along the Gondwanan passive margin succeeded by syn-Cadomian arc sequences;

(b) the Late Ediacaran-Early Cambrian Cadomian orogeny culminating in accretion of the OMZ to the CIZ;

(c) a Late Cambrian - Early Ordovician sedimentary and igneous succession inferred to record a rifting event (opening of the Rheic Ocean);

(d) deposition of an Ordovician – Devonian passive margin succession along the Gondwanan margin as the Rheic Ocean opened.

Volcanic and plutonic rocks with calc-alkalic affinities of Visean age occur along the southern margin of the OMZ. This magmatism ended by ca. 330 ma and is thought to be genetically related to late Paleozoic subduction beneath the OMZ (Jesus et al., 2007; Castro et al., 2002).

1.2.5. Pulo do Lobo Zone and Beja Acebuches Ophiolite

The Pulo do Lobo Zone(PDLZ) is in faulted contact with the Beja Acebuches Ophiolite (BAO) to the north (Fig. 1.5). The BAO (Ca. 334 $\pm$ 2 Ma; Azor et al., 2008) is commonly correlated with the closure of the Rheic Ocean and delineates the northern contact between the PDLZ and OMZ(Silva et al., 1990;Fonseca et al., 1993;Quesada et

al., 1994). It has been suggested that Geochemical analysesindicate the primary igneous rocks of the BAO have a MORB affinity(e.g. Quesada et al., 1994). The BAO was thought to be correlative with the ca. 390 Ma Lizard complex (Davies, 1984). However recent ca. 334 Ma age date (Azor et al., 2008) suggests the BAO formed during the final stages of Rheic Ocean closure.Azor et al., 2008 have interpreted the BAO to have formed during a transtensional event following the main continent-continent collision (390-345 Ma).

Across strike, the BAO displays an increasing metamorphic grade to the north (i.e. highest temperature mineral assemblages located along the contact with the OMZ). This metamorphic grade is interpreted as the result of Variscan thrusting of the OMZ over the BAO (e.g. Quesada et al., 1994; Castro et al., 1996). The contact between the BAO and the PDLZ exhibits intense shearing and retrograde metamorphism, as a result of mylonitization along the South Iberian Shear Zone (SISZ) (Crespo-Blanc and Orozco, 1988, 1991) (Fig 1.2).

The PDLZ consists of fault-bounded tectono-stratigraphic units that strike east-west and dip steeply to the north (Eden 1991). The nomenclature and description of these units vary from Spanish to Portuguese sections (e.g. Silva et al., 1990; Oliveira, 1990; Eden, 1991; Giese et al., 1994) (Fig. 1.4). However, there is a consensus that the lowermost units of the PDLZ comprise phyllites, quartzites and mica schists and the uppermost units are a varied siltstone and greywacke flysch sequence (Santa Iria Flysch, SIF). Various tectonic and sedimentary mélanges are also recognized (Eden, 1991). To the south, the

Gil Márquez granodiorites (Ca. 330 Ma.; De la Rosa et al., 2001) locally intrude the PDLZ metasediments. These granodiorites are locally foliated parallel to the east-west orogenic grain and are commonly interpreted to have been emplaced during the latest stages of deformation in the PDLZ (e.g. Castro et al., 1995). Taken together, the units of the PDLZ are considered to have evolved from a pre-early orogenic to a syn-orogenic sequence that accreted to the OMZ during northward-directed subduction beneath the OMZ (Eden, 1991;Quesada et al., 1994; Onézime et al.,1999, 2003).However, the specific timing of deposition and deformation of units within the PDLZ remains poorly constrained. Within the Ribeira de Limas Formation, palynomorphs yielded Givetian-Frasnian ages (Oliveira et al., 1986; Giese et al., 1988) while spores and acritarchs indicate a Late Famennian age for the Santa Iria Formation (Eden, 1991;). Onézime et al.(2003) suggest that these data indicate an Early-to-Middle Devonian age for the basal formation (Pulo do Lobo Formation) of the accretionary wedge.

The regional structure of the PDLZ has been interpreted as a broad antiform (Pulo do Lobo (Portugal) - Los Ciries (Spain) Antiform) that reveals a complex internal structural history (Crespo Blanc, 1989; Silva et al., 1990; Eden, 1991; Onézimeet al., 2002). It has been suggested the type area has undergone three distinct deformation events (D1, D2, D3) (Silva et al., 1990; Giese et al., 1994; Giese et al., 1999), attributed to changing tectonic conditions during subduction of Rheic oceanic crust under the OMZ (Eden, 1991; Quesada et al., 1994; Onézimeet al., 1999, 2003).

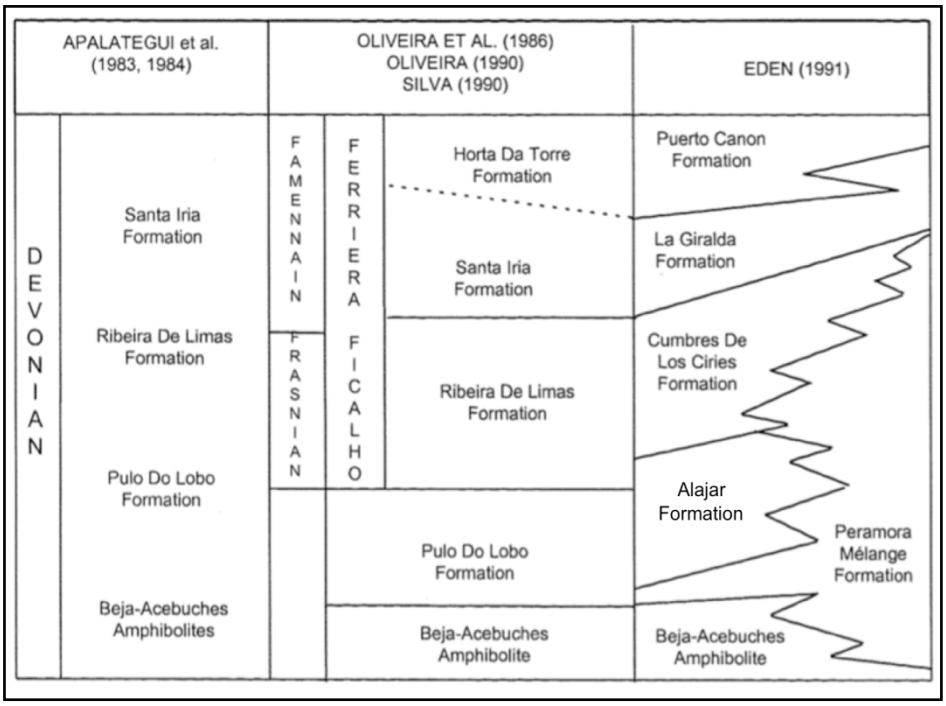

Fig. 1.4 Previously defined formations in the Pulo do Lobo Spanish section. Relativeages from palynologic data (Apalategui et al., 1983, 1984; Oliveira et al., 1986; Oliveira, 1990; Silva et al., 1990; Giese et al., 1988;Eden, 1991).

1.2.6. South Portuguese Zone

The SPZ crops out directly to the south of the PDLZ (Fig. 1.5) and consists mainly of Late Devonian–Late Carboniferous metasedimentary and metavolcanic rocks that are interpreted to have been deposited in an intracontinental transtensional basin (Fonseca et al., 1993). The SPZ is classically divided into three tectonostratigraphic units (Schermerhorn, 1971): (i) Devonian continental shelf quartzites and phyllites, which are interpreted as a passive margin sequence and the oldest unit exposed in the SPZ; (ii) an overlying bimodal volcano – sedimentary complex (VSC) dominated by Fammenian to Tournaisian (Munhá, 1983; Rosa et al., 2008) volcanic rocks interbedded with silicious

shale and chert; and (iii) a Visean to Westphalian flysch sequence known as “Culm” or Baixo Alentejo flysch (Oliveira et al., 1979; Oliveira, 1983, 1990). Flysch sediments contain mainly metamorphic lithic fragments and have been interpreted to reflect derivation from an OMZ and/or PDLZ source (Oliveira, 1988). Higher up, the Culm contains numerous volcanic clasts suggesting that the SPZ and the VSC in particular are also possible sources. Intrusive bodies of granitic, tonalitic, gabbroic and dioritic compositions (Ca. 350 to 300 Ma), are exposed in the northeastern part of the SPZ (Sierra Norte Batholith) and are considered to be syn- to post-tectonic with respect to Variscan events (Simancas et al., 1986; De la Rosa et al., 1993; Soriano et al., 2002).

During the Variscan orogeny, the SPZ is interpreted to have undergone a transition from a passive margin shelf environment, through a transtensional basin where the VSC was emplaced, to a syn-orogenic flysch setting (Silva, 1990; Quesada, 1991). Southwest-verging folds and thrusts, together with a general decrease of deformation intensity to the southeast, suggest that both fold vergence and syn-tectonic sedimentation propagated toward the southwest (Oliveira et al., 1990; Quesada, 1998; Onézime et al., 2002). This southward propagation of sedimentation and intensity of deformation, together with the younging of tectonstratigraphic units to the south (Early-Middle Devonian Pulo do Lobo Antiform, LateDevonian-Visean Iberian Pyrite Belt, Early Wesphalian flysch sequences),are interpreted to reflect a north-directed subduction beneath the OMZ (e.g. Quesada, 1998).

Metamorphism is low grade, ranging from epizonal in the southeast to anchizonal in the southwest, typical of shallow crustal environments within external orogenic domains (Munhá, 1990). Quesada (1998) proposed that SPZ records three distinct Variscan tectonic events:

(i) an initial transtensional event accompanied by lateral escape of marginal units of the SPZ and by extensional collapse of the pre-existing passive margin;

(ii) an inversion of the previous transtensional basin by major transpressional deformation associated with the obduction the OMZ onto the SPZ;

(iii) a late-stage transtensional event associated with the collapse of the previously thickened orogen in the OMZ and SPZ, during which the emplacement of the Sierra Norte Batholith took place.

Deformation recorded within the PDLZ (D1, D2, and D3) is considered to be directly related to the second tectonic event (transpression associated with collision).

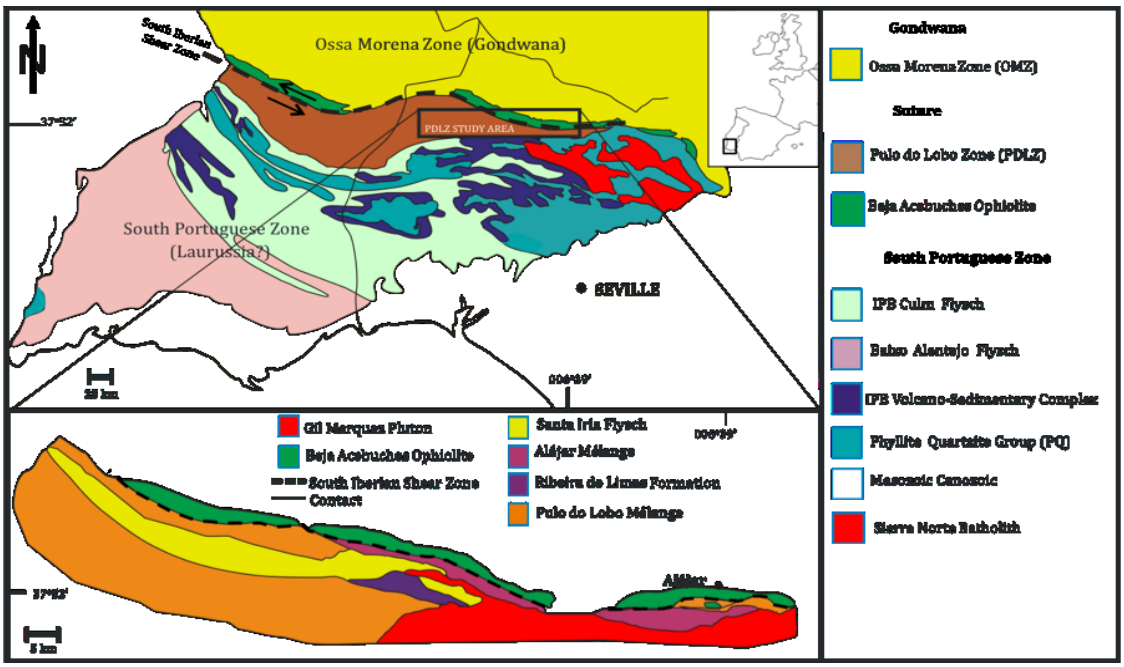

Fig. 1.5 Variscan tectonic terranes of Southern Iberia showing proposed suture zone (PDLZ and BAO) between the South Portuguese Zone and the Ossa Morena Zones (adapted from Onézime et al., 2003). Inset black square shows detailed PDLZ study area.

1.3 Objectives and Approach

This thesis provides a detailed examination of a potential exposure of a Pangean suture zone of the Variscan orogen. In order to test models concerning the development of this suture zone detailed fieldwork and mapping were completed as a framework for geochronological analyses (provenance) as well as geochemical and isotopic tracing.

1.3.1. Deformation in Accretionary Systems

The PDLZ is classically considered an accretionary complex developed during the formation of Pangea (e.g. Eden, 1991). However a detailed analysis of the structural geology in the Spanish portion of the PDLZ has not been published. This thesis presents the first detailed maps and structural analyses of the PDLZ and proposes new methods for interpreting deformation in highly deformed rocks within accretionary-type settings.

1.3.2. Provenance of the Pulo do Lobo Zone

Accretionary complexes are generally considered to be derived from either (i) sediment scraped from the lower plate or (ii) sediments eroded from the overriding plate and carried by turbidity currents in to the bottom of the trench (e.g. Twiss and Moores, 2007). Although these complexes mark important geologic divisions and events throughout geologic time, little is known about their evolution prior to incorporation into the upper plate, as intense deformation often overprints evidence of their derivation. Furthermore most orogenic events involve oblique collision, suggesting evolution of accretionary complexes may be in some cases more complex than generally thought. Based on field mapping and previous work the Variscan collision is thought to be highly oblique. An important objective of this thesis is to test the provenance of the PDLZ in order to determine how accretionary complexes evolve in oblique collisional settings. These data also help to provide regional constraints on the tectonic relationship of the PDLZ and the SPZ.

1.3.3. Provenance of the South Portuguese Zone

Determining the pre-orogenic provenance of allochthonous terranes that are covered by syn-orogenic and post orogenic geologic sequences is key to unraveling paleogeographic history. This scenario is recognized in the southern Iberia where the oldest exposed units in the SPZ are Late Devonian. Determining the provenance of the SPZ basement has broad implications not only for determining the tectonic development of southern Iberia but also for understanding the relationships of these Variscan events to the development of the Appalachian orogen. A main objective of this thesis is to test various hypotheses surrounding the paleogeographic history of the SPZ basement by determining the composition of the SPZ basement.

1.3.4. Summary of Thesis Objectives

(i) To constrain how accretionary systems are deformed in oblique collisional settings.

(ii) To test whether the PDLZ is a Pangean suture zone and Variscan accretionary prism.

(iii) To determine the provenance of the PDLZ and its relationship to the development of the Variscan-Appalachian orogens.

(iv) To determine the provenance of the SPZ and its relationship to the development of the Variscan and Appalachian orogens.

(v) To provide insights into the timing, geometry and processes associated with the formation of the supercontinent Pangea

1.4. Thesis Structure and Organization

1.4.1. Relationship to Published Work

The main chapters of this thesis are written as independent but complementary manuscripts that have been published or submitted for publication. Some repetition of background material is therefore unavoidable. Furthermore, geological interpretations evolved during this study as a result of the acquisition of new data, resulting in some differences in interpretation between the manuscripts. These differences are reconciled in the synthesis and discussion chapter (Chapter 5).

Chapter 2 presents results from detailed field mapping in the Spanish portion of the PDLZ. This chapter presents new interpretations on the structural evolution of the PDLZ, the lithologic and structural relationship of the PDLZ to the OMZ and SPZ, and supplies the groundwork for targeted sampling within the PDLZ and SPZ as described and analyzed in subsequent chapters. Furthermore this paper presents a possible template for interpreting similar collisional accretionary events. This chapter is a journal manuscript published in a special issue of*Gondwana Research* entitled *The Rheic Ocean: Palaeozoic Evolution from Gondwana and Laurussia to Pangaea.* Co- authors are J.B. Murphy and Cecilio Quesada. I did the primary fieldwork and manuscript preparation myself. Both J.B. Murphy and C. Quesada contributed significantly to ideas and discussions in the field and to editing the manuscript.

Chapter 3 discusses the provenance of the PDLZ and the SPZ and demonstrates that (i) the SPZ was outboard of Gondwana in the Late Devonian (ii) the PDLZ is also exotic to Gondwana and (iii) in general what was thought to be a simple accretionary style deposition may have had a complex and long lived history. This chapter is a journal manuscript accepted for publication in the *Journal of theGeological Society of London*and is co-authored by J.B. Murphy, Cecilio Quesada and Jim Mortensen. This paper presents new LA-ICPMS U/Pb detrital zircon data from the PDLZ and SPZ. These samples were collected based on fieldwork presented in Chapter 2. I completed zircon separations, sample preparation, U/Pb analytical work and data reduction, with help from Jim Mortensen and the Pacific Centre for Isotopic and Geochemical Research (PCIGR) at the University of British Columbia. I have interpreted the geochronological data myself with helpful suggestions from J.B. Murphy and C. Quesada.

Chapter 4 discusses the composition of the SPZ basement and its potential pre-Devonian tectonothermal and paleogeographic history.This chapter is under review for publication in the *Canadian Journal of Earth Sciences*, co-authored by J.B. Murphy, C. Quesada, L. Bickerton and J. Mortensen. There may be some discrepancy in text of this journal article and the text in this thesis pending suggestions by reviewers. This paper presents new LA-ICPMS zircon geochronological data, geochemical and Sm–Nd isotopic data from representative samples from a granite batholith that cuts both the PDLZ and the SPZ. This paper also presents new lithogeochemical and Sm-Nd isotopic data from exposed sedimentary sequences in the SPZ and PDLZ. These data facilitate (i)

comparison between the SPZ and various tectonostratigraphic zones in the northern Appalachians; and (ii) an interpretation of the geometry and age of the closure of the Rheic Ocean and the formation of Pangea. All samples were selected based on field relationships outlined in Chapter 2. Zircon separations, sample preparation, U/Pb analytical work and data reduction were done myself, with help from Jim Mortensen and the Pacific Centre for Isotopic and Geochemical Research (PCIGR) at the University of British Columbia. The major and selected trace elements were analyzed by X-ray fluorescence at the Nova Scotia Regional Geochemical Centre at St. Mary's University, Halifax. Rare Earth Elements (REE) by neutron activation for Sm-Nd compositions at the Atlantic Universities Regional Isotopic Facility (AURIF) at Memorial University. J.B. Murphy and Cecilio Quesada provided valuable assistance in the tectonic interpretations and manuscript editing. Luke Bickerton assisted with the geochemical and geochronological plots and interpretation.

1.4.2. Originality Summary

I have done the following myself with important input and writing corrections from my thesis committee and co-authors on submitted papers:

- Fieldwork, mapping and structural interpretations
- Sample selection
- U/Pb zircon sample separation, analyses and interpretation
- SEM backscatter imaging and interpretation

- Geochemical and isotopic interpretations
- Petrographic analyses and interpretation
- Manuscript writing

CHAPTER 2

STRUCTURAL ANALYSIS OF AN ACCRETIONARY PRISM IN A CONTINENTAL COLLISIONAL SETTING, THE LATE PALEOZOIC PULO DO LOBO ZONE, SOUTHERN IBERIA

2.1. Abstract

Models concerning the tectonic evolution of accretionary complexes typically relate outcrop-scale to plate-scale multiphase deformation as a smooth variation of strain on all scales. However, at oblique convergent margins, regional-scale brittle faults in the shallow crust are commonly parallel to the main orogenic grain. These faults impose a strong structural anisotropy and can subsequently control deformation at subordinate scales.As a result, finite strain in each domain may not record local kinematics consistent with the overall orogenic-scale motion implying that structural data must be analyzed selectively from a large area in order to relate outcrop-scale kinematics to global plate-scale dynamics. Field mapping and preliminary structural analysis of the Late Devonian Pulo do Lobo (PDLZ) Formation, and suspect "exotic" South Portuguese Zone (SPZ) in southern Iberia indicate tectonic juxtaposition of diverse deposits such as foreland basin flysch, sedimentary and tectonic mélange, and passive margin sediments showing an overall geometry consistent with an accretionary wedge setting. Variations in finite strain, lithology and regional structure were used as proxies for defining tectonic domains for structural analysis. Numerous local kinematic indicators within the PDLZ suggest a

complex regional deformation with several enigmatic features that can be explained by sequential compartmentalization of strain during the development of the imbricate stack followed by late-stage bulk strain imposed across the entire complex. Structural data produced by local strain partitioning reveals kinematic indicators, which contradict the overall regional structural style (e.g. spatial juxtaposition of sinistral and dextral fabrics). When viewed at larger scales (i.e. regional scale), however, these data indicate that significant sinistral strike-slip movement occurred in conjunction with both an extension and shortening. Outcrop-scale deformation in polydeformed domains is controlled by local conditions resulting from brittle deformation coeval with orogenic-scale bulk strain. The entire Pulo do Lobo Zone is dominated by a pervasive late-stage vertical to sub-vertical E-W cleavage, axial planar to chevron folds which overprint earlier deformation in the older passive margin units. This overprinting suggests that in the late stages of the evolution of the accretionary complex, bulk strain was imposed over the entire complex as a result of internal locking of the accretionary complex and reduced strain rates during the waning stages of collision between Gondwana and Laurentia. Stereographic analysis of fabric elements from each distinct tectonic domain, together with regional geological constraints, support this hypothesis and are indicative of progressive deformation imposed on the PDLZ during the Variscan Orogeny.

2.2. Introduction

Although accretionary complexes are an integral manifestation of convergent margins, their internal structural complexities make it difficult to relate outcrop and regional-scale observations to orogenic scale events. These internal complexities are typically characterized by an imbricate structure (at both outcrop and regional scale) and by pervasive thrusting and shearing (e.g. Pini, 1999; Kusky et al., 2004). Accretionary complexes also typically develop a block-in-matrix "mélange" fabric due to layer-parallel extension and shearing (Niwa, 2006).

Despite the recognition that (i) deformation in accretionary complexes can be considered progressive (e.g. Ujiie, 2001) and (ii) there is a kinematic requirement for variability in strain compatibility from a bulk orogenic scale across all subordinate scales in orogenic belts(Jones et al., 2005), most studies of late Palaeozoic accretionary complexes in western Europe and southern Iberia (Variscan orogen; Lotze, 1945) interpret outcrop-scale and map-scale structures as fractal with respect to larger orogen-scale kinematics and processes (e.g. Díaz et al., 1999, Martínez Catalán et al., 1997). As a result, there are a plethora of tectonic models that attempt to explain plate-scale processes from regional structural interpretations across the Variscan orogenic belt. For example, some models claim deformation in accreted terranes is genetically linked to a westward subduction beneath the Laurussian margin (e.g. Martínez Catalán et al., 1997; Díaz et al., 1999; Sánchez Martínez et al., 2007), with Gondwana situated on the lower

plate, whereas others ascribe late Paleozoic Variscan events to an eastward-dipping subduction zone beneath the Gondwanan margin (e.g. Rapela et al., 1992; Fonseca et al., 1993; Onézime et al., 2003).

In southern Iberia, a late Paleozoic accretionary complex, known as the Pulo do Lobo Zone, (PDLZ) (Fig. 1.2) separates the Ossa Morena Zone (OMZ), which has Gondwanan affinities throughout the Paleozoic, from the South Portuguese Zone (SPZ), which is considered to be underlain by Avalonian or Meguma basement (e.g. De la Rosa et al., 2001; Simancas et al., 2005). As Avalon was accreted to Laurussia by the Mid-Silurian (Murphy et al., 1996; Van Staal et al., 1998; Nance et al., 2002; Keppie et al., 2003), the accretionary complex (known as the Pulo do Lobo Zone, PDLZ), potentially represents an exposed suture zone that records the closure of the late Paleozoic Rheic Ocean and the amalgamation of Pangea. This suture zone was first recognized by the occurrence of rocks with oceanic type geochemistry (Beja Acebuches Ophiolite, BAO) (Quesada et al., 1994) outcropping along the boundary between the OMZ and the PDLZ. The BAO is historically interpreted as a Variscan ophiolite of the Rheic Ocean (i.e. Munhá et al., 1986; Castro et al., 1996; Fonseca et al., 1993). However, recently the BAO has been dated at 334 $\pm$ 2 Ma (U/Pb zircon, SHRIMP, Azor et al., 2008) and interpreted as formed during post-collisional (Laurussia-Gondwana) extension (Azor et al., 2008). Both models for the BAO have in common the hypothesized exotic nature of the SPZ and imply subsequent deformation in the PDLZ potentially records an important part of the

accretionary history. As a result, the PDLZ is an ideal field laboratory to study the structural evolution of accretionary prisms in late Paleozoic orogenic systems.

To date, most studies detailing the geologic evolution of the PDLZ have focused on describing internal lithostratigraphic relationships (Carvalho et al., 1976; Eden, 1991; Giese et al., 1994). The internal structural development and kinematic relationship of deformation in the PDLZ to Variscan orogenic processes remains poorly understood.

In this paper, we present field relationships and structural data which suggest that (i) the complex deformation of the PDLZ can be explained by compartmentalization of bulk strain at a regional-scale, and (ii) outcrop-scale structures in the shallow crust were controlled primarily by a strong structural anisotropy which developed within the accretionary system. Our data indicate that deformation of the PDLZ was progressive with the development of different structural styles in distinct tectonic domains as a function of time and changing boundary conditions. However, we suggest that although kinematics on an outcrop to regional scale may not be directly indicative of orogen-scale kinematics and processes, recognition of the scales at which compatibility is maintained is predictable and may provide a template for interpreting coeval systems throughout the Variscan orogenic belt. To view maps, field notes and field pictures please refer to the supplementary DVD.

2.3. Tectonic Domains ~ General Considerations

In accretionary complexes, bulk strain on a regional scale typically changes progressively with time (e.g. Ramsey and Lisle, 2000; Jones et al., 2005). Finite strain recorded at an outcrop scale is a composite of different strains as a result of temporal changes in stress fields. Rheologic contrasts and secondary strain regimes (e.g. riedel shears on a subordinate scale) add to the complexity. As a result, systems affected by regional-scale simple shear or non-coaxial non-plane strain exhibit a variety of brittle or ductile structures at subordinate scales (Jones et al., 2005). If regional-scale deformation includes an array of shear zones or faults, the magnitude and orientation of coaxial and non-coaxial components will be heterogeneous, and the extent to which bulk strain is recorded in the rock record varies both in space and time (e.g. Jones et al., 2005). Consequently, the use of non-penetrative or outcrop-scale structures, as evidence for distinct deformational events (the so-called deformation phases) is typically misleading. Added complexity arises in accretionary complexes such as the PDLZ that contain sedimentary or tectonic mélange units. Tectonic and sedimentary mélanges form mappable (1:25,000 or smaller scale) units in the PDLZ that are internally fragmented and consist of mixed rock bodies containing a variety of blocks in a deformed matrix (Silver and Beutner, 1980). Although mélanges are typically represented as coherent units on a geologic map, internally they are chaotic, and are discontinuous along strike and in the subsurface (Wakabayashi, 2004). By implication, most investigations of mélanges using classical mapping techniques do not adequately characterize their spatial

distribution, lithological and tectonic character. Although mélanges are considered in integral component of accretionary complexes, the use of this term has been mostly descriptive, given the lack of consensus concerning their genesis. Most researchers have interpreted asymmetric shear fabrics and sheared block/matrix contacts in mélanges as indicative of a primary tectonic origin. On the other hand, sedimentary mélanges are considered to have a primary sedimentary origin due to the lack of such shear fabrics. The presence of rounded blocks or "cobbles" and preserved sedimentary structures internal to mélange blocks is also indicative of a primary sedimentary origin. However, recently Osozawa et al., 2009 point out that mélange "blocks" with pre-existing fabrics, which potentially record older tectonic events, can be incorporated into the mélange by sedimentary processes and deformed following deposition. In this case the mélange records independent sedimentary and tectonic processes (deposition and subsequent deformation) as well as pre-accretionary tectonic events (pre-existing fabrics in blocks).

As the PDLZ is fault-bounded, internally sheared and mélange-bearing (Eden, 1991; Giese et al., 1999), the above considerations suggest that conventional mapping and structural analysis techniques may not be practical in determining the tectonic history of the area. As a result, tectonostratigraphic domains were selected in the PDLZ (Fig. 2.1) by: (1) relating similar brittle and ductile structural styles over a maximum spatial extent (i.e. outcrop-microscopic-scale strain patterns, which could be related spatially over the mapping area), and (2) recording variations in the relative development of strike-slip, shortening and extensional features. Using this approach we were able to identify and

map five domains (A through E). Domain Ais defined by the presence of a well-developed shallowly plunging stretching lineation and by outcrop-to-microscopic scale ptygmatic folds. *Domain B* is defined by complex outcrop-scale folding patterns, conical and intrafolial folds, pervasive anastamosing schistosity and a localized block-in-matrix mélange fabric. *Domain C* is defined by outcrop-scale folding patterns and crenulation cleavage. *Domain D* is defined by a block-in-matrix mélange fabric, a shallowly-plunging stretching lineation, duplexing and conjugate fault sets. *Domain E* is defined by outcrop-scale upright cylindrical folds, pervasive fracture cleavage and conjugate fracture sets. *Domain A* corresponds with the northern margin of the Pulo do Lobo Formation (southern margin of the SISZ), *domain B* with the Pulo do Lobo Formation and Permora mélange, *domain C* with the Ribeira de Limas Formation, *domain D* with the Alajar Formation (a mélange) and *domain E* with the Santa Iria flysch (Figs 1.4, 2.2).

Although internal structures in each domain are interpreted as part of a domain-specific system, for comparison, relatable events in the structural evolutionary path for a given domain are separated into distinct events (e.g. A-D_1=domain A, event 1; A-D_2 = domain A, event 2; A-D_3 = domain A, event 3…etc.).

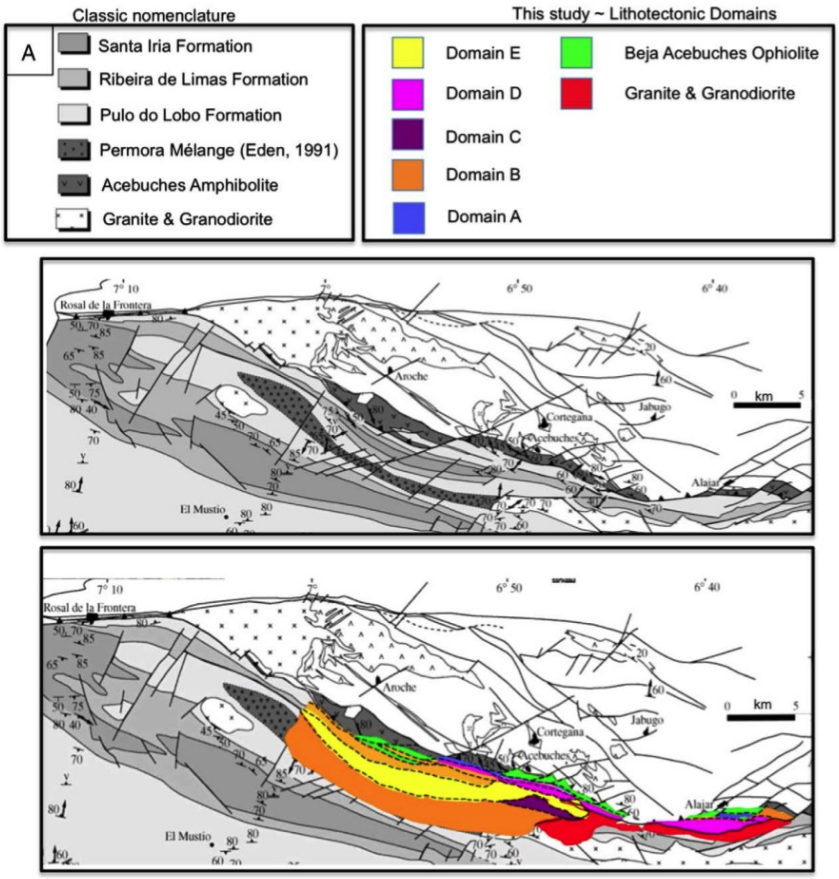

Fig 2.1 Comparison of tectonostratigraphic domains with current geologic maps (adapted fromOnézime et al., 2003).

2.4. Field Observations

2.4.1. Domain A

Observations

Domain A crops out along the northern margin of the PDLZ (Fig. 2.1) and is bordered to the north by the BAO and the South Iberian Shear Zone (SISZ) of Crespo Blanc and Orozco (1988, 1991). The domain is characterized by L-tectonite, and by fine-

grained pelitic schists composed predominantly of muscovite, biotite and quartz. Pre-tectonic plagioclase-rich layers occur locally in the schists and are enveloped by a mylonitic foliation. This mylonitic foliation, defined by muscovite and minor chlorite, strikes east-west, and is sub-vertical (A-D_1) (Fig. 2.2a). A well-developed stretching lineation (A-L_1) defined by quartz rods is visible along foliation planes and plunges shallowly to the southeast and to the northwest (Fig. 2.2a). Plagioclase is boudinaged along foliation planes and displays both brittle and plastic deformation (Fig. 2.2b). On a microscopic scale, the mylonitic foliation is also locally deformed into ptygmatic folds with steeply plunging hinges (A-D_2) in oriented sections cut parallel to the A-L_1 stretching lineation (A-D_2) (Fig. 2.2c). Plagioclase boudins show sinistral back-rotation (A-D_3) (Fig. 2.2d).

Interpretation

To a first order, the pervasive occurrence of shallowly plunging stretching lineations suggests the main deformation coeval with fabric development was predominantly strike-slip (A-D_1). The east-west strike of the mylonitic foliation and the sinistral kinematics displayed by plagioclase boudins associated with this deformation implies relative bulk sinistral kinematics. In this case, the shallow easterly plunge of the stretching lineations also suggests a minor reverse component (i.e. north side up). The steep plunge of A-D_2 minor folds of the mylonitic foliation indicates subsequent rotation of the main fabric and that strain was predominantly non-coaxial. This sinistral strike-

slip motion constitutes the bulk of internal deformation in the domain. However, a plot of minor fold axis orientations from outcrop-scale (A-D_2) folds also shows potential bulk cylindrical rotation of conical minor fold axial planes about an axis shallowly plunging to the west (A-D_4) (Fig. 2.2e).

The presence of muscovite, biotite, and chlorite indicate peak metamorphic conditions were at maximum upper-greenschist facies during A-D_1. This interpretation is consistent with textural evidence for the close spatial juxtaposition of both plastic and brittle deformation in the plagioclase suggests deformation potentially took place at the brittle-plastic transition zone (~450 ºC) (van der Pluijm et al., 1997).

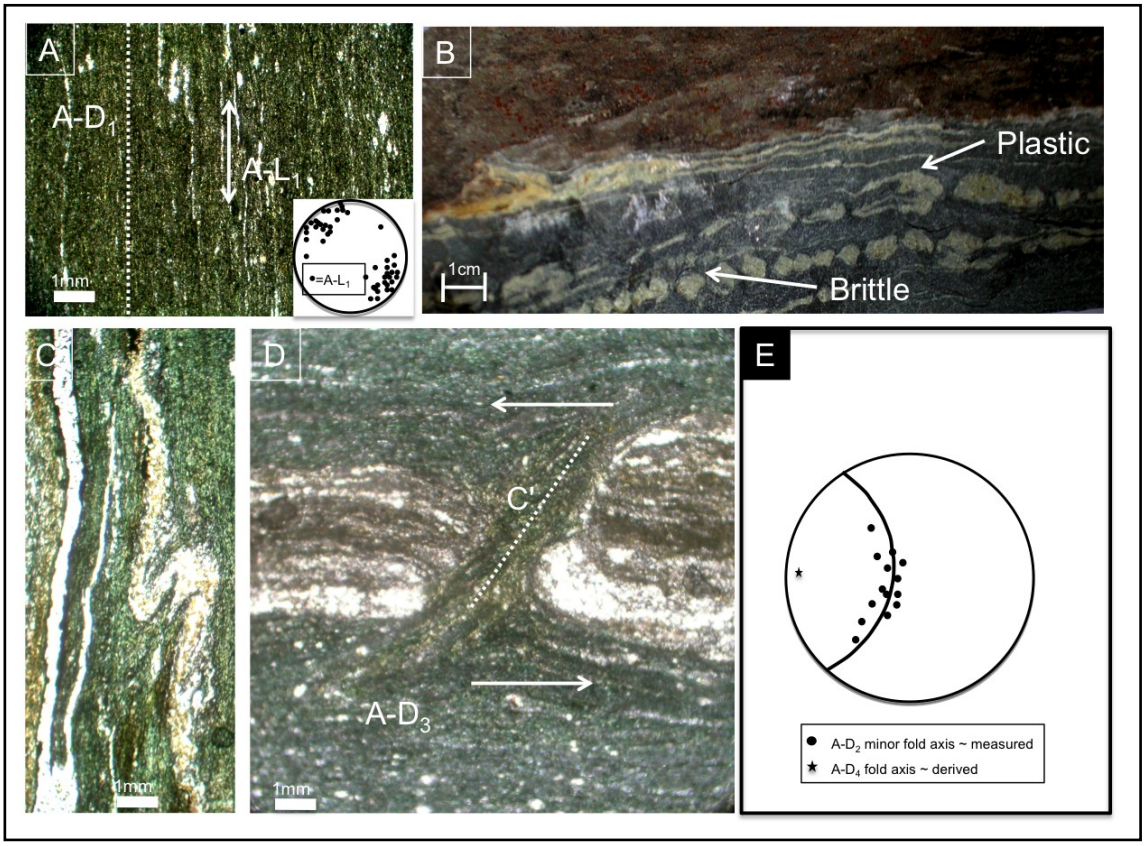

Fig. 2.2 Domain A (A) Mylonitic Foliation (A–D1) (east–west striking) trace with shallowly plunging stretching lineations A–L1in thin section (plane polarized). (Inset) equal anglestereoplot of stretching lineations measured throughout the domain on outcrop-scale. (B) Plagioclase-rich layers displaying spatially juxtaposed brittle and plastic behaviorassociated with A–D1. (C) Photo micrograph of minor ptygmatic fold showing sinistral kinematics (plane polarized) (A–D2). (D) Plagioclase boudins show sinistral back-rotation(A–D3). (E) Equal angle stereoplot showing conical rotation of (A–D2) minor fold axes by (A–D4).

2.4.2. Domain B

Observations

Domain B (Fig. 2.3) is dominated by quartz-mica phyllite and schist comprised of quartz, sericite, minor biotite, chlorite and plagioclase. Both phyllites and schistsarebandedonamicroscopicscale (from0.05to1mm) and these bands are definedby

varying abundances ofquartzandphyllosilicates. Quartz-rich bands, however,arenotpersistent laterally andcommonlypinch out (Fig. 2.3a). Locally, minor phacoidal quartzite and greenschist (metabasalt) blocks (cm to m scale) enveloped by the schists and phyllites are exposed and grade continuously into zones dominated entirely by the schist and phyllite. The greenschist blocks contain a mylonitic foliation (B-D_1) (Fig. 2.3b). A well-developedpenetrative foliation (B-D_2) envelopes the greenschist and quartzite blocks, is defined by muscovite and biotite, strikes predominantly east-west and is consistently steeply dipping (Fig. 2.3c). A stretching lineation (B-L_1) (plunging shallowly to the east) defined by quartz is weakly developed along the foliation planes in the schists and the long axis of the coarser grained (quartz-rich) bands are commonly boudinaged parallel to this lineation (Fig. 2.3c). The long axes of greenschist and quartzite blocks (where present) are also commonly boudinaged parallel to the stretching lineation. Slickensides are also common along block/matrix contacts.

Minor folds (B-D_3) of the foliation are visible throughout the domain on an outcrop and microscopic scale (Fig. 2.3d). At an outcrop scale, this foliation is folded into meter-scale folds (B-D_3), which locally envelope intrafolial folds (of similar pelitic schist) (Fig. 2.3e). Using the methos described in Keppie et al., 2002, stereographic projections show that these meter-scale folds (B-D_3) have a conical geometry. Petrographic examination shows that textures in the schists are defined by sutured grain boundaries between quartz grains and micas, and S/C fabric development with micas oriented parallel to the S and C-fabrics.

Interpretation

The occurrence of quartzite and greenschist blocks in the schistose matrix suggests that, locally, lithologies in this domain attain a mélange-type character. Although the overall structural style is consistent throughout the domain (S/C fabric, conical folds) the local occurrence of block-in-matrix mélange enveloped by a strong tectonic fabric and sheared block/matix contacts (slickensides) suggest the entire domain may be tectonically shuffled, implying that the original stratigraphy is not preserved. The presence of this strong tectonic fabric is further supported by the occurrence of intrafolial folds in the matrix, enveloped by the main foliation. These intrafolial folds potentially represent bulk shortening ($B\text{-}D_1$) prior to the main shearing event ($B\text{-}D_2$). The well-defined S/C fabric and stretching lineations in the schistose units may be indicative of this strong shearing and suggest a dominant overall sinistral strike-slip component during $B\text{-}D_2$. However, the presence of numerous conical folds of the schistosity, from microscopic to outcrop scale, also implies that shortening ($B\text{-}D_3$) occurred following fabric development. Stereoplots of these fold axes reveal evidence of two discrete phases of conical folding. Minor folds of the schistosity are each defined by conical folds axes with an internally consistent orientation. However, a synoptic plot shows that these cone axes are rotated about late-stage regional cone axes that plunge shallowly to the east and the west ($B\text{-}D_4$) (Fig. 2.3f). Taken together, the development of the primary schistosity, the two different phases of conical folding of this schistosity and the subsequent rotation

of those folds about axes with different orientations suggest a minimum of three different stress regimes imposed on the domain throughout its tectonic evolution. The presence of minor biotite, sericite and chlorite along B-D_2 foliation planes in the schists indicate that peak metamorphism associated with B-D_2 was greenschist facies.

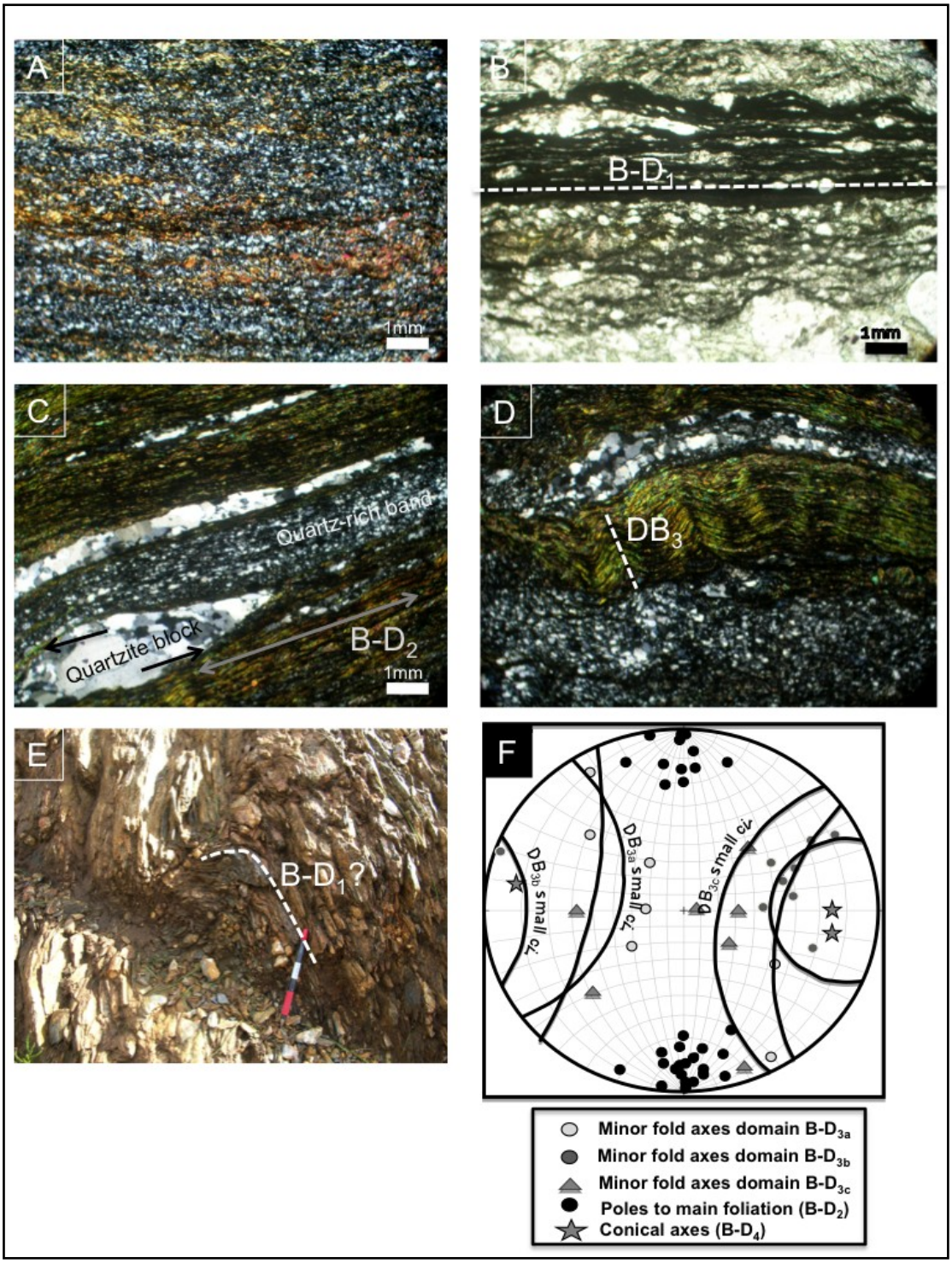

Fig. 2.3 Domain B (A) Photo micrograph showing laterally discontinuous quartz-rich bands in a metapelitic matrix (crossed polarized). (B) Mylonitic foliation (B–D1) from agreenschist"block"(photo micrograph). (C) Main foliation (B–D2) defined by muscovite, sericite and biotite with boudinaged quartzite block emplaced prior to B–

D2(crossedpolarized thin section). (D) Photo micrograph of minor folds of B–D2foliation (by B–D3) (crossed polarized). Dashed line along B–D3hinge trace. (E) Main foliation B–D2surroundsintrafolial fold (B–D1?). (F) Equal angle stereoplot of measured B–D3minor fold axes rotated by B–D4where B–D3a,b,crepresent outcrop-scale sub-domains within domain B.

2.4.3. Domain C

Observations

Domain C (Fig. 2.4) is dominated by bedded quartzwacke (ca. 40cm thick) comprised of angular quartz clasts in a groundmass of finer grained quartz and plagioclase. The quartzwacke is interbedded with thin (ca. 10 cm) layers of phyllitic metasediments comprised mainly of quartz, biotite, chlorite, and sericitized plagioclase. On an outcrop scale, minor folds of quartzwacke beds (C-D_1) are locally developed about vertical hinges (Fig. 2.4a) and are asymmetric. Phyllites are characterized by a penetrative cleavage defined by sericite, biotite and chlorite.

Minor folds are also developed about horizontal hinges (C-D_2) (Fig. 2.4b) which rotate the C-D_1 fabric and show both “s” and “z” symmetry. A fracture cleavage (C-D_3) that is weakly developed in the quartzwacke units is near vertical and east-west striking. A crenulation cleavage (Fig. 2.4c) in the phyllites (D-C_3) crenulates the pre-existing C-D_1 penetrative cleavage. Locally, cordierite porphyroblasts in phyllitic horizons exhibit poikiloblastic textures and their growth is post-tectonic with respect to C-D_1 penetrative cleavage and C-D_3 crenulation cleavage. These cordierite porphyroblasts occur only in close spatial proximity to exposed granites and granodiorites to the south.

Interpretation

The preservation of bedding throughout the domain (as seen in the quartzwacke units) indicates the domain was not strongly internally sheared during the main phase of deformation. Minor "z" and "s" fold vergences of upright folds (C-D_2), however, are inconsistent with the tectonic facing as indicated by bedding/cleavage relationships, suggesting they formed prior to the larger-scale structural development (C-D_3). This inconsistency implies the (C-D_2) minor folds are related to an earlier shortening-dominated regime and the fracture cleavage is associated with the regional structure. A synoptic plot of the poles to minor fold axial planes measured throughout the domain define a great circle distribution about an axis plunging shallowly to the east (C-D_3) which lies on the C-D_3 crenulation axial plane (Fig. 2.4d). Fracture cleavage intersection lineations also lie on the crenulation cleavage plane suggesting fracture cleavage was developed during C-D_3.

The presence of biotite and chlorite on C-D_1 suggests a peak metamorphism of greenschist to lower greenschist facies (i.e. phyllitic fabric crenulated by C-D_3). The development of crenulation cleavages on pre-existing C-D_1 cleavage planes also suggests continued progressive shortening (C-D_3) at higher structural levels than C-D_1.

Given the regional scale of typical greenschist facies minerals, the presence of cordierite mineral post (C-D_{1-2}) overgrowths on the fabric suggests proximity to an intrusive igneous body (i.e. contact metamorphism), which, therefore, intruded after the main deformation. The Gil Márquez (Ca 330 Ma; De la Rosa et al., 2001) granodiorite

crops out directly to the south (Fig. 1.5) and is a likely heat source for the contact metamorphism evidenced in Domain C. In this case, C-D_{1-3} occurred prior to 330 Ma. and post-emplacement movement would be limited.

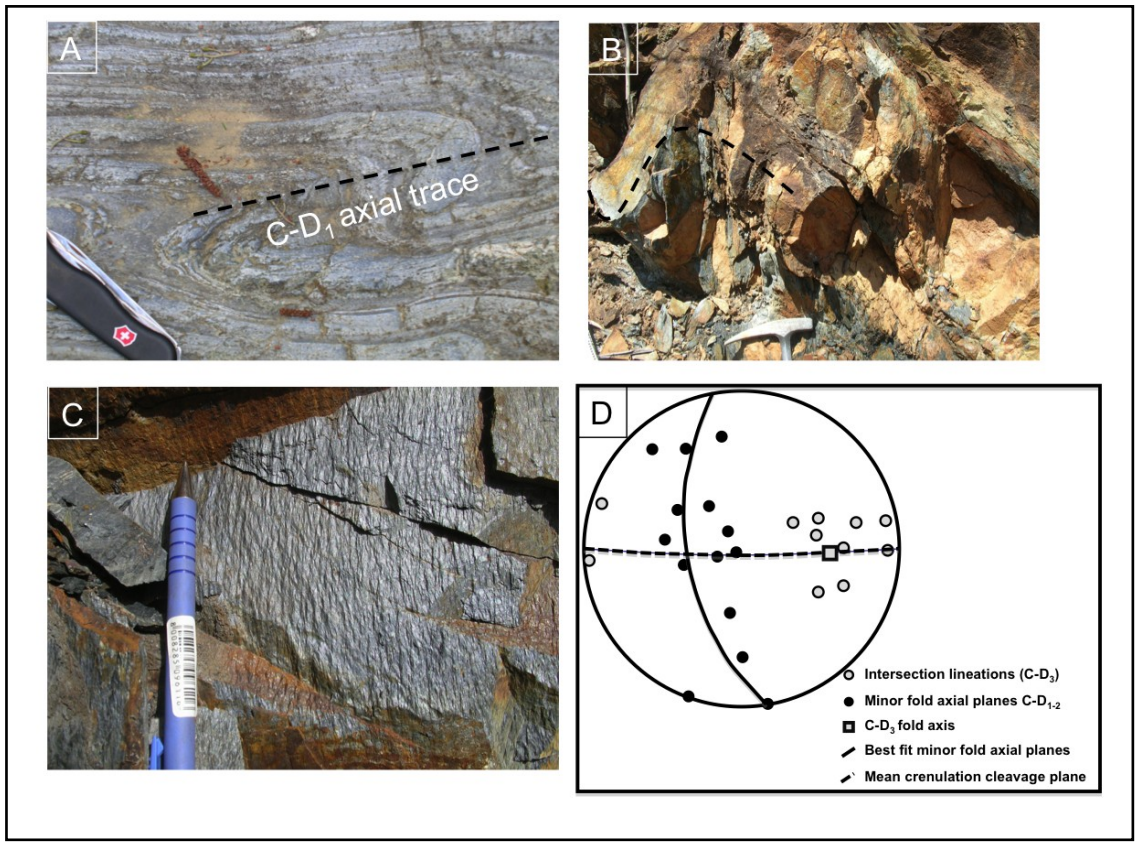

Fig. 2.4 Domain C (A) Minor C–D1folds of quartzwacke bed with sub-vertical hinge (plunging into page). (B) Minor"s"C–D2fold of quartzwacke bed with sub-horizontal hinge(plunging into page). (C) Lineation formed by crenulation of the phyllitic cleavage (C–D2). (D) Equal angle stereoplot domain C fabric elements (C–D3).

2.4.4. Domain D

Observations

Domain D (Fig. 2.5) consists of hectometer-size sigmoidal, phacoidal quartzites and centimeter-to-meter-size rounded quartzite "cobbles" enveloped in a slate/phyllite/quartzite matrix (Fig. 2.5a). The main fabric in the phyllitic matrix is defined by sericite and chlorite. Individual quartzite cobbles are elongate along an east-west trend that is parallel to the phyllitic fabric in the finer grained matrix and to the major lithological contacts. The entire domain forms a regional topographic high. To the west, the domain is dominated by interbedded planar quartzite and phyllite. The thickness (perpendicular to strike) varies considerably along strike and is directly proportional to cobble abundance. The quartzite cobbles are resistant to erosion and the portions of this domain that contain abundant cobbles tend to occupy high elevations. The meter to hectometer size phacoidal quartzite cobbles preserve sedimentary structures such as cross bedding and load casts, and internally contain interbedded pelitic horizons (Fig. 2.5b). Graded bedding in zones of quartzite-rich matrix also occurs where deformation is less intense. Locally the smaller centimeter to meter size rounded cobbles contain an internal folded tectonic fabric (folded fabric=D-D_1) (Fig. 2.5c).

Deformation in the domain is accommodated primarily in the matrix as indicated by a moderately developed stretching lineation (D-L_1) along the main phyllitic foliation that plunges shallowly to the east. An S/C fabric is also locally developed in the matrix

(Fig. 2.5d) and the intersection of the S/C planes is observed to be perpendicular to the stretching lineation ($D\text{-}D_2$). The larger phacoidal quartzites (hectometer size) display only minor internal duplexing and conjugate fault sets, and are internally undeformed. Most of the smaller cobbles, however, show internal sinistral duplexing (Fig. 2.5e) and an overall sigmoid geometry with "tails" displaying predominantly sinistral kinematics when viewed parallel to the stretching lineation.

Interpretation

Although the domain exhibits an asymmetric shear fabric ($D\text{-}D_2$) the presence of (1) isolated rounded quartzite cobbles, (2) preservation of sedimentary structures internal to cobbles, (3) quartzite in the matrix, (4) preserved ($D\text{-}D_1$) fabric in cobbles, suggest the primary formation of the mélange was a sedimentary process and the block-in-matrix fabric is olistostromal. In this case, the $D\text{-}D_1$ fabric may be indicative of sedimentary recycling within the accretionary system (e.g Osozawa et al., 2009) and the tectonic fabric ($D\text{-}D_2$) represents an independent post-emplacement tectonic process imposed on the mélange. The fact that only a small portion of the cobbles show this pre-emplacement tectonic fabric indicates either multiple sedimentary sources, or a uniform source with a partitioned pre-emplacement deformation.

The main fabric in the matrix ($D\text{-}D_2$) wraps these cobbles and the $D\text{-}D_1$ fabric, indicating progressive deformation ($D\text{-}D_2$), as denoted by fabric development and rotation of the quartzite cobbles. Field observations of stretching lineation traces in the

sigmoidal quartzite cobbles (i.e. stretching directions defined by sigmoid tails) indicate that they are oblique sections whose orientation varies depending upon the planar surface on which the measurement is made. This variation indicates that they represent apparent rather than true stretching directions. Using the stereographic method described by Ragan (1985), which incorporates measurement of both the stretching lineation traces and the planar surface on which the lineation was measured, yields a true stretching direction orientation moderately plunging to the east ($D\text{-}L_1$) (Fig. 2.5f). The observed moderate plunge to the east is consistent with an oblique shear sense for $D\text{-}D_2$. This obliquity is also supported by the coexistence of both outcrop-scale ramp thrust faults ($D\text{-}D_2$) and sinistral S/C fabrics ($D\text{-}D_2$).

A stereoplot of the main fabric in the matrix suggests the entire domain is tightly folded about an axis that gently plunges to the east ($D\text{-}D_3$) (Fig. 2.5g). The occurrence of slate in the matrix and the presence of sericite and chlorite suggest a lower greenschist facies metamorphic grade associated with $D\text{-}D_2$ (i.e. visible in the phyllitic foliation).

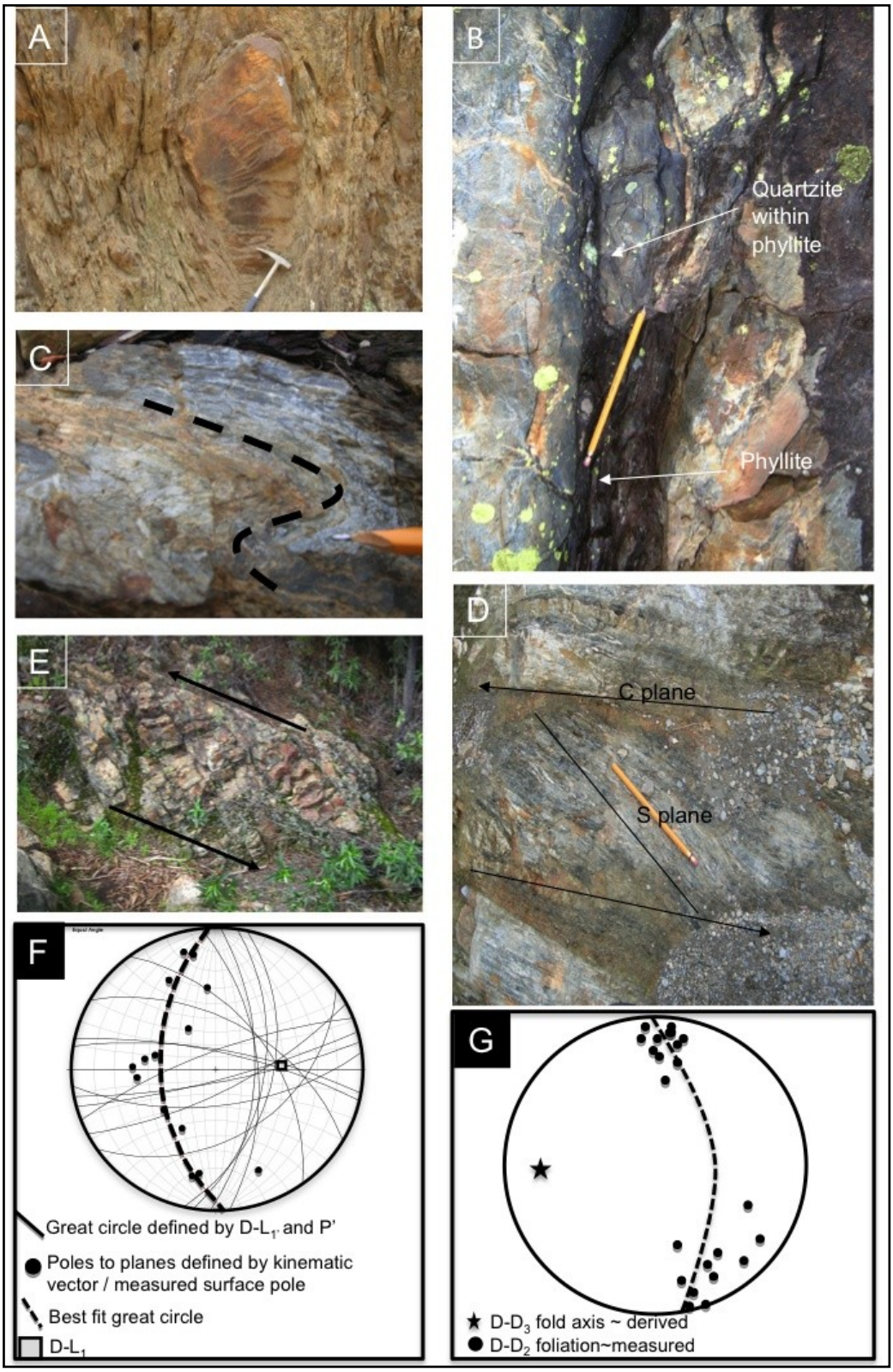

Fig. 2.5 Domain D (A) Quartzite cobble enveloped by a phyllitic matrix. (B) Phyllite

internal to hectometer size quartzite cobble (load cast structure). (C) Quartzite cobble withan internal folded fabric (D–D1). (D) S/C fabric showing sinistral kinematics in phyllitic matrix (D–D2). (E) Cobble with an internal duplex structure showing sinistral kinematics(D–D2). (F) Derivation of true stretching direction D–L1from apparent lineations measurements (D–L1) and exposure planes (P′) (method afterRagan, 1985). (G) Equal anglestereoplot showing rotation of D–D2fabric by (D–D3).

2.4.5. Domain E

Observations

Domain E (Fig. 2.6) is dominated by feldspar-rich greywacke and shale. Grain size in the greywacke varies from coarse to very fine sand and the quartz grains are angular. Bedding is preserved (E-S_0) and crossbeds indicate that the strata throughout the domain are right way up. Repeated fining-upward sequences are recognized from meter- to kilometer-scale. Minor folds (E-D_1) predominantly occur in the coarser grained units, are locally chevron in style and range from centimeter to decameter in wavelength. Open, cuspate, upright folds (Fig. 2.6a, b) also occur in conjunction with chevron geometries. A fracture cleavage is axial planar to these folds and no crenulation cleavage is visible within the shale. Bedding -cleavage intersections (E-L_1) (Fig. 2.6d) are well defined and consistently plunge shallowly to the east or west (Fig. 2.6c). Locally granites and granodiorites of the Sierra Norte Batholith intrude and crosscut E-D_1 structures.

Interpretation

The angular quartz grains and lithic fragments in the greywacke suggest the sedimentary sequence is texturally immature. This immaturity, together with the presence

of simple fold geometries and limited metamorphism, suggests a simple tectonic history compared to domains A-D. Pervasive chevron fold geometries imply (i) E-D_1 occurred at upper crustal levels and (ii) are indicative of a shortening-dominated regime. A stereoplot of a representative minor folds show a simple cylindrical geometry with a near-vertical axial plane and a shallowly plunging fold axis (E-D_1) (Fig. 2.6c).

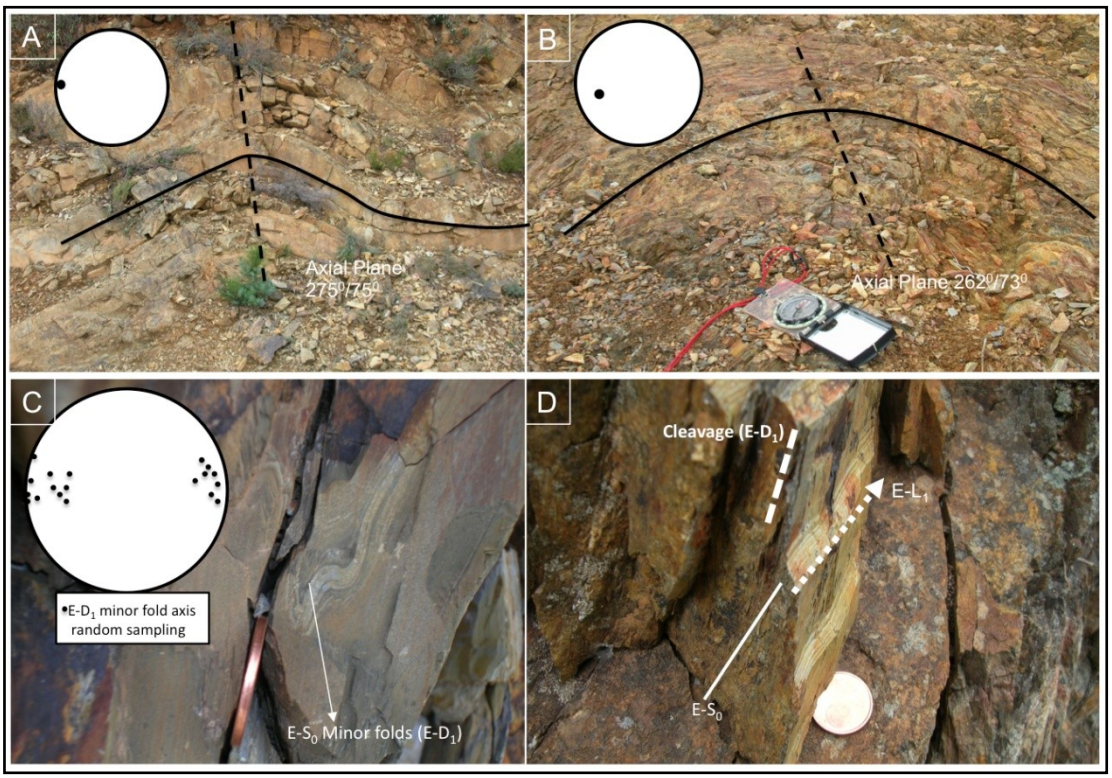

Fig. 2.6 Domain E (A) Open folds of greywacke and (B) shale. Insets: equal angle stereoplot showing orientations of minor fold axes (E–D1). (C) Minor fold of bedding with shallowplunge. Inset = synoptic equal angle stereoplot of fold axes (random sampling). (D) Cleavage / Bedding (E–S0) intersections (E–L1).

2.5. Summary and Synthesis

2.5.1. Structural Relationships Between Domains

Domain A exhibits structures (A-$D_{1, 2, 3}$) consistent with a major sinistral strike-slip component (Figs 2.7a, b). Although the various structures are sequential (i.e. A-D_2 folds A-D_1) their respective orientations are associated with non-coaxial sinistral rotation (Figs. 2.7a, b). Consequently, if their orientations are associated with the same overall bulk strain, A-D_{1-3} deformation can be viewed as progressive. The higher metamorphic grade associated with A-D_1 (upper greenschist) and the brittle-plastic behavior suggests that A-D_1 of domain A exposes deeper structural level than the other domains. The lower metamorphic grades of A-D_{2-4} suggest these phases occurred at higher crustal levels (no recrystallization) suggesting exhumation coeval with progressive deformation. A-D_4, however, is a bulk rotation of all pre-existing fabric elements and is therefore clearly not associated with the same bulk strain conditions and consequently constitutes a later change in bulk strain.

Domain B deformation also records a major non-coaxial bulk strain component (B-D_2) suggesting a possible transient linkage with A-$D_{1,2,3}$ (Figs. 2.7a, b). However, the presence of a pre-existing fabric in mélange blocks and intrafolial folds suggest that a deformation (B-D_1) pre-dated B-D_2 fabric development and metamorphism. Upright conical folds (B-D_3) imply progressive shortening associated with a complex sinistral non-coaxial-non-plane strike-slip regime (Figs. 2.7a, b) (e.g. Jones et al., 2004, 2005) and

the absence of new metamorphic minerals associated with B-D_3 suggests ensuing deformation occurred at higher structural levels. The latest deformation phase (B-D_4) is linked to A-D_4, as its internal structure (i.e. B-D_3) is a bulk rotation about an axis of similar orientation to A-D_4 of domain A.

The multiphase folding patterns in domain C (C-$D_{1, 2}$) suggests bulk strain was shortening dominated (Figs. 2.7a, b) and that overall internal shear component was minimal. The final deformation event (C-D_3) is again consistent with the later deformation in domain A (A-D_4) and domain B (B-D_4) and its internal structures are folded about a similar axis.

Domain D shear fabric development (D-D_2) suggests an overall non-coaxial bulk strain (i.e. S/C fabrics in matrix; conjugate fault sets) (Figs 2.7a,b). Pre-existing D-D_1 fabric in quartzite cobbles suggests tectonic activity prior to emplacement in the mélange and potential cannibalization of the cobbles during their incorporation into the mélange. However, the final deformation (D-D_3) is again similar to A-D_4, B-D_4 and C-D_3, in that its structures are folded about a similar axis.

Taken together these data suggest that (i) although structural styles vary among each domain there are transient linkages between both progressive deformational style within each domain and among the domains (Figs. 2.7a, b) and (ii) the entire package (domains A-D) was rotated about the same axis during the final stages of deformation.

When compared to structural elements in domain E, this axis which internal structures of A-D_{1-3}, B-D_{1-3}, C-D_{1-2}, D-D_{1-2} are rotated about has the same orientation as

measured minor fold hinges and cleavage / bedding intersections (E-D_1), implying a genetic link between the deformation in domain E and the final deformation of domains A-D (Fig. 2.8).

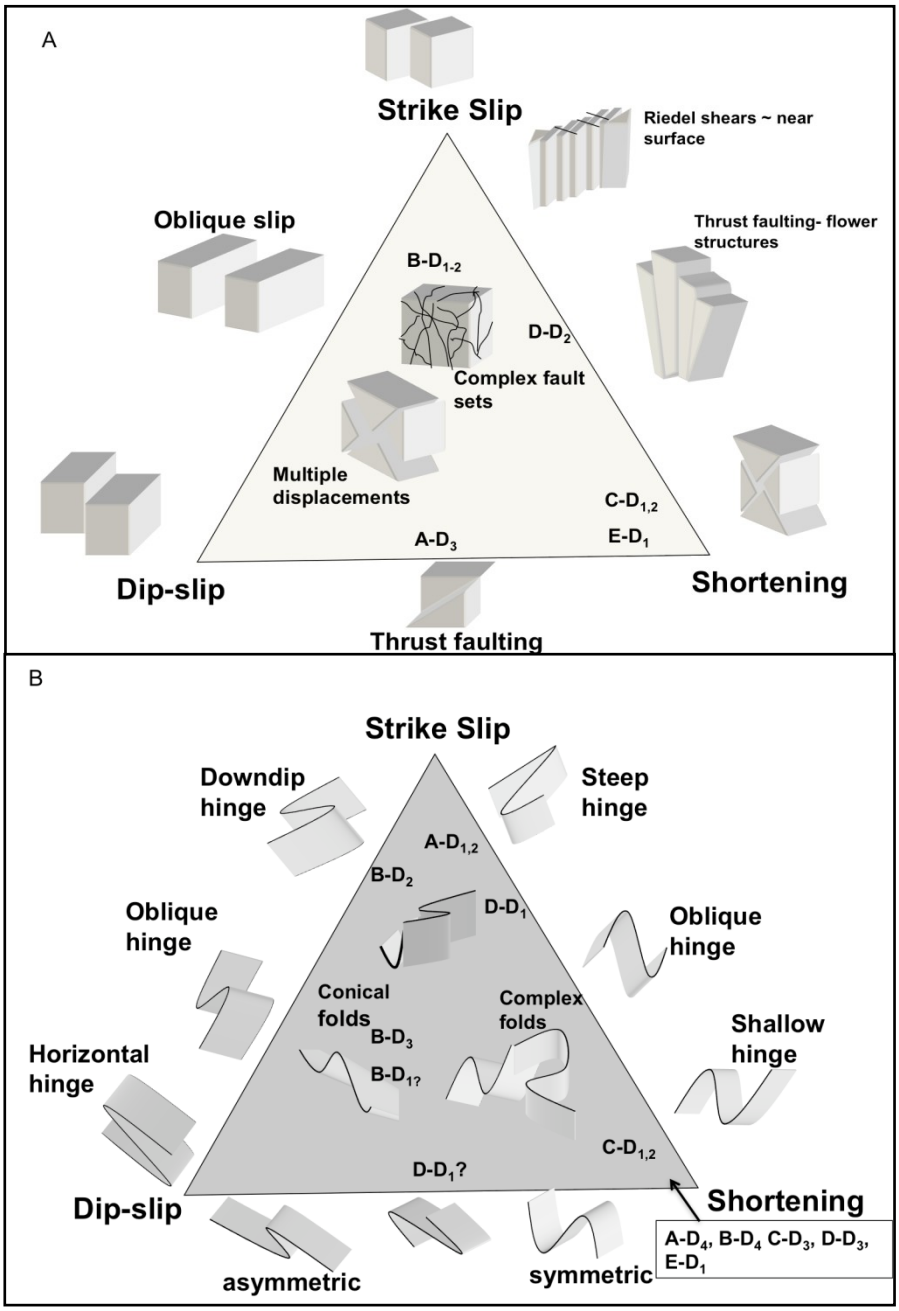

Fig. 2.7 The structures are plotted on a strain triangle in which the apices represent

individual plane strain components and the inside of the triangle represents combinations of thesecomponents to give non-coaxial non-plane strains (Modified fromJones et al., 2005). (A) Brittle structures associated with domain specific deformation, (B) ductile structuresassociated with domain specific deformation.

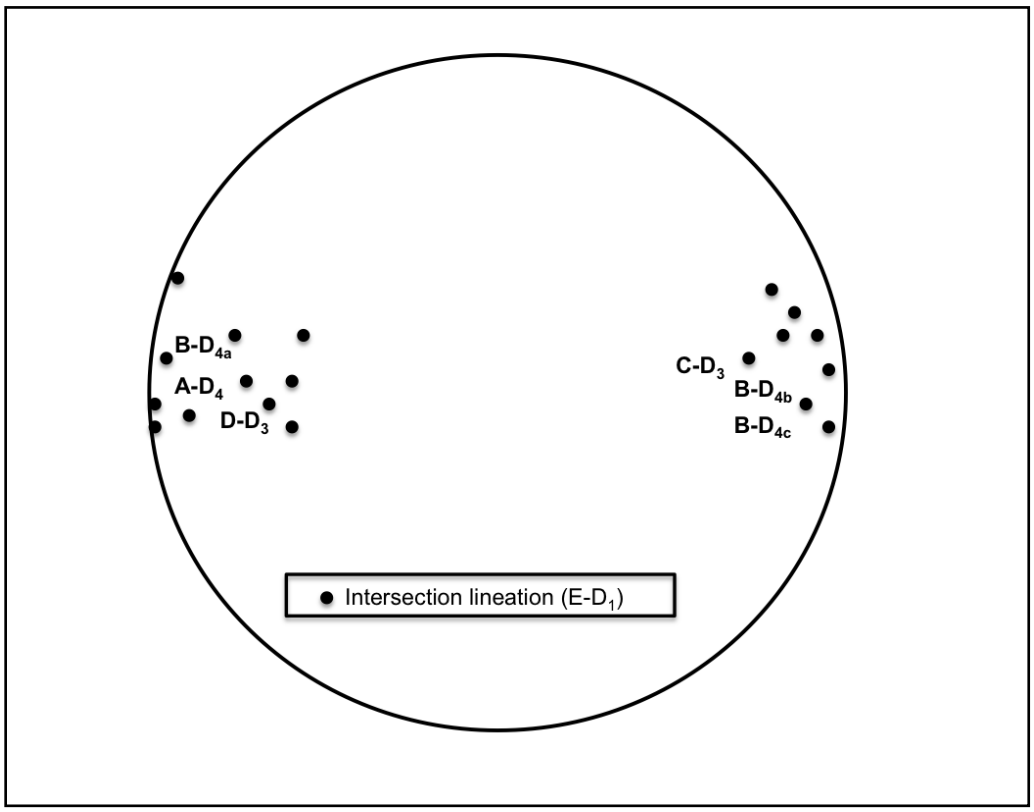

Fig. 2.8 Equal angle stereoplot of E–D1intersection lineations compared with fold axesA–D4, B–D4, C–D3, and D–D3.

2.5.2. Mélange Fabric and Scale

Variscan deformation recorded by domains A-E in the PDLZ shows a complex history characterized by changing regional bulk strain conditions and variations of structural style with scale. These complexities suggest traditional structural interpretation techniques are not applicable in determining the regional tectonostratigraphic history (e.g. Wakabayashi, 2004). On a regional scale, domains (A-D) in the PDLZ are characterized by:

(i) Original stratigraphy not preserved (domains A,B,D)

(ii) Fault-bounded units (domains)

(iii) Various mélange fabrics

(iv) Changing true thickness along strike

Domains B and D display classic characteristics of a mélange (Greenly, 1919). Domain B contains both amphibolite and quartzite blocks in a schistose matrix. Domain D contains phacoidal quartzites of varying sizes (centimeter to hectometer in scale) and rounded quartzite cobbles, which locally preserve internal sedimentary structures. In this case, the domain displays a block-in-matrix aspect characteristic of a sedimentary mélange (olistostrome; Pini, 1999). However, domain D also locally displays some structural order (parallel orientation of phacoidal quartzites and outcrop-scale boudinage), which is characteristic of a tectonic mélange (tectonosome; Pini, 1999). On a map scale, although

the cobbles are aligned in an east-west orientation (parallel to the orogenic grain) individual units are not traceable along strike. As boudins are traceable parallel to the main fabric, the inability to map phacoidal quartzites along strike, suggests the isolation of phacoidal quartzites is not a tectonic process. Furthermore, evidence of deformation (D-D_1) of quartzite cobbles prior to incorporation into the mélange suggests sedimentary recycling within the accretionary system (e.g. Osozawa et al., 2009). As a result, the dominant lithology of this domain is interpreted as a sedimentary olistostromal mélange where cobbles were deformed prior to erosion and emplacement and subsequently deformed and metamorphosed by D-D_2 during continued subduction.

Domain B is marked by highly variable abundances of "blocks" and matrix and boudinaged structures. Boudinaged greenschist blocks contain a pre-emplacement fabric and the inherent higher metamorphic grade than the surrounding matrix is evidence of exposure of deeper crustal levels. There is, however, no definitive evidence to support an olistostromal interpretation. The seemingly random variability in block composition, size and shape and contrast of block and matrix composition (i.e. domain D blocks similar in composition to matrix) and strong pervasive internal deformation along block-matrix contacts suggest a primary tectonic derivation of the mélange fabric.

Alternatively, domains A and C do not contain "blocks" or "cobbles" typical of a tectonic or sedimentary mélange. Although internal deformation is complex (A-$D_{1\text{-}4}$, C-$D_{1\text{-}3}$) and the units are internally untraceable along strike, on a local scale they can be considered coherent (e.g. Wakabayashi, 2003). At regional scales (Fig. 1.5), however,

domains A and C can be viewed as tectonically imbricated with the mélange units of domains B and D (i.e. fault-bounded). At these regional scales bulk strain asymmetry is evidenced in the changing internal deformation for a given domain. As it is now widely accepted that extensive asymmetric shear fabric is a defining characteristic of tectonic mélanges and that all block-in-matrix fabrics should exhibit shear planes (Onishi and Kimura, 1995; Osozawa et al., 2009), together domains (A-D) can be interpreted to as a tectonic mélange at regional scales. In this case each domain records mélange formation during different tectonic and metamorphic conditions during the evolution of the accretionary wedge (i.e. domain D is a sedimentary mélange within a larger scale tectonic mélange).

2.5.3. Regional Tectonic Evolution

Various theoretical models can be applied to describe the deformation and tectonic evolution of the PDLZ (i.e. non-cohesive, cohesive, elastic, plastic and Coulomb wedge) (e.g. Davis et al., 1983; Fletcher, 1989). Coulomb wedge models are widely used in describing the regional shape and overall mechanical behavior of accretionary prisms (e.g. Davis et al., 1983; Schott et al., 2001). In the Coulomb wedge model, the material within the wedge deforms internally until a critical taper (shape for which the wedge is on the verge of failure under horizontal compression) is attained, after which faults continue to grow at constant taper as additional material is incorporated at the toe. Eventually, as friction (related to fault angle, thickness, internal rheology, etc.) along

existing thrust faults increases (assuming constant subduction angle) and as horizontal stresses along the active imbricate surface within an accretionary wedge attain a "critical" limit, a new thrust will develop at the toe, forming a new imbricate system (Koyi et al., 2001).

As the PDLZ is defined by fault-bounded domains, each showing discrete episodes of internal deformation, the Coulomb model is applicable to describing the regional behavior of the system. In the PDLZ, domain A shows evidence of both plastic and brittle deformation of quartz, suggesting deformation (A-$D_{1,2}$) occurred at higher temperatures and pressures than deformation of domains B,C,D and E. If one assumes that domain A constitutes the earliest imbricate wedge (i.e. close to the basal décollement) then subsequent domains were deformed at higher structural levels and Domain A exhumed by continued transcurrent motion. In this case, if classic Coulomb wedge dynamics are applied, each domain records internal deformation before a critical taper is attained. Following the development of a new frontal thrust, a new imbricate slice will form (i.e. domain B) (Fig. 2.9). Structures internal to each domain (e.g. B-D_{1-3}) within the PDLZ (Fig. 2.7a, b), however, suggest that the fault movement was predominantly non-coaxial. As a result, the relative amount of shortening vs. strike-slip shear together with the regional orientation of the stretching lineation and the changing fault angle will dictate the amount of time needed for the fault to reach a critical taper.

In the PDLZ, as all domains show a bulk rotation, coeval with the deformation of domain E (i.e. minor folds rotated by same stress field), a critical taper must have been

attained for each domain prior to E-D_1. Domains A-D locally record earlier strain compartmentalization during internal structural development and each were subsequently overprinted by the deformation seen in domain E. This common internal deformation implies that the steeply dipping faults (which bound each domain within the PDLZ and do not cut the domain E) were not active during the final stages of deformation. Therefore, domain E cannot be considered a new frontal thrust developed in the "bulldozer" Coulomb wedge model but rather implies that domain E was deposited during the final stages of collision unconformably over domains A-D. In this case, the final deformation (E-D_1) could be indicative of the final stages of collision (i.e. OMZ and SPZ are juxtaposed) and the flysch sequence of domain E could potentially be derived from the OMZ, SPZ or domains A-D (Fig. 2.9). In domain E, bedding is internally preserved and the presence of cylindrical, outcrop scale chevron folds and the lack of variation of structures on smaller scales within the domain suggest strain was internally homogeneous. These characteristics imply a discrete change in deformational style between the domain E and domains (A-D) supporting the interpretation that domain E is the youngest unit in the PDLZ (e.g. Giese et al., 1999).

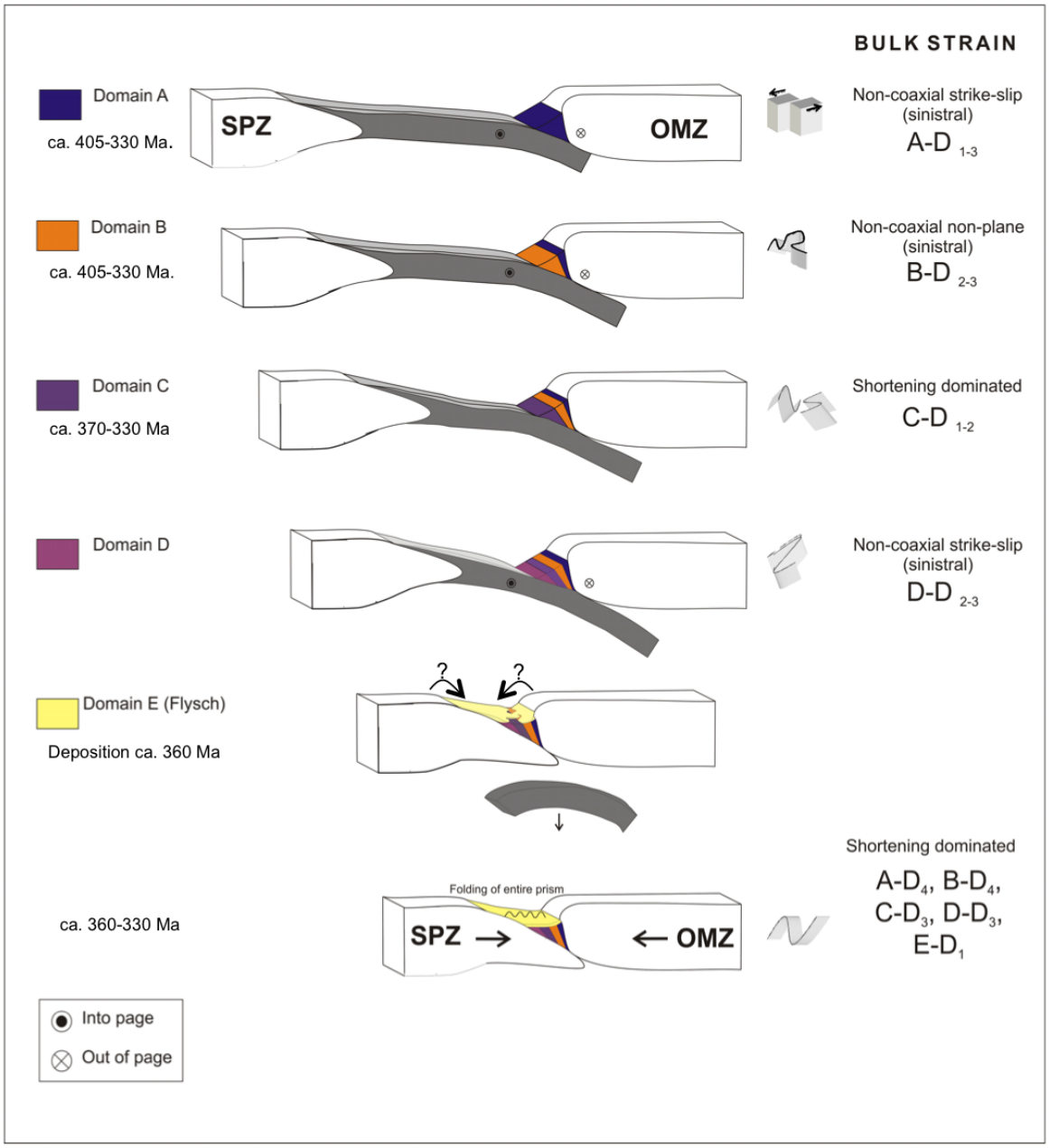

Fig. 2.9 Evolutionary model for the Pulo do Lobo Accretionary complex assuming north directed subduction: (1) non-coaxial strike–slip bulk strain (deformation domain A);(2) Non-coaxial non-plane bulk strain (deformation domain B); (3) Bulk shortening (deformation Domain C); (4) Non-coaxial strike–slip bulk strain (Domain D); (5)"locking"of regional faults, deposition of domain E, Deformation of domain E and rotation of domains A–D.

2.5.4. Constraints on the Timing of Deformation

The age of the deformation events are only broadly constrained, and a detailed U-Pb geochronological investigation is in progress. The best constraint on the age of deformation is in domain E, and is bracketed between ca. 360 (the depositional age of the Santa Iria flysch) and 330 Ma (the intrusive age of the Gil Márquez pluton). The plutons locally crosscuts domain E, however, as the plutonic rocks are locally foliated, they may by synkinematic to deformation of domain E.

On a regional scale domains A-D are interpreted as a tectonic mélange and consequently their internal age relationships are difficult to determine. However, in domain C, fabrics C-$D_{1,}$ and C-D_3 are crosscut by the Gil Márquez granodiorite suggesting internal deformation in this domain occurred prior to ca. 330 Ma. The Gil Márquez granodiorite is assumed partly coeval with the granites which intrude domain E, thus suggesting that at least a part of these plutons (Sierra Norte Batholith) intruded the PDLZ following deposition of domain E and bulk rotation of domains (A-D).

The internal deformational events in domains A-D must pre-date the regional E-D_1 deformation, which involved bulk rotation of all domains, and is younger than the Devonian age of their respective protoliths. For example, the Frasnian depositional age for the Ribeira de Limas Formation (Oliveira et al., 1986; Giese et al., 1988) constrains the internal deformation of domain C to ca. 370-330 Ma. The Early Devonian age for the Pulo do Lobo Formation (Onézime et al., 2003), constrains the deformation in domain A between ca. 405-330 Ma.

If the BAO represents a vestige ocean lithosphere deformed during accretion to the Gondwanan margin (e.g. Crespo-blanc and Orozco, 1988; Diaz-Apiroz et al., 2005), then the ca. 334 ± 2 Ma (protolith) age (Azor et al., 2008) of the ophiolite would constrain the internal deformation of the PDLZ accretionary prism to between 334-330 Ma. On the other hand, if the BAO was generated in a post-collisional setting, then the BAO age does not constrain deformation in the accretionary prism. The strong mylonitic foliation in domain A (D-A_1) suggests a possible genetic link with deformation of the adjacent BAO and South Iberian Shear Zone (SISZ, Crespo-Blanc and Orozco, 1988). The recent 334 ± 2 Ma age for the BAO protolith implies that if D-A_{1-3} were coeval with development of the SISZ then deformation in domain A should be coeval or post ca. 334 Ma. However, domains A-D were rotated coeval with deformation in domain E (Fig. 2.8) suggesting internal deformation in these domains must have occurred prior to the Late Fammenian. Consequently, internal deformation of domains A-D cannot be genetically related to the deformation in the SISZ as it is today, though nothing precludes such a relationship during initial, presently exhumed, parts of this important shear zone. This apparent lack of association of deformation between the PDLZ and SISZ supports the internal compartmentalization regional strain within lithotectonic domains and further suggests that later deformation in the SISZ (post-330 Ma.) was also internally localized within the shear zone (i.e. PDLZ kinematically isolated from bulk strain). This apparent isolation may be a result of late Variscan re-activation of regional-scale faults within the

PDLZ allowing for localized deformation of the BAO-domain A contact and may also be responsible for localized fabrics within the granites and granodiorites.

Field and paleontological data therefore support the hypothesis that the PDLZ deformation and accretion was associated with an extremely diachronous (as is typical of largely oblique convergent processes) Late Devonian-Early Carboniferous oblique (sinistral) subduction/collisional event, propagating from NW to SE, (e.g. Quesada et al., 1994, 2006). This oblique subduction/collision event (Variscan orogeny) may have been punctuated in time and/or space (e.g. at releasing bends along the suture zone) by localized transtensional events eventually leading to marginal oceanic basin opening (formation of BAO at Ca. 334 Ma) or massive emplacement of late plutonic rocks (Sierra Norte Batholith). In this case, the deformation of the entire package (domains A through E of the PDLZ) (Fig. 2.9, stage 5) would have taken place before the formation of the BAO. Subsequent inversion of the BAO and the SISZ would be responsible for internal deformation/exhumation of the former and the present geometric arrangement of lithotectonic units.

2.6. Conclusions

Previous studies have interpreted the PDLZ in the type area as affected by three distinct phases of deformation (e.g. Silva et al., 1990; Giese et al., 1994; Giese et al., 1997). Although our findings show evidence of polyphase deformation, field evidence suggests that strain compatibility is highly scale dependent. Although deformation across

the entire map area is highly heterogeneous, homogeneity is generally achieved within each tectonostratigraphic domain. Also, although observed structures on a local scale (microscopic, outcrop, etc.) may conflict with the overall kinematics of the given domain, a large sampling of structural data shows general consistency of structural style, where both brittle and ductile deformation show a combination of dip-slip, strike-slip, oblique slip, or shortening (Fig. 2.7a, b).

The variation in structural style from each domain in the map area suggests that bulk strain orientations on a regional scale changed during progressive deformation, which directly influenced the spatial extent of observed structures in the field. This variation suggests that the kinematics associated with regional-scale faults, which border each domain, directly controlled the style of internal deformation (Fig. 2.8). The Late Fammenian SIF is generally considered to show only one deformation phase. Our findings are consistent with this conclusion; however, we suggest this deformation affected not only the SIF but was recorded internally by all units within the PDLZ, where earlier deformation was only locally developed. By implication, it can be hypothesized that during the waning stages of continent-continent collision and accretionary wedge development, energy-release mechanisms along internal structural breaks became less efficient, causing a shift in boundary conditions to a higher scale level. This shift would subsequently result in a "locking" of bounding faults and the distribution of strain across larger scales. Recognition of these systems (where strain is homogenous on higher scales)

across assumed coeval accretionary systems may help to improve our understanding of the Variscan Orogenic belt.

2.7 Acknowledgements

JAB thanks Nick Culshaw and Rebecca Jamieson for discussions related to the project as advisors on JAB thesis committee. The support of theNatural Sciences and Engineering Research Council, Canada throughthe PGS-D grant to JAB and Discovery and Research Capacity grants toJBM. JAB also acknowledges the support of the Dalhousie Killampredoctoral scholarship program. St. Francis Xavier University Councilfor Research grants to JBM. We are grateful to Stephen Johnston and ananonymous reviewer for their very insightful and constructive reviewsand to Rafael López-Guijarro for help withfieldwork and discussions.

CHAPTER 3

EXCISION OF A CRUSTAL FRAGMENT DURING THE CLOSURE OF THE RHEIC OCEAN: U-PB DETRITAL ZIRCON DATA FROM THE LATE PALAEOZOIC PULO DO LOBO AND SOUTH PORTUGUESE ZONES, SOUTHERN IBERIA

3.1 Abstract

The Pulo do Lobo Zone (PDLZ), which crops out immediately north of the allochthonous South Portuguese Zone (SPZ) in southern Iberia, is classically interpreted as a polydeformed accretionary complex developed along the southern margin of the Gondwanan para-autochthon (Ossa Morena Zone, OMZ), during the late Palaeozoic closure of the Rheic Ocean. This closure was a major event during the amalgamation of Pangea. U/Pb laser ablation inductively coupled mass spectrometry dating of detrital zircons from late Palaeozoic Devonian-Carboniferous clastic units in the SPZ and PDLZ yield contrasting age populations and attest to the exotic nature of both zones. Detrital zircons from the SPZ display populations typical of detritus derived from either Gondwana (OMZ), or peri-Gondwanan terranes. In contrast, rocks from the PDLZ contain populations consistent with derivation from Baltica, Laurentia or recycled Early Silurian deposits along the Laurentian margin. An example of one such deposit is the Southern Uplands terrane of the British Caledonides. Taken together, these data can be

reconciled by a model involving tectonic transport of a crustal fragment that was laterally equivalent to the Southern Uplands terrane between the allochthonous SPZ and Gondwana as a result of an Early Devonian collision between an Iberian indenter with Laurussia.

3.2 Introduction

The geology of the middle to late Palaeozoic era was dominated by the amalgamation of the supercontinent Pangea, which produced orogens in eastern North America and Western Europe that lay within Pangea's interior (Murphy and Nance, 2008; Cawood and Buchan, 2007). The Appalachian-Caledonide-Variscan orogens were produced by (i) the Ordovician-Silurian accretion of peri-Gondwanan terranes (e.g. Ganderia, Avalonia, Meguma) to Laurentia, which resulted in closure of the Iapetus Ocean, followed by (ii) the Carboniferous closure of the Rheic $\pm$ Palaeotethys oceans and ensuing terminal collision between Gondwana and Laurussia (e.g. van Staal et al., 1998, 2009; Stamfli and Borel, 2002) (Fig. 3.1). The former continuity of these belts was sundered in the Early Mesozoic by the opening of the Atlantic Ocean. As a result, many of the suture zones, particularly those that formed by consumption of the Rheic Ocean during Pangea amalgamation, were either destroyed or are hidden beneath the Atlantic continental shelves.

In Southern Iberia, the Pulo do Lobo Zone (PDLZ) has been interpreted as a rare exposure of part of a suture zone that records the final stages of the closure of the Rheic Ocean and the terminal collision between Gondwana and Laurussia (e.g. Eden, 1991; Onézime et al., 2003). The PDLZ is an Early to Middle Devonian polydeformed tectonic mélange of oceanic metasediments and olistostromal phacoidal quartzites unconformably overlain by a simply deformed Visean flysch sequence (Eden, 1991; Giese et al., 1999; Braid et al., 2010). Together with (i) adjacent portions of the Ossa Morena Zone (OMZ) to the north, (ii) a sequence of dismembered mafic rocks with ophiolitic affinities (Beja Acebuches Ophiolite) and (iii) the South Portuguese Zone (SPZ) to the south, these rocks are generally thought to preserve a segment of the Pangean suture (e.g. Quesada et al., 1994; Onézime et al., 2003) (Fig. 3.2)

Fig. 3.1 Schematic late-Devonian palaeocontinental reconstruction (modified from Woodcock et al., 2007) assuming a unified Iberia and Armorica with Gondwana. White star shows approximate location of the Southern Uplands terrane of the British Caledonides and black rectangle the approximate location of figure 3.2.

In this scenario, the OMZ, which has Palaeozoic Gondwanan faunal affinities (Robardet, 2003), represents the Gondwanan parautochthon and the SPZ is underlain by exotic basement of unknown origin (Quesada et al., 1994; Onézime et al., 2003; Pous et al., 2004). Based on palaeogeographic reconstructions (e.g. Scotese, 2003; McKerrow and Scotese, 1990), it has been suggested that the SPZ basement can be correlated with extensions of either Avalonia (e.g. Simancas et al., 2005; Leistel et al., 1998) or the Meguma terrane (e.g. Martínez Catalán et al., 1997; de la Rosa et al., 2001). Avalonia and Meguma are among several terranes collectively known as peri-Gondwanan, that originated along the northern Gondwanan margin in the Neoproterozoic but lay along the

southern flank of Laurussia by the middle Devonian as a result of the closure of the Iapetus Ocean (Van Staal et al., 1998, 2009; Murphy and Nance, 2002) (Fig. 3.1). Despite these correlations there is considerable debate surrounding the late Palaeozoic palaeogeographic history of the SPZ and the relationship of the SPZ to Gondwana and peri-Gondwanan terranes, which flanked the Rheic Ocean during its consumption.

In order to further investigate the processes associated with the formation and evolution of this putative Pangean suture zone, we sampled the clastic metasedimentary rocks and phacoidal quartzites in the PDLZ and the Late Devonian metasedimentary rocks in the SPZ and present laser ablation inductively coupled plasma mass spectrometry (LA-ICPMS) U/Pb analyses of detrital zircons from these samples. Our data provide new insights into the timing of collision between Gondwana and Laurussia and demonstrate that the PDLZ mélange and metasedimentary rocks are not simply derived from the flanking Laurussian or Gondwanan margins. To account for the detrital zircon populations in the PDLZ we propose derivation from a crustal fragment, which escaped laterally as the result of an Early Devonian collision between an Iberian indenter (Gondwana) with Laurussia. Our model not only provides a method for emplacement of the PDLZ but also potentially explains genetic linkages between enigmatic voluminous magmatism and widespread mineralization in both the Meguma terrane of the northern Appalachians and the Iberian Pyrite Belt of the SPZ not accounted for in other models.

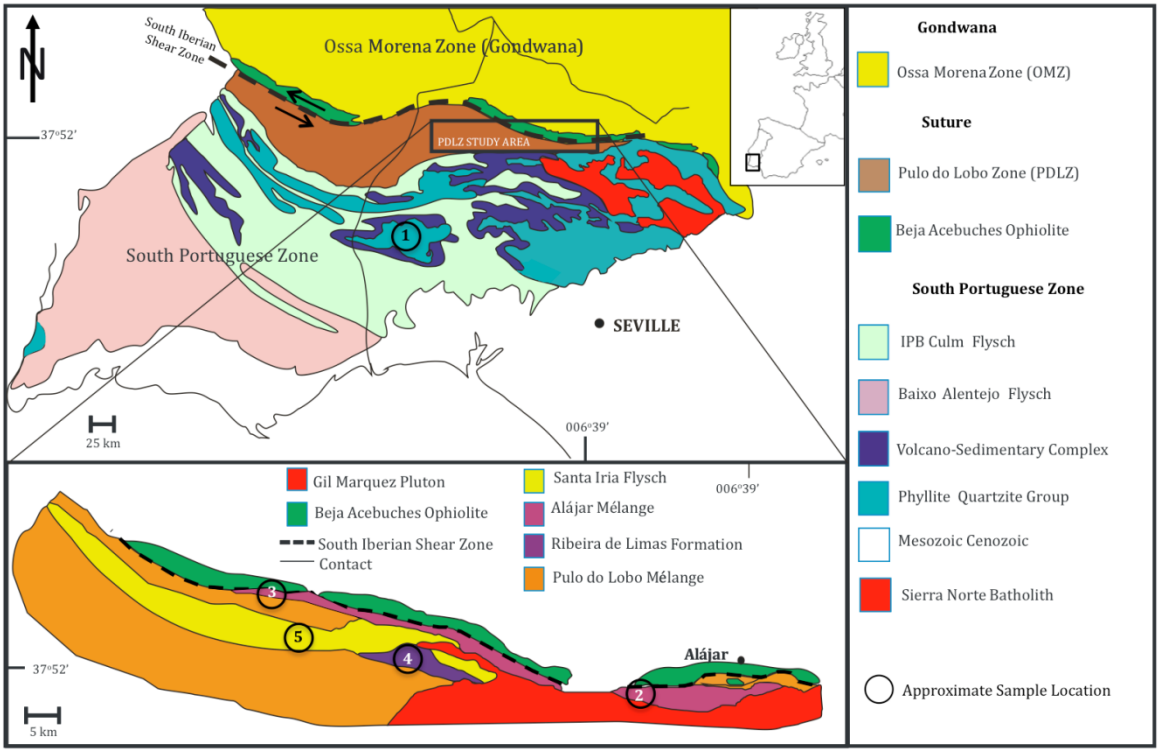

Fig. 3.2 Variscan tectonic terranes of Southern Iberia showing suspect suture zone (PDLZ) between the South Portuguese Zone (Laurussia?) and the Ossa Morena Zone (Gondwana) (sample locations in PDLZ inset) (adapted fromOnézime et al., 2003). Sample locations numbered: **(1)** Quartzite (sample JB-17) from the Phyllite Quartzite Group, Virgen de la Peña nappe (N37°36.153 W007°12.223); **(2)** Alájar Mélange along Rivera de Santa Ana, phacoidal quartzite (sample RSA-01) (N37°51.429 W006°42.013) and quartzite matrix (sample RSA-02) (N37°51.202 W006°41.817); **(3)** Alájar Mélange phacoidal quartzite (sample JB-43) (N 37°53.954 W 006°56.013); **(4)** Ribeira de Limas formation along Rivera de Acebuches (sample AC-03) (N37°52.049 W006°49.044); **(5)** Santa Iria Flysch greywacke (sample JAB-08) (N37°52.310 W006°51.642).

3.3. Geology and Tectonic Framework

3.3.1. South Portuguese Zone

The oldest exposed units in the SPZ are Late Devonian continental shelf strata of the Phyllite Quartzite Group. The Phyllite Quartzite Group is composed of siliciclastic

rocks deposited in a subtidal environment from fan delta and sand bar systems on a shallow marine continental platform (Moreno and Sáez, 1990; Oliveira, 1990; Moreno et al., 1996). The base of this unit is not exposed and has a minimum thickness of 300–400 m (Soriano and Martí, 1999). Its depositional age is constrained by the presence of Fammenian conodonts in limestone lenses interbedded with the clastic strata (Boogaard and Schermerhorn, 1980; 1981). The Phyllite Quartzite Group is conformably overlain by the Late Famennian - Late Visean (Oliveira, 1990) bimodal volcanic and sedimentary successions of the Volcano-Sedimentary Complex deposited in a transtensional basin (Schermerhorn, 1971; Rosa et al., 2009). The Volcano-Sedimentary Complex is in turn overlain by a Late Visean to the Serpukhovianturbiditic flysch group, (Schermerhorn,1971; Oliveira,1990) (Fig. 3.2).

3.3.2. Pulo do Lobo Zone

The PDLZ is classically interpreted as an accretionary prism formed during the closure of the Rheic Ocean (e.g. Eden, 1991) and is comprised of four polydeformed fault-bounded lithotectonic units: (i) the quartz-mica schists and local quartzite mélange of the Pulo do Lobo formation, (ii) a sequence of quartzwackes and phyllites of the Ribeira de Limas formation, (iii) hectometre to metre-scale internally deformed olistostromal quartzites in a polydeformed phyllite/quartzite matrix of the Alájar mélange (Eden, 1991) and (iv) tectonically emplaced mafic blocks in a volcaniclastic matrix (Peramora Mélange) (Eden, 1991). Together these polydeformed units are

unconformably overlain by the relatively simply- deformed (Giese et al., 1999) greywackes and shales of the Santa Iria Flysch, interpreted to have been deposited during terminal collision between Gondwana and Laurussia (e.g. Braid et al., 2010). Locally, these flysch deposits are crosscut by the ca. 330 Ma Gil Márquez pluton, which is part of the voluminous ca. 350-300 Ma Sierra Norte Batholith (de la Rosa, 1992). The protolith ages of the PDLZ are constrained by Givetian-Frasnian palynomorphs (Ribeira de Limas formation) andLate Devonian-Early Carboniferous spores and acritarchs in the flysch deposits (Santa Iria Flysch) (Giese et al., 1988;Lake et al., 1988).

To the north of the PDLZ, a sequence of dismembered mafic rocks, known as the Beja Acebuches Ophiolite (ca. 330-345 Ma) (U/Pb Shrimp; Azor et al., 2009), delineates the boundary between the PDLZ an the OMZ. The genesis of the Beja Acebuches Ophiolite remains controversial and is thought to represent either (i) obducted primary Rheic oceanic lithosphere (e.g. Castro et al., 1996) or (ii) mafic rocks formed during a transtensional event following the maincontinent–continent collision (ca. 345–390 Ma) (Quesada et al., 1994; Azor et al., 2008; Braid et al., 2010.)

3.3.3. Tectonic Evolution

In the late Paleozoic, regional Late Devonian to Early Carboniferous south–southeasterly propagating (e.g. Quesada, 1998) deformation in the SPZ occurred as a result of northward-directed oblique (sinistral)subduction of the Rheic Ocean lithosphere beneath the OMZ (Gondwana) (Crespo Blanc and Orozco, 1988; Quesada, 1998).

Subsequently, this subduction would have led to the eventual collision of the continental margin of the SPZ (which may have been part of Avalonia or Meguma, e.g. Leistel et al., 1998; de la Rosa et al., 2001),with the OMZ. In this scenario, oblique sinistral convergence resulted in the development of an accretionary prism (PDLZ) and is evidenced by widespread ca. 355-300 Ma calc-alkaline andesitic magmatic arcin the OMZ (Jesus et al., 2007).

The PDLZ also preserves evidence of this pervasive Late Devonian regional sinistral shear, compartmentalized within Pulo do Lobo formation, the Ribeira de Limas formation and the Alájar Mélange (Braid et al., 2010). Furthermore, the Beja Acebuches Ophiolite is deformed along a sinistral orogen-scale shear zone localized along the boundary with the PDLZ (South Iberian Shear Zone; Crespo-Blanc and Orozco, 1988) (Fig. 3.2).

3.4. Sample Selection and Methodology

To investigate the development of this putative suture zone, six samples were collected for detrital zircons from Devonian to Early Carboniferous units of the PDLZ and SPZ (Fig. 3.2). We analysed (i) one sample from the Late Devonian passive margin quartzites (Phyllite Quartzite Group) from the SPZ to test the provenance of the SPZ and its relationship to the PDLZ and (ii) two samples of phacoidal quartzites and one sample of matrix from the mélange deposits (Alájar Mélange) and one sample of quartzwacke

(Ribeira de Limas formation) from the PDLZ (suture zone). The samples from the PDLZ test the provenance of the PDLZ and potential changes in sediment provenance in different lithotectonic units within the suture zone. We also analysed (iii) a sample of greywacke from the overlying Late Devonian Early Carboniferous flysch (Santa Iria Flysch) from the PDLZ to investigate the potential changes in sediment provenance with proposed changes in tectonic environment.

Approximately sixty-five zircon grains from each sample were mounted, polished, imaged by electron back-scatter, and analysed for their U and Pb isotopic composition (one analysis per zircon grain) using an Thermo Element 2 high resolution Inductively Coupled Plasma-Mass Spectrometer coupled to a New Wave Research 213 nm Nd-YAG laser. Detailed description of analytical instrumentation, analytical protocol and methodology, data reduction and age calculation at the Pacific Centre for Isotopic and Geochemical Research (PCIGR) at the University of British Columbia are described in Mortensen et al. (1995, 2007). All zircons were analysed using line scans with a laser spot diameter of 20 μm. Data were reduced using theprogram GEMOC Glitter and plots generated using Isoplot (Ludwig 1999). Age uncertainties are reported at 2σ and either the Pb^{207}/Pb^{206} or the Pb^{206}/U^{238} age is reported depending on which value gives the lower uncertainty. Of the six samples (~65 analyses per sample) only eight analyses revealed >10% discordance and were discarded. Probability distribution plots for all remaining concordant grains are shown in Figure 3.3.U-Pb concordia diagrams and full tables of results can be found in *appendix B*.

3.5. Results

3.5.1. South Portuguese Zone

A sample of quartzite (JB-17) was selected from the Late Devonian continental shelf deposits (Phyllite Quartzite Group), which are considered the oldest exposed unit in the SPZ proper. Of the sixty concordant analyses, only four grains (~7%) are Mesoproterozoic. The bulk of the sample (~52%) is dominated by Neoproterozoic (ca. 0.5-0.7 Ga) zircons, with a strong peak at ca. 590 Ma. The remainder of the detritus (~35%) is dominated by (ca. 1.8-2.3 Ga) Palaeoproterozoic zircons with only four grains (<7%) yielding Archean ages (Figs. 3.3, B.7) (Table B.3).

3.5.2. Pulo Do Lobo Zone

Both the phacoidal quartzites (RSA-01, JAB-43) and quartzite matrix (RSA-02) from the Alájar mélange in the suture zone have similar detrital zircon age distributions (Figs. B.7, B.8, B.9) (Tables B.2, B.4, B.5), but display a very different distribution than the JB-17 sample from the SPZ. For each of the three samples (i) the largest population is Mesoproterozoic (ca. 1.0-1.5 Ga) comprising approximately (55-70%) of zircons analysed, (ii) a significant population (15-25%) is Palaeoproterozoic (ca. 1.6-1.9 Ga) but younger on average than the Palaeoproterozoic population in the JB-17 sample from the SPZ and (iii) small populations (< 10%) of Archean (ca. 2.5-3.0 Ga) and ca. 440 Ma Early Silurian zircons (<5%) occur (Fig. 3.3). A concordant grain (JB-43) at 438.7± 4.38

Ma provides a maximum depositional age for the phacoidal protolith. SEM backscatter images of these ca. 440 Ma zircons reveal a zoned, euhedral, multifaceted zircon morphology, whereas older populations are generally well-rounded (Fig. 3.5).

The quartzwacke (Ribeira de Limas formation) sample from the PDLZ (AC-03) lacks ca. 440 Ma zircons but otherwise displays a similar detrital zircon age distribution (Fig. 3.3). The dominant population (~55%) is Mesoproterozoic (ca. 1.0-1.5 Ga) in age. A second large population (~35%) is late Palaeoproterozoic (ca. 1.6-1.9 Ga), and one zircon is early Palaeoproterozoic (2447.6 ±10.2 Ma) in age. The remainder of the detrital zircons are Archean (~10%) in age. The youngest concordant zircon in the sample is 947.6 ± 4.3.

3.5.3. Flysch

A sample of Greywacke (JAB-08) from the flysch (Santa Iria Flysch), which unconformably overlies the mélange phacoids and matrix (Alájar Mélange) and quartzwacke (Ribeira de Limas formation) in the PDLZ, displays the widest range of detrital zircon ages and contains the most Devonian-Carboniferous detritus (~32%) of all samples, with a strong peak at ca. 347 Ma. The sample also displays a variety of Proterozoic populations (~ 30% Neoproterozoic, ~12% Mesoproterozoic and 21% Palaeoproterozoic) with only minor (<5%) Archean detritus (Fig. 3.3). An elongate, multifaceted and zoned concordant grain at 347.2 ± 5.5 Ma provides a maximum depositional age.

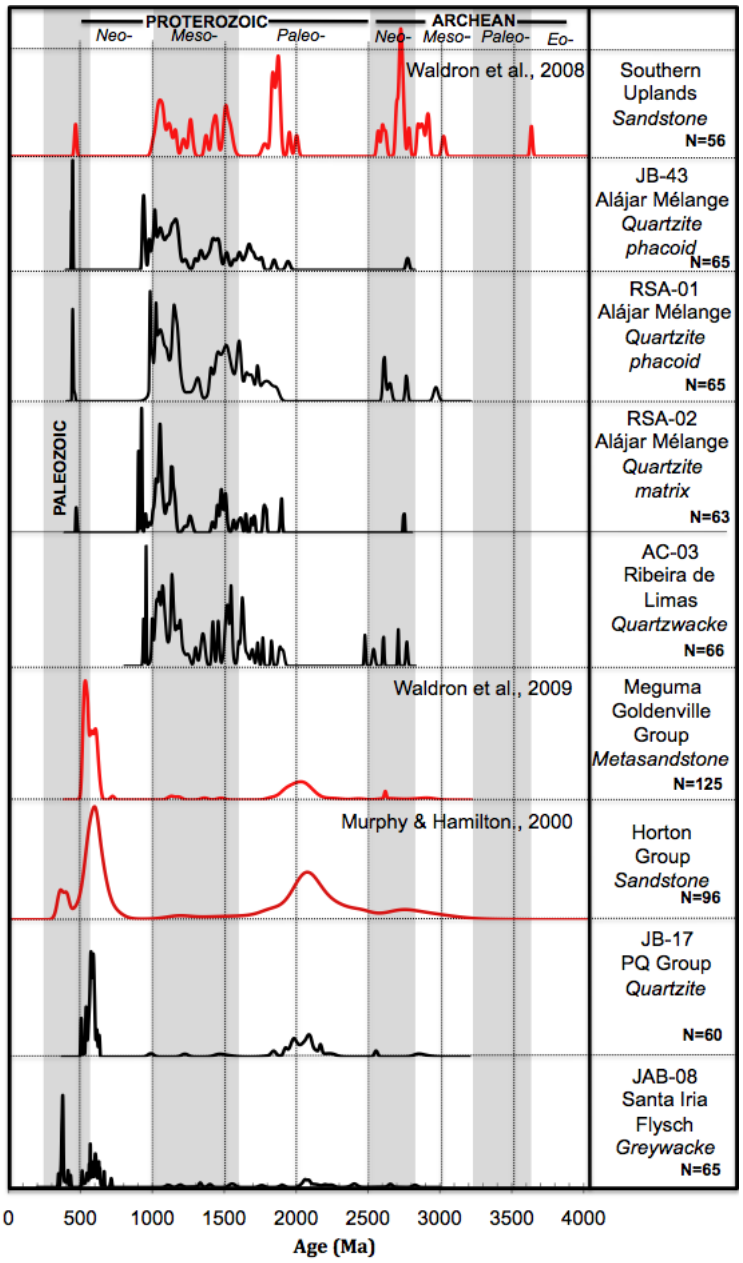

Fig. 3.3 U-Pb detrital zircon relative probability distribution plots for samples from the PDLZ (suture) and the SPZ (Laurussia?) from this study compared with samples (highlighted in red) from Early Silurian Kirkcolm Formation of the Southern Uplands terrane of the British Caledonides (after Waldron et al., 2008), the Cambrian-Ordovician Meguma terrane from the northern Appalachians (after Waldron et al., 2009) and the Devonian-Carboniferous Horton Group from the St. Mary's Basin of the northern Appalachians (after Murphy and Hamilton., 2000) (in red). Plots were generated by ISOPLOT (Ludwig, 2003).

3.6. Tectonic Significance

3.6.1. Origins of the Pulo do Lobo and South Portuguese Zones

A comparison between U/Pb detrital zircon ages in the samples and the ages of detrital zircon populations and tectonothermal events in potential source areas are shown in Figure 3.4. The dominant Neoproterozoic (ca. 0.5-0.7 Ga) and Palaeoproterozoic (ca. 2.0-2.5 Ga) zircon populations in the continental clastic rocks (Phyllite Quartzite Group) of the SPZ are typical of derivation from either West Africa (e.g. Rocci et al., 1991), or the peri-Gondwanan Meguma terrane which is the only known location in Laurussia with such detrital zircon populations (Krogh and Keppie, 1990; Murphy et al., 2004; Waldron et al., 2009) (Fig. 3.4). However, the presence of minor Mesoproterozoic zircons in the Phyllite Quartzite Group sample are not typical of derivation from West Africa but are present in peri-Gondwanan Avalonia and Meguma. Mesoproterozoic zircons (ca. 1.0 Ga) are common in Avalonia but rare in Meguma. As a consequence the Meguma terrane is a more likely candidate for the source of the PQ group detrital zircon distribution.

In contrast, the dominant Mesoproterozoic (ca. 1.0-1.5 Ga) and late Palaeoproterozoic populations (ca. 1.6-1.9 Ga) in the phacoidal quartzites and matrix (Alájar mélange) and from the quartzwacke (Ribeira de Limas formation) in the PDLZ are typical of both Laurentia and Baltica (Laurussia) (e.g. Cawood et al., 2007). The PDLZ samples also lack Neoproterozoic and early Palaeoproterozoic zircon populations, which are typically abundant in Neoproterozoic through Devonian units derived from

Gondwana (e.g. Martínez Catalán et al., 2004; Fernández Suárez et al., 2002a, 2002b; Gutiérrez-Alonso et al., 2007; López-Guijarro et al., 2007) and from peri-Gondwanan terranes (i.e. Meguma, Avalonia) (e.g. Murphy and Hamilton, 2000; Murphy et al., 2004; Fyffe et al., 2009) but typically absent in clastic rocks derived from both Laurentia and Baltica (Fig. 3.4). Consequently, the age distributions of these samples suggest that the detritus in the PDLZ was neither derived from Gondwana (OMZ), nor from the sources of the Late Devonian clastic rocks (Phyllite Quartzite Group) of the SPZ or peri-Gondwanan terranes which flanked the margin of Laurentia and Baltica in the Devonian-Carboniferous.

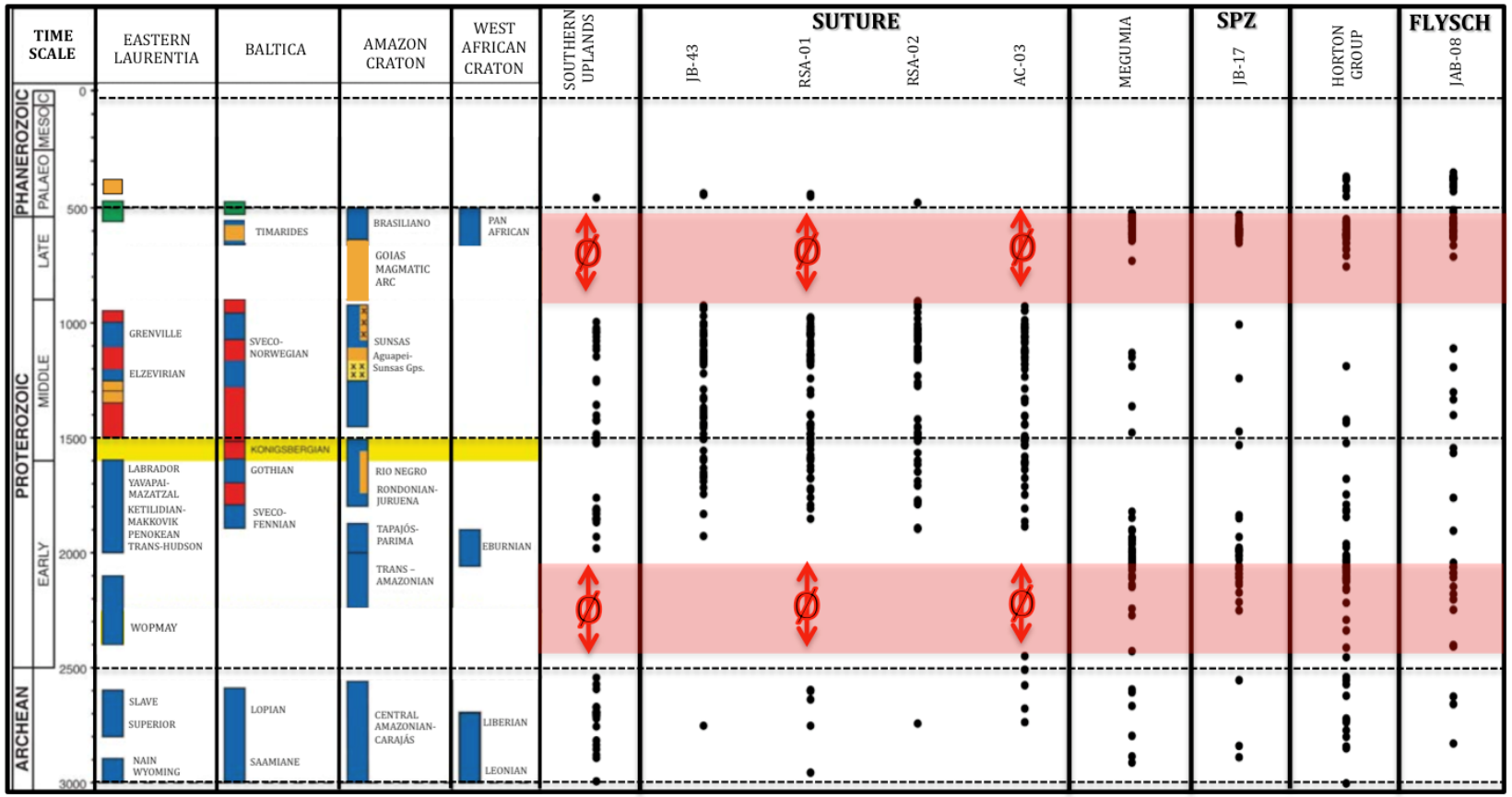

Fig. 3.4 Detrital Zircon ages from samples from the Alájar Mélange phacoids (RSA-01, JB-43), matrix (RSA-02) and Ribeira de Limas formation quartzwacke (AC-03) and Santa Iria Flysch (JAB-08) of the suture zone and quartzite (JB-17) from the Phyllite Quartzite Group of the SPZ. These data are compared with detrital zircon data from theEarly Silurian Kirkcolm Formation of the Southern Uplands Terrane of the British Caledonides (Waldron et al., 2008), Meguma Terrane from the Northern Appalachians (after Waldron et al., 2009) and the Devonian-Carboniferous Horton Group from the St. Mary's Basin of the Northern Appalachians (Murphy and Hamilton, 2000). Also shown are tectonothermal events in

Taken together these interpretations suggest that the quartzite phacoids and matrix (Alájar mélange) and metasediments (Ribeira de Limas formation) of the PDLZ were derived from either Baltica or Laurentia. The presence of euhedral, multifaceted ca. 440 Ma zircons in the mélange phacoids (RSA-01 and JB-43) suggests a local Early Silurian volcanic source. Volcanism of this age is rare in Gondwana but common along eastern Laurentia (e.g. Midland valley terrane; Grahame et al., 2008). As this volcanism is generally associated with the closure of the Iapetus Ocean, the presence of these euhedral ca. 440 Ma zircons (Fig. 3.5) is indicative of a source proximal to the Iapetan suture zone located between eastern Laurentia and peri-Gondwanan terranes (Fig. 3.4). As a result, the PDLZ sediments were not only derived from Laurentia and/or Baltica but also likely derived from Early Silurian rocks associated with the closure of the Iapetus, along the eastern margin of Laurentia.

An example of one such potential source is the Early Silurian Southern Uplands terrane of the British Caledonides (Fig. 3.1), which borders the Midland Valley terrane to the south. The Southern Uplands terrane is interpreted as a quartzite-dominated accretionary prism (McKerrow et al., 1977) that developed along the eastern margin of Laurentia during the closure of the Iapetus Ocean. A comparison of the PDLZ detrital zircon data with the detrital zircon ages obtained from quartzite units in the Southern Uplands terrane (Waldron et al., 2008) reveals striking similarities (Figs. 3.3, 3.4). Most notably, similar to the detritus in the PDLZ, detritus from the Southern Uplands terrane contains abundant Mesoproterozoic and late Palaeoproterozoic zircons as well as ca. 440

Ma Palaeozoic zircons. Furthermore, the Southern Uplands terrane also lacks early Palaeoproterozoic and significant Neoproterozoic zircons. As the Southern Uplands terrane has potential lateral equivalents in Newfoundland (Waldron et al., 2008) this connection refers not only to the Southern Uplands terrane sensu stricto but also coeval units developed along the Laurentian margin during similar processes, which have been identified in Scotland, Ireland and Atlantic Canada (Waldron et al., 2008).

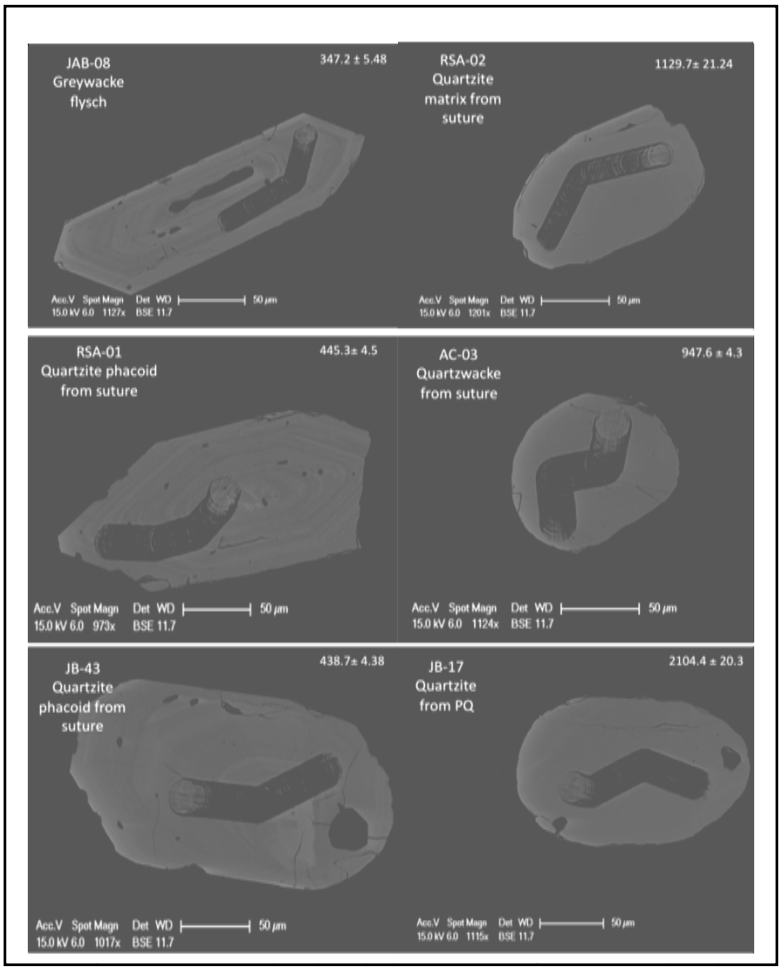

Fig. 3.5 SEM Backscatter images of selected zircon grains from the PDLZ.

To a first order, the data suggest that during at least the Early to Middle Devonian the SPZ was outboard of the Gondwanan margin (OMZ). This interpretation is consistent with late Palaeozoic calc-alkaline andesitic arc magmatism present in the OMZ (Jesus et al., 2007), which suggests subduction of oceanic lithosphere beneath the OMZ margin. Therefore the SPZ basement is either (i) a rifted Silurian West African ribbon continent which derived Late Devonian passive margin clastic rocks from itself or (ii) peri-Gondwanan Meguma basement with Phyllite Quartzite Group clastic rocks sourced from the Meguma Group, which is dominated by ca. 0.6-2.1 Ga detritus (Krogh and Keppie, 1990; Waldron et al., 2009). However, the Phyllite Quartzite Group (JB-17) contains a paucity of Mesoproterozoic zircons (Fig. 3.4), the lack of which is generally considered a fingerprint of West African provenance (e.g. Linneman and Romer, 2002). In addition, the fact that (i) palaeogeographic reconstructions propose that the Meguma terrane was immediately outboard of the Southern Iberia margin during the Early Devonian (e.g. Martínez-Catalán et al., 1997; Onézime et al., 2003; Simancas et al., 2003) and (ii) West Africa lacks Silurian-Early Devonian rift to passive margin deposits that would reflect a separation of the SPZ along the periphery of West Africa, we support the former scenario where the SPZ basement is part of the peri-Gondwanan Meguma terrane.

3.6.2. Timing of Ossa Morena Zone / South Portuguese Zone Collision

The detrital zircon signature of the flysch (Santa Iria Flysch) in the PDLZ displays

a broad range of Neoproterozoic to Palaeoproterozoic zircons consistent with derivation from sources located in Gondwana, peri-Gondwanan terranes and Laurussia (Fig. 3.4). This signature is also similar to the detrital zircon data obtained from the PQ group of the SPZ. These data imply that by the Visean, detritus was being shed to the PDLZ from the SPZ (Meguma?). Therefore, juxtaposition of the SPZ and OMZ occurred between ca. 347.2 Ma and ca. 330 Ma as constrained by the maximum age for deposition of the Santa Iria Flysch and the age of the crosscutting Gil Márquez Pluton. These data suggest that if the ophiolites (Beja Acebuches Ophiolite) formed during ca. 330-345 Ma (Azor et al., 2008) then they are likely related to transtensional bend along the sinistral South Iberian Shear Zone. In this case, later transpressional deformation recorded along the South Iberian Shear Zone (e.g. Crespo Blanc and Orozco, 1988) was likely a result of continued transpression during continent-continent collision, and was isolated from the simply deformed Visean Santa Iria Flysch (Braid et al., 2010). However our data do suggest that, despite the possibility that the Beja Acebuches Ophiolite may not be primary Rheic oceanic lithosphere as was already suggested by Quesada et al. (1994), the SPZ did not contribute detritus to the suture zone until the Visean and therefore supports an exotic SPZ palaeogeographic history with respect to Gondwana (OMZ).

3.6.3. Synthesis and Evolutionary Model

Taken together, the detrital zircon data from the PDLZ and the SPZ indicate that (i) the polydeformed Alájar mélange and metasediments of the PDLZ were all derived from

a similar source, (ii) the PDLZ polydeformed sediments were neither derived from the (OMZ) nor from the (SPZ) during Devonian subduction of an oceanic basin beneath the OMZ, (iii) a source for the PDLZ polydeformed deposits similar to the Southern Uplands terrane of the British Caledonides is required, (iv) the SPZ is likely exotic with respect to both the PDLZ and the OMZ and contains Late Devonian continental clastic rocks (Phyllite Quartzite Group) similar to the Devonian detritus from the Meguma terrane of the northern Appalachians and (v) the SPZ accreted to the PDLZ and the OMZ by ca. 347 Ma, the age of the youngest concordant detrital zircon in the PDLZ flysch (Santa Iria Flysch), which contains zircon populations similar to the SPZ as well as younger zircons consistent with upper plate arc magmatism (ca. 350 Ma).

Interpretation of a source equivalent to the Southern Uplands terrane for the PDLZ requires either (i) a substantial across-strike fluvial transport during the Devonian from a source northwest of the peri-Gondwanan terranes (e.g. Avalonia, Meguma, Ganderia) or (ii) a tectonic transport of a crustal fragment along strike of the Southern Uplands to a location between the SPZ and the OMZ. In our view, the latter scenario is favored by (i) presence of ca. 440 Ma grains with a euhedral morphology, consistent with a short lived sedimentary history, in both the quartzite phacoids and quartzite matrix as well as (ii) the absence of peri-Gondwanan detritus in the PDLZ samples that would be expected in a fluvial system spanning from the Laurentian margin to a Devonian basin outboard of Gondwana and (iii) our interpretation that both the polydeformed olistostromal phacoidal quartzites (samples RSA-01, JB-43) of the Alájar mélange as well as the quartzite matrix

(sample RSA-02) were derived from the same source. These factors favor a proximal source for the PDLZ deposits over a distal fluvial derivation of individual zircon grains. This interpretation requires that the quartzite phacoids and matrix (Alájar mélange) and metasediments (Ribeira de Limas formation) were all derived locally and not the result of distal fluvial systems where the phacoids would be expected to yield different zircon populations from the matrix. Taken together these data and interpretations suggest the deposition of the PDLZ units requires not only a source along the Early Silurian Laurentian margin (Southern Uplands terrane?) but also the subsequent spatial juxtaposition of this source with the OMZ, prior to ca. 347 Ma (i.e. a many hundred kilometers relative displacement).

A model, which satisfies these requirements, should also be consistent with late Palaeozoic continental reconstructions. Although most late Palaeozoic reconstructions agree on the general relative positions of Gondwana and Laurussia during the closure of the Rheic Ocean, the relative positions of Iberia and Gondwana are debated. There are essentially two versions which may affect the details of models concerning Iberian late Palaeozoic geological evolution: (i) Iberia was part of autochthonous Gondwana throughout the Palaeozoic (e.g. McKerrow and Scotese, 1990; Scotese, 2003; Robardet, 2002; 2003; Martinez Catalan et al., 2004) or (ii) Iberia was part of the Armorican Composite terrane (ACT) which separated from Gondwana during the Silurian and collided with Laurussia prior to its terminal collision with Gondwana (e.g. Van der Voo, 1979; 1982; Stampfli and Borel, 2002). The latter is largely based on palaeomagnetic

evidence and the interpretations of the age of magnetization of units in the Iberian autochthon remain controversial (e.g. Perroud et al., 1991). On the other hand, faunal, lithological and palaeoclimatic indicators are in general agreement and indicate that the southern European regions (e.g. OMZ) remained connected with Gondwana throughout the late Palaeozoic (e.g. Robardet, 2002, 2003). Furthermore the OMZ records an Early Ordovician to late Palaeozoic passive margin (RobardetandGutiérrez Marco, 2004), which lacks Silurian rift to drift deposits predicted by an early Palaeozoic separation of an Armorican Composite terrane from Gondwana. Therefore in terms of understanding the enigmatic and contrasting Devonian-Carboniferous evolution of the PDLZ, SPZ and the OMZ we adopt a reconstruction with a unified Iberia and Gondwana. Although this choice may affect the details of our model, it does not affect the basic processes involved.

Reconstructions, which unify Gondwana and Iberia, also indicate Iberia as a promontory of Gondwana, with a re-entrant between this promontory and North Africa (e.g. McKerrow and Scotese, 1990; Scotese, 2003; Woodcock et al., 2007). This promontory likely experienced post-orogenic oroclinal bending to form the Iberian-Armorican arc (e.g. Weil et al., 2010), however we adopt the view that the continental margin was likely non-linear prior to the Variscan orogen (e.g. Matte, 1991; Woodcock et al., 2007).

Using this general reconstruction, we propose that Early Devonian oblique collision between an Iberian indenter and Laurussia and the existence of a small remnant ocean basin (re-entrant) between southern Iberia, North Africa and the northern Appalachians

resulted in excision of a crustal fragment correlative with the Southern uplands of the British Caledonides across the remnant ocean. This excision was accommodated by development of a new subduction zone beneath the OMZ (Fig. 3.5b). A collision originating at ca. 390-400 Ma between a late Palaeozoic Iberian indenter and Britain and Ireland (Woodcock et al., 2007) (Fig. 3.5b) is supported by (i) Early Devonian Acadian shortening in central Britain, (ii) coeval dextral Early Devonian deformation along the Bristol Fault zone in Southeastern England, (iii) opposing sinistral deformation in the Southern Uplands of Scotland (Phillips et al., 1995) and the South Iberian Shear Zone (Crespo-Blanc and Orozco, 1988) and other major lineaments (Quesada, 1991) in Southern Iberia (Fig. 3.6) and (iv) onset of deformation and flysch deposition in Iberia (Quesada et al., 1990; González Clavijo, 1996).

In this model, northwesterly subduction beneath Laurussia in the Late Silurian was disrupted by collision with the Iberian promontory of Gondwana such that oblique subduction with a sinistral component commenced beneath the OMZ. This subduction was accompanied by the generation of the sinistral South Iberian Shear Zone (Crespo Blanc and Orozco, 1988) and a tectonic free face (e.g. Mann, 1997) along the re-entrant between Iberia and North Africa (Fig. 3.6b,c). This situation is analogous to the generation of microplates and tectonic escape (excision) of crustal blocks away from a continental indenter in modern Mediterranean (e.g. Dhont et al., 2006) and Himalayan (e.g. Tapponier and Molnar, 1976; Kapp et al., 2004) collisional zones.

During the stages of excision of the crustal block, Late Devonian passive margin deposits (Phyllite Quartzite Group), likely sourced from the Meguma terrane, were deposited on SPZ basement, which was part of the escaping block. As these are passive margin deposits they are only indicative of a local passive margin setting in basins]. Following deposition of these continental clastic rocks, Late Devonian-Early Carboniferous extension occurred within the SPZ, typical of internal deformation in escaping blocks (e.g. Mann et al., 1997; see also the model by Castroviejo et al. 2010 for the particular case of the SPZ and how this transtensional event facilitated ascent and eruption of the bimodal volcanism in the Iberian Pyrite Belt). This model is consistent with (i) documented dextral movement in the Meguma terrane relative to Avalonia in the northern Appalachians (Keppie and Dallmeyer, 1987) (ii) the Late Devonian-Early Carboniferous transtension required for bimodal volcanism (ca. 355-330 Ma) of the Iberian Pyrite Belt (e.g. Quesada, 1998; Solomon and Quesada, 2003; Castroviejo et al., 2010) in the SPZ and (iii) extension-related voluminous magmatic episodes evident in the Meguma terrane in Maritime Canada (ca. 380–300 Ma) and the SPZ (Sierra Norte Batholith, ca. 350-300 Ma). Although these connections are independent of the derivation of the PDLZ they further support both a detrital zircon genetic linkage between the SPZ and the Meguma terrane and a Devonian-Carboniferous excision of a crustal block as the probable mode of transport for part of the Laurentian / Iapetan suture (Southern Uplands?) toward the OMZ.

The eventual juxtaposition of rocks from the Southern Uplands equivalent terrane with a Rheic subduction zone beneath the OMZ (Fig. 3.6c) led to cannibalization and deposition of metasediments (PDLZ) from this terrane and spatial juxtaposition of the SPZ, PDLZ and OMZ. In this case, the internal fabric evident in the cannibalized phacoidal quartzites of the PDLZ (Alájar mélange) (Braid et al., 2010) potentially preserves a record of the closure of the Iapetus, whereas deformation in the quartzite matrix and the quartzwacke (Ribeira de Limas formation) records subduction of the Rheic related ocean basin and terminal collision between the OMZ and the SPZ.

The data presented here suggest that both the PDLZ and the SPZ terranes should be regarded as exotic to the Gondwanan parautochthon (OMZ) and terminal collision between the OMZ and SPZ occurred between ca. 347 Ma and ca. 330 Ma. The PDLZ records the juxtaposition of an exotic crustal fragment with southern Iberia and occurred as a result of movement along orogen-scale shear zones (e.g. South Iberian Shear Zone, and probably others), which spanned across the Iapetan suture.

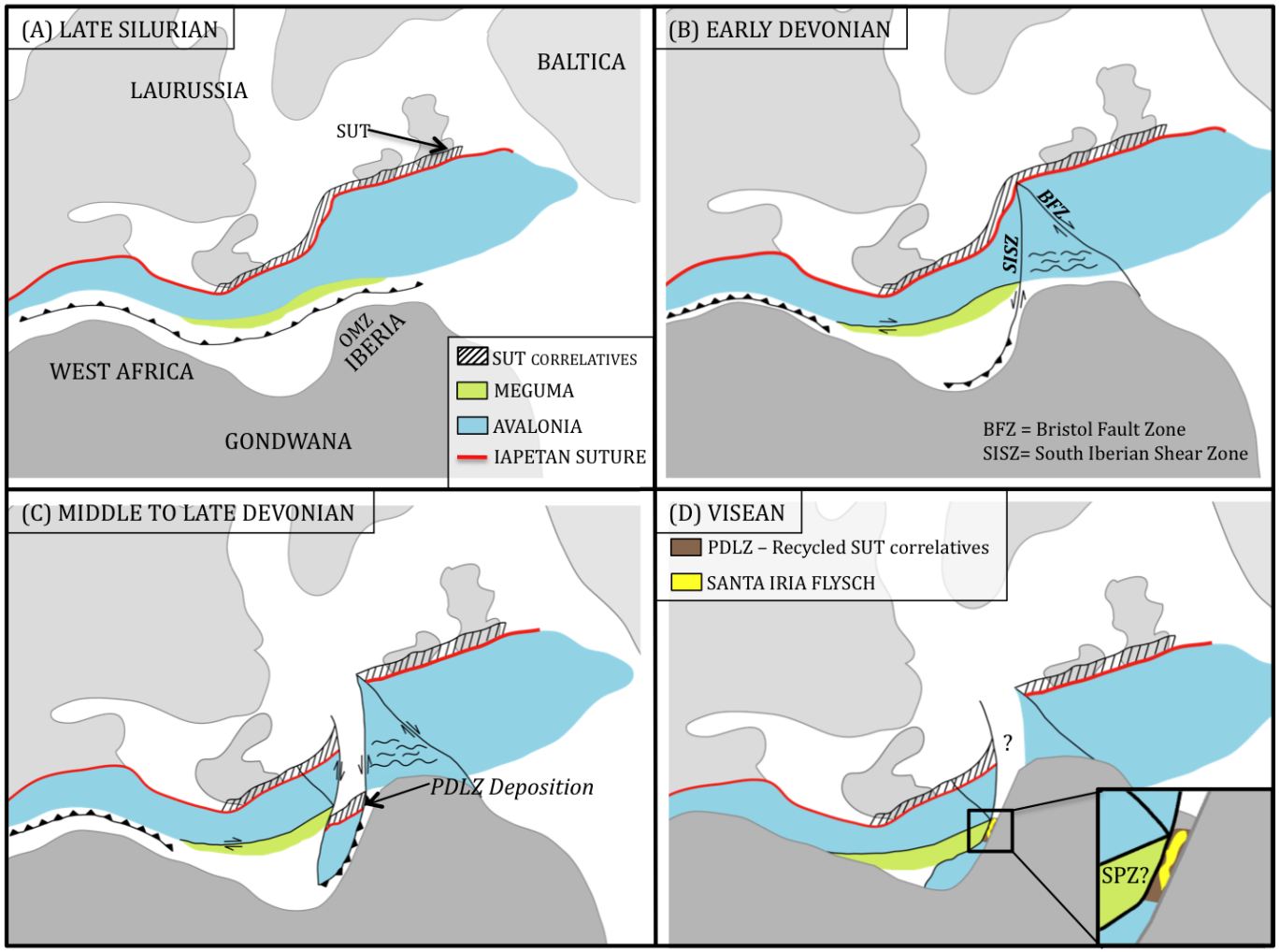

Fig. 3.6 Tectonic model showing juxtaposition of the Iapetan suture and a Southern Uplands equivalent crustal block with the OMZ assuming juxtaposition of the OMZ with West Africa (e.g. Robardet, 2003) and the Bay of Biscay closed (e.g. Ries, 1978). (a) late Silurian closure of the Rheic Ocean (b) early Devonian collision of the Iberian promontory with the British Caledonides (c) late Devonian-early Carboniferous movement of a crustal fragment toward a Gondwana re-entrant with associated local extension and deposition of the PDLZ (d) Visean juxtaposition of the SPZ, PDLZ and OMZ and deposition of the Santa Iria flysch.

3.7. Acknowledgements

We would like to thank Nick Culshaw and Rebecca Jamieson for discussions related to the project as advisors on JAB thesis committee. The support of theNatural Sciences and Engineering Research Council, Canada throughthe PGS-D grant to JAB and Discovery and Research Capacity grants toJBM. JAB also acknowledges the support of the Dalhousie Killampredoctoral scholarship program. St. Francis Xavier University Councilfor Research grants to JBM. We are grateful to Peter Cawood and and twoanonymous reviewers for their very insightful and constructive reviewsand to Rafael López-Guijarro for help withfieldwork and discussions

CHAPTER 4

PROBING THE COMPOSITION OF UNEXPOSED BASEMENT, SOUTH PORTUGUESE ZONE, SOUTHERN IBERIA: IMPLICATIONS FOR THE CONNECTIONS BETWEEN THE APPALACHIAN AND VARISCAN OROGENS

4.1. Abstract

The SPZ of southern Iberia is an allochthonous terrane of the late Paleozoic Variscan orogen. The oldest exposed units in the SPZ are Late-Devonian continental clastics and as a result the origins of the SPZ are unknown.Geochemistry and Sm-Nd and U-Pb (magmatic zircon) isotope data from a post-collisional batholith that crosscuts the allochthonous South Portuguese Zone (SPZ) suggest that the basement is compositionally more juvenile than the exposed upper crust.. Multifaceted inherited zircon cores from a granitoid batholith (Sierra Norte Batholith reveal) Neoproterozoic (ca. 561 Ma to 647 Ma) and Mesoproterozoic ages (ca. 1075 to ca. 1116). Granitoid samples are characterized by εNdvalues ranging from +1.4 to –9.6 and model ages ca. 0.76-1.8 Ga. Conversely the exposed Late Devonian clastics of the SPZ are characterized by more negative εNd values (-7.5 to -10.4). Taken together U-Pb and Sm-Nd data indicate the lower crust that melted to yield the SNB was (i) Neoproterozoic (ca. 560- 650 Ma) to Mesoproterozoic (ca. 1.0 -1.2 Ga) in age (ii) was not compositionally similar to the

overlying Devonian-Carboniferous continental detritus, but was instead more juvenile with model ages between ca. 0.9-1.2 Ga. This unusual relationship is similar to the relationship between the relatively juvenile basement and ancient upper crust documented in the exposed portion of the Meguma terrane in the northern Appalachians, which paleogeographic reconstructions show was immediately outboard of southern Iberia in the Late Devonian.

4.2. Introduction

Allochthonous terranes typically preserve evidence of their original tectonic setting as well as events relating to their accretion and subsequent dispersal (e.g. McWilliams and Howell, 1982; Beck, 1989; Dallmeyer et al., 1991; Van der Voo, 1993; Fernández Suárez et al., 2002). Therefore determining the geologic history of orogenic belts typically requires an understanding of the tectonic evolution and paleogeography of allochthonous terranes prior to accretion.

Terrane accretion is commonly accompanied by the deposition of syn- to post - orogenic sedimentary sequences, which overstep terrane boundaries and cover the pre-orogenic geology. Such a scenario occurs in southern Iberia where an allochthonous terrane in the late Paleozoic Variscan orogen of Western Europe, known as the South Portuguese Zone (SPZ, Lotze, 1945), exposes only late Paleozoic clastic rocks and granitoid rocks which intrude across the terrane boundary (Fig. 4.1). The SPZ is located outboard of a suture zone (Pulo do Lobo Zone; PDLZ) to the north, which separates SPZ from the Iberian autochthon (Fig. 4.1). The suture zone is particularly significant as it is widely thought to have developed during the closure of the late Paleozoic Rheic Ocean and terminal collision between Gondwana and Laurussia (Quesada et al., 1994; Onézime et al., 2003), which is a major event in the formation of the supercontinent Pangea.

Lithologic (Onézime et al., 2003; Simancas et al., 2005) and geochronological data (e.g. Braid et al., *in press*) indicate the SPZ was outboard of the Gondwanan margin at

least until the Late Devonian. However, the oldest exposed units in the SPZ are Late Devonian continental clastic strata and as a result the composition of the SPZ basement cannot be directly determined.

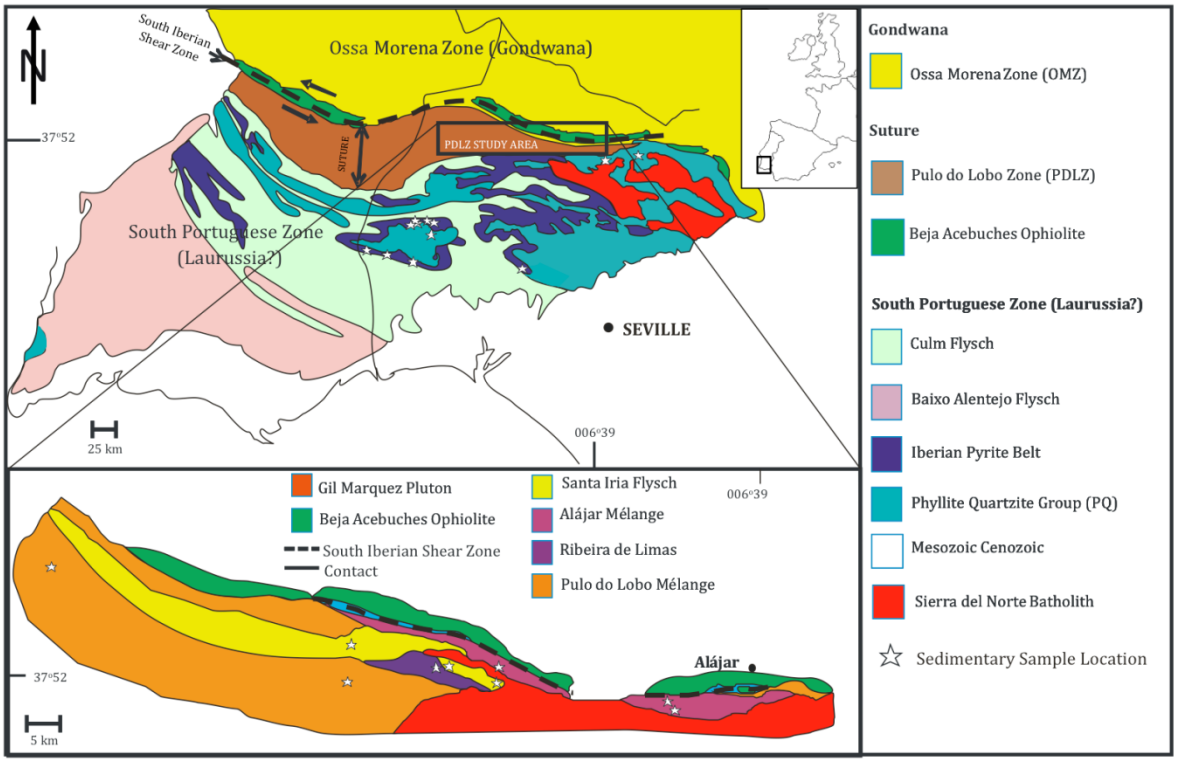

Fig. 4.1 Summary of the geology of the South Portuguese and Pulo do Lobo Zones in the study area (adapted fromOliveira, 1990). For detailed PDLZ geology see Braid et al., 2010. Location of sedimentary samples for lithogeochemistry and Sm- Nd isotopes shown.

Despite this limited geologic record, the pre-Variscan SPZ crust is thought to be a fragment of a peri-Gondwanan terrane; either the Meguma terrane (Martínez Catalán et al., 1997; de la Rosa et al., 2001) or Avalonia (e.g. Leistel, 1998; Simancas et al., 2005). These interpretations of the potential connection between the SPZ and these peri-Gondwanan terranes is inferred from late Paleozoic reconstructions (e.g. McKerrow and Scotese, 1990; Scotese, 2003; Woodcock et al., 2007), which place southern Iberia adjacent to Maritime Canada during the formation of Pangea. These terranes are currently exposed in the northern Appalachians and in southern Britain (e.g. Keppie, 1985, 1993; Murphy et al., 2004; Hibbard et al., 2006; Waldron et al., 2009; *in press;*Nance et al., 2010).

Although these Late Devonian reconstructions provide a general paleogeographic framework for the Paleozoic evolution of the SPZ, the potential connections between the SPZ and the northern Appalachians remain poorly documented. Therefore determining the original affinity of the SPZ has profound implications on our understanding of the processes affecting the Appalachian and Variscan orogens as well as the timing and geometry of the formation of Pangea.

As the basement to the Late Devonian clastic successions is unexposed in the SPZ, its age and composition must be determined by indirect methods, such as U-Pb geochronology of detrital zircons in the clastic successions and of xenocrystic cores of zircons in plutonic rocks. In addition, Sm-Nd isotopic analyses of clastic rocks can provide information on the provenance and tectonic processes such as uplift or terrane

accretion that accompanied deposition, (e.g. Thorogood, 1990; Murphy et al., 1996; Murphy and Nance, 2002) and of crustally-derived plutonic and volcanic rocks can provide constraints on isotopic composition of basement sources (e.g. DePaolo, 1981, 1988).

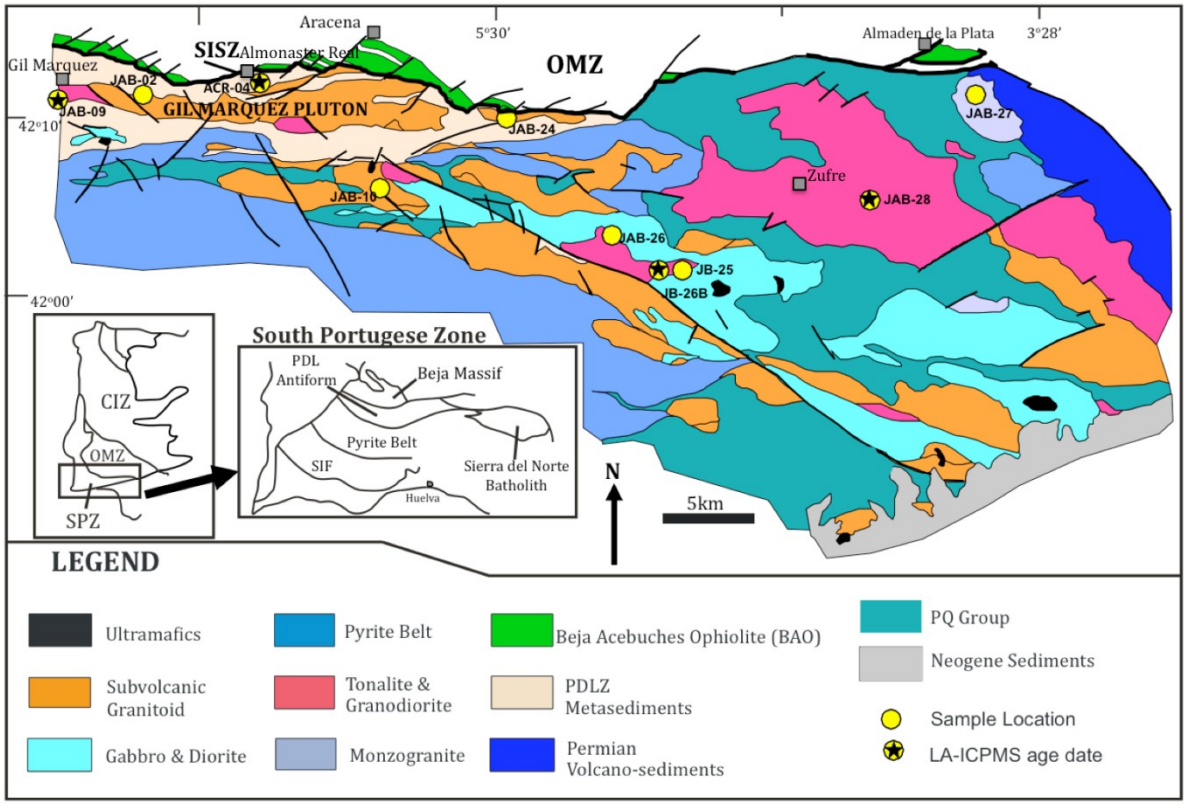

Fig. 4.2 Summary of the geology of the Sierra Norte Batholith (adapted from de la Rosa, 1993). Granitoid samples for lithogeochemistry, Sm-Nd isotopes and La-ICPMS zircon age dating shown.

In order to constrain the composition and origin of the SPZ basement, we present new LA-ICPMS zircon geochronological data, geochemical and Sm–Nd isotopic data from representative samples from a granite batholith (Sierra Norte Batholith, SNB; de la Rosa, 1992), which crosscuts both the PDLZ and the SPZ. We also present new lithogeochemical and Sm-Nd isotopic data from exposed sedimentary sequences in the SPZ and PDLZ. These data facilitate a comparison between the SPZ and various tectonostratigraphic zones in the northern Appalachians (e.g. peri-Gondwanan terranes), which may have been connected to SPZ in the late Paleozoic. Finally, we attempt to evaluate the significance of these connections in interpreting the geometry and timing surrounding the closure of the Rheic Ocean and the formation of Pangea.

4.3. Geology

The SPZ of the Iberian Massif forms part of the Variscan orogenic belt inWestern Europe (Leistel et al., 1998; Carvalhoet al., 1999; Franke, 2000). The SPZ isin faulted contact to the north with the PDLZ, which contains a sequence of mafic rocks known as the Beja-Acebuches ophiolite complex (BAO). The PDLZ is in faulted contact to the northeast with the OssaMorena Zone (OMZ) (Fig. 4.1). The OMZ has faunal affinities with Gondwana throughout the Paleozoic (e.g. Robardet et al., 2003) and is generally thought to have accreted obliquely to Gondwana (Iberian autochthon) in the Neoproterozoicalong an orogen-scale transcurrent shear zone (Tomar-Badajoz-

Córdobashear zone). This shear zone was reactivated in the Carboniferous during the collision between Laurussia and Gondwana (Quesada andDallmeyer, 1994). During the Late Devonian, the continental margin of the SPZ,is widely held to have drifted northward by subduction beneath the OMZ margin of Gondwana until ca. 330 Ma (Jesus et al., 2007). The PDLZ crops out between the SPZ and Gondwana and is classically interpreted as an accretionary complex between SPZ and OMZ that developed during the closure of the Rheic Ocean (e.g. Eden, 1991) in the Late Devonian-Early Carboniferous time span.

4.3.1. South Portuguese Zone

The exposed geology of the SPZ is dominated by the Late Devonian–Early Carboniferous sedimentary and bimodal volcanic sequences of the Iberian Pyrite Belt (IPB) (Fig. 4.1) (e.g. Schermerhorn, 1971; Onézime et al., 2003). Three lithostratigraphic formations are recognized in the IPB (Schermerhorn, 1971) from the oldest to the youngest: (i) the Late-Devonian detrital Phyllite-QuartziteGroup (PQ), which are continental clastic strata; (ii) theVolcanic Siliceous Complex (VSC), hosting the VMSmineralization of Late Famennian to middle Visean age (Rosa et al., 2008);and (iii) a Late Visean to the Serpukhovianturbiditic flysch group, (Schermerhorn,1971; Oliveira,1990).

The PQ is composed of siliciclastic pre-volcanic rocks deposited in a subtidal environment from fan delta and sand bar systems on a shallow marine continental

platform (Moreno and Sáez, 1990; Oliveira, 1990; Moreno et al., 1996). The base of this unit is not exposed and, has a minimum thickness of 300–400 m (Soriano and Martí, 1999). The depositional age is constrained by the presence of Fammenian conodonts in limestone lenses interbedded with the clastic strata (Boogaard and Schermerhorn, 1980; 1981). Detrital zircon U/Pb age data from the PQ group display age populations dominated by Paleoproterozoic (ca. 1.8-2.3 Ga) and Neoproterozoic (ca. 0.5-0.7 Ga) zircons with minor Archean zircons (ca. 2.5-2.9 Ga) (Braid et al., 2010 *in press*).

VSCvolcanicandsedimentary strata accumulatedconformablyonthePQGroupshelffaciesbasement (Oliveira, 1990).The VSC is comprised ofmaficandfelsicrocks,interfingered with purpleshales,siltstones,tuffitesandminorlimestones. These rocks are further subdivided into three sedimentary and igneous successions (termed V1, V2 and V3, from lowermost to uppermost).A unit of purple shale occurs along the contact between the V2 and V3, and is generally referred to as the purple shale horizon. Limestonesoftheintermediatesuccession (V2)aredatedbyconodontsandcephalopodsasupperFamennian/ToumasiantoLowerUpperVisean(Boogaard1963;Oliveira1983;Oliveiraetal.1986.). The large variation in the geochemistry of the volcanic rocks compared to that of the sedimentary strata suggests that the sedimentary rocks were not derived from the coeval mafic and felsic volcanics (Boulter et al., 2004).

4.3.2. Pulo Do Lobo Zone & Beja Acebuches Ophiolite

The PDLZ is characterized by a series of tectonically imbricated polydeformed metasediments, olistostromal mélange and tectonic mélange deposits overlain by a relatively simply deformed flysch sequence (e.g. Eden, 1991; Braid et al., 2010) (Fig. 4.1). Although nomenclature and lithologies vary between Spanish and Portuguese sections there is a general consensus that the lowermost unit is a tectonic mafic mélange (e.g. Eden, 1991) with local occurrences of amphibolite blocks in a tectonically imbricated volcaniclastic and schistose matrix. These mélange deposits are also crosscut by mafic dykes and are in fault contact with a polydeformed sedimentary mélange deposit comprised of olistostromal phacoidal quartzites in a phyllite/quartzite matrix, which in turn are in fault contact with a sequence of polydeformed quartzwackes and phyllites. Collectively, these units are unconformably overlain by a Visean (ca. 330 Ma to ca. 347 Ma); (Braid et al., *in press*) simply deformed sequence of siltstone and greywacke known as the Santa Iria Flysch (SIF). For detailed descriptions of the mélange, metasedimentary and flysch deposits see Braid et al., 2010.

The PDLZ is classically interpreted as an accretionary complex developed along the margin of the OMZ during the collision between Gondwana and Laurussia (e.g. Eden, 1991; Onézime et al., 1999, 2003). However, recent detrital zircon U/Pb age data (Braid et al., in press) reveal a more complex history. Olistostromal quartzite clasts and matrix from the polydeformed PDLZ have detrital zircon populations that cannot be derived from either the SPZ or Gondwana. These rocks are both characterized by an abundance

of Mesoproterozoic zircons (ca. 1.0-1.5 Ga), a subordinate Paleoproterozoic (ca. 1.6-1.9 Ga) population, as well as minor Archean and euhedral ca. 440 Ma zircons. PDLZ polydeformed samples lack the Neoproterozoic (ca. 0.6-0.9 Ga) and Paleoproterozoic (ca. 2.0-2.5 Ga) detrital zircons that are typical of late Paleozoic sedimentary rocks derived from either Gondwana (OMZ), peri-Gondwanan terranes (e.g. Meguma terrane) or the middle Devonian continental clastics (PQ) of the SPZ. These data suggest the PDLZ mélange and metasediments were derived from neither the upper plate (OMZ) nor the lower plate (SPZ) (La-ICPMS; Braid et al., *in press*). Braid et al., *in press* suggest this enigmatic scenario can be reconciled by derivation of the PDLZ from an excised crustal fragment laterally equivalent to the Southern Uplands terrane of the British Caledonides, during oblique collision between Gondwana and Laurussia in the Late Devonian.

To the north, the PDLZ is in fault contact with theBAO (ca. 334 ± 2 Ma;Azor et al., 2008), which has ophiolitic affinities (Silvaet al., 1990; Fonseca and Ribeiro, 1993; Quesada et al., 1994) anddelineates the northern contact between the PDLZ and OMZ.Geochemical analyses (e.g.Quesada et al., 1994) have shown theprimary igneous rocks of the BAO have a MORB affinity. Across strike,the BAO displays an increasing metamorphic gradient to the north(i.e. highest temperature mineral assemblages located along contactwith OMZ). This metamorphic gradient is interpreted to be the result ofVariscan thrusting of the OMZ over the BAO (e.g.Quesada et al., 1994; Castro et al., 1996). The contact between the BAO and the PDLZ showsintense shearing and retrograde metamorphism, related to themylonitization along the South Iberian Shear

Zone (SISZ) (Crespo-Blanc and Orozco, 1988, 1991). The genesis of the BAO remains controversial and is thought to represent either (i) obducted primary Rheic oceanic lithosphere (e.g. Castro et al., 1996) or (ii) mafic rocks formed during a transtensional event following the maincontinent–continent collision (ca. 345–390 Ma) (Quesada et al., 1994; Azor et al., 2008; Braid et al., 2010; Braid et al., *in press*).

4.3.3. Sierra Norte Batholith

The Sierra Norte Batholith (SNB) is a composite batholith (Fig. 4.2) that intrudes the PDLZ and the SPZ (de la Rosa, 1992; Castro et al., 1995). One of its components, the Gil Márquez granodiorites (ca. 330 Ma La-ICPMS;de la Rosa et al., 2001)locally intrudes both the polydeformed mélange and metasediments and the flysch of the PDLZ. These granodiorites are typically foliated parallel to the east–west orogenic grain and are interpreted to have been emplaced during the latest stages ofdeformation in the PDLZ (e.g.Castro et al., 1995). The ca. 330 Ma age date was obtained exclusively from these foliated granodiorites.The remainder of the SNB is comprised of non-foliatedgabbro,diorite,tonalite, monzograniteandgraniteand crops outintheNEpartoftheIberianPyriteBelt(Soler,1980;Schultzetal.1987)(Fig. 4.2).

ThisbatholithisinterpretedtorepresenteitherthedeepequivalentsoftheVolcanic-SiliceousComplexvolcanics of the IPB in the SPZ (Soler,1980;Schultzetal.1987),orlate-orogenicintrusives, which areunrelatedtotheVSC volcanics(Simancas1983). Rb–Sr wholerock isotopic data are interpreted to indicate that the SNB calc-alkalinegranitoids

are the product of interaction the of magmasderived from the lithospheric mantle with magmasdeveloped by partial melting of a deep mafic andpelitic granulitic crust in an active continental margin(de la Rosa et al., 1993, 2001).

4.4. Sample Selection and Analytical Methods

In order to further constrain the composition of the SPZ basement, representative samples were collected from granitoid rocks of the SNB for LA-ICPMS U/Pb dating, lithogeochemical and Sm-Nd isotope analysis (Fig. 4.2). As the granitoids were emplaced following collision of the SPZ and the OMZ and are generally considered a product of melting the deep continental crust, these samples may possibly preserve an inherited signature of the SPZ basement. To date a LA-ICPMS age (ca. 330 Ma; de la Rosa et al., 2001) has been obtained only from one unit in the SNB (i.e. the foliated Gil Márquez pluton), which locally crosscuts the PDLZ suture. In order to better assess the potential contribution of SPZ basement to the granitoid melt away from the suture zone as well as the range in age of magmatism across the batholith, representative samples were selected from both the foliated Gil Márquez pluton and non-foliated rocks of the SNB outboard of the PDLZ (Fig. 4.2). Furthermore in order to assess (i) the relative contribution of the exposed sedimentary units in the SPZ and PDLZ to the granitoid melts and (ii) potential differences in composition of the lower and upper crust, we also present lithogeochemistry and Sm-Nd isotopic data from representative samples collected from

sedimentary units in both the SPZ and the PDLZ, which are crosscut by the SNB (Fig. 4.1). Full tables of results can be found in the appendix.

4.4.1. Lithogeochemistry and Sm-Nd Isotopes

The major and selected trace elements were analyzed by X-ray fluorescence at the Nova Scotia Regional Geochemical Centre at St. Mary's University, Halifax. The accuracy and precision of all analyses are generally better than 10%. Details of the analytical methods are given in Dostal et al. (1994).Rare earth element analyses were also determined at Memorial University, Newfoundland by ICP-MS according to methods described in Jenner et al. (1990). Samples were analyzed for Sm-Nd compositions at the Atlantic Universities Regional Isotopic Facility (AURIF) at Memorial University, Newfoundland. Analytical procedures for Sm-Nd analyses are described in Kerr et al. (1995).The Nd isotope signature in clastic sedimentary rocks is interpreted to represent the weighted average of values for detrital contributions from the various source areas (see Arndt and Goldstein, 1987; Thorogood, 1990; Murphy and Nance, 2002). The geochemical and Sm-Nd data are available in *appendix C and D*.

4.4.2. U/Pb LA-ICPMS

Approximately sixteen to thirty zircon grains from each of four representative granitoid samples taken from both the Gil Márquez granodiorite (two samples) and across the SNB (two samples) were mounted, polished, imaged by electron backscatter (samples

JAB-09; JAB 28) and cathode luminescence (ACR-04; JB-26B). Of these samples, two were foliated (JAB-09; ACR-04) and two were non-foliated (JB -26B; JAB-28). SEM imaging was done at the Pacific Centre for Isotopic and Geochemical Research (PCIGR) at the University of British Columbia. Cathode luminescence images were obtained at the Zircon and Accessory Phase Laboratory (ZAPLab) at the University of Western Ontario. Zircon grains were analyzed for their U and Pb isotopic composition using a Thermo Element 2 high resolution Inductively Coupled Plasma-Mass Spectrometer coupled to a New Wave Research 213 nm Nd-YAG laser. Detailed description of analytical instrumentation, analytical protocol and methodology, data reduction and age calculation at the Pacific Centre for Isotopic and Geochemical Research (PCIGR) at the University of British Columbia are described in Mortensen et al. (1995, 2007). All zircons were analyzed using line scans with a laser spot diameter of 20 μm along either a zircon core or rim. For each line scan (one analysis), which crossed both a core and a rim, data was selected from either the core or rim section. In some cases where the rims were thick (i.e. > 20 μm) two lines scans (two analyses) were performed on an individual zircon grain.

Age uncertainties are reported at 2σ and either the Pb^{207}/Pb^{206} or the Pb^{206}/U^{238} age is reported depending on which value gives the lower uncertainty (Ludwig, 1998). A total of ninety analyses were obtained in the four samples. Six analyses revealed >10% discordance and were discarded. U/Pb concordia distribution plots for the remaining eighty-four concordant grains are shown in *figures 4.8 and 4.9*and compared in a relative probability plot (Fig.4.12).

4.5. Results ~ Sierra Norte Batholith

4.5.1. Lithogeochemistry

Ten representative samples were selected from the SNB (Fig. 4.2). Sample ACR-04 and sample JAB-24 were taken from foliated granitoid bodies within the SNB that crosscut the SIF within the PDLZ. Two SNB samples were selected from foliated granodiorites near the town of Gil Márquez (JAB-09, JAB-02) and the remaining six samples (JAB-10, JAB-25, JB-26B, JAB-26, JAB-27, JAB-28) were selected from various non-foliated SNB intrusive bodies. All samples display sericitization of feldspars in thin section indicative of post-emplacement alteration and/or weathering. The major- and trace-element chemistry (Table D.1) for theSNB samples can be found in Appendix D.

Most of the SNB samples are felsic (SiO_2 > 67 wt %, on a volatile-free basis) but one sample (JB-26B) has a SiO_2 content of ~ 60 wt%. TiO_2,Fe_2O_3, Al_2O_3 (with exception of JB-26B), and CaO display negative linear correlationswith SiO_2, whereas Na_2O and K_2O display more complex patterns (Fig. 4.3). Trace element correlations with SiO_2display more complexpatterns than the major elements, although Zr displays a clear negative correlation (Fig. 4.4).

As all samples from the SNB display petrographic evidence of alteration and/or weathering, ratios involving HFSE (high field strength elements) and REEs are generally considered more reliable indicators of the rock's original geochemistry because they are relatively unaffected by those processes (e.g., McLennan et al., 1980; Bhatia and Crook, 1986). HFSE and REE abundances are emphasized, as they are more reliable geochemical indicators of SNB magmatic affinity and tectonic setting.

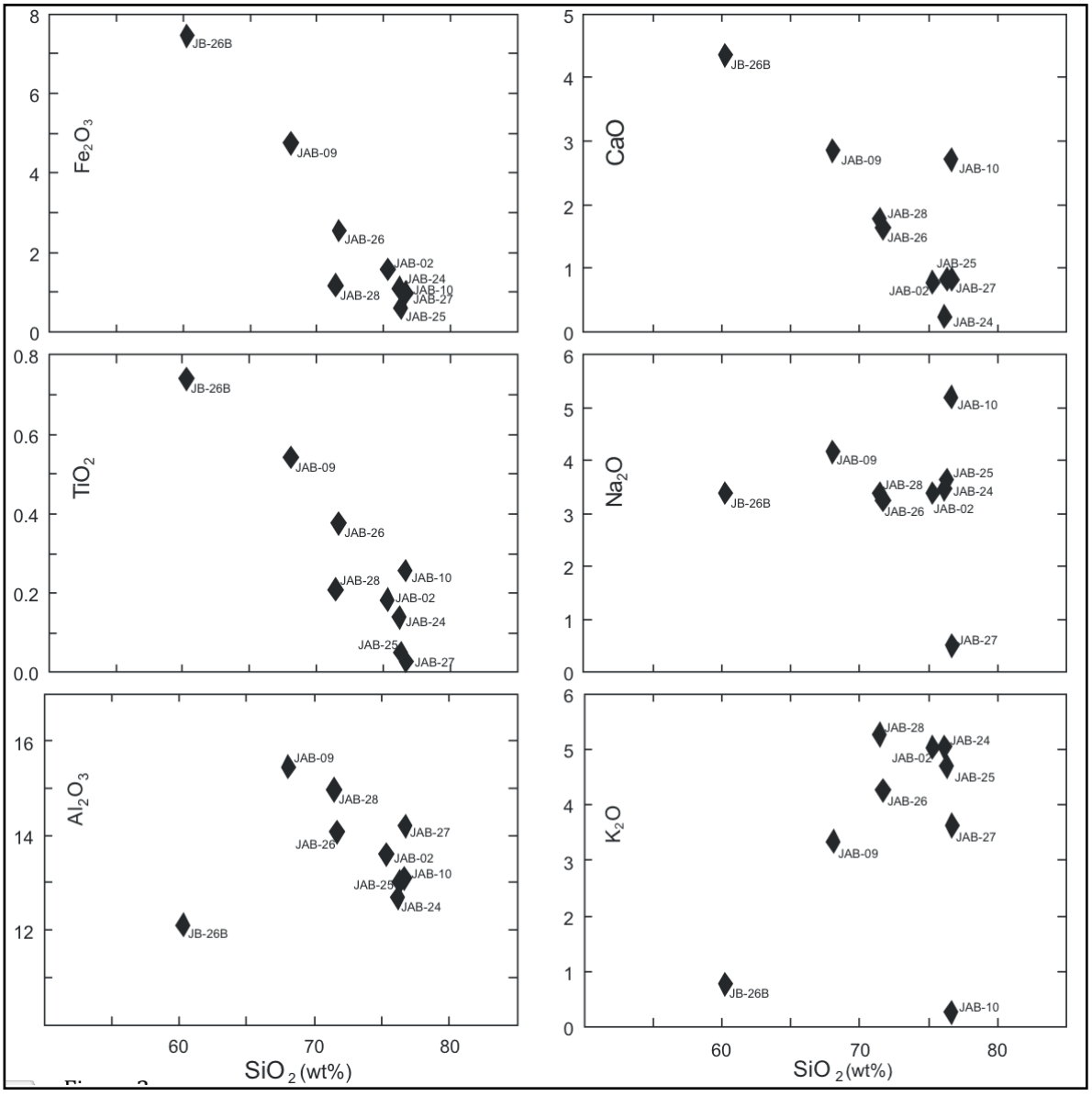

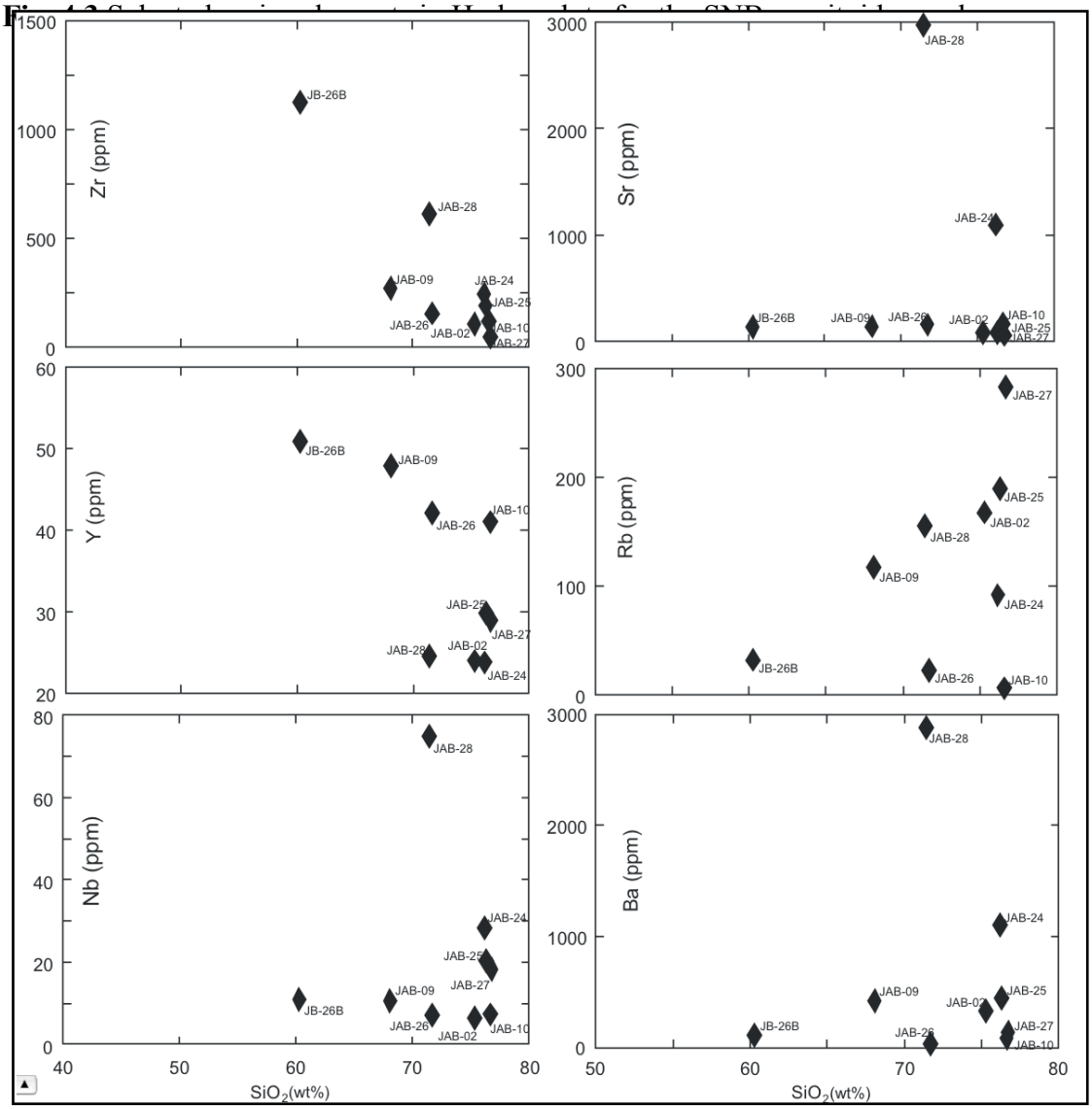

Fig. 4.4 Selected trace elements in Harker plots for the SNB granitoid samples.

Chondrite and primitive mantle normalized plots of rare earth elements (REE) are shown

in *figure 4.6*. A moderate enrichment in light rare earth elements (LREE) in most SNB samples is reflected the range in $(La/Sm)_n$ ratio from 2.3 to 5.7. Sample JAB-27 displays a slightly positive Sm anomaly and a relatively flat LREE profile reflected by a $(La/Sm)_n$ ratio of 1.6. Heavy rare earth element abundances (HREE) generally show flat profiles which are reflected in the range in $(Gd/Lu)_n$ ratio of 0.59 to 1.5. All samples are characterized by a negative europium anomaly, with [(Eu*/Eu) -1] varying between 0.2 (JAB-28) and 4.6 (JAB-24), with a mean value of 1.41 (see inset Fig. 4.5a).

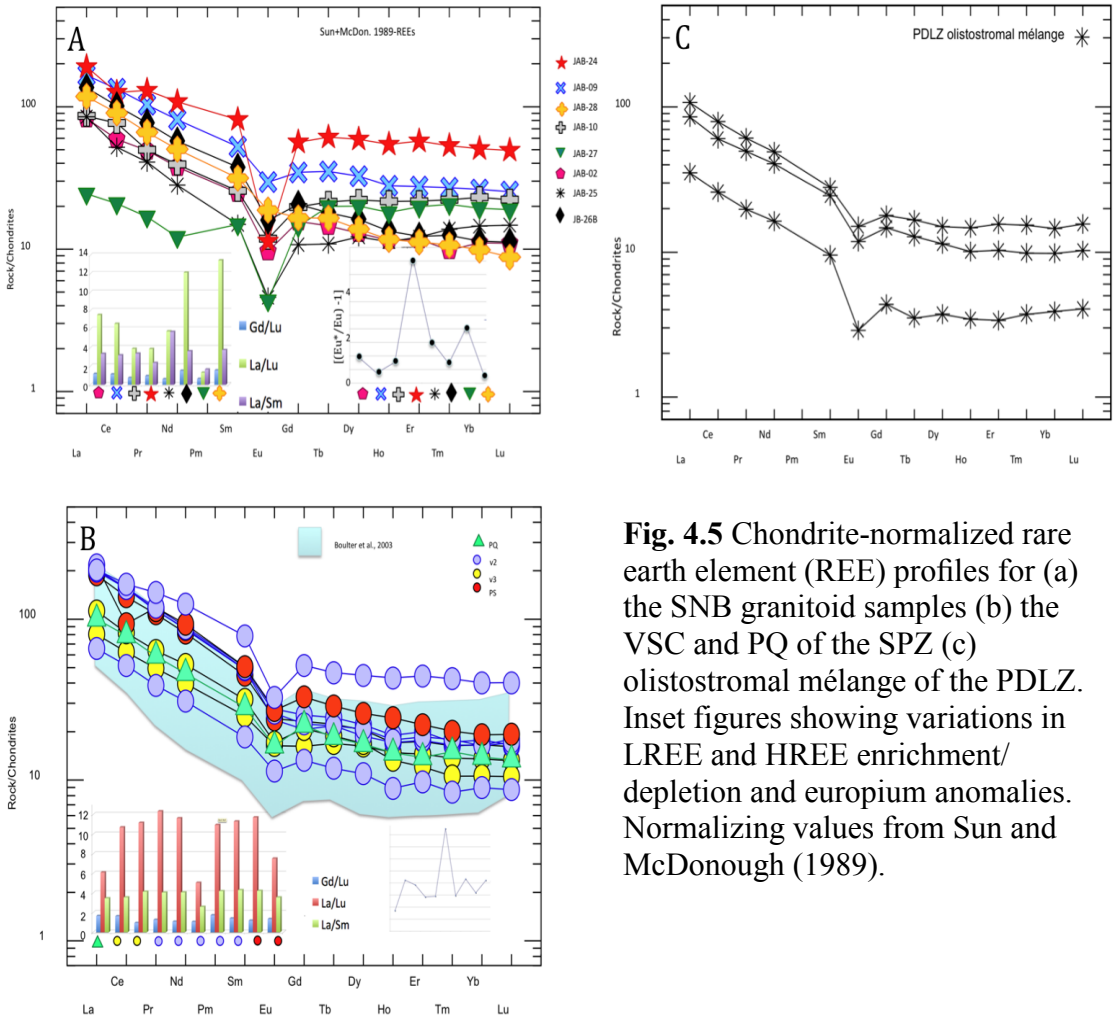

Fig. 4.5 Chondrite-normalized rare earth element (REE) profiles for (a) the SNB granitoid samples (b) the VSC and PQ of the SPZ (c) olistostromal mélange of the PDLZ. Inset figures showing variations in LREE and HREE enrichment/ depletion and europium anomalies. Normalizing values from Sun and McDonough (1989).

4.5.2. Sm Nd Isotopes

The Sm-Nd data for nine SNB samples (Table C.2) can be found in Appendix C. To facilitate comparison between formations, εNd values (relative to CHUR [chondritic uniform reservoir]) given in the text are for its intrusive age (t = 330 Ma). Following Stern (2002), we report T_{DM} ages only for samples with $^{147}Sm/^{144}Nd < 0.165$. Of the nine samples, one sample (JAB-27) displays a $^{147}Sm/^{144}Nd > 0.165$ and therefore its T_{DM} age is not reported. Of the remaining eight samples T_{DM} ages vary from ca. 0.76 to 1.80 Ga. Taken together, all samples in the batholith are characterized by a wide range in εNd values from +1.4 to –9.6 (Fig. 4.6). Two samples, (JAB-28 and JAB-27) display comparatively more negative εNd values at T=330 (-9.6 and -7.5 respectively). The remainder of samples display a more limited range in εNd (-3.0 to 1.4) at T=330 with model ages ca. 0.9 – 1.2 Ga.

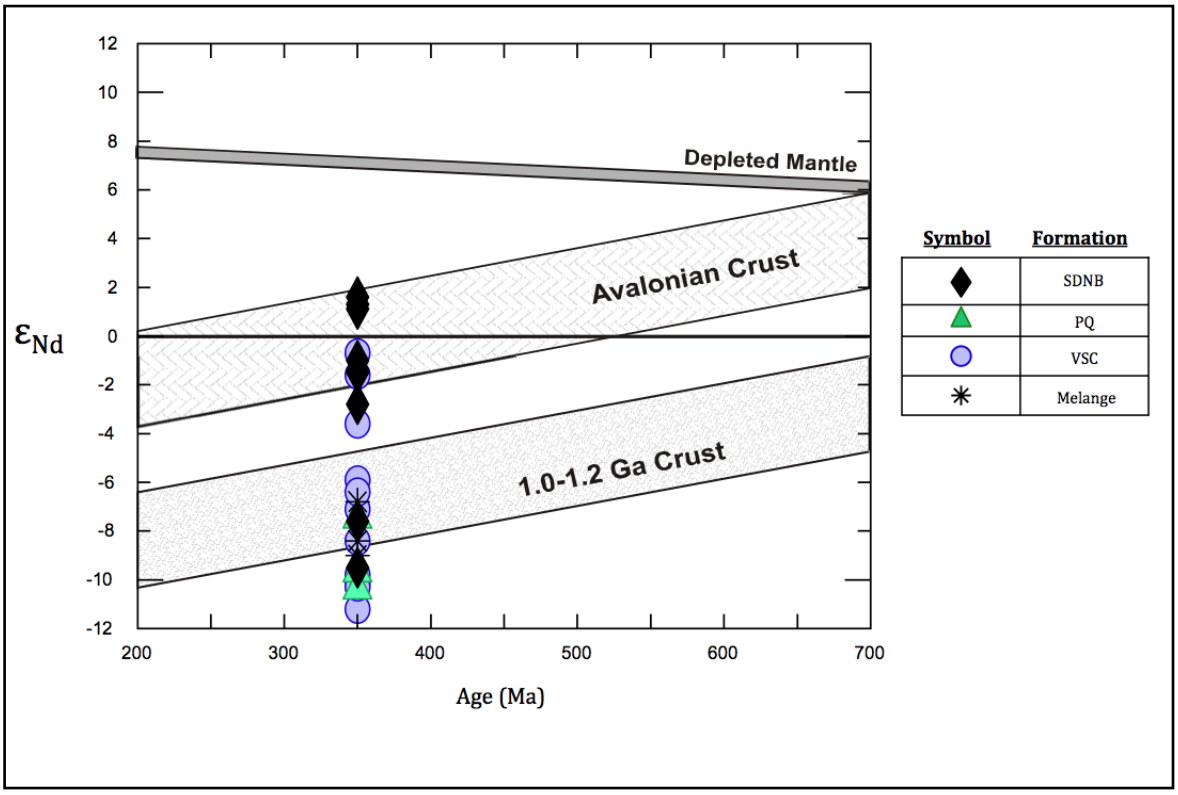

Fig. 4.6 εNd (*t*) vs. time (Ga) diagram (at *t* = 350 Ma) comparing Sm-Nd isotope data for the PDLZ, SPZ and SNB with typical Sm-Nd isotope compositions of Avalonian crust (Murphy et al., 1996b, 2000), 1.0–1.2 Ga (Samson et al., 2000) for rocks in the North American Grenville Province, Meguma Metasedimentary Rocks (MMS) and Meguma Granitoids Rocks (MGR) (Clarke et al., 1997). Depleted mantle evolution curve isfrom the model of DePaolo (1981).

4.5.3. U-Pb Isotopic Data, Foliated Rocks

Sample JAB-09 is a strongly foliated granodiorite collected from a large outcrop exposed along a roadcut immediately south of the village of Gil Márquez (Fig. 4.2). The sample is coarse-grained (5 to 10 mm), and is dominated by quartz, plagioclase,K

feldspar, biotiteand amphibole, with subordinateapatite, sphene, zircon and opaque minerals. Zircons from sample JAB-09 typically show multifaceted terminations with either a stubby euhedral or elongate morphology. SEM backscatter images reveal: (i) zircon cores that are either multifaceted or rounded with a thin rim or (ii) zircons without cores that are zoned and multifaceted (Fig. 4.7a). To determine both the age of igneous crystallization and the ages of potential inherited cores, line scans were performed on either the core or rim of thirty representative grains.The results are listed in table B.7 in the appendix and plotted in *Figure 4.8*. Of the thirty analyses, three are discordant and are not considered further. Twenty-four analyses were performed on either multifaceted zircons with no rims or rims of zircons with cores. These analyses yielded ages ranging from ca. 327 Ma to ca. 386 Ma. Two analyses were also performed on rounded zircon cores and revealed concordant ages of ca. 2040 and ca. 2075 Ma. One analysis was also performed on a multifaceted zircon core and revealed a concordant age of ca. 1180 Ma.

*Sample ACR-04*was collectedsouth of the Almonaster la Real village from a granite body that locally crosscuts the metasediments and the Santa Iría Flysch of the PDLZ (Fig. 4.2). The sample is representative of a granite body that is mildly foliated and is comprised predominantly of quartz, plagioclase,K feldspar, biotiteand amphibole. Most of the zircon grains (~70%) are medium to large (100-200 μm length), elongate subeuhedral prisms. The grains range from translucent yellow-brown to turbid, and generally have inclusions and fractures. The remainder of the grains (~30%) are medium (~100 μm diameter) stubby and subeuhedral to euhedral. Stubby grains generally have

more inclusions and fractures. CL imaging reveals that most zircons are characterized by complex zoning patterns. Inherited cores are irregular in shape but appear multifaceted and zoned (Fig. 4.7b). To determine both the age of igneous crystallization and the ages of potential inherited cores, line scans were performed across sixteen representative grains. The U-Pb isotopic data (Table B.10) can be found in the appendixandare plotted in *Figure 4.8*. Of the sixteen analyses, fifteen yielded concordant or nearly concordant ages (i.e. < 10% discordance). Of these fifteen analyses twelve yielded concordant ages ranging from ca. 325 Ma to ca. 357 Ma. Three analyses of multifaceted zircon cores yielded concordant ages of ca. 1075 to ca. 1116 Ma.

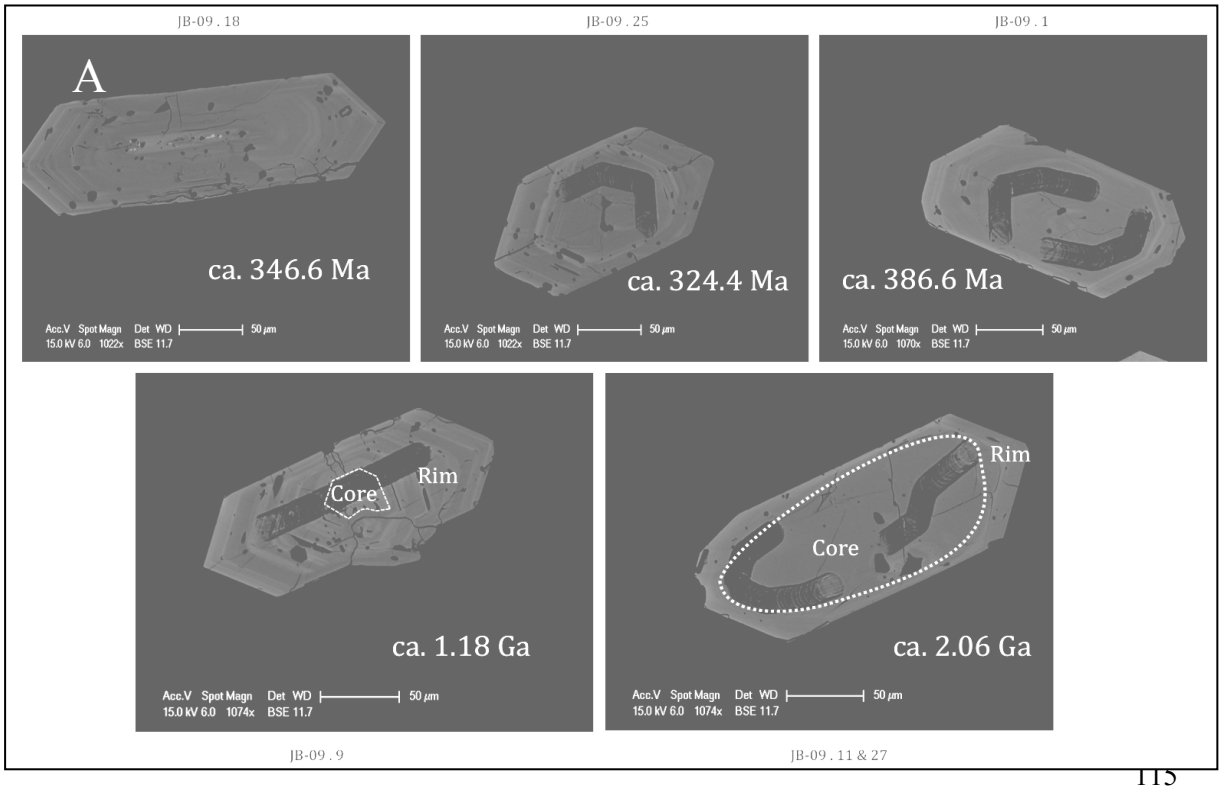

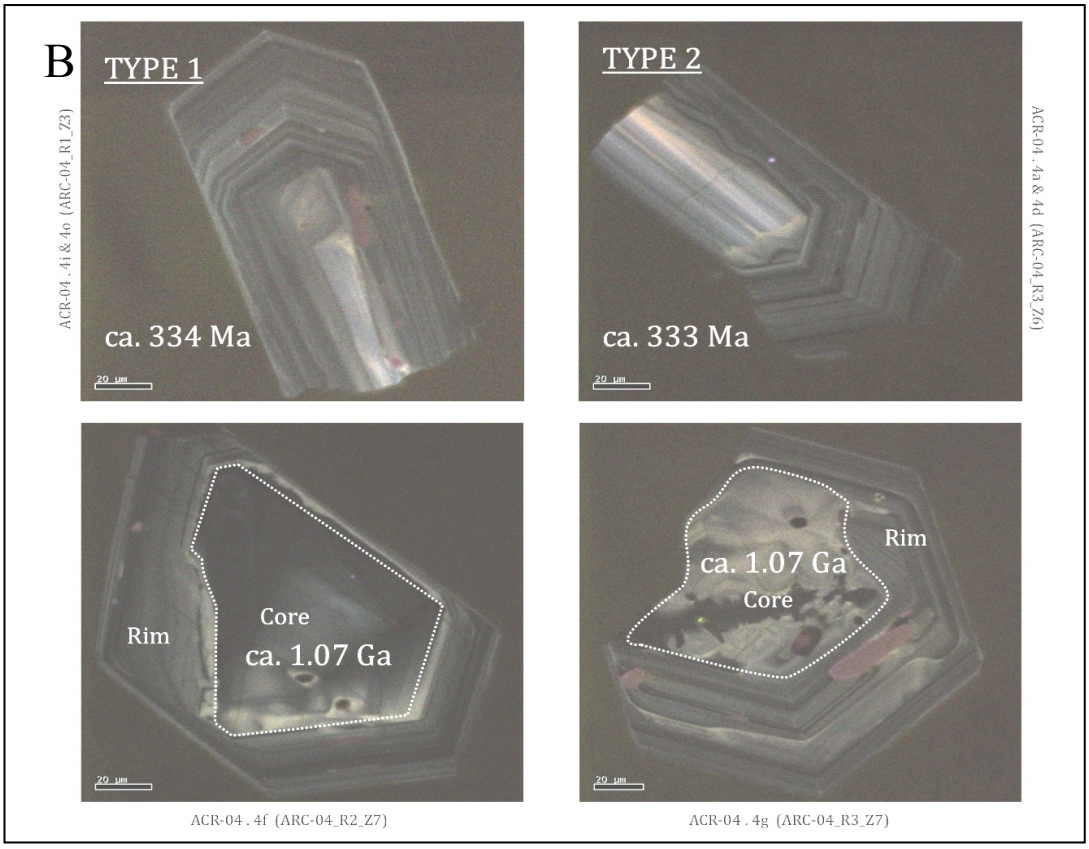
B
TYPE 1
ca. 334 Ma
20 µm
ACR-04 . 4i & 4o (ARC-04_R1_Z3)
TYPE 2
ca. 333 Ma
20 µm
ACR-04 . 4a & 4d (ARC-04_R3_Z6)
Rim
Core
ca. 1.07 Ga
20 µm
ACR-04 . 4f (ARC-04_R2_Z7)
ca. 1.07 Ga
Rim
Core
20 µm
ACR-04 . 4g (ARC-04_R3_Z7)

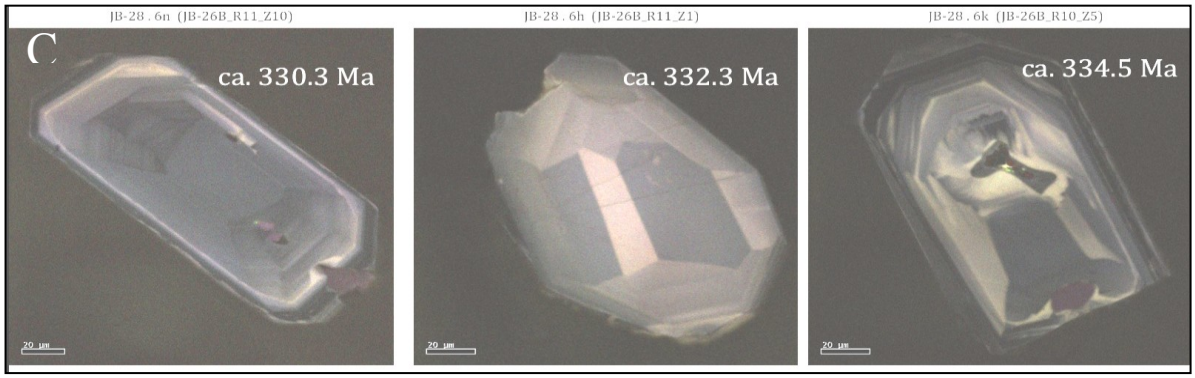
JB-28 . 6n (JB-26B_R11_Z10)
C
ca. 330.3 Ma
20 µm
JB-28 . 6h (JB-26B_R11_Z1)
ca. 332.3 Ma
20 µm
JB-28 . 6k (JB-26B_R10_Z5)
ca. 334.5 Ma
20 µm

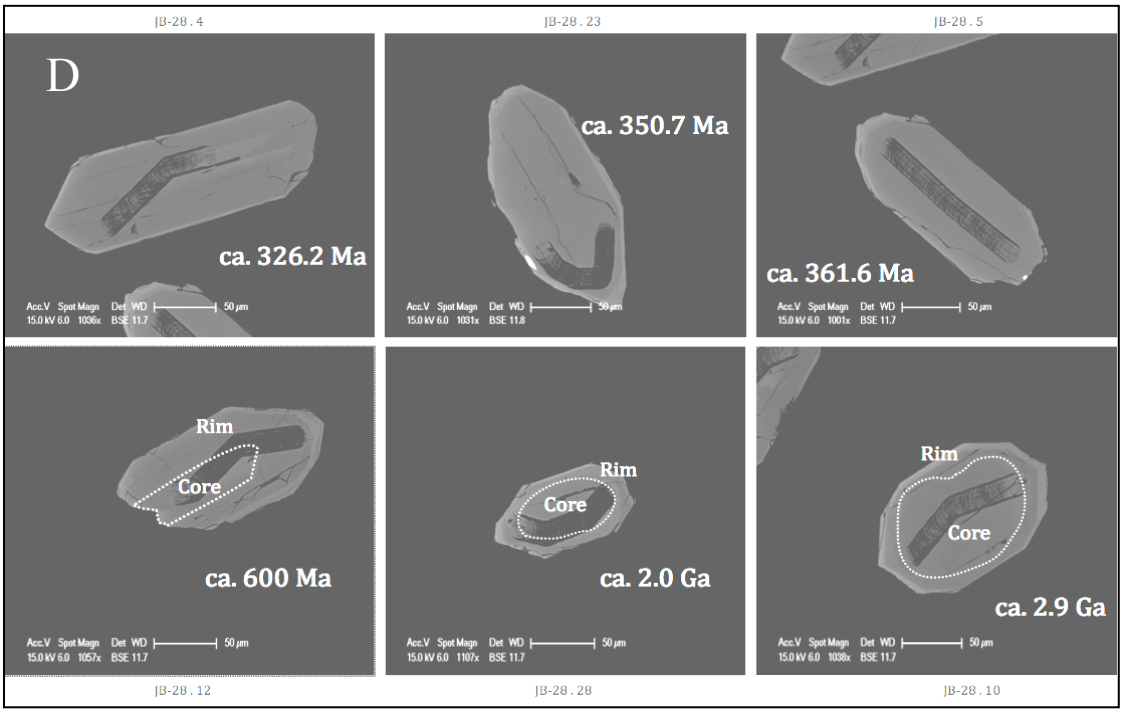

Fig. 4.7 SEM backscatter images of representative zircons in sample JAB-09. (b) Representative CL images of zircons in sample ACR-04. (c) Representative CL images of zircons in sample JB-26B. (d) SEM backscatter images of representative zircons in sample JAB-28. Dark lines in SEM images are the raster ionprobe analysis.

4.5.4. U-Pb Isotopic Data, Non-foliated Rocks.

Sample JB-26B is from an outcrop of non-foliated granodiorites exposed along a roadcut near the town of Castillo de las Guardas (Fig. 4.2). The granodiorite is composed primarily of quartz, plagioclase,K feldspar, biotiteand amphibole, with minorapatite, monazite, titanite, zircon and opaques. Zircons from sample JB-26B show a broad range of morphologies including (i) pale yellow slightly elongate, prismatic and multifaceted

(~40%) and (ii) clear, stubby, prismatic and multifacted (~30%) to (iii) magmatically resorbed (~15%) and (iv) multifaceted and fractured (~15%). CL imaging reveals most zircons contain complex zoning patterns with no inherited cores (Fig. 4.7c). Fourteen representative grains were analyzed from sample JB-26B. All yielded concordant or near concordant ages (<10% discordance) with a mean age of 330.8 ± 1.8 Ma.The U-Pb isotopic data (Table B.9) can be found in the appendixand are plotted in *Figure 4.8*.

Sample JAB-28 was collected from a granitoid that crops out near the town of Zufre (Fig. 4.2). The sample is non-foliated and composed primarily of quartz, plagioclase,K- feldspar, biotiteand muscovite.Most of the zircon grains (~70%) from sample JAB-28 are medium to large (100-200 μm length), euhedral to subeuhedral prisms. The grains range from translucent yellow-brown to turbid, and generally have inclusions and fractures. The remainders of the grains (~30%) are medium sized (~100 μm diameter), stubby to rounded. BSE imaging shows that the majority of zircons (~70%) show no zonation and the remainder (20%) have multifaceted elongate cores rimmed by thick overgrowths or are rounded un-zoned zircons rimmed by thin overgrowths (Fig. 4.7d). To determine both the age of igneous crystallization and the ages of potential inherited cores, line scans were performed across thirty representative grains (one analysis per grain).The U-Pb isotopic data (Table B.8) can be found in the appendixand are plotted in *Figure 4.9*. Of these thirty analyses, all yielded concordant ages. Analysis of multifaceted prismatic zircons and zircon rims (fifteen analyses) reveal concordant ages ranging from ca. 309 Ma to ca. 361 Ma. Ten analyses of multifaceted

zircon cores reveal concordant ages ranging from ca. 561 Ma to ca. 647 Ma and five analyses of rounded zircon cores with thin overgrowths yield concordant ages ranging from ca. 1989 Ma to ca. 2910 Ma (Fig. 4.9).

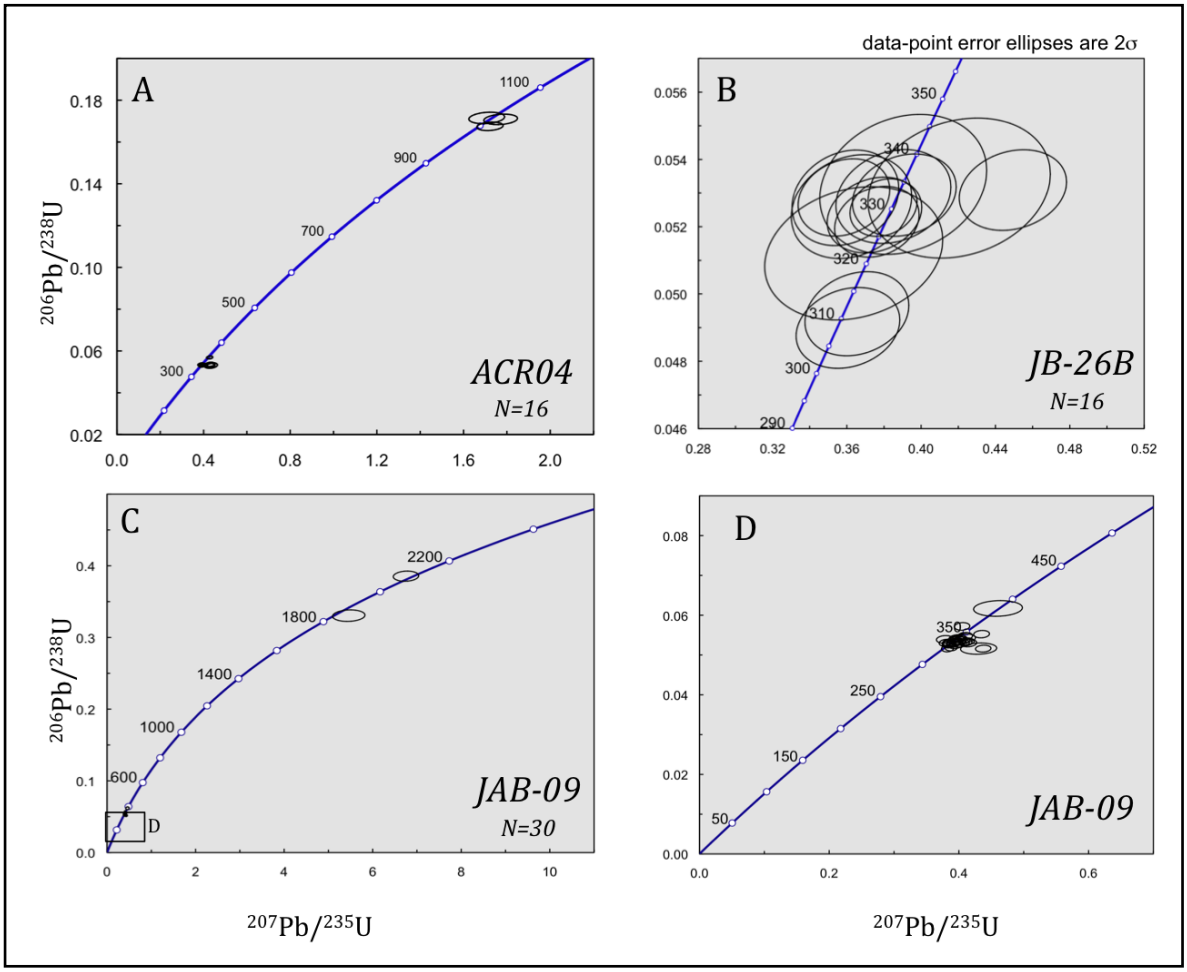

Fig. 4.8U-Pb concordia plot of samples (a) ACR-04; (b) JB-26B; (c) JAB-09; (d) Enlargement of concordia plot for Paleozoic zircons of sample JAB-09 (ellipses are 2σ).

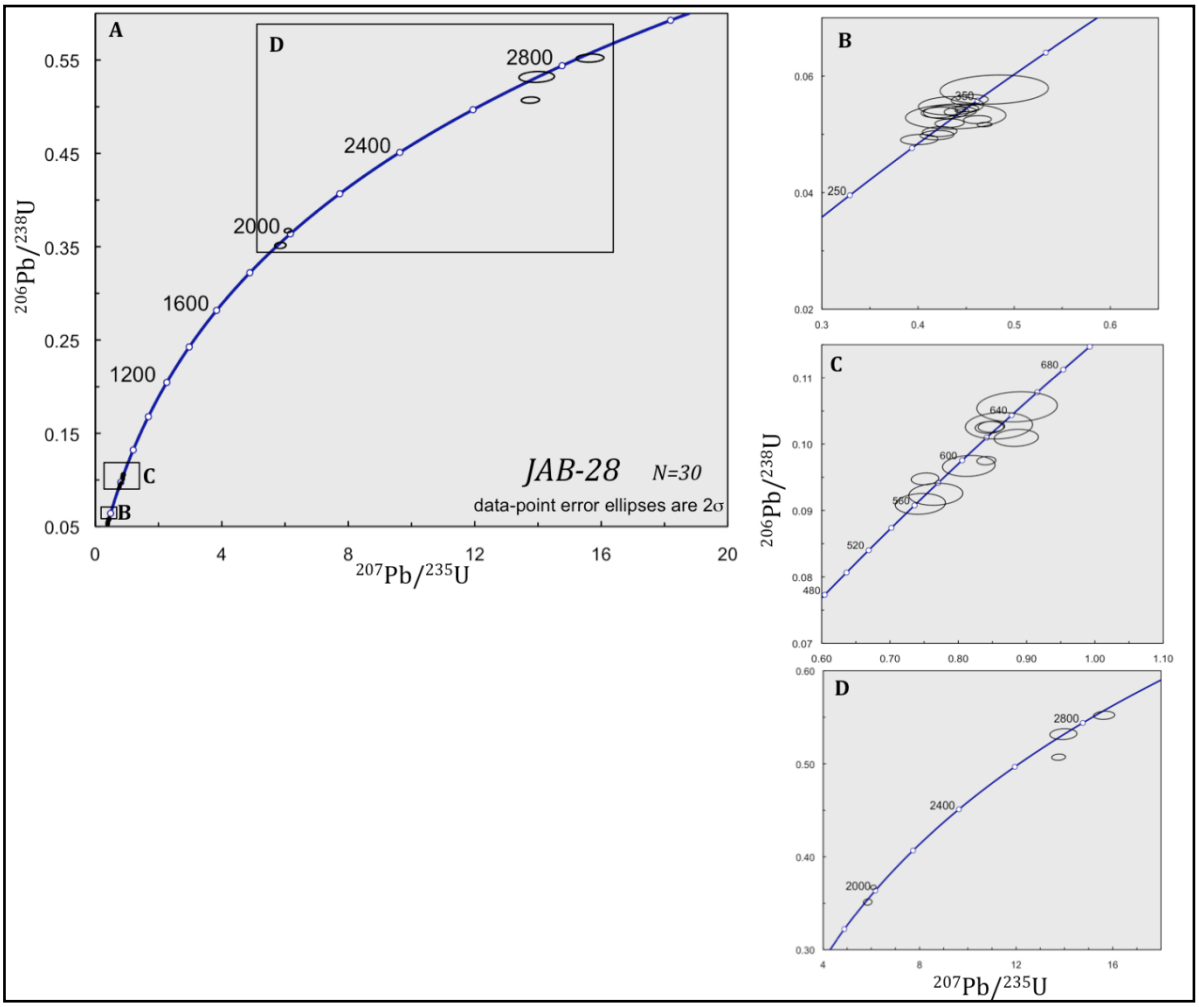

Fig. 4.9 (a) U-Pb concordia plot of sample JAB-28. (b) Enlargement of concordia plot for Paleozoic zircons. (c) Enlargement of Neoproterozoic to Cambrian zircons. (d) Enlargement of concordia plot for Paleoproterozoic to Archean zircons

4.6. Results~Sedimentary Units

4.6.1. Lithogeochemistry and Sm-Nd

SPZ

Twelve samples were selected from clastic rocks in the V2, V3 and purple shale (PS) horizon of the VSC and three samples were selected from the Late Devonian PQ group (JB-17, JB-24, JB-25) in the SPZ. These sedimentary units are all crosscut by the SNB. The major-and trace-element chemistry for theVSC and PQ rocks is given in table D.3 and Sm-Nd data in table C.3 of the Appendix.

Overall, major-oxide concentrations show large ranges in concentrations. One sample from the V2 contains nearly 100% SiO_2. In the other V2 samples, SiO_2 ranges from ~ 57 to 86 wt %, Al_2O_3 from trace amounts to ~ 20 wt %, TiO_2 from trace amounts to 1.07 wt %, CaO from 0.03 to 0.24 wt %, and Fe_2O_3 from ~4.2 to 10 wt %. By comparison, major element abundances in the V3 samples show a more restricted range in concentration with SiO_2 ranging from ~ 72 to 77 wt %, Al_2O_3 from ~10.8 to 13.7 wt%, TiO_2 from ~0.3 to 0.9 wt %, CaO from 0.05 to 0.3 wt %, and Fe_2O_3 from ~4.6 to 7.2 wt %. Major element geochemistry of the PS samples reveal SiO_2 ranging from ~ 64 to 65 wt %, Al_2O_3 from ~18.3 to 21.2 wt %, TiO_2 from ~0.7 to 0.8 wt %, CaO from 0.09 to

0.18 wt %, and Fe_2O_3 from ~7.3 to 7.7 wt %. PQ samples reveal SiO_2 ranging from ~ 54 to 74 wt %, Al_2O_3 from ~2 to 25 wt %, TiO_2 from ~0.23 to 0.96 wt %, CaO from 0.04 to 0.12 wt %, and Fe_2O_3 from ~6 % to 36 wt %.

In order to more fully document the geochemistry of the SPZ, published major element (40 samples) and REE data (5 samples) of the VSC (Boulter et al., 2004) are included on geochemical plots (Figs. 4.5b, 4.10). Complex patterns on plots such as log (SiO_2/Al_2O_3) vs. log (Na_2O/K_2O) VSC rocks (Fig. 4.10a) likely reflect alkali mobility during sedimentary processes such as weathering and diagenesis. On a Fe_2O_3 + MgO vs. Al_2O_3/SiO_2 diagram, the samples display a linear, positive correlation between Fe_2O_3 + MgO and Al_2O_3/SiO_2 (Fig. 4.10d). According to Bhatia (1983) this trend is indicative of an arc to active-margin to passive-margin signature, which could reflect the tectonic setting either of the strata or of the source rocks.

On a plot of Zr/Nb vs. Ti/Nb (Fig. 4.11a), VSC samples show a general trend of increasing Ti/Nb with increasing Zr/Nb and PQ samples display little variation in the Ti/Nb. On a Zr/Y vs. Ti/Y diagram (Fig. 4.11b) the VSC samples show a positive correlation between Zr/Y and Ti/Y. Similarly, on a Zr/V vs. Ti/V diagram (Fig. 4.11c), VSC samples lie on a trend of higher Zr/V with higher Ti/V.

Chondrite-normalized REE patterns for all SPZ samples (Fig. 4.5b) are moderately sloping and display moderate and relatively restricted LREE enrichment reflected in $(La/Sm)_n$ of 2.6-4.3. HREE generally display a flat profile with $(Gd/Lu)_n$ ranging from 0.94-1.72. All samples are characterized by a slight negative europium anomaly,

with[(Eu*/Eu) -1] of 0.17 (JAB-12, V3) and 0.84 (JAB-11, V2) (see inset Fig. 4.5b). Sample JAB-19 displays a negative Ce anomaly.

To facilitate comparison between formations, εNd values (relative to CHUR [chondritic uniform reservoir]) given in the text are for the same depositional age (t = 350 Ma). Taken together, the VSC samples are characterized by a wide range of εNd values. V2 samples range from -11.2 to -0.7, purple shale samples from -7.1 to -8.4 and V3 samples from -5.9 to -1.6 (Fig 4.6). On the other hand PQ samples show a relatively restricted range from -10.4 to –7.5.

PDLZ

Samples were selected from the polydeformed mélange, matrix and metasediments of the PDLZ (RSA-01, quartzite phacoid; RSA-02, matrix; and AC-03; quartzite) and siltstones from the overlying SIF (samples JAB-01, JAB-03, JAB-08). The major-element chemistry (*Table D.5*) for samples from the polydeformed PDLZ rocks displays high SiO_2> 85wt%, whereas SIF samples display SiO_2 between 70-80 wt%. TiO_2 in the PDLZ samples varies from 0.21 to 0.58 wt%, CaO from 0.04 to 0.13 wt%, Fe_2O_3 from ~2.5 to 3.5 wt%. Na_2O typically occurs in very low concentrations. By comparison, SIF samples are higher in TiO_2 (from ~0.8 to 0.9 wt%) and Fe_2O_3 (from ~4.6 to 6.7 wt%) and lower in CaO (from 0.02 to 0.04 wt%). On plots such as log SiO_2/Al_2O_3 vs. log Na_2O/K_2O PDLZ polydeformed rocks display extremely low Na_2O/K_2O (due to the very minor abundance of Na_2O in the samples) and a slightly negative correlation (Fig. 4.10a).

On the Fe_2O_3 + MgO vs. Al_2O_3 / ($CaO+Na_2O$) and the Fe_2O_3 + MgO vs. Al_2O_3 / SiO_2 diagrams (Figs. 4.10 b, c,) the rocks display more complex patterns suggesting alkali mobility during weathering. However on the Al_2O_3/SiO_2 vs. Fe_2O_3 + MgO diagram (Fig. 4.10d), the polydeformed PDLZ and SIF samples display increasing Al_2O_3/SiO_2 with increasing Fe_2O_3 +MgO. The relatively low Fe_2O_3 + MgO and Al_2O_3/SiO_2 in the PDLZ samples are typical of upper crustal rocks either deposited in, or derived from, a passive margin setting (after Bhatia et al., 1983).

On a plot of Zr/Nb vs Ti/Nb (Fig. 4.11a) PDLZ polydeformed samples (RSA-01, RSA-02, RSA-03) display a general trend of increasing Ti/Nb ratio with increasing Zr/Nb whereas SIF samples display a limited range in Ti/Nb and Zr/Nb. Alternatively, on a plot of Zr/Y vs. Ti/Y, SIF samples exhibit a positive relationship between Zr/Y and Ti/Y (Fig. 4.11b). On a plot of Ti/V vs. Zr/V both SIF and PDLZ polydeformed samples together display an increasing trend between Ti/V and Zr/V (Fig. 4.11c)

Chondrite-normalized REE patterns for the polydeformed PDLZ are gently sloping (Fig. 4.5c) and display moderate LREE enrichment with a relatively restricted range (La/Sm = 3.5–3.8). HREE display flat profiles as reflected in $(Gd/Lu)_n$ which ranges from 0.88-1.2. All polydeformed PDLZ samples also display a negative europium anomaly ([(Eu*/Eu) -1]=0.41-1.27).

Sm-Nd compositions of the olistostromal mélange and the metasedimentary rocks (RDL) are characterized by negative εNd values (calculated at T=350 Ma) (-0.9; metasediments), (-8.4; phacoidal quartzite) and (-6.8; phyllitic matrix) (Fig. 4.6) (Table

C.1).

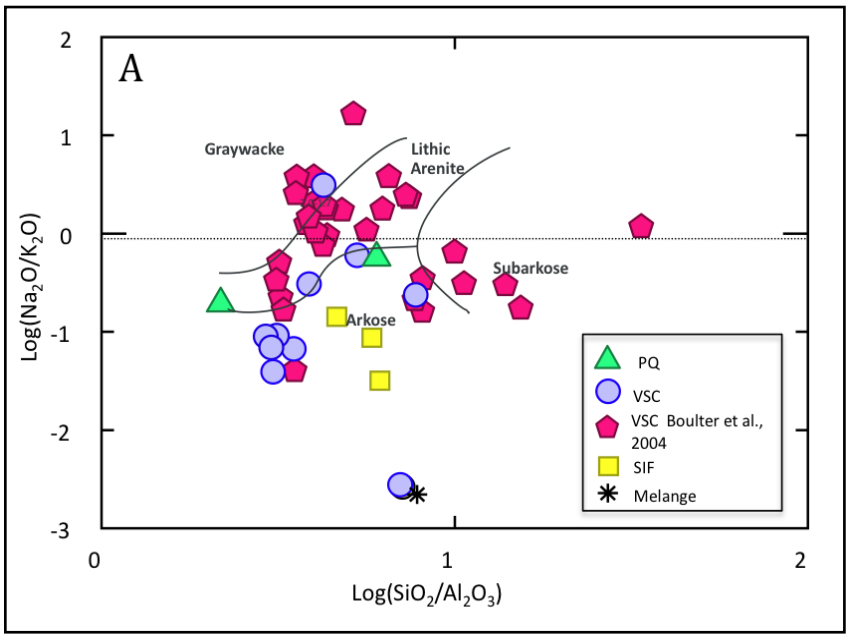
A
Graywacke
Lithic Arenite
Subarkose
Arkose
PQ
VSC
VSC Boulter et al., 2004
SIF
Melange
Log(Na2O/K2O)
Log(SiO2/Al2O3)

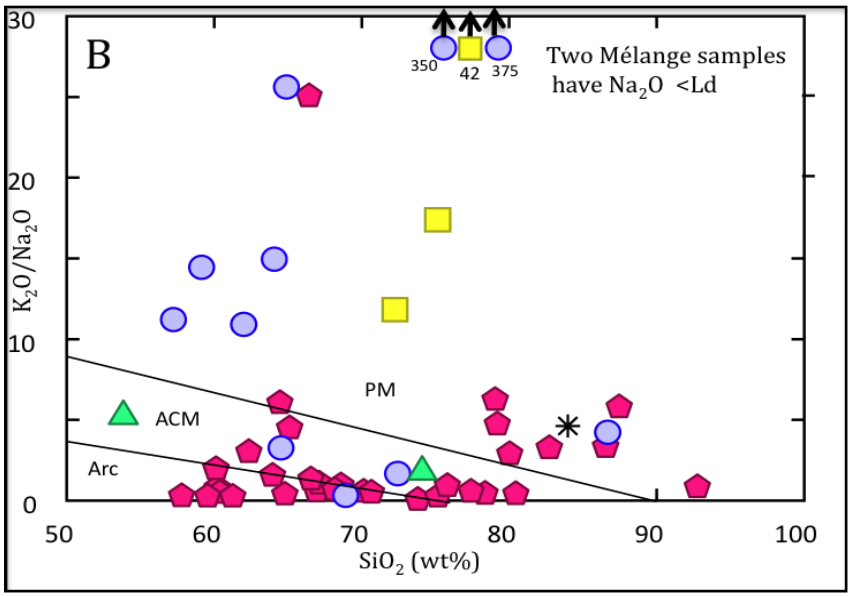
B
350
42
375
Two Mélange samples have Na2O <Ld
PM
ACM
Arc
K2O/Na2O
SiO2 (wt%)

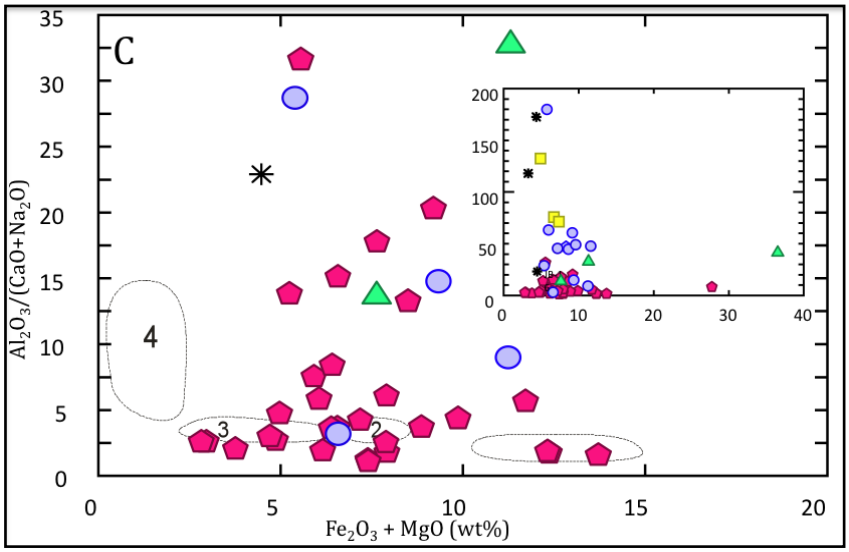
C
4
3
2
Al2O3/(CaO+Na2O)
Fe2O3 + MgO (wt%)

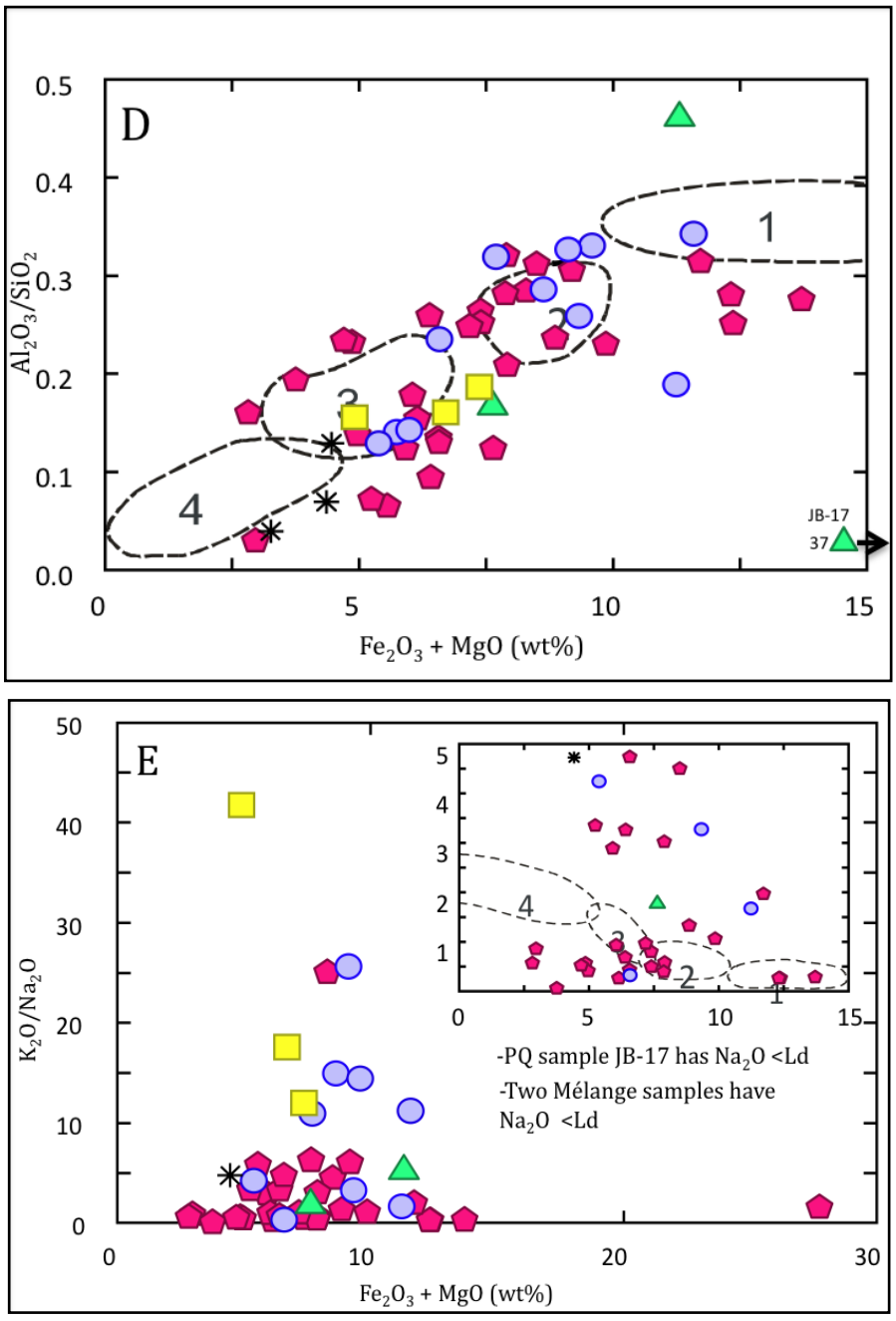

Fig. 4.10SPZ and PDLZ sedimentary rocks plotted on selected published discrimination diagrams emphasizing major element chemical variations: (A) log Na_2O/K_2O vs. log

SiO_2/Al_2O_3; (B) K_2O/Na_2O vs. SiO2 (after Roser and Korsch, 1986); (C) $Al_2O_3/(CaO + Na_2O)$ vs. Fe_2O_3 + MgO (after Bhatia, 1983); (D) Al_2O_3/SiO_2 vs. Fe_2O_3 + MgO (after Bhatia, 1983); (E) K_2O/Na_2O vs. Fe_2O_3 + MgO (after Bhatia, 1983). In B, ACM-active continental margin; PM-passive margin. In C, D, and E, 1-oceanic island arc; 2-continental island arc; 3-active continental margin; 4-passive margin.

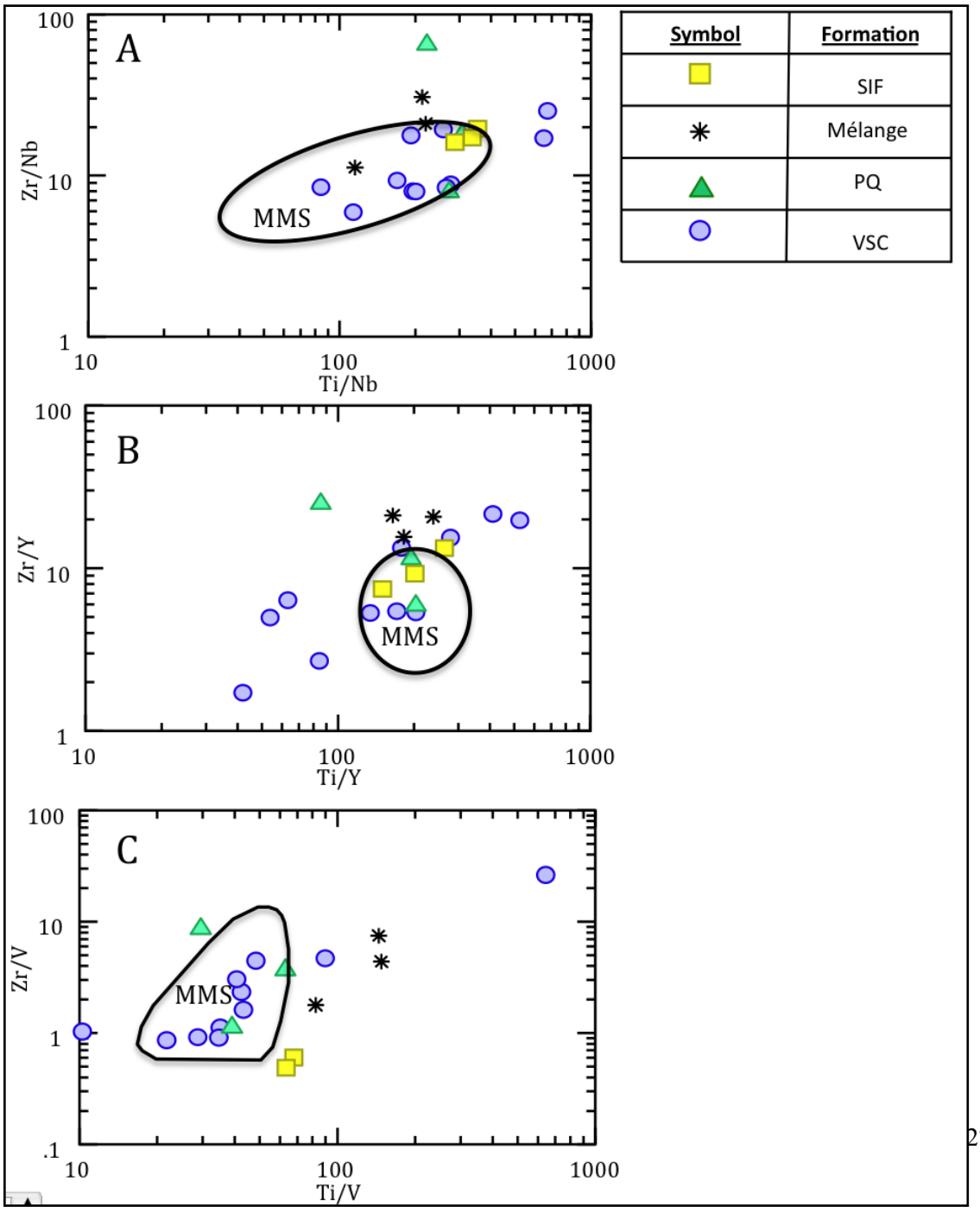

Fig. 4.11 Plots using interelement ratios of high field strength elements: (A) Zr/Nb vs. Ti/Nb; (B) Zr/V vs. Ti/V; (C) Zr/Y vs. Ti/Y. MMS—Meguma Group metasedimentary rocks.

4.7. Interpretation

4.7.1. Magmatic Age of the Sierra Norte Batholith

The youngest ages yielded by prismatic zircon crystals and rims indicate a concordant age ranging from 325.5 ± 1.74 Ma (sample ACR-04) to 333± 4.78 Ma (sample JAB-09) for the foliated Gil Márquez pluton, which within our uncertainty isindistinguishable from the U–Pb age on a late leucogranite dated by de la Rosa et al., 2001 (ca. 330 Ma). For the non-foliated rocks of the SNB magmatic ages range from 308.3 ± 3.03 Ma (sample JB-26B) to 309 ± 4.43 Ma (sample JAB-28) (Fig.4.8, 4.12). This range in age suggests the non-foliated rocks are younger than the foliated rocks (Gil Márquez pluton) and the batholith as a whole composite recording two main stages of magmatism.

4.7.2. Inherited Ages of the Sierra Norte Batholith

The zircon cores in SNB samples, which reveal ages ranging from ca. 561 Ma to 647 Ma in sample JAB-28, ca. 1075 Ma to ca. 1116 Ma in sample ACR-04 and ca. 1185 Ma in sample JAB-09 all display a multifaceted inherited core morphology (Fig. 4.7).

On the other hand, older Paleoproterozoic inherited cores with concordant ages of

ca. 2005 Ma (sample JAB-28) and ca. 2073 Ma (sample JAB-09) as well as Archean inherited cores with concordant ages of ca. 2759 Ma, ca. 2828 Ma, and ca. 2910 Ma in sample JAB-28 all display a well-rounded morphology (Fig. 4.7). Multi-faceted zircons are generally indicative of a magmatic protolith (e.g. Timmerman et al., 2000). Therefore most likely the protoliths for the multifaceted cores are igneous rocks whereas the rounded cores probably originated from sedimentary rocks containing late Paleoproterozoic and Archean detrital zircons. As a result the magmatic inherited cores in the SNB samples likely preserve zircons from the melting of SPZ basement, whereas the rounded zircon cores are xenocrysts probably derived from the Devonian-Carboniferous sedimentary rocks of the PQ or PDLZ (which both contain late Paleoproterozoic and Archean detrital zircons; Braid et al., *in press*). Furthermore most rounded inherited cores contain thin magmatic rims, in contrast with thicker well-zoned rims that occur on prismatic cores of Neoproterozoic age. These different morphological characteristics suggest that the rounded inherited cores are xenocrysts, which were likely incorporated into the melt from the adjacent host rock, late in the evolution of the pluton. The numerous Paleoproterozoic and Archean inherited cores in sample JAB-28 suggest that this sample was derived from a more evolved granite, which was contaminated by the upper crust of the PQ and / or VSC.

4.7.3. Sm-Nd Isotopes and Geochemistry of the Sierra Norte Batholith

The SNB samples display εNdvalues ranging from +1.4 to –9.6 and model ages ca.

0.76-1.8 Ga. One sample (JAB-27) with high $^{147}Sm/^{144}Nd$ (>0.165) also has a flat LREE profile, consistent with fractionation of accessory phase during crystallization of the granite melt, thereby invalidating T_{DM} calculations (Arndt and Goldstein, 1987). On average the bulk of the SNB samples have less negative εNd values (-3.0 to 1.4) than the PQ detritus (εNd ~ -7.5 to -10.4), the VSC detritus (εNd ~ 11.2 to -0.7) and the PDLZ detritus (εNd ~ -6.8 to -9.0). However, two samples (JAB-28 and JAB-27) display more negative εNd (-9.6 and -7.5 respectively) compared to the other SNB samples suggesting either melting of a relatively ancient basement or significant contamination from the upper crust.

Samples JAB 28 and JAB 27 have εNd signatures similar to the PQ group (which they crosscut) suggesting potential contamination from PQ detritus. Furthermore the presence of rounded Paleoproterozoic (ca. 2.0 Ga) and Archean (ca. 2.7-2.9 Ga) inherited cores in sample JAB-28 supports a late-stage crustal contamination. These zircon populations (ca. 1.8-2.3 and ca. 2.5-2.9 Ga) are also present in PQ detrital zircons samples (Braid et al., *in press*).

Taken together Sm-Nd and U-Pb data suggest that (i) the granitoid melts of samples JAB-28 and JAB-27 were contaminated by the overlying SPZ strata, and (ii) the source for the SNB was on average more juvenile than the sedimentary units. This relationship indicates the lower crust that melted to yield the SNB was not compositionally similar to the Devonian-Carboniferous continental detritus (PQ, VSC and PDLZ), but was instead derived from a more juvenile lower crustal source with model ages between ca. 0.9-1.2

Ga.

4.7.4. Relationship between the PDLZ and SPZ

Geochemical comparison of rocks involving interelement ratios of high field strength elements are especially significant because these plots are relatively insensitive to sedimentary processes that affect the modal abundance of the accessory phases in which these elements reside (McLennan et al., 1980). The geochemical signatures of the all SPZ rocks compared with PDLZ rocks show fundamental geochemical differences suggesting that derivation from a similar source is unlikely. On interelement ratio plots, PDLZ samples generally display a more restricted range in Ti/Nb, Zr/Y and Ti/Nb than detritus from the SPZ (Fig. 4.11). Chondrite-normalized REE patterns in the SPZ rocks compared to PDLZ mélange samples are characterized by higher REEs, especially Ce to Tb, and gentler HREE profiles. To a first order, differences in REE profiles suggest the PDLZ and SPZ detritus were not derived from the same source and support the exotic origin of the quartzite mélange and associated metasediments suggested by Braid et al., *in press*.

Within the SPZ, PQ samples generally display more restricted Ti/Nb, Zr/Y and Ti/Nb ratios than the VSC sedimentary rocks (Fig. 4.11). VSC sedimentary rocks also contain a wider ranger in εNd (-11 to -0.7) (Fig. 4.6) suggesting a variable contribution from more juvenile sources probably associated to coeval bimodal magmatic activity. On

the other hand, the PQ samples show a relatively restricted range (εNd ~ -6.8 to -9.0), suggesting detritus was derived from (on average) a much older source than in the VSC. In this case, the wide range in εNd values for the VSC detritus may be attributed to the variable isotopic characteristics of the source rocks (e.g. juvenile volcanics and more ancient sedimentary rocks).

4.8. Synthesis and Discussion

Taken together, geochemistry, Sm-Nd isotopes and zircon geochronology and morphology suggest that the SNB granitoids: (i) are the product of melting a Neoproterozoic (ca. 560- 650 Ma) to Mesoproterozoic (ca. 1.0 -1.2 Ga) basement source that (ii) in some cases were contaminated when they incorporated older detrital zircon xenocrysts from the rocks they intrude and (iii) are a product of melting a source which was isotopically more juvenile compared to the Devonian-Carboniferous SPZ and PDLZ strata.

Late Devonian paleogeographic reconstructions provide constraints for the SPZ provenance and show West Africa and Laurussia both flanking the Rheic Ocean and in relative proximity to the Iberian autochthon (e.g. Scotese, 2003). In addition, Braid et al., (*in press)* interpret the PDLZ as a displaced portion of the Laurentian margin that escaped towards a Rheic Ocean subduction zone at this time. Therefore potential candidates for the basement of the SPZ in the Late Devonian are: (i) Gondwana (Iberian autochthon or

West Africa) (ii) the PDLZ (which would have a Laurentia signature) or (iii) peri-Gondwanan terranes which lay along the outer Laurussian margin.

The West African Craton is generally characterized by Neoproterozoic (ca. 500 - 700 Ma) and ca. 1.9 – 2.1 Ga orogenic events (Pan African and Eburnian orogens) (Rocciet al., 1991; Boheret al.,1992; Potrelet al., 1998; Hirdes and Davis, 2002). Tectonothermal events of these ages are also recorded in the Iberian autochthon and together are reflected in the abundance of local sedimentary deposits with ca. 500-700 Ma and ca. 2.0-2.2 Ga detrital zircons typical of derivation from Gondwana (e.g. Martínez Catalán et al., 2004; Fernández Suárez et al., 2002; López-Guijarro et al., 2007). On the other hand Mesoproterozoic zircons are typically absent in the West African craton (Linnemann et al., 2002; Abati et al., 2010). As a result, Nance and Murphy (1996) and Linnemann et al. (2004) suggest that an abundance or lack of Mesoproterozoic zircon may be used as a diagnostic tool to differentiate terranes originally adjacent to West Africa.Paleoproterozoic tectonothermal events (ca. 2.0-2.2 Ga) typical of Gondwana are rare in eastern Laurentia (Rocci et al., 1991; Lerouge et al., 2006), which is instead dominated by Cambrian–Ordovician (ca. 440-550 Ma) (McNicoll et al. 2001), and Grenvillian (ca. 1.0-1.2 Ga) sources (e.g., Cawood et al., 2007; Hoffman, 1989).

The Avalon terrane, originated as one of several peri-Gondwana terranes that formed along the periphery of western Gondwana in the Neoproterozoic (Johnson and Van der Voo, 1986; Murphy and Nance, 1991; Keppie et al., 1996; O'Brien et al., 1996;

Murphy et al., 1997). Abundant Neoproterozoic (ca. 570-630 Ma) igneous rocks record tectonic activity on a margin of Gondwana, from which the Avalon terrane was rifted, probably in Cambrian time. Furthermore Murphy et al. (2000) suggest the formation of proto-Avalonian basement occurred at ca. 1.2-1.0 Ga. Avalonian derived rocks also typically have abundant Mesoproterozoic (ca. 1.0 Ga) detrital zircons (e.g. Keppie et al., 1998) and relatively juvenile Sm-Nd signatures (εNd ~+1 to -4 at T=350) (Murphy and Nance, 2002).

The Meguma terrane, the most outboard of peri-Gondwana terranes in North America, is principally characterized by a thick (>10 km) succession of Cambrian to Ordovician turbiditic meta-sandstones and slates (the Meguma Group). The Meguma Group sedimentary rocks typically display (on average) a relatively ancient source (εNd~ -8 to -12; T=370 Ma) (Clarke et al., 1997) and detrital zircon populations dominated by late Neoproterozoic (ca. 550-700 Ma) and early Paleoproterozoic zircons (ca. 2.0 -2.2 Ga) (Krogh and Keppie, 1990; Waldron et al., 2009). In some samples late Mesoproterozoic zircons occur (Waldron et al., 2009). Together, this age distribution is thought to indicate the Meguma terrane was originally located between Avalonia and West Africa, in the rift system along which the Rheic Ocean opened (Waldron et al., 2009).Although the basement to the Meguma Group is not exposed the geochemistry of ca. 375 Ma Meguma granitoid rocks (Clarke etal., 1988) and the geochemistry and mineralogy of lowercrustal xenoliths (Owen et al., 1988; Owen and Greenough,1991; Eberz et al., 1991; Greenough et al., 1999) suggest the Meguma terrane, in the Late

Devonian was underlain by 1.0-1.2 Ga juvenile basement similar in composition to Avalonia. As a result the Meguma terrane, as a whole, displays a rather unusual scenario where a comparatively juvenile basement is overlain by strata derived from a more ancient cratonic source.

When compared to the above potential sources for the SPZ basement the presence of Mesoproterozoic zircons in the primary SNB melt suggests that the basement to the SPZ is not West African. Furthermore the PQ clastics also contain a paucity of Mesoproterozoic detrital zircons (Braid et al., *in press*) indicating the West African craton was not a source for the Late Devonian cover in the SPZ. The PQ also contains an abundance of Paleoproterozoic (1.8-2.3 Ga) zircons, which are rare in Laurentia (e.g. Rocci et al. 1991) and lack the Cambrian–Ordovicianzircons that are typical Laurentia-derived sedimentary rocks (McNicoll et al., 2001). The Neoproterozoic (ca. 560- 650 Ma) and Mesoproterozoic (ca. 1.0-1.2 Ga) inherited zircons and the ca. 0.9-1.2 Ga model ages of the SNB granitoid samples, which are not crustally contaminated, are consistent with the main range of Avalonian magmatism (e.g. Murphy et al., 2000) and a basement source that is isotopically indistinguishable to the Avalon terrane (Fig. 4.12). However, the abundant Paleoproterozoic detrital zircons (ca. 1.8-2.3 Ga) (Braid et al., *in press*), the lack of ca 1.0 Ga zircons and time older model ages (ca. 2.0 Ga) from the PQ Group contrast sharply with typical of strata deposited on Avalonia or Avalonian derived rocks (εNd ~+1 to -4 at T=350) (Murphy and Nance, 2002). Therefore, although the SPZ basement displays an Avalonian-type signature, the basement and PQ clastics, together

are not consistent with derivation from one of West Africa, Avalonia or Laurentia sensu stricto. Taken together these data imply either (i) the PQ was not derived from the SPZ basement or (ii) the SPZ was derived from a crust with an Avalonian-type basement beneath strata derived from a more ancient cratonic source.

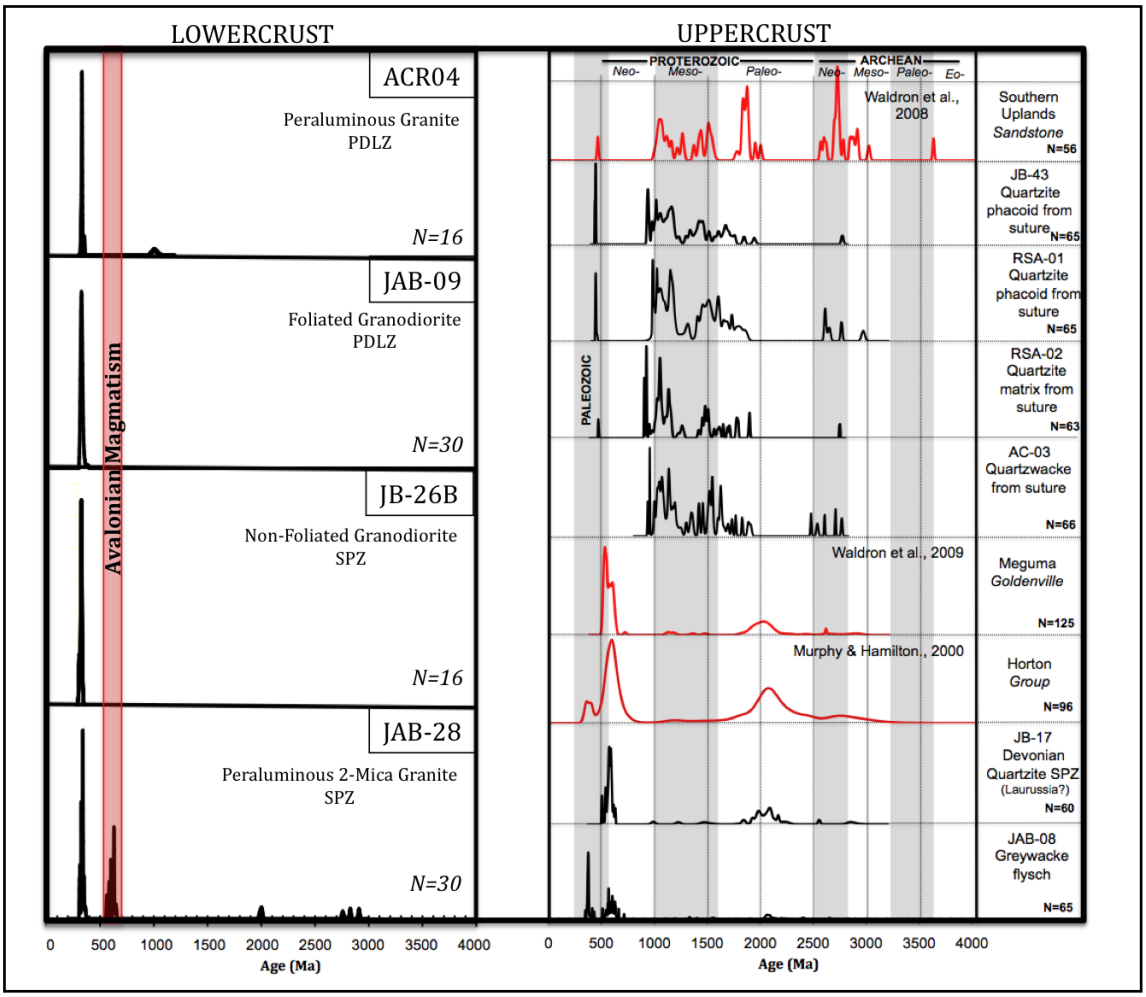

Fig. 4.12 Relative Probability Plots of U/Pb data from SNB granitoid samples compared with U-Pb detrital zircon relative probability distribution plots for samples from the PDLZ (suture) and the SPZ (Laurussia?) from this study compared with samples (highlighted in red) from Early Silurian Kirkcolm Formation of the Southern Uplands terrane of the British Caledonides (after Waldron et al., 2008), the Cambrian-Ordovician

Meguma terrane from the northern Appalachians (after Waldron et al., 2009) and the Devonian-Carboniferous Horton Group from the St. Mary's Basin of the northern Appalachians (after Murphy and Hamilton., 2000) (in red). Plots were generated by ISOPLOT (Ludwig, 2003).

Deposition of the PQ group and the VSC sediments in the Late Devonian is generally considered the result of local extension) in an intracontinental rift basin (e.g. Mullane, 1998; Quesada, 1998; Rosa et al., 2010). Therefore the local dominant source for the relatively immature sediments of the PQ was likely the SPZ basement (Mullane, 1998). If so, the SPZ is characterized by Late Devonian strata derived from Paleoproterozoic rocks (εNd=6.8 to -9) that were deposited above a relatively juvenile basement (εNd = +1.4 to –3.0) (Fig. 4.6).

This unusual relationship is similar to the relationship between the relatively juvenile basement and ancient upper crust documented in the exposed portion of the Meguma terrane in the northern Appalachians. Therefore a likely candidate for the derivation of Neoproterozoic (ca. 560- 650 Ma) and Mesoproterozoic zircons (ca. 1.0-1.2 Ga) in magmatic inherited cores of the SNB is basement equivalent to the peri-Gondwanan Meguma terrane. SNB Neoproterozoic and Mesoproterozoic inherited zircon ages and model ages are consistent with the relatively juvenile basement, which underlies the Meguma terrane in Atlantic Canada (Fig. 4.12). Furthermore, detrital zircons from the Late Devonian PQ of the SPZ reveal similar detrital zircon populations to the Cambrian-Ordovician Goldenville Group of the Meguma terrane and the Late Devonian Horton

Group that was deposited on the Meguma terrane at the same time as deposition of the PQ Group (Fig. 4.12). These data support a Meguma basement for the SPZ where the PQ group was deposited in basins and derived sediment locally.

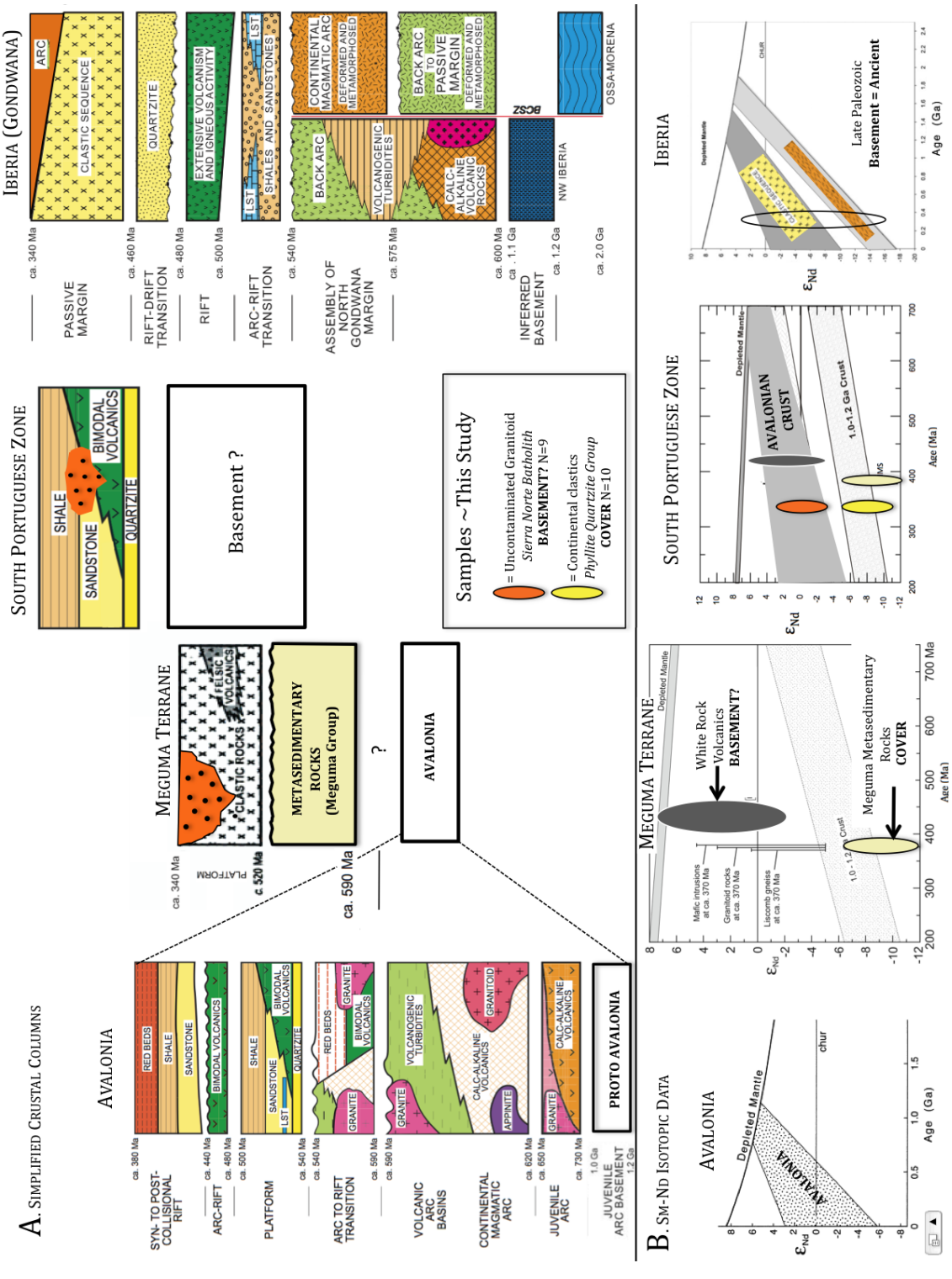

Fig. 4.13 (A). Simplified tectonstratigraphy of crustal blocks that bounded the Rheic Ocean in the late Paleozoic (modified from Nance et al., 2008). (B) Comparative analysis of Sm-Nd data from each crustal block; Avalonia field from Murphy et al., 2004; Meguma data from Macdonald et al., 2002; OMZ data from Lopez-Guijarro et al., 2008.

However the geochemical and isotopic differences of the PQ Group rocks compared to the VSC rocks suggest both suites were not directly derived from underlying basement rocks. When compared to the Meguma terrane metasedimentary rocks (Goldenville Group) the PQ rocks are broadly similar inTi/Nb, Zr/Y and Ti/Nb ratios, but VSC rocks show a somewhat wider range. These data support the detrital zircon data (Braid et al., *in press*), which indicate the Meguma terrane as a potential source for the PQ group. Taken together, geochemical and detrital zircon data suggest the PQ group may have been derived directly from Meguma terrane bedrock,whereas the VSC sediments were likely derived from a more heterogeneous source. This heterogeneity is likely a reflection of the contribution of the coeval mafic and felsic volcanics to VSC sediments.

The Meguma terrane extends offshore in Maritime Canada along the Scotian shelf where it is thought to be underlain by West African basement (Pe Piper and Jansa, 1999; Pe Piper et al., 2010). This interpretation is based largely on the geochemical signature of granitoid samples retrieved in drill core, which indicate a granite melt source (εNd ~-12; T_{dm}=1857 at T=375). These data contrast with the geochemistry of onshore Meguma terrane plutons and xenoliths of the lower crust, which generally indicate derivation from a younger more juvenile basement (e.g. Eberz et al., 1991) similar to the εNd of the basement signature of the SPZ and Avalonia.

Taken together, these interpretations imply that either (i) the basement to the Meguma terrane is highly variable in composition switching across strike from more juvenile to more ancient and back to juvenile or (ii) the SPZ is along strike of a lateral equivalent of the portion of the Meguma terrane that was close to the suture zone between Meguma and Avalonia (Fig. 4.13). However late Paleozoic reconstructions show that the OMZ and the orogen parallel shear zones (e.g. South Iberian Shear Zone, Badajoz Cordoba Shear Zone) in the Variscan belt were roughly perpendicular to the contact between the Meguma terrane and Avalonia in Maritime Canada (e.g. Braid et al., 2010 in press; Woodcock et al., 2007). Therefore we suggest the latter scenario is more likely, where the SPZ is a lateral equivalent of the onshore Meguma terrane in Maritime Canada rather than an eastward correlative of offshore Meguma crust (Fig. 4.13).

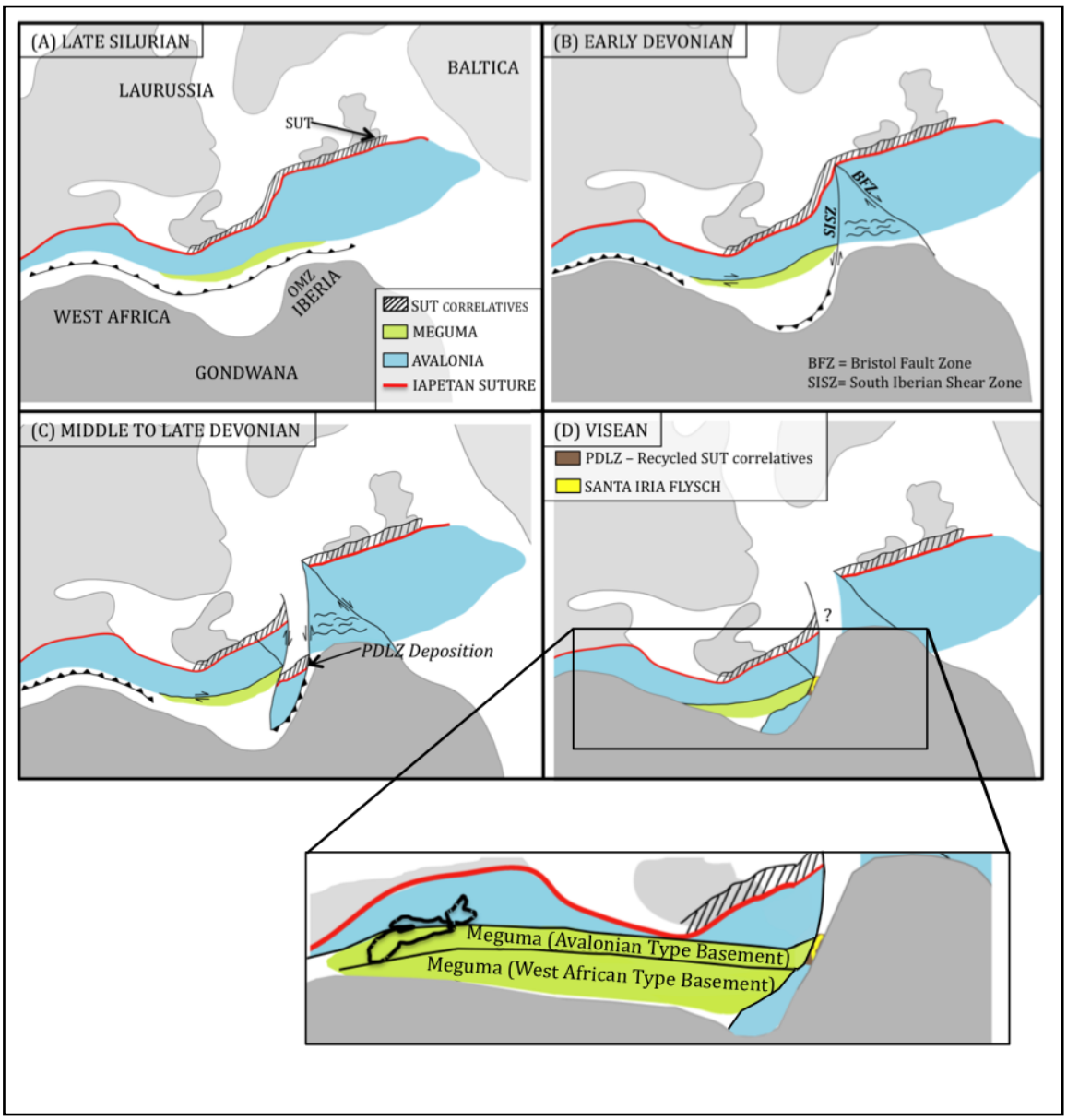

Fig. 4.14 Tectonic model showing juxtaposition of the Iapetan suture and a Southern Uplands equivalent crustal block with the OMZ assuming juxtaposition of the OMZ with West Africa (e.g. Robardet, 2003) and the Bay of Biscay closed (e.g. Ries, 1978) (a) Late Silurian closure of the Rheic Ocean (b) Early Devonian collision of the Iberian

promontory with the British Caledonides (c) Late Devonian-Early Carboniferous excision of a crustal fragment toward a Gondwana re-entrant with associated local extension and deposition of the PDLZ (d) Visean juxtaposition of the SPZ, PDLZ and OMZ and deposition of the Santa Iria flysch. Inset showing the along strike equivalent of onshore Meguma terrane adjacent to southern Iberia in the Late Devonian (after Braid et al., *in press*)

4.9. Acknowledgements

The support of theNatural Sciences and Engineering Research Council, Canada throughthe PGS-D grant to JAB and Discovery grants to JKM and JBM and Research Capacity grants toJBM. JAB also acknowledges the support of the Dalhousie Killampredoctoral scholarship program and to St. Francis Xavier University Councilfor Research grants to JBM.

CHAPTER 5

DISCUSSION AND CONCLUSIONS

5.1 Regional Geologic Constraints

This thesis has contributed to the understanding of southern Iberian regional geology in the following ways:

(i) U/Pb zircon geochronology and Sm/Nd isotopic data demonstrate that the composition of the SPZ is different than that of Gondwana suggesting that the SPZ was likely exotic with respect to Gondwana in the late Paleozoic, a subject which has been extensivelydebated in the literature;

(ii) U/Pb zircon geochronology (chapter 3) demonstrates that the PDLZ, which was previously considered an accretionary prism derived from the SPZ plate, is also exotic with respect to Gondwana and the SPZ;

(iii) U/Pb zircon geochronology indicates the maximum depositional age of the Santa Iria flysch is ca. 347 Ma and the age of the crosscutting Gil Márquez pluton is 325.5 ± 1.74 Ma. Together these data provide age constraints on the

spatial juxtaposition of the OMZ (Gondwana) and the SPZ in the late Paleozoic;

(iv) Detailed mapping provides the first in-depth structural analysis of the PDLZ and demonstrates that lithotectonic domains in the PDLZ were deformed as the result of strain compartmentalization during oblique subduction.

5.2. Implications of Regional Geologic Constraints

5.2.1. Complexities in Accretionary Systems in Oblique Collisional Settings

Relevant conclusions of this work

- The PDLZ was derived from neither the upper nor lower plates but rather a far travelling crustal fragment inboard of the Rheic suture.
- The PDLZ structures show highly compartmentalized strain during oblique collision

Discussion

Most accretionary complexes are typically analyzed within a 2-D framework, including previous analysis of the PDLZ in southern Iberia (e.g. Eden, 1991; Giese et al., 1997) an approach that influenced the understanding of the geodynamic evolution of the orogen. This thesis reveals two important attributes of the PDLZ that provide additional

insights into how accretionary systems evolve in three dimensions. First, the PDLZ is characterized by highly compartmentalized deformation, where bounding faults between lithotectonic units control deformation of subordinate levels. Second, detritus in the PDLZ was derived from a crustal fragment, which traveled toward the subduction system beneath the OMZ. In this case the characteristics of the PDLZ suggest that in oblique subduction and collisional settings, with the existence of promontories and re-entrants along a continental margin involved in the collision, accretionary prisms are not necessarily simply derived from the upper or lower plates. Instead excision of crustal blocks along the peripheries of promontories have the potential to deliver crustal fragments as well as detritus from crustal fragments, which were once located in crust which was inboard of the margins of a closing oceanic basin (i.e. Rheic). Furthermore these processes also result in intense strike-slip shear parallel to the orogenic grain. In the case of the PDLZ, what was previously interpreted as a simple off-scraping of sediments from the lower plate during Variscan subduction of the Rheic Ocean is a complex process of involving excision of crustal blocks and juxtaposition of lithotectonic units with variable provenance. The PDLZ contains three groups of lithotectonic units, which may have variable provenance:

(i) a mafic mélange (provenance unknown)

(ii) a quartzite mélange and metasediments (exotic origin)

(iii)a flysch sequence (derived from the upper and lower plates)

Identifying similar scenarios where portions of a so-called accretionary prism are exotic facilitates comparison between exotic units and units derived locally (e.g. SIF). By comparing the timing of deposition of overlying units to exotic units, the timing of collision between two continental landmasses can be tightly constrained. In the case of the PDLZ, because of the exotic nature of the mélange and metasedimentary rocks, the maximum depositional age (ca. 347 Ma) of the flysch (which displays local derivation) provides an upper age constraint on the juxtaposition of the SPZ and OMZ.

Suggestions for Further Work

- *More detailed petrographic and provenance study of the PDLZ to more tightly constrain its original protolith prior to recycling.*

- *Detailed U-Pb, Isotopic and sampling along strike of the PDLZ (along the Rheic suture) to identify other potential allochthonous units. These data will help constrain the extent, geometry and timing of the tectonics associated with transport of the PDLZ.*

5.2.2. Implications and Relationship of the Tectonic Development of Southern Iberia to the Variscan Orogen

Relevant conclusions of this work

- The SPZ basement is possibly an equivalent to a correlative of the onshore Meguma terrane in Maritime Canada
- Structural analyses show no Late Carboniferous to Permian re-activation along major structures

Discussion

The SPZ is typically correlated with the Rheno-Hercynian domain of the Iberian-Armorican arc, which delineated the outer arc of the Variscan macrostructure (Fig. 5.1). The existence of this arc has provided a template for tectonic studies in the Variscan orogen for more than 20 years. This interpretation is based on (i) the correlation of the BAO with the Lizard ophiolites and (ii) the correlation of Late Devonian to Carboniferous deposits of Iberia of coeval "Avalonian" strata of southern Britain and northern Europe (e.g. Franke, 2000).

However, the results of this thesis suggestcorrelation of the SPZ with an along strike equivalent of the Meguma terraneof the northern Appalachians and imply the SPZ cannot be directly linked with the foreland basin deposits of the Rheno-Hercynian zone on the northern limb of the Iberian-Armorican arc. In addition, a recent ca. 334 Ma age of crystallization for the BAO (Azor et al., 2008) suggests the BAO formation occurred during the final stages of continent-continent collision and isconsiderably younger than the formation of the lizard ophiolite (ca. 397 $\pm$ 2 Ma, U-Pb, zircon; Clark et al. 1998).

The along strike correlation of the exposed portion of the Meguma terrane with southern Iberia is also consistent with Late Devonian paleogeographic reconstructions which place southern Iberia adjacent to Maritime Canada during the formation of Pangea (e.g. Scotese, 2003). This interpretation implies that after the opening of the Atlantic Ocean southern Iberia (SPZ) was not rotated significantly. Paleomagnetic data, however, suggests that SPZ delineates the southern limb of the Iberian-Armorican arc, which was formed by Late Carboniferous to Early Permian thick-skinned oroclinal bending (Weil et al., 2010; Gutiérrez-Alonso et al., 2008; Weil et al., 2002). At the core of this arc the Cantabrian Asturias Arc (CAA) displays apparent folding of over 180 degrees (Fig. 5.2).

As a result, a complete tectonic evolution of the Iberian-Armorican arc from the Late Devonian through to the Permian requires re-evaluation. Any new model should consider the ramifications of (i) the apparent correlation of the SPZ with the Meguma terrane (ii) the discontinuity of the Rheno-Hercynian zone from the southern to northern limb of the arc and (iii) the apparent post-Variscan folding of the orogen. Furthermore the contrasting orogen-scale Early Devonian strike-slip tectonics recognized on the northern and southern limbs of the arc (SISZ, BFZ) are consistent with tectonics associated with the collision of a Gondwanan promontory with Laurussia. Excision of crustal blocks during this collision is also suggested by the juxtaposition of Laurentian deposits along the Iapetan suture with the OMZ (which were re-deposited as the PDLZ) (Fig 5.2). Alone, the oroclinal bending model does not explain the highly transpressional strain regime in both limbs of the arc since the inception of Variscan

convergence,suggesting that probably both models are not exclusive but rather complementary of each other.Together these observations suggest that the Gondwanan margin prior to collision with Laurussia was at least not entirely linear.

The tectonic development of the Iberian-Armorican Arc, therefore, appears to be the result of both a pre-collisional Gondwanan promontory and post-collisional oroclinal bending. As a result the geologic evolution of the belts which define the arc were likely originally linear, whereas the continental margin defined a Gondwanan promontory. Post-collision bending, however, likely affected only part of the orogen as the SPZ is tectonically severed from the interior of the Iberian-Armorican arc and major structures bounding the SPZ (i.e. SISZ) show no evidence of Late Carboniferous to Permian reactivation. As a result, the southern limb of the arc was tectonically isolated from the core of the arc (CAA). This isolation was likely accommodated by movement along pre-existing shear zones (i.e. Badajoz Cordoba shear zone; South Iberian Shear Zone) (Fig 5.2). In this case the SPZ was isolated from the Iberian-Armorican arc during Late Carboniferous to Permian shortening in the core of the arc, and remained along strike of the Meguma terrane in Maritime Canada.

Suggestions for Further work

- *Further study of the Badajoz-Cordoba and associated orogen-parallel shear zones is needed to confirm Early Permian reactivation and test this model.*
- *The correlation of Meguma with maritime Canada implies that the geometry of the Iberian-Armorican arc is a result of a combination of complex shuffling of tectonic blocks, as well as oroclinal bending. U-Pb detrital zircon studies are needed from the northern limb of the arc to test for shuffling of crustal blocks associated with collision of a Gondwanan promontory.*

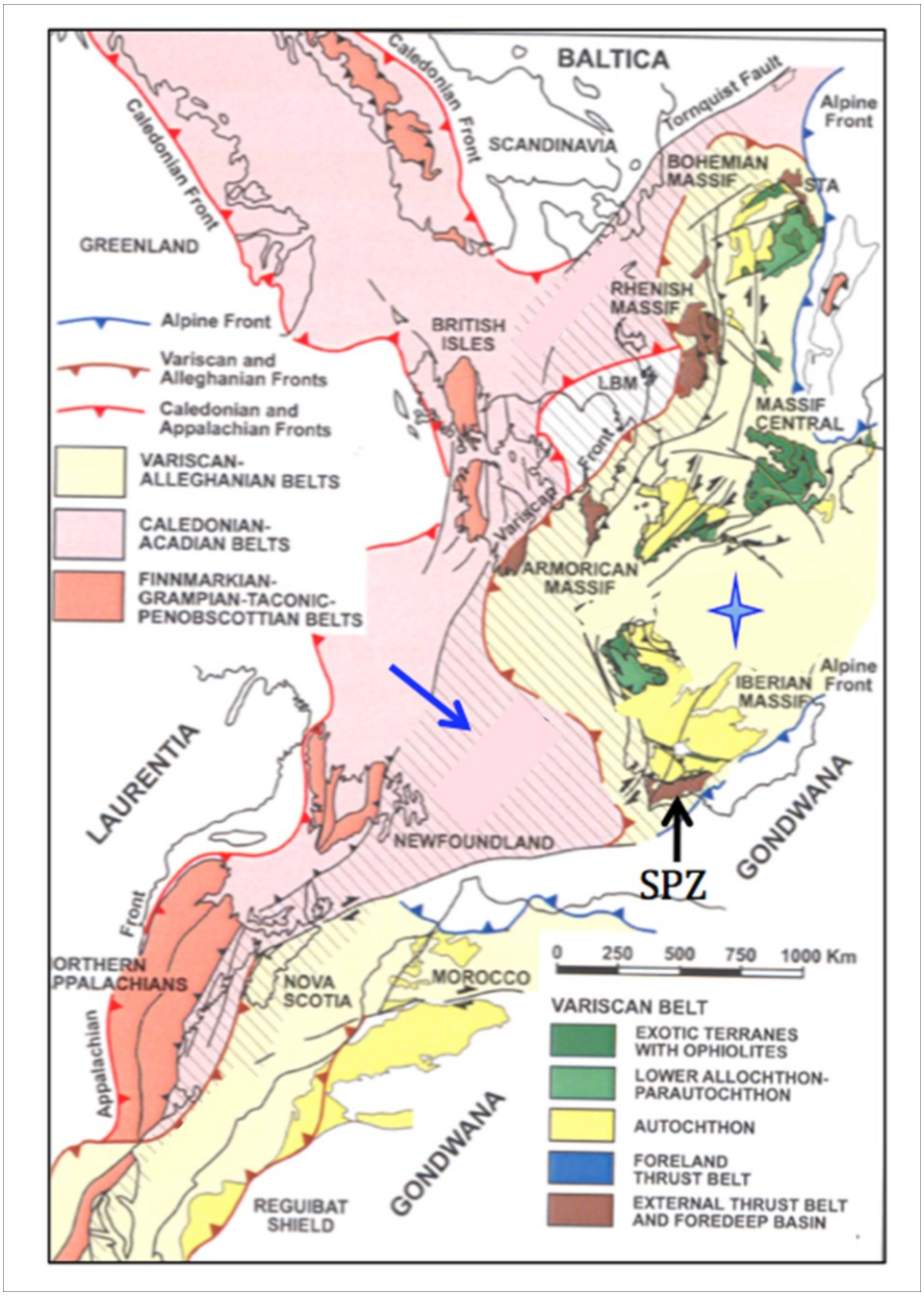

Fig 5.1 Reconstruction showing the position of Iberia and the SPZ in relation to the Appalachian, Caledonide and Variscan belts at the end of Gondwana / Laurussia convergence. Blue star = site of the future core of the Iberian-Armorican arc (following Late Carboniferous bending). Blue arrow shows excision of Laurussian crust towards a Gondwanan re-entrant. (Modified from Martinez Catalan et al., 2002).

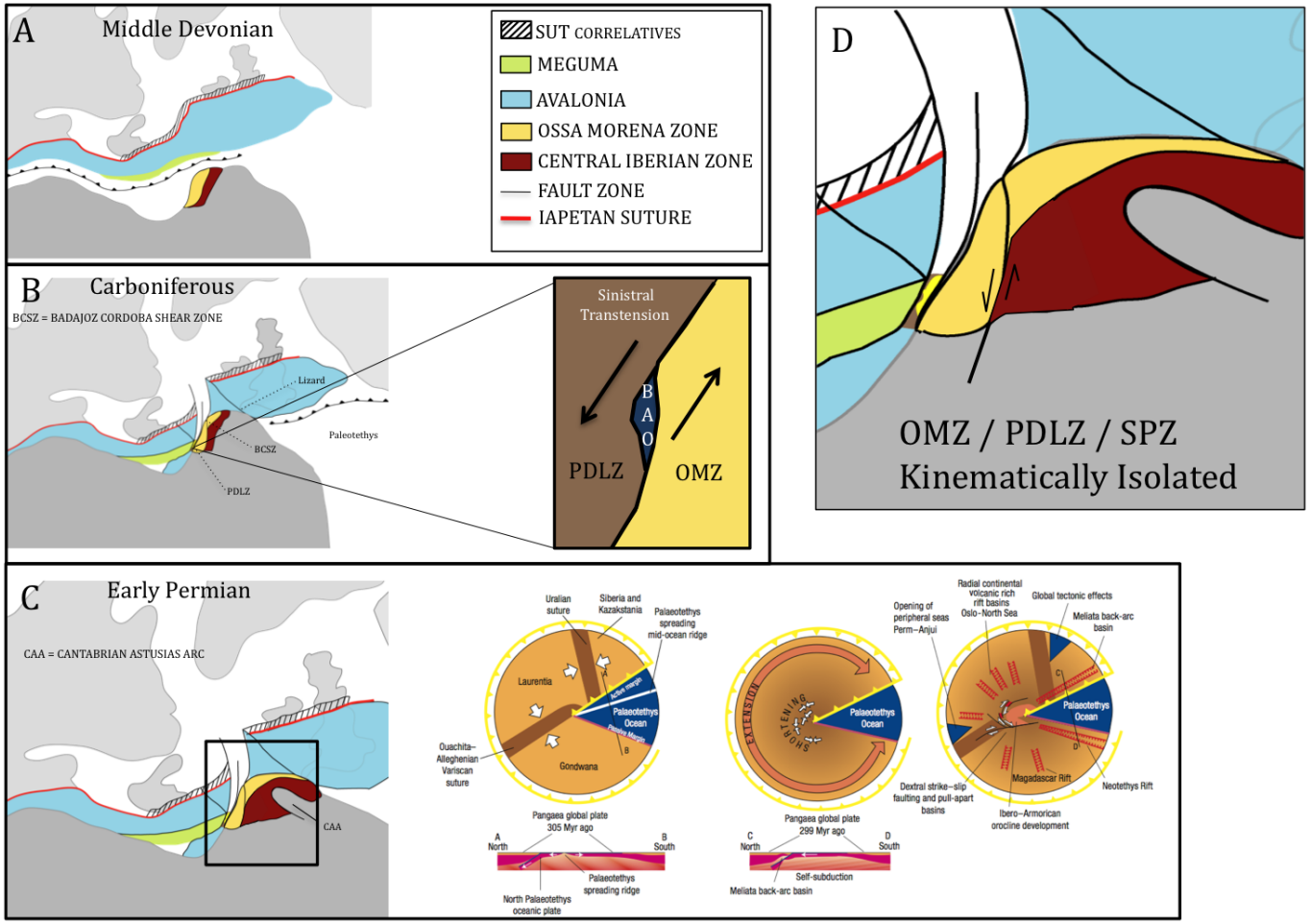

Fig. 5.2 Simplified reconstruction showing the proposed tectonic evolution of the Ibero-Armorican arc. (A) Devonian closure of the Rheic Ocean (B) Impingement of an Iberian indenter into the Laurussian margin and lateral escape of Silurian-Ordovician crustal block from the Iapetan suture. This escape nucleated along orogen-parallel shear zones(e.g. South Iberian Shear zone), which likely produced the BAO in a transtensional setting. (C) Oroclinal bending of the OMZ and CIZ during closure of the Paleotethys as proposed by Gutierrez-Alonso et al., (2008). (D) During this bending the PDLZ and SPZ were kinematically isolated from the event that formed the orocline.

5.2.3. Preferential Extrusion of Pre-Existing Suture Zone in Indenter Style Collisional Orogenesis

Relevant conclusions of this work

- The PDLZ was likely derived from part of the Iapetan accretionary complex between peri-Gondwana and Laurentia. This derivation implies excisions of a crustal block containing these accretionary deposits toward a Gondwanan re-entrant.

Discussion

The PDLZ was classically considered as an accretionary prism deriving its detritus from the lower plate (SPZ) during Pangean amalgamation (e.g. Eden, 1991; Giese et al., 1999). However, detrital zircon U-Pb data (Braid et al., in press; chapter 3 *this study*) demonstrates that part of the PDLZ (polydeformed) records a long-lived tectonic history and likely traveled as an excised crustal fragment far from its original source.

Thismovement appears to have nucleated along the pre-existing boundary between peri-Gondwanan terranes and Laurentia (Iapetan suture), which would provide the appropriate crustal weakness. Similar processes are well documented in modern orogens. For example in the Mediterranean the Mesozoic-Cenozoic tectonic escape of the Anatolian microplate is accommodated largely by deformation of the weak Anatolian

accretionary collage between the southern margin of the Eurasian Plate and the Arabian Plate (e.g. Piper, 2008). In terms of the closure of the late Paleozoic collision between Gondwana and Laurussia, the intervening suture zones between peri-Gondwana terranes and Laurentia would have been favorable for nucleating the excision of a crustal block. In this scenario, similar to the Anatolian accretionary collage, suture zones and accretionary prisms marking the closure of the Iapetus Ocean (e.g. southern uplands terrane) would havemoved toward a tectonic free face along the re-entrant between West Africa and Iberia. This movement was marked by dominant Devonian-Carboniferous dextral tectonics in Atlantic Canada and sinistral tectonics in the British Caledonides (Fig. 5.3).

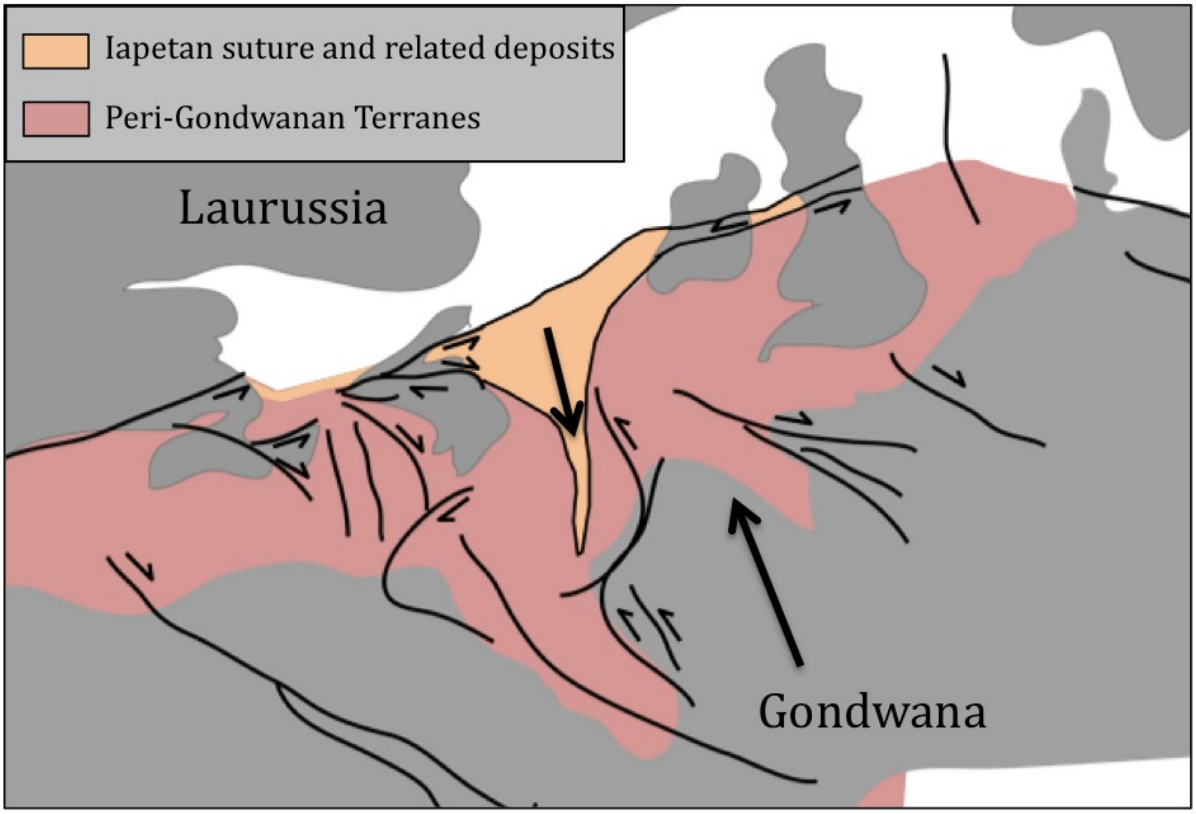

Fig. 5.3 Simplified Late Devonian- Carboniferous reconstruction showing movement of structurally weaker Iapetan suture zone deposits toward a Gondwana re-entrant (modified from Simancas et al., 2005; Braid et al., *in press*).

Suggestions for Further work

- *More geochronological data is needed from other accretionary- type deposits along strike of the PDLZ to test for exotic provenance*
- *Offshore data is needed from the Continental shelf near the interface with oceanic lithosphere to test for structural discontinuities and Laurentian-type deposits.*

5.2.4. Timing of the formation of Pangea

Relevant conclusions of this work

- The regional expression of collision between the SPZ and Gondwana (OMZ) can be bracketed between ca. 347 Ma (the maximum age for deposition of the flysch) and ca. 325 Ma (the age of the foliated granite which crosscuts the flysch)
- The SPZ basement can be correlated with a lateral equivalent of the Meguma terrane in Maritime Canada.

Discussion

Like in any supercontinent formation involving non-linear margins (i.e. promontories and re-entrants) the collision of Gondwana and Laurussia resulted in variations in the timing of collision as recorded by regional geologic sequences around the Pangean suture zone. However it is generally considered the final closure of the Rheic occurred by the Early Visean (e.g. Nance et al., 2010).

The correlation of the SPZ with the onshore Meguma terrane provides an important insight into the timing of Rheic closure in the Appalachians as well as the timing of the Variscan Orogen. Reconstructions show that the OMZ of southern Iberia, in the late Paleozoic, was located on the margin of a re-entrant between an Iberian and a North African promontory. To a first order, the movement of crustalblocks toward this re-entrant likely resulted in the juxtaposition of the SPZ with the PDLZ and OMZ. However this re-entrant would also be one of the last ocean basins to close between the

northern Appalachians and the Variscides in Europe. As a result the ca. 325 Ma Gil Marquez Granodiorite, which crosscuts both the PDLZ flysch deposits (ca. 347 Ma) and the SPZ, potentially provides an upper age constraint on the collision between Gondwana and Laurussia. In this case, the final closure of the Rheic occurred much earlier than has been suggested (e.g. ca 300 Ma; Pe-Piper et al., 2010 or Early Permian; Nance et al., 2010) and younger granitoid bodies in the Meguma are the result of post collisional processes associated with crustal thickening and/or extension.

5.2.5. Geometry of the Formation of Pangea

Relevant conclusions of this work

- The SPZ basement is an along strike correlative of the Meguma terrane in Maritime Canada.

Discussion

The Wegenerian configuration of Pangea, also known as Pangea 'A', is the generally accepted paleogeographic geometric arrangement in the Early Jurassic just prior to opening of the North Atlantic (e.g. Muttoni et al., 2003). The earlier history of Pangea in the late Paleozoic is, however, still debated since the introduction of the Pangea 'B' model (Irving, 1977). Paleomagnetic analyses demonstrate that a substantial amount of overlap of continental crust would have occurred in the Early Permian

between Gondwana and Laurasia if reconstructed in a Pangea 'A' configuration (Muttoni et al., 1996). The overlap could be eliminated by sliding Gondwana along lines of latitude to the east with respect to Laurasia, which would maintain the coherence of the paleomagnetic poles. This modification results in a Pangea 'B' configuration which markedly differs from the Wegenerian Pangea 'A' and places South America (and Africa) adjacent to the southern margin of Europe. It has been suggested that the transformation from Pangea 'B' to Pangea 'A' was the result of intra-Pangea megashear that occurred, according to paleomagnetic data, within the Permian, after the Variscan orogeny but prior to the Triassic (Muttoni et al., 2003).

In this scenario, however, the along strike preservation of terranes along both the Laurussian and Gondwanan margins following the Variscan and Appalachian orogenies would be unlikely as megashear between the two continents would offset or destroy continuity between the two continental margins. However, the suggestion that Southern Iberia preserves an along strike remnant of the Meguma terrane as exposed in Atlantic Canada suggests a Late Devonian connection between the Laurussia and Gondwana similar to a Pangea 'A' configuration. As this arrangement predates the supposed post Variscan megashear required for the transition between Pangea 'B' to Pangea 'A' the along strike connection between the SPZ basement and the onshore Meguma terrane in the Late Devonian suggests Pangea 'A' was formed during primary Pangean amalgamation.

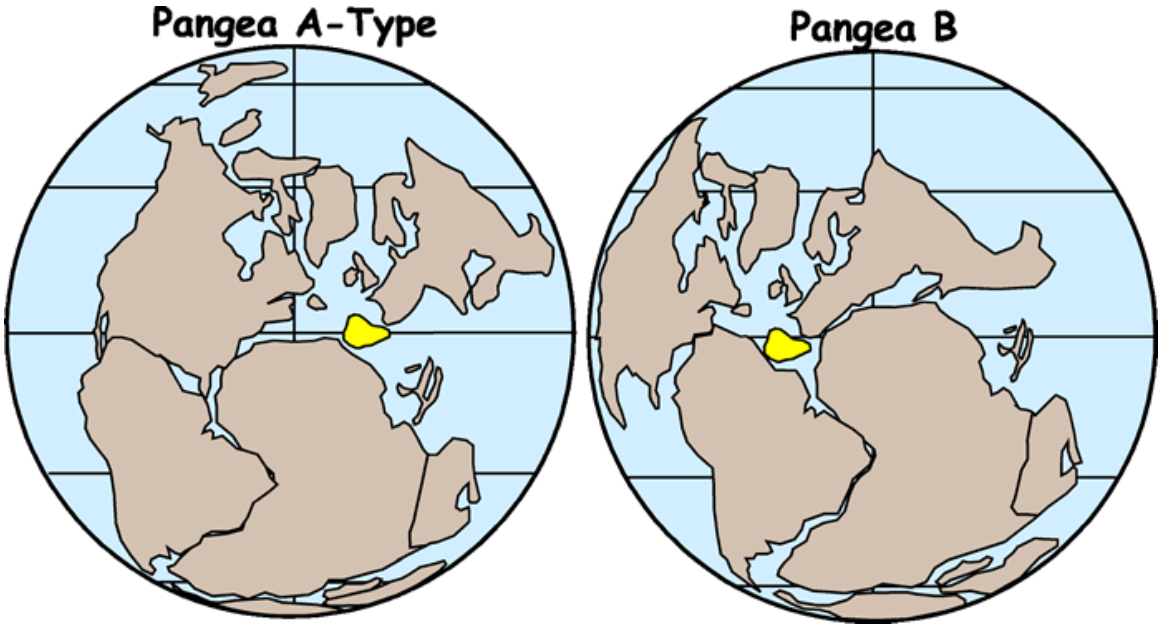

Figure 5.4 Pangea reconstructions highlighting latitudinal adjustment of Gondwana relative to Laurussia in Permian. Pangea A after Van der Voo and French (1974); Pangea B after Morel and Irving (1981).

5.2.6. Influences of Pangean Amalgamation on the Geometry of Atlantic Ocean Rifting

Relevant conclusions of this work

- Excision of the Iapetan suture-zone / Laurentian margin occurred in the Late Devonian – Early Carboniferous toward a Gondwanan re-entrant between Iberia and West Africa

- This excision likely nucleated along / resulted in development of orogen parallel shear zones which crosscut peri-Gondwana Avalonian and Meguma

Discussion

It has been well documented that rifting events of tend nucleate along pre-existing suture zones (e.g. Murphy et al., 2006; Murphy et al., 2008). For example it is believed that the Rheic Ocean originated as a result of rifting along pre-existing suture zones which delineated the divisions between peri-Gondwanan Avalonian-type and Cadomian-type terranes along the Gondwana margin in the late Neoproterozoic.

Therefore if rifting occurs preferentially along pre-existing zones of weakness, the dispersal of Pangea should have been the result of rifting events parallel to either (i) suture zones between peri-Gondwanan terranes and Laurentia or (ii) the primary Pangean suture between Laurussia and Gondwana. However, although the rifting of the Atlantic was roughly parallel to the orogens, which lay in Pangea's interior, the rifting of the Atlantic crosscut peri-Gondwanan Avalonia and Meguma. This crosscutting resulted in remnants of along strike Meguma in southern Iberia (SPZ) and Western Avalonia and the separation of the Appalachians and the British Caledonides. In this case either (i) rifting did not occur along pre-existing crustal weaknesses or (ii) crustal weaknesses existed perpendicular to the orogen across peri-Gondwanan terranes.

The juxtaposition of part of the Iapetan suture along southern Iberia, which transported the source for the PDLZ toward southern Iberia in the late Paleozoic, was

likely accompanied by shear zones parallel with the southern flank of the Iberian indenter. In this case the shear zones, which accompanied the movement of this crustal block would have truncated the orogen between the northern Appalachians and the British Caledonides. As a result these shear zones would have provided a favorable structural weakness for nucleation of the Atlantic rift system across Meguma and Avalonia (Fig. 5.4).

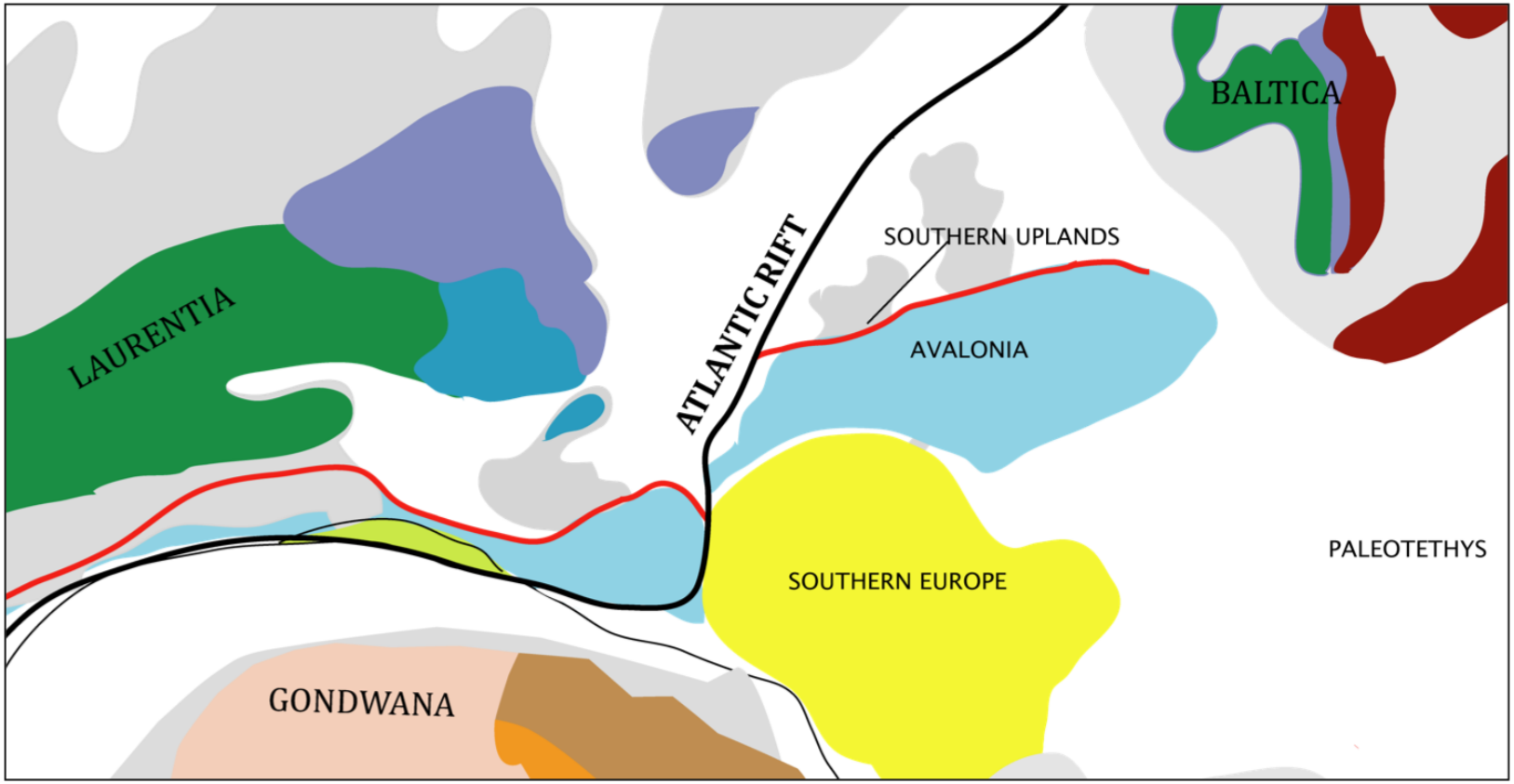

Fig. 5.5 Simplified Carboniferous reconstruction showing the future Atlantic rift nucleating along the Rheic suture to the south and across peri-Gondwanan Avalonia and Meguma where shear zones crosscut the orogenic fabric.

5.3. Proposal for Future Project

Discussion

A major issue, which was not directly addressed in this thesis, is determining the processes by which the Rheic Ocean closed. Addressing this issue is of fundamental importance because as the closure of the Rheic runs contrary to modern understanding of ocean basin closure. Two general characteristics of the Rheic Ocean indicate these enigmatic features.

(i) a wealth of geologic evidence indicates that the Rheic began to close some ca. 50 Ma after its formation (e.g. Scotese, 2003).Murphy and Nance (2008) suggest this closure indicates subduction rates of the younger more buoyant Rheic Ocean lithosphere exceeded those of the older and denser Paleopacific Ocean, which surround the external margins of Gondwana and Laurussia. In this scenario, modern geodynamic models for supercontinent assembly, whereby the dispersingcontinental fragments of a supercontinent break up and migratefrom newly formed oceanic lithosphere to reassemble at subduction zones of older oceanic lithosphere, fail to accountfor the amalgamation of Pangea.

(ii) Murphy et al. (2009) noted that Devonian and Carboniferous mafic complexes representing vestiges of the Paleozoic Rheic Ocean are characterized by unusually depleted Sm-Nd isotopic compositions. Some of these mafic complexes (e.g. Lizard,

Britain; Caréon, NW Iberia) preserve many of the lithotectonic characteristics of ophiolites whereas other complexes, although oceanic in origin, do not contain the full ophiolitic suite of lithologies. Murphy et al., 2010 *in press* suggest these signatures are indicative of derivation from a mantle with time-integrated depletion of Nd relative to Sm, and are consistent with a mantle source that previously had yielded basalt at some time in the Neoproterozoic. In this case the Rheic Ocean would have incorporated this older mantle sometime during its evolution.

In terms of the geology of southern Iberia, the BAO is one such mafic complex, which displays an uncharacteristically high Sm Nd isotopic signature ($\varepsilon_{Nd(t)}$ +7.9 to +9.2) (Castro et al., 1996). However this thesis supports the notion that the BAO is not genetically related to other primary Rheic Ocean ophiolitic complexes (e.g. Azor et al., 2008) despite the fact that its uncharacteristically high Sm-Nd signature indicated that it may have sourced the same ultra-depleted Neoproterozoic mantle. In any case, if the BAO is younger than terminal collision between Gondwana and Laurussia then the exact location of the Rheic suture is cryptic beneath the PDLZ.

The Peramora mélange (Eden, 1991), which is the lowermost tectonstratigraphic unit within the PDLZ, contains amphibolite blocks (part of Domain B; chapter 2), which have previously been thought derived from the BAO. However, if the BAO formed during a transtensional event in the Carboniferous (e.g. Azor et al., 2008) then this relationship is unlikely as the mélange is (i) polydeformed and (ii) overlain by less deformed Late Devonian tectonstratigraphic units. As a result the Peramora Mélange,

which was not studied in detail in this thesis, may be a more likely candidate for rocks genetically related to primary Rheic Ocean lithosphere. If so, then constraining the tectonic evolution of the Peramora mélange is critical in better understanding the tectonic evolution of the Rheic Ocean.

Proposed Model

Why the Rheic Ocean closed so early in its development may also be linked to the potential incorporation of this older mantle. As a result of implied earlier (to Rheic development) basalt extraction, this mantle would be relatively buoyant and thus preferentially preserved (Prelević and Foley, 2007). According to Murphy et al., 2010 *in press*this process many have occurred as portions of more buoyant Paleopacific were transferred to the upper plate (interior Rheic Ocean) along transform fault induced subduction zones at its out margins. These subduction zones would have nucleated where younger Rheic Ocean lithosphere was spatially juxtaposed with denser Paleopacific lithosphere.

Incorporation of buoyant Paleopacific lithosphere would ultimately create microplates bounded by subduction zones, which merged with the continental margins of Gondwana and Laurussia (Fig. 5.4). In this scenario, if enough fragments of buoyant Paleopacific lithosphere were incorporated into the interior Rheic realm then these subduction zones could merge to form Rheic subduction zones parallel to the continental margins. Furthermore the simple subduction of Paleopacific lithosphere beneath Rheic

lithosphere at the outer margins could facilitate crustal weakness and slab tear along the Rheic margins (Fig. 5.5). Taken together these suppositions seem to suggest that subduction at an early stage during Rheic development was entirely possible and accounts for the enigmatically high Sm Nd isotopic signatures of Rheic Ocean mafic complexes.

Suggestions for Project

- *In order to gain further insight into the development of Rheic Ocean mafic complexes the tectonothermal history of the Peramora Mélange needs to be better understood. Asa result further detailed field based mapping and sampling, geochemical and isotopic analysis and uranium lead isotope dating of this mafic mélange is needed. Taken together these data will test (i) the regional relationship of the mafic mélange to the PDLZ (ii) the timing of formation of the mafic mélange with respect to the rest of the PDLZ and the BAO and (iii) the genetic linkages between the mélange and the primary Rheic Ocean lithosphere. Constraining these relationships will greatly improve our understanding of the geodynamic evolution of this enigmatic ocean and the processes, which led to the formation of Pangea.*

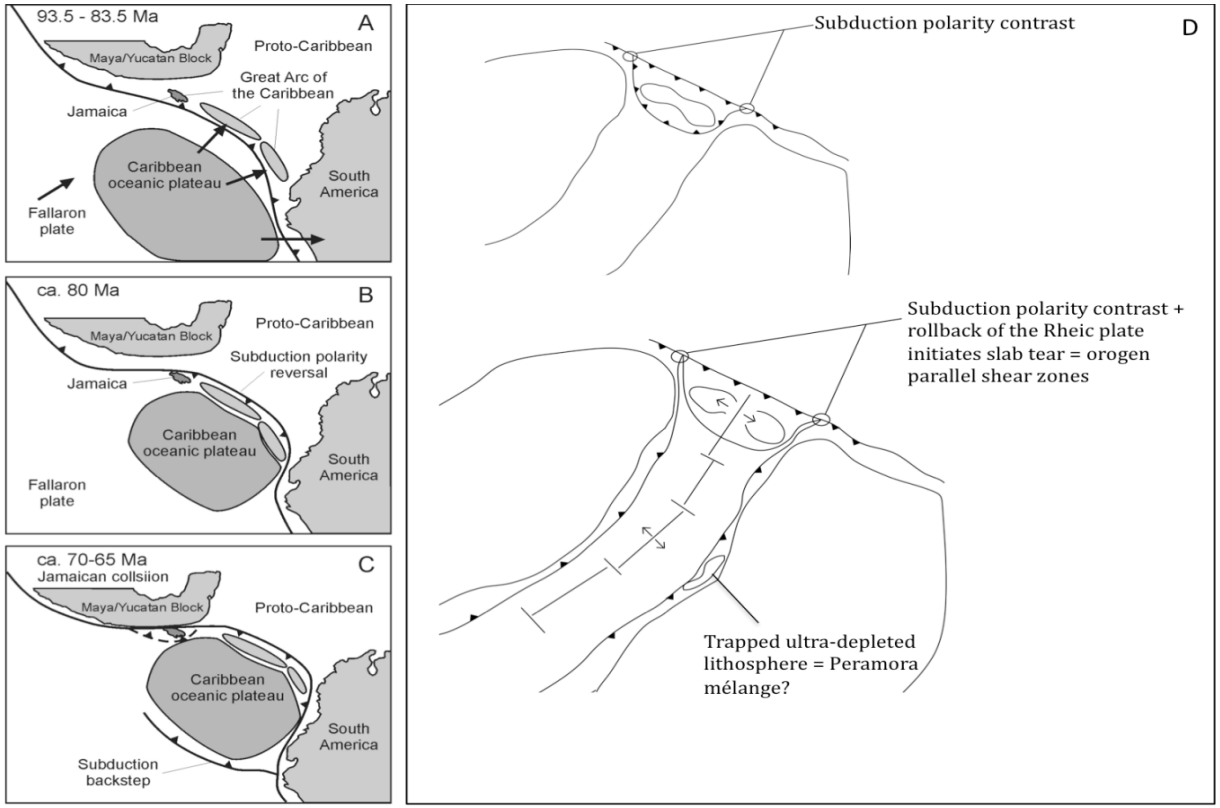

Fig. 5.5 Simplified model showing incorporation of Ultra-Depleted mantle into the Rheic ocean (After Murphy et al., 2010, *in press*), analogous to the capture of the Caribbean plate. Rollback and tear faults at the outer margins of the Rheic initiates orogen parallel shear zones in the interior ocean.

REFERENCE LIST

Abati, J., Mohsine Aghzer, A., Gerdes, A., Ennih, N. 2010. Detrital zircon ages of Neoproterozoic sequences of the Moroccan Anti-Atlas belt. *Precambrian Research*, **181**, 115-128.

Apalategui,O.,Barranco,E.,Contreras,F.,Roldan,F.J.1983.MapaGeologico1:50000,HojaAroche916.Serv.Publ.Minist.IndustriayEnergia,Madrid.

Apalategui,O.,Barranco,E.,Contreras,F.,Delgado,M.,Roldan,F.J.1984.MapaGeologico1:50000,HojaAracena917.Serv.Publ.Minist.IndustriayEnergia,Madrid.

Arndt, N.T., and Goldstein, S.L. 1987. Use and abuse of crust formation ages. *Geology*, **15**, 893-895.

Azor, A., Rubatto, D., Simancas, J. F., González Lodeiro, F., Martínez Poyatos, D., Martín Parra, L.M., Matas, J. 2008. Rheic Ocean ophiolitic remnants in southern Iberia questioned by SHRIMP U-Pb zircon ages on the Beja-Acebuches amphibolites. *Tectonics*, **25.**

Beck, M.E. 1989. Paleomagmatism of Continental North America, implications for the displacement of crustal blocks within the Western Cordillera, Baja California to British Columbia. *Geological Society of America Bulletin*, **101**, 471-492.

Bhatia, M.R. 1983. Plate tectonics and geochemical composition of sandstones. *Journal of Geology*, **91**, 611–627.

Bhatia, M.R., and Crook, K.A.W. 1986. Trace element characteristics of greywackes and tectonic setting discrimination of sedimentary basins. *Contributions to Mineralogy and Petrology*, **92**, 181–193.

Boher, M., Abouchami, W., Michard, A.N., Albarede, F., and Arndt, N. 1992. Crustal growth in West Africa at 2.1 Ga. *Journal of Geophysical Research*, **97**: 345–369.

Boogaard, M.V. 1963. Geology of Pomarão region (Southern Portugal). Thesis Graffisch Centrum Deltro, Rotterdam.

Boogaard, M.V.D., and Schermerhorn, L.J.G. 1980. Conodont faunas from Portugal and southwestern Spain. Part 4: A Famennian conodont fauna near Nerva (Rio Tinto). *Scripta Geologica*, **56**, 1-14.

Boulter, C.A., Hopkinson, L.J., Ineson, M.G., and Brockwell,J.S. 2004. Provenance and geochemistry of sedimentary components in the Volcano-Sedimentary Complex, Iberian Pyrite Belt: discrimination between the sill–sediment-complex and volcanic-pile models. *Journal of the Geological Society*,**161**, 103-115.

Braid, J.A., Murphy, J.B., Quesada, C., and Mortensen, J.K. 2010. Tectonic Escape of a Crustal Fragment During the Closure of the Rheic Ocean: U-Pb detrital zircon data from the Late Palaeozoic Pulo do Lobo and South Portuguese Zones, Southern Iberia. *Journal of the Geological Society*, **in press**.

Braid, J.A., Murphy, J.B., and Quesada, C. 2010. Structural analysis of an accretionary prism in a continental collisional setting, the Late Paleozoic Pulo do Lobo Zone, Southern Iberia. *Gondwana Research*, **17**, 422–439.

Brun, J.P., Burg, J.P. 1982. Combined thrusting and wrenching in the Ibero-Armorican arc: a corner effect during continental collision. *Earth and Planetary Science Letters*, **61**, 319–332.

Burg, J.P, Balé, P., Brun, J.P, Girardeau, J. 1987. Stretching lineation and transport direction in the Ibero-Armorican Arc during the Siluro-Devonian collision. *Geodynamica Acta*, **1**, 71–87.

Carvalho, D., Correia, H.A.C., Inverno, C., 1976. Contribuiçao para o conhecimento geológico do Grupo de Ferreira-Ficalho. Suas relaçoes cum a Faixa Piritosa e o Grupo do Pulo do Lobo. *Memorias e Noticias Universidad de Coimbra*, **82**, 145-169.

Castro, A., De la Rosa, J.D., Fernández, C., Moreno-Ventas, I. 1995. Unstable flow, magma mixing and magma-rock deformation in a deep-seated conduit: the Gil-Márquez Complex, south-west Spain. *Geologische Rundschau*, **84**, 359–374.

Castro, A., Fernández, C., de la Rosa, J., Moreno-Ventas, I., Rogers, G. 1996. Significance of MORB-derived amphibolites from the Aracena metamorphic belt, southwest Spain. *Journal of Petrology*, **37**, 235–260.

Castro, A., Corretgé, L.G., de la Rosa, J., Enrique, P., Martínez, F.J., Pascual, E., Lago, M., Arranz, E., Galé, C., Fernández, C., Donaire, T., López, S., 2002. Palaeozoic Magmatism. *In:* The Geology of Spain, W. Gibbons and T. Moreno *(Eds.)*. *Journal of the Geological Society,* 117-153.

Castroviejo, R., Quesada, C., Soler, M. 2010. Post-depositional tectonic modification of VMS deposits in Iberia and its economic significance. *In:* Allen, R. and Tornos, F. (eds) Geology of VMS deposits. *Mineralium Deposita*.

Cawood, P.A., McCausland, P.J.A., Dunning, G.R. 2001. Opening Iapetus: Constraints from the Laurentian margin in Newfoundland. *Geological Society of America Bulletin*, **113**, 443-453.

Cawood, P.A., Nemchin, A.A., Strachan, R.A, Prave, T., Krabbendam, M. 2007. Sedimentary basin and detrital zircon record along East Laurentia and Baltica during assembly and breakup of Rodinia. *Journal of the Geological Society,* **164**, 257-275.

Clark, A.H., Scott, D.J., Sandeman, H.A., Bromley, A.V., Farrar, E. 1998. Siegenian generation of the Lizard ophiolite; U–Pb zircon age data for plagiogranite, Porthkerris, Cornwall. *Journal of the Geological Society,* **155**, 595–598.

Clarke, D.B., Halliday, A.N., and Hamilton, P.J. 1988. Neodymium and strontium isotopic constraints on the origin of the peraluminous granitoids of the South Mountain Batholith, Nova Scotia, Canada. Chemical Geology. *Isotope Geoscience Section*, **73**: 15–24.

Crespo-Blanc, A. and Orozco, A. 1988. The southern Iberian shear zone: A major boundary in the Hercynian folded belt.*Tectonophysics,* **148**, 221-227.

Crespo-Blanc, 1989. Evolución geotectónica del contacto entre la Zona de Ossa-Morena y la Zona Surportuguesa en las sierras de Aracena y Aroche (Macizo Ibérico

Meridional): un contacto mayor en la cadena hercínica europea. *Ph. D. Thesis*, Univ. Sevilla.

Crespo-Blanc, A., Orozco, A. 1991. The boundary between the Ossa-Morena and South portuguese Zones (Southern Iberian Massif): a major suture in the European Hercynian Chain. *Geologische Rundschau*, **80**, 691-70.

Dallmeyer R. D., Ribeiro, A., and Marques, F. 1991. Polyphase Variscan emplacement of exotic terranes (Morais and Bragança Massifs) onto Iberian successions: Evidence from $^{40}Ar/^{39}Ar$ mineral ages. *Lithos*, **27**, 133-144.

Davies, G.R. 1984. Isotopic evolution of the Lizard Complex. *Journal of the Geological Society*,**141**, 3-14.

Davis, D., Suppe J., Dahlen, F.A. 1983. Mechanics of fold-and-thrust belts and accretionary wedges. *Journal of Geophysical Researc*h, **88**, 1153–1172.

de la Rosa, J.D. 1992. Petrología de las Rocas Básicas y Granitoides del batolito de la Sierra Norte de Sevilla, Zona Surportuguesa, Macizo Ibérico*,PhD Thesis*, Univ. Sevilla.

de la Rosa J.D., Rogers G., Castro A., 1993. Relaciones 87Sr/86Sr de rocas básicas y granitoides del batolito de la Sierra Norte de Sevilla. *Rev. Soc. Geol. España*, **6**, 141–149.

de la Rosa, J., Jenner, J., Castro, A. 2001. A study of inherited zircons in granitoid rocks from the South Portuguese and Ossa-Morena Zones, Iberian Massif: support for the exotic origin of the South Portuguese Zone. *Tectonophysics,***352**, 245-256.

DePaolo, D.J. 1981. Neodymium isotopes in the Colorado Front Range and crust–mantle evolution in the Proterozoic. *Nature*, **29**: 193–196

DePaolo, D.J. 1988. Neodymium Isotope Geochemistry: An Introduction. Minerals and Rocks. 187pp.

Dhont, D., Chorowicz, J., Luxey, P. 2006. Anatolian escape tectonics driven by Eocene crustal thickening and Neogene–Quaternary extensional collapse in the eastern Mediterranean region. *In:* Dilek, Y. and Pavlides, S. (eds) Postcollisional tectonics and magmatism in the Mediterranean region and Asia. *Geological Society of America, Special Paper*, **409**, 411-462.

Dostal, J., Dupuy, C. and Caby, R. 1994. Geochemistry of the Neoproterozoic Tilemsi belt of Iforas (Mali, Sahara): a crustal section of an oceanic island arc. Precambrian Research, **65**, 55-69.

Dias, R. and Ribeiro, A. 1995. The Ibero-Armorican Arc: A collision effect against an irregular continent?. *Tectonophysics,***246**, 113-128.

Díaz Azpiroz, M., Fernández, C. 2005. Kinematic analysis of the Southern Iberian shear zone and tectonic evolution of the Acebuches metabasites (SW Variscan Iberian Massif). *Tectonics*, **24**.

Díaz García F., Arenas R., Martínez Catalán, J.R., González de Tanago J., Dunning G.R. 1999. Tectonic evolution of the Careón Ophiolite (northwest Spain): a remnant of oceanic lithosphere in the Variscan Belt. *Journal of Geology*, **107**, 587-605.

Dickin, A.P., 2005. Radiogenic Isotope Geology 2nd ed. Cambridge. *Cambridge University Press*. 101pp.

Eberz, G.W., Clarke, D.B., Chatterjee A.K. and Giles, P.S. 1991. Chemical and isotopic composition of the lower crust beneath the Meguma Lithotectonic Zone, Nova Scotia: evidence from granulite facies xenoliths. *Contributions to Mineralogy and Petro*logy, **109**, 69–88.

Eden, C.P. 1991. Tectonostratigraphic analysis of the northern extent of the oceanic exotic terrane, Northwestern Huelva Province, Spain.*Ph.D. The*sis, University of Southampton, England.

Fernández-Suárez, J., Gutiérrez-Alonso, G., Cox, R., Jenner, G.A. 2002. Assembly of the Armorica microplate: a strike-slip terrane delivery? Evidence from U-Pb ages of detrital zircons. *Journal of Geology,* **110**, 619-626.

Fernández-Suárez, J., Gutiérrez-Alonso, G., Jeffries, T.E. 2002. The importance of along-margin terrane transport in northern Gondwana: insights from detrital zircon parentage in Neoproterozoic rocks from Iberia and Brittany. *Earth and Planetary Science Letters,* **204**, 75-88.

Fletcher, R.C., 1989. Approximate analytical solutions for a cohesive fold-and-thrust wedge: some results for lateral variation in wedge properties and for finite wedge angle. *Journal of Geophysical Research,* **94**, 10347-10354.

Fonseca, P., Ribeiro, A. 1993. Tectonics of the Beja-Acebuches Ophiolite: a major suture in the Iberian Variscan Foldbelt. *Geologische Rundschau*, **82**, 440-447.

Franke, W. 1989. Tectonostratigraphic units in the Variscan belt of central Europe, *Geological Society of America, Special Paper,* **230,** 67-90.

Franke, W. 2000. The mid-European segment of the Variscides: Tectonostratigraphic units, terrane boundaries and plate tectonic evolution. *Journal of the Geological Society, Special Publications,***179**, 35-61.

Fryer, B.J., Kerr, A., Jenner, G.A., Longstaffe, F.J., 1992. Probing the crust with plutons: regional isotopic geochemistry of granitoid intrusions across insular Newfoundland. *Geological Survey Branch, Newfoundland Department of Mines and Energy Report*,**92-1**, 119–140.

Fyffe, L.R., Barr, S.M., Johnson, S., McLeod, M., McNicoll, V., Valverde-Vaquero, P., van Staal, C.R., White, C.E. 2009. Detrital zircon ages from Neoproterozoic and Early Paleozoic conglomerate and sandstone units of New Brunswick and coastal Maine:: implications for the tectonic evolution of Ganderia. *Atlantic Geology,* **45**, 100-144.

González, A., Córdoba, D., Vegas, R., Matias, L.M. 1998. Seismic crustal structure in the southwest of the Iberian Peninsula and the Gulf of Cádiz. *Tectonophysics,***296**, 317–331.

Giese, U., Reitz, E., Walter, R. 1988. Contribution to the stratigraphy of the Pulo do Lobo succession in southwest Spain. *Comunicações dos Serviços Geológicos de Portugal,***74**, 79–84.

Giese, U., Nierhoff, R., Walter, R., 1994. Geology of the southwestern Iberian Meseta III. The northern margin of the South Portuguese Zone between Almonaster la Real

and Río Tinto (Huelva Province, SW Spain). *Neues Jahrbuch für Mineralogie Abh*., **192**, 361–381.

Giese, U., Hoymann, K., Glodny, J., Kramm, U., Dallmeyer, R.D. 1999. Age constraints for the tectonometamorphic evolution of the Pulo do Lobo Zone in SW Spain. *Zeitschrift der Deutschen Geologischen Gesellschaft,* **150**, 65-582.

González Clavijo, E. 1996. La geologia del sinforme de Alcañices, oeste de Zamora.*PhD Thesis*, Univ. Salamanca.

Greenough, J.D., Krogh, T.E., Kamo, S.L., Owen, J.V., and Ruffman, A. 1999. Precise U/Pb dating of Meguma basement xenoliths: New evidence for Avalonian underthrusting. *Canadian Journal of Earth Sciences*, **36**, 15–22.

Greenly, E. 1919. The Geology of Anglesey: Geological Survey of Great Britain. *Memoir*, **1**, 980 pp.

Grahame, J.H.O., Wilde, S.A., Yushengwan, W. 2008. Geochronology and geodynamics of Scottish granitoids from the late Neoproterozoic break-up of Rodinia to Palaeozoic collision. *Journal of the Geological Society,* **165**, 661–674.

Griffin, W.L., Powell, W.J., Pearson, N.J. and O'Reilly, S.Y. 2008. Glitter: Data reduction software for laser ablation ICP-MS; In Sylvester, P.J. (ed.), Laser Ablation ICP-MS in the Earth Sciences: Current Practices and Outstanding Issues, *Mineralogical Association of Canada Short Course Series, Short Course 40, Vancouver, B.C.*, 308-311.

Gutiérrez-Alonso, G., Gross, M.R. 1999. Structures and mechanisms associated with development of a fold in the Cantabrian zone thrust belt, NW Spain. *Journal of Structural Geology*, **21**, 653-670.

Gutiérrez-Alonso, G., Fernández-Suárez, J.,Gutiérrez Marco, J.C., Corfú, F., Suárez, M., Murphy,J.B. 2007. Depositional age of the Armorican Quartzite in the Cantabrian Zone of Iberia: Paleogeographic and biostratigraphic implications. *In:* Linnemann, U., Nance, R.D., Kraft, P. and Zulauf, G. (eds) The evolution of the Rheic Ocean: From Avalonian-Cadomian active margin to Alleghenian-Variscan collision. *Geological Society of America, Special Paper*, **423**, 287-296.

Gutiérrez-Alonso, G., Fernández-Suárez, J., Weil, A.B., Murphy, J.B., Nance, R.D., Corfú, F. and Johnston, S. 2008. Self-subduction of the Pangean global plate. *Nature Geoscience,***1**, 549-553.

Hibbard, J.P., van Staal, C.R., Rankin, D.W., and Williams, H. 2006. Lithotectonic map of the Appalachian Orogen, Canada–United States of America. Geological Survey ofCanada Map 2096A, scale 1:1,500,000.

Hirdes, W., and Davis, D.W. 2002. U–Pb geochronology of Paleoproterozoic rocks in the southern part of the Kedougou-Ke´nie´ba inlier, Senegal, West Africa: evidence for diachronous accretionary development of the Eburnian province. *Precambrian Research*, **118**, 83–99.

Hoffman, P.F. 1989. Precambrian geology and tectonic history of North America, *in* Bally, A.W., and Palmer, A.R., eds., The geology of North America: An overview. *Geological Society of America, The Geology of North America*, **A**: 447-512.

Hoffman, P.F., Kaufman, A.J., Halverson, G.P., Schrag, D.P. 1998. A Neoproterozoic snowball Earth. *Science,***281**, 1342–1346

Irving, E. 1977. Drift of the major continental blocks since the Devonian. *Nature*,**270**, 304–309.

Jamieson, R.A. 1981. Metamorphism during Ophiolite Emplacement the Petrology of the St. Anthony Complex. *Journal of Petrology*, **22**, 397-449.

Jenner, G.A., Longerich, H. P., Jackson, S.E., and Fryer, B.J. 1990. ICP-MS; a powerful tool for high-precision trace-element analysis in earth sciences; evidence from analysis of selected U.S.G.S. reference samples. *Chemical Geology*, **83**, 133-148

Jesus, A., Munhá, J., Mateus, A., Tassinari, C., Nutman, A. 2007. The Beja Layered Gabbroic Sequence (Ossa-Morena Zone, Southern Portugal): geochronology and geodynamic implications. *Geodinamica Acta,***20**, 139–157.

Johnson, R.J.E., and Van der Voo, R. 1986. Paleomagnetism of the Late Precambrian Fourchu Group, Cape Breton Island, Nova Scotia. *Canadian Journal of Earth Science*,**23,** 1673–1685.

Jones, R.R., Holdsworth, R.E., McCaffrey, K.J.W., Clegg, P., Tavarnelli, E. 2005. Scale dependence, strain compatibility and heterogeneity of three-dimensional deformation during mountain building: a discussion. *Journal of Structural Geology*, **27**, 1190-1204.

Jones, R.R., Holdsworth, R.E., Clegg, P., McCaffrey, K.J.W., Tavarnelli, E., 2004. Inclined transpression. *Journal of Structural Geology*, **26**, 1531-1548.

Kapp, P., Guynn, J.H. 2004. Indian punch rifts Tibet.*Geology,***32**, 993-996.

Keppie, J.D. 1985. The Appalachian College. *In* The Caledonide Orogen, Scandinavia, and Related Areas. *Edited by* D.G. Gee, and B. Stun., 1217-1226pp.

Keppie, J.D. and Dallmeyer, R.D. 1987. Dating transcurrent zone accretion: An example from the Meguma and Avalon composite terranes in the northern Appalachians. *Tectonics,***6**, 831–847.

Keppie, J.D., Dostal, J., Murphy, J.B., and Nance, R.D. 1996. Terrane transfer between eastern Laurentia and western Gondwana in the early Paleozoic: constraints on global reconstructions. *In*Avalonian and Related Peri-Gondwanan Terranes of the Circum-North Atlantic. *Edited by*D. Nance and M. Thompson. *Geological Society of America Special Paper*,**304**, 369–380.

Keppie, J.D., Nance, R.D., Murphy, J.B., and Dostal, J., 1991, The Avalon terrane: *in* Dallmeyer, R.D., and Lecorché, J.P., eds., The western African orogens and circum Atlantic correlatives: New York, Springer-Verlag, pp. 315-333.

Keppie, J.D., Davis, D.W., Krogh, T.E. 1998. U-Pb geochronological constraints on Precambrian stratified units in the Avalon composite terrane of Nova Scotia, Canada, Tectonic implications. *Canadian Journal of Earth Sciences,***35**, 222-23.

Keppie, J.D. and Krogh, T.E. 2000. 440 Ma igneous activity in the Meguma Terrane, Nova Scotia, Canada; part of the Appalachian overstep sequence?. *American Journal of Science,***300**, 528-538.

Keppie, D.F., Keppie, J.D., and Murphy, J.B., 2002. Saddle-reef auriferous veins in a conical fold termination (Oldham Anticline, Meguma Terrane, Nova Scotia, Canada): reconciliation of structural and age data. *Canadian Journal of Earth Sciences*, **39**, 53-63.

Keppie, J.D., Nance, R.D., Murphy, J.B., Dostal, J. 2003. Tethyan, Mediterranean, and Pacific analogues for the Neoproterozoic–Paleozoic birth and development of peri-Gondwanan terranes and their transfer to Laurentia and Laurussia. *Tectonophysics*, **365**, 195-220.

Kerr, A., Jenner, G.A., and Fryer, B.J. 1995. Sm-Nd isotopic geochemistry of Precambrian to Paleozoic granitoid suites and the deep-crustal structure of the southeast margin of the Newfoundland Appalachians.*Canadian Journal of Earth Sciences*, **32**, 224-245.

Koyi, H., Schott, B. 2001. Stress estimations from fault geometries applied to sand-box accretionary wedges. *Geophysical Research Letters*, **28**, 1087-1090.

Kurth, M., Sassen, A., Suhr, G., Mezger, K. 1998. Precise ages and isotopic constraints for the Lewis Hills (Bay of Islands Ophiolite): Preservation of an arc–spreading ridge intersection. *Geology*, **26**, 1127-1130.

Kusky, T., Bradley, D. 1999. Kinematic analysis of mélange fabrics: examples and applications from the McHugh Complex, Kenai Peninsula, Alaska. *Journal of Structural Geology*, **21**, 1773-1796.

Krogh, T.E. and Keppie, J.D. 1990. Age of detrital zircon and titanite in the Meguma Group, southern Nova Scotia, Canada: Clues to the origin of the Meguma Terrane.

Tectonophysics, **177**, 307–323.

Jacobs, J., and Thomas, R. 2004. Himalayan-type indenter-escape tectonics model for the southern part of the late Neoproterozoic–early Paleozoic East African– Antarctic orogen. *Geology*, **32**, 721-724.

Julivert, M., Fontboté, J.M., Ribeiro, A., Conde, L.N. 1974. Mapa Tectónico de la Peninsula Ibérica y Baleares. *Memoria explicativa*, Inst. Geol. Min. España, 113pp.

Lake, P.A., Oswin, W.M., Marshall, J.E.A. 1988. A palynologoical approach to terrane analysis in the South Portuguese Zone. *Trabajos de Geología*, Univ. de Oviedo.

Landing, E. 1996. Avalon; insular continent by the latest Precambrian (*in* Avalonian and related peri-Gondwanan terranes of the Circum-North Atlantic) *Geological Society of America*, *Special Paper*, **304**, 29-63.

Lefort, J.P. 1989. Basement correlation across the North Atlantic. Berlin, Germany, Springer, 148.

Lefort, J.P., Agarwal, B.N.P. 1999. Of what is the centre of the Ibero-Armorican arc composed? *Tectonophysics*, **302**, 71–81.

Leistel, J.M., Marcoux, E., Thiéblemont, D., Quesada, C., Sánchez, A., Almodóvar, G.R., Pascual, E. and Sáez, R. 1998. The volcanic-hosted massive sulphide deposits of the Iberian pyrite belt. *Mineralium Deposita,* **33**, 2-30.

Lerouge, C., Cocherie, A., Toteu, S.F., Penaye, J., Milesi, J.P., Tchameni, R., Nsifa, E.N., Fanning, C.M., and Deloule, E.2006. Shrimp U–Pb zircon age evidence for Paleoproterozoic sedimentation and 2.05 Ga syntectonic plutonism in the Nyong

Group, south-western Cameroon; consequences for the Eburnean–Transamazonian belt of NE Brazil and Central Africa. *Journal of African Earth Sciences*, **44**, 413–427.

Linnemann, U. andRomer, R.L. 2002. The Cadomian orogeny in Saxo- Thuringia, Germany, geochemical and Nd-Sr-Pb isotopic characterization of marginal basins with constraints to geotectonic setting and provenance. *International Journal of Earth Science*s, **93**, 683-705.

Linnemann, U., McNaughton, N.J., Romer, R.L., Gehmlich, M., Drost, K., and Tonk, C. 2004. West African provenance for Saxo-Thuringia (Bohemian Massif); Did Armorica ever leave pre-Pangean Gondwana? U/Pb–SHRIMP zircon evidence and the Nd-isotopic record. *International Journal of Earth Sciences*, **93**, 683–705.

López-Guijarro, R., Quesada, C., Fernández-Suárez, J., Jeffries, T. and Pin, Ch. 2007. Age of the rift-drift transition of the Rheic Ocean in the Ossa Morena Zone: K-bentonite in the Early Ordovician succesion at "Venta del Ciervo". *In*: The rootless Variscan suture of NW Iberia (Galicia, Spain*)*. The International Geoscience Programme. IGCP 497: "*The Rheic Ocean: Its Origin, Evolution and Correlatives*"**.** Publicaciones del Instituto Geológico y Minero de España, 142-143.

López-Guijarro, R., Armendáriz, M., Quesada, C., Fernández-Suárez, J., Murphy, J.B., Pin, C. and Bellido, F. 2008. Ediacaran–Palaeozoic tectonic evolution of the Ossa Morena and Central Iberian zones (SW Iberia) as revealed by Sm–Nd isotope systematics. *Tectonophysics,***461**, 202–214.

Lotze, F.,1945. Zur gliederung des Varisciden der Iberischen Meseta, *Geotektonische Forschungen*, **6**, 78–92.

Ludwig, K.J. 2003. Isoplot 3.00. *Berkeley Geochronology Center Special Publication*, **4**, 70.

Mann, O. 1997. Model for the formation of large, transtensional basins in zones of tectonic escape.*Geology,***25**, 211-214.

Martínez Catalan, J.R., Arenas, R., Díaz García, F., Abati, J. 1997. Variscan accretionary complexo f northwest Iberia: Terrane correlation and sucesión of tectonothermal events. *Geology,***25**, 1103.

Martínez Catalan, J.R., Fernandez-Suarez, J., Jenner, G.A., Belousova, E.A., Diez Montes, A. 2004. Provenance constraints from detrital zircon U-Pb ages in the northwestern Iberian Massif: Implications for Paleozoic plate configuration and Variscan evolution. *Journal of the Geological Society,***161**,463-476.

Martínez Catalán, J.R., Arenas, R., Díaz García, F., Gómez-Barreiro, J., González Cuadra, P., Abati, J., Castiñeiras, P., Fernández-Suárez, J., Sánchez Martínez, S., Andonegui, P., González Clavijo, E., Díez Montes, A., Rubio Pascual, F.J., Valle Aguado, B. 2007. Space and time in the tectonic evolution of the northwestern Iberian Massif. Implications for the comprehension of the Variscan belt. In: Hatcher, R.D.Jr., Carlson, M.P., McBride, J.H., Martínez Catalán, J.R. (Eds.), 4-D framework of continental crust. *Journal of th*e *Geological Society Memoir 200*.

Matte P., Ribeiro, A., 1975. Forme et orientation de l'éllipsoide de déformation dans la virgation hercynienne de Galice. Rélations avec le plissement et hipothèses sur la génèse de l'arc Ibero-Armoricain. *C.R. Ac. Sc. Paris, ser. D.,***280**, 2825-2828.

Matte, P. 1986. Tectonics and plate tectonic model for the Variscan belt of Europe. *Tectonophysics*, **126**, 329-374.

Matte, P. 1991. Accretionary history and crustal evolution of the Variscan belt in Western Europe. *Tectonophysics,***196**, 309-337.

McCulloch, M.T. and Wasserburg, G.J. 1978. Sm–Nd and Rb–Sr chronology of continental crust formation. *Science,***200**, 1003–1011.

McKerrow, W.S., Leggett, J.K., Eales, M.H. 1977. Imbricate thrust model of the Southern Uplands of Scotland. *Nature,***267**, 237-239.

McKerrow, W.S. and Scotese, C.R. 1990. Palaeozoic Biogeography and Paleogeography. *Journal of the Geological Society,***12**, 435.

McLennan, S.M., Nance, W.B., and Taylor, S.R. 1980. Rare earth element–thorium correlations in sedimentary rocks and the composition of the continental crust. *Geochimica et Cosmochimica Acta*, **44**, 1833–1840.

McNicoll, V.J., Van Staal, C.R., and Waldron, J.W.F. 2001. Accretionary history of the northern Appalachians: SHRIMP study of Ordovician syntectonic sediments in the Canadian Appalachians. *Geological Association of Canada Programme with Abstracts*, **26**, 100.

McWilliams, M.O., and Howell, D.G. 1982. Exotic terranes of western California. *Nature*, **297**, 215-217.

Morel, P., and Irving, E., 1981, Palaeomagnetism and the evolution of Pangaea: Journal of Geophysical Research, v. 86p. 1858-1872.

Moreno, C., Sierra, S., and Saez, R. 1996. Evidence for catastrophism at the Famennian-Dinantian boundary in the Iberian Pyrite Belt. *In* Recent advances in Lower Carboniferous geology. *Edited by* P.S. Strogen, I.D. Somerville, and G.L. Jones. Geological Society Special Publication, **107**,153-162

Mortensen, J.K., Brand, A., Liverton, T. 2007. Laser ablation ICP-MS U-Pb zircon ages for Cretaceous plutonic rocks in the Logtung and Thirtymile Range areas of southern Yukon. *In:* Emond, D.S., Lewis, L.L. and Weston, L.H. (eds) *Yukon Exploration and Geology 2006.* Yukon Geological Survey, 213-221.

Mortensen, J.K., Ghosh, D., Ferri, F. 1995. U-Pb age constraints of intrusive rocks associated with copper- gold porphyry deposits in the Canadian Cordillera. *In:* Schroeter, T.G. (ed) Porphyry Deposits of the Northwestern Cordillera of North Amer*ica*. CIM Special Volume, **46**, 142-158.

Mullane, E.1998.The geochemistry of the south Portuguese zone, Spain and Portugal.*Ph.D. Thesis*, University of Southampton, Faculty of Science, School of Ocean and Earth Science,469pp.

Munhá, J. 1983. Hercynian magmatism in the Iberian Pyrite Belt. *Memórias Serviços Geológicos de Portugal*, **29**, 39-81.

Munhá, J. 1990. Metamorphic evolution of the South Portuguese/Pulo de Lobo Zone. *In*: Pre-Mesozoic Geology of Iberia, Dallmeyer, R.D., Martínez García, E. (Eds.), Springer-Verlag, Berlín, 361-368.

Munhá J., Oliveira, J.T., Ribeiro, A., Oliveira, V., Quesada, C., Kerrich, R., 1986. Beja–Acebuches Ophiolite: characterization and geodynamic significance. *Maleo (Bol. Soc. Geol. Portugal)*, **2**, 1–3.

Murphy, J.B., Keppie, J.D., Dostal, J., Waldron, J.W.F., Cude, M.P. 1996. Geochemical and isotopic constraints on the accretion of Avalonia in the Appalachian-Caledonide orogen: evidence from Early Silurian clastic sequences in Antigonish Highlands, Nova Scotia, Canada. *Canadian Journal of Earth Sciences*, **33**, 379-388.

Murphy, J.B., Keppie, J.D., Davis, D., Krogh, T.E. 1997. Regional significance of new U–Pb age data for Neoproterozoic igneous units in Avalonian rocks of northern mainland Nova Scotia, Canada. *Geological Magazine*, **134**: 113–120.

Murphy, J.B. and Hamilton, M.A. 2000. U-Pb detrital zircon age constraints on evolution of the Late Paleozoic St. Marys Basin, central mainland Nova Scotia. *Journal of Geology,***108**, 53-72.

Murphy, J.B., Strachan, R.A., Nance, R.D., Parker, K.D., Fowler, M.B. 2000. Proto-Avalonia: a 1.2–1.0 Ga tectonothermal event and constraints for the evolution of Rodinia. *Geology*, **28**, 1071–1074.

Murphy, J.B., 2001. Geochemistry and tectonic significance of the middle to late Devonian McAras Brook and the Visean Martin Road Formation, Merigomish sub-basin, Nova Scotia. *Atlantic Geology*, **37**, 161-173.

Murphy, J.B. and Nance, R.D. 2002. Nd-Sm isotopic systematics as tectonic tracers: an example from West Avalonia, Canadian Appalachians. *Earth Science Reviews,* **59**, 77-100.

Murphy, J.B., Fernandez-Suarez, J., Keppie, J.D., Jeffries, T. 2004. Contiguous rather than discrete Paleozoic histories for the Avalon and Meguma terranes based on detrital zircon data. *Geology,* **32**, 585–588.

Murphy, J.B. and Nance, R.D. 2005. Do Supercontinents Turn Inside-in or Inside-out? *International Geology Review,* **47**, 591-619

Murphy, J.B., Gutiérrez-Alonso, G., Nance, R.D., Fernández-Suárez, J., Keppie, J.D., Quesada, C., Strachan, R.A., Dostal, J. 2006. Origin of the Rheic Ocean: rifting along a Neoproterozoic suture? *Geology*, **34**, 325-328.

Murphy, J.B. and Nance, R.D. 2008. The Pangean Conundrum. *Geology*, **36**, 703-706.

Murphy, J.B., Gutierrez-Alonso, G., Nance, R.D., Fernandez-Suarez, J., Keppie, J.D., Quesada, C., Dostal, J., Braid, J.A. 2009. Rheic ocean mafic complexes: overview and synthesis. In: Murphy, J.B., Keppie, J.D., Hynes, A.J. (Eds.), Ancient Orogens and Modern Analogues.*Journal of the Geological Society, Special Publication*,**327**, 343-369.

Murphy, J.B., Cousens, B., Braid, J.A., Strachan, R.A., Dostal, D., Keppie, J.D., Nance, R.D. *In press*.Highly Depleted Oceanic Lithosphere In The Rheic Ocean: Implications For Paleozoic Plate Reconstructions. *Lithos*.

Muttoni, G., Kent, D.V., and Channell, J.E.T. 1996. Evolution of Pangea: Paleomagnetic constraints from the Southern Alps, Italy. *Earth and Planetary Science Letters*, **140**, 97–112.

Muttoni, G., Kent, D.V., Garzanti, E., Brack, P., Abrahamsen, N., and Gaetani, M. 2003.Early Permian Pangea 'B' to Late Permian Pangea 'A'. *Earth and Planetary Science Letters*, **215**, 379-394

Nance, R. D., and Murphy, J. B. 1989. Break-up of a late Precambrian supercontinent and the evolution of the Avalonian-Cadomian belt. *In:* Tectonostratigraphic expression of terrane accretion in the Circum-Atlantic Paleozoic orogens, Athens, Georgia, 75-78.

Nance, R.D., and Murphy, J.B. 1994. Contrasting basement isotopic signatures and the palinspastic restoration of peripheral orogens: Example from the Neoproterozoic Avalonian-Cadomian belt. *Geology*, **22**, 617-620.

Nance, R.D., Murphy, J.B., Keppie, J.D. 2002. A Cordilleran model for the evolution of Avalonia. *Tectonophysics*, **352**, 11-31.

Nance, R.D., Miller, B., Keppie, J.D., Murphy, J.B., Dostal, J. 2006. Acatlán Complex, Southern Mexico. Record spanning the assembly and breakup of Pangea. *Geology*, **34**, 857-860.

Nance,R.D., Murphy, J.B., Strachan, R.A., Keppie, J.D., Gutiérrez-Alonso, G., Fernandez- Suarez, J., Quesada, C., Linnemann, U., D'lemos, R., Pizarevsky, S. 2008. The late Neoproterozoic-early Palaeozoic extension along the West African craton and the Peri-Gondwanan terranes *In* Neoproterozoic-early Palaeozoic tectonostratigraphy and palaeogeography of the peri-Gondwanan terranes:

Amazonian v. West African connections *Geological Society, London, Special Publications*, **297**, 345-383.

Nance, R.D., Keppie, J.D., Miller, B.V., Murphy, J.B., Dostal, J. 2009. Paleozoic Paleogeography of Mexico: constraints from detrital zircon age data. *Journal of the Geological Society, Special Publications,* **327**, 239-269.

Nance,R.D., Gutiérrez-Alonso, G., Keppie, J.D., Linnemann, U., Murphy, J.B., Quesada, C., Strachan, R.A., Woodcock, N., 2010. Evolution of the Rheic Ocean. Gondwana Research 17, 194-222.

Niwa, M., 2006. The structure and kinematics of an imbricate stack of oceanic rocks in the Jurassic accretionary complex of Central Japan: an oblique subduction model. *Journal of Structural Geology*, **28**, 1670-1684.

Nance,R.D., Gutiérrez-Alonso, G., Keppie, J.D., Linnemann, U., Murphy, J.B., Quesada, C., Strachan, R.A., Woodcock, N. 2010. Evolution of the Rheic Ocean. *Gondwana Research*, **17**, 194-222.

Nutman, A.P., Green, D.H., Cook, C.A., Styles, M.T., Holdsworth, R.E. 2001. SHRIMP U/Pb zircon dating of the exhumation of the Lizard Peridotite and its emplacement over crustal rocks, Cornwall, England: constraints for tectonic models. *Journal of the Geological Society,* **158**, 809–820.

O'Brien, S.J., Wardle, R.J., and King, A.F. 1983. The Avalon zone: A Pan-African terrane in the Appalachian orogen of Canada. *Geological Journal*, **18**, 195–222.

O'Brien, S.J., O'Brien, B.H., Dunning, G.R., and Tucker, R.D. 1996. Late Neoproterozoic Avalonian and related peri-Gondwanan rocks of the Newfoundland Appalachians. *In* Avalonian and Related Peri-Gondwanan Terranes of the Circum-North Atlantic. *Edited by*R.D. Nance and M.D. Thompson. *Geological Society of America SpecialPaper*. **304**, 9–28.

Oliveira, J.T., Horn, M., Paproth, E. 1979. Preliminary note on the stratigraphy of the Baixo Alentejo Flysch Group, Carboniferous of southern Portugal and on the paleogeographic development, compared to corresponding units in northwest Germany. *Commun. Serv. Geol. Portugal*, **65**, 151-168.

Oliveira, J.T. 1983. The marine stratigraphy of south Portugal: a stratigraphical and sedimentological approach. *In* 'The Carboniferous of Portugal'. Mem. Servicos Geologicos de Portugal. **29**, 3–37.

Oliveira, J.T., Cunha, T., Streel, M., Vanguestaine, M. 1986. Dating the Horta da Torre Formation, a new lithostratigraphic unit of the Ferreira-Ficalho Group, South Portuguese Zone: Geological consequences. *Comunicacoes dos Servicos Geologicos de Portugal,***72**, 26-34.

Oliveira, J.T., 1988. Contribution to the knowledge of the tectonos-stratigraphic evolution of the South Portuguese Zone in Portugal. *Doctoral Thesis*. Serv. Geol. Portugal, Lisboa 88

Oliveira, J.T. 1990. Stratigraphy and syn-sedimentary tectonism in the South Portuguese Zone. *In:* Dallmeyer, R.D. and Martínez García, E. (eds) *Pre-Mesozoic Geology of Iberia*, Springer-Verlag, Berlín, 334-347.

Onézime, J., Charvet, J., Faure, M., Chauvet, A., Panis, D. 1999. Thrusting and wrenching in the Pulo do Lobo antiform (South Portuguese Zone, Spanish area). In: Gámez, J.A., Eguiluz, L., Palacios, T., Editors,. *XV Reunión de Geología del Oeste Peninsular. Diputación de Badajoz*, Badajoz, Spain, 185-189.

Onézime, J. Charvet, J., Faure, J., Chauvet, A., Panis, D. 2002. Structural evolution of the southernmost segment of the West European Variscides: the South Portuguese Zone (SW Iberia). *Journal of Structural Geology*, **24**, 451-468.

Onézime, J., Charvet, J., Faure, M., Bourdier, J., Chauvet, A. 2003. A new geodynamic interpretation for the South Portuguese Zone (SW Iberia) and the Iberian Pyrite Belt genesis. *Tectonics,***22**, 1-16.

Onishi, T.C., Kimura, G., 1995. Change in fabric of mélange in the Shimanto Belt, Japan: Change in relative convergence? *Tectonics*, **14**, 1273-1289.

Osozawa, S., Morimoto, J., Flower, M., 2009. "Block-in-matrix" fabrics that lack shearing but possess composite cleavage planes: A sedimentary mélange origin for the Yuwan accretionary complex in the Ryukyu island arc, Japan. *Geological Society of America Bulletin*, **121**, 1190-1203.

Owen, J.V., Greenough, J.D., Hy, C., and Ruffman, A. 1988. Pelitic xenoliths in a mafic dyke at Popes Harbour, Nova Scotia: implications for the basement of the Meguma Group. *Canadian Journal of Earth Sciences*, **25**, 1464–1471.

Owen, J.V., and Greenough, J.D. 1991. An empirical sapphirine–spinel Fe–Mg exchange thermometer and its application to highgrade xenoliths in the Popes Harbour dyke, Nova Scotia. *Lithos*, **26**, 317–332.

Pe-Piper, G. and Jansa, L.F. 1999. Pre-Mesozoic basement rocks offshore Nova Scotia, Canada: new constraints on the accretion history of the Meguma terrane. *Geological Society of America Bulletin*,**111**, 1773–1791.

Pe-Piper, G., Kamo, S.L., McCall, C. 2010. The German Bank pluton, offshore SW Nova Scotia: Age, petrology, and regional significance for Alleghanian plutonism. *Geological Society of America Bulletin*, **122**, 690-700.

Perroud, H., Calza, F., Khattach, D. 1991. Paleomagnetism of the Silurian volcanism at Almaden, Southern Spain. *Journal of Geophysical Research,* **96**, 1949-1962.

Potrel, A., Peucat, J., Fanning, C.M. 1998. Archean crustal evolution of the West African Craton: example of the Amsaga Area (Reguibat Rise). U–Pb and Sm–Nd evidence for crustal growth and recycling. *Precambrian Research*, **90**, 107–117.

Phillips, E.R., Barnes, R.P., Boland, M.P., Fortey, N.J., McMillan, A.A. 1995. The Moniaive Shear Zone: a major zone of sinistral strike-slip deformation in the Southern Uplands of Scotland. *Scottish Journal of Geology,* **31**,139-149.

Pini, G.A., 1999. Tectosomes and olistostromes in the Argille Scagliose of the Northern Apennines, Italy. *Geological Society of America Special Paper*, **335**, 70pp.

Piper, J.D.A., Tatar, O., Gursoy, H., Mesci, B.L., Kocbulut, F., Huang, B. 2008. Post-collisional deformation of the Anatolides and motion of the Arabian indenter: A paleomagnetic analysis *OP Conf. Ser.: Earth Environ. Sci.,*2 012011

Pous, J., Munoz, G., Heise, W., Melgarejo, J.C., Quesada, C. 2004. Electromagnetic imaging of Variscan crustal structures in SW Iberia: the role of interconnected graphite. *Earth and Planetary Science Letters,* **217**, 435-450.

Poulsen, C.J., Pollard, D., Montanez, I., Rowley, D. 2007. Late Paleozoic tropical climate response to Gondwanan deglaciation, *Geology*, **35**, 771-774.

Prelević, D., Foley, S.F. 2007. Accretion of arc-oceanic lithospheric mantle in the Mediterranean: Evidence from extremely high-Mg olivines and Cr-rich spinel inclusions in lamproites. *Earth and Planetary Science Letters*,**256**, 120-135.

Quesada, C., Robardet, M., Gabaldón, V. 1990. Ossa-Morena Zone Stratigraphy: Synorogenic phase (Upper Devonian-Carboniferous - Permian). *In:* Dallmeyer, R. D. and Martínez García, E. (eds) *Pre-Mesozoic Geology of Iberia.* Springer-Verlag, Berlin, 273-279.

Quesada, C. 1991. Geological constraints on the Paleozoic tectonic evolution of tectonostratigraphic terranes in the Iberian Massif. *Tectonophysics,***185**, 225–245.

Quesada, C., Bellido, F., Dallmeyer, R.D., Gil-Ibarguchi, I., Oliveira, J.T., Peréz-Estaún, A., Ribeiro, A., Robardet, M., Silva, J.B. 1991. Terranes within the Iberian Massif: correlations with West African sequences. *In:* Dallmeyer, R.D. and Lécorché, J.P. (eds) The West African Orogens and Circum-Atlantic Correlatives, Springer-Verlag, Berlin, 267–294.

Quesada, C., Fonseca, P.E., Munhá, J., Oliveira, J.T., Ribeiro, A. 1994. The Beja-Acebuches Ophiolite (Southern Iberia Variscan fold belt): geological characterization and significance. *Boletín Geológico Minero,***105**, 3-49.

Quesada, C. and Dallmeyer, R.D. 1994. Tectonothermal evolution of the Badajoz-Cordóba shear zone (SW Iberia): characteristics and $^{40}Ar/^{39}Ar$ mineral age constraints. *Tectonophysics*,**231**, 195-213.

Quesada, C., 1997. Evolución geodinámica de la Zona Ossa Morena durante el ciclo Cadomiense. In: A.A. Araújo and M.F. Pereira, Editors, Estudo sobre a geología da zona de Ossa Morena (Maciço Ibérico), Livro homenagem Prof. Francisco Gonçalves, University of Évora, 205–230.

Quesada, C. 1998. A reappraisal of the structure of the Spanish segment of the Iberian Pyrite Belt. *Mineralium Deposita,***33**, 31-34.

Quesada, C., Sánchez-García, T., Bellido, F., López-Guijarro, R., Armendáriz, M., Braid, J., 2006. Introduction: the Ossa-Morena Zone — from Neoproterozoic arc through Early Palaeozoic rifting to late Palaeozoic orogeny. In: M.F. Pereira and C. Quesada, Editors, Ediacaran to Viséan Crustal Growth Processes in the Ossa-Morena Zone (SW Iberia), Évora Meeting 2006: Conference abstracts and Field trip guide, Instituto Geológico y Minero de España, 51–73.

Ragan, D.M., 1985. Structural Geology: An Introduction to the Geometrical Techniques (3rd edition). *New York: McGraw-Hill*, 393 pp.

Ramsay, J.G., Lisle, R.J., 2000. The Techniques of Modern Structural Geology, vol. 3. Applications of Continuum Mechanics in Structural Geology. *Academic Press, London*.

Rapela, C.W., Coira, B., Toselli, A., Saavedra, J. 1992. The lower Paleozoic magmatism of southwestern Gondwana and the evolution of the Famatinian orogen. *International Geology Review*, **34**, 1081–1142.

Reading, H.G., Allen, P.A., Talbot, M.R., 1996. Sedimentary Environments: processes, facies and stratigraphy. *Blackwell Science*.

Ribeiro, A., Silva, J.B. 1983. Structure of South Portuguese Zone. In: Sousa, M.J.L. and Oliveira, J.T., (Eds), 1983. *The Carboniferous of Portugal. Comunicações dos Serviços Geológicos de Portugal*, **29**, 83-90.

Ribeiro, C., Quesada, C., Dallmeyer, R.D. 1990. Geodynamic evolution of the Iberian Massif. *In:* Dallmeyer, R.D. and Martínez García, E. *(eds)* Pre-Mesozoic Geology of Iberia. Springer-Verlag, Berlin, 399–409.

Ribeiro, A., Sanderson, D. 1996. SW-Iberia. Transpressional Orogeny in the Variscides. In: Lithosphere Dynamics. Europrobe–ESF, 90–98.

Ries, A.C. 1978. The opening of the Bay of Biscay – A review. *The Earth Science Reviews,***14**, 35-63.

Robardet, M. 2002. Alternative approach to the Variscan Belt in southwestern Europe: Pre-orogenic paleobiogeographical constraints. *In:* Martinez Catalan, J.R., Hatcher, R.D., Arenas, R. and Diaz García, F. *(eds)* Variscan-Appalachian Dynamics: The Building of the Late Paleozoic Basement. *Geological Society of America, Special Paper,***364**, 1-15.

Robardet, M. 2003.
TheArmorica‘microplate’:Factorfiction?Criticalreviewoftheconceptandcontradictorypalaeobiogeographicaldata.*Palaeogeography, Palaeoclimatology,Palaeoecology*,**195**, 125–148.

Robardet, M. and Gutiérrez Marco, J.C. 2004. The Ordovician, Silurian and Devonian sedimentary rocks of the Ossa Morena Zone (SW Iberian Peninsula), Spain. *Journal of Iberian Geology,* **30**, 73–92.

Rocci, G., Bronner, G., Deschamps, M. 1991. Crystalline basement of the West African craton. *In* The West African Orogens and Circum-Atlantic Correlatives. *Eds* by R.D. Dallmeyer and J.P. Le´Corche. *Springer-Verlag*, New York, 31–61.

Rosa, D.R., Finch, A.A., Andersen, T., Inverno, C.M. 2008. U–Pb geochronology and Hf isotope ratios of magmatic zircons from the Iberian Pyrite Belt. *Mineralogy and Petrology,***95**, 47-69.

Rosa, C.J.P., McPhie, J., Relvas, J.M.R.S. 2010. Type of volcanoes hosting the massive sulfide deposits of the Iberian Pyrite Belt. *Journal of Volcanology and Geothermal Research*, **194**, 107-126

Roser, B.P. and Korsch, R.J. 1986. Determination of tectonic setting of sandstone-mudstone suites using SiO_2 content and K_2O/Na_2O ratio. *Journal of Geology*, **94**, 635–650.

Samson, S.D., Barr, S.M., White, C.E. 2000. Nd isotopic characteristics of terranes within the Avalon zone, southern New Brunswick. *Canadian Journal of Earth Sciences*, **37**, 1039–1052.

Sánchez-García, T., Bellido, F., Quesada, C., 2003. Geodynamic setting and geochemical signatures of Cambrian–Ordovician rift-related igneous rocks (Ossa-Morena Zone, SW Iberia). *Tectonophysics*, **365**, 233-255.

Sánchez Martínez, S., Arenas, R., Díaz García, F., Martínez Catalán, J., Gómez-Barriero, J., Pearce, J. 2007. Careón ophiolite, NW Spain: Suprasubduction zone setting for the youngest Rheic Ocean floor. *Geology*, **35**, 53-56.

Sánchez-García, T., Quesada, C., Bellido, F., Dunning, G.R., González de Tánago, J. 2008. Two-step magma flooding of the upper crust during rifting: The Early Paleozoic of the Ossa Morena Zone (SW Iberia). *Tectonophysics*, **461**, 72-90.

Schenk, P.E. 1997. Sequence stratigraphy and provenance on Gondwana's margin: The Meguma zone (Cambrian–Devonian) of Nova Scotia, Canada. *Geological Society of America Bulletin*, **109**, 395-409.

Schermerhorn, L.J.G. 1971. An outline stratigraphy of the Iberian Pyrite Belt. *Boletín Geológico y Minero,***82**, 239-268.

Schültz, W., Ebneth, J., Meyer, K.D. 1987. Trondhjemites, tonalites and diorites in the South Portuguese Zone and their relations to the volcanics and mineral deposits of the Iberian Pyrite Belt. *Geologische Rundschau*, **76**, 201–212.

Scotese, C.R. 2003. Paleomap project. World Wide Web Address: www.scotese.com.

Scott, B. and Koyi, H. 2001. Estimating basal friction in accretionary wedges from the geometry and spacing of frontal faults. *Earth and Planetary Science Letters*, **194**, 221-227.

Silver, E. and Beutner, E. 1980. Mélanges. *Journal of Geology*, **8**, 32-34.

Silva, J.B., Oliveira, J.T., Ribeiro, A. 1990. Structural outline of the South Portuguese Zone. *In:* Dallmeyer, R.D. and Garcia, E.M., *(Eds).* Pre-Mesozoic Geology of Iberia, Springer, Berlin*,* 348-362.

Simancas, J.F. 1983. Geología de la extremidad oriental de la Zona Sudportuguesa. *Ph.D. Thesis*, University of Granada, 439 pp.

Simancas J.F., 1986. La deformación en el sector oriental de la zona Sudportuguesa. *Bol. Geol. Minero*, **97**,148-159.

Simancas, J.F., Carbonell, R., González-Lodeiro, F., Pérez-Estaún, A., Juhlin, C., Ayarza, P., Kashubin, A., Azor, A., Martínez-Poyatos, D., Almodóvar, G.R., Pascual, E., Sáez, R., Expósito, I. 2003. Crustal structure of the transpressional Variscan orogen of SW Iberia: SW Iberia deep seismic reflection profile (IBERSEIS). *Tectonics,***22.**

Simancas, J.F., Tahiri, A., Azor, A., González Lodeiro, F., Martínez Poyatos, D. and El Hadi, H. 2005. The tectonic frame of the Variscan–Alleghanian Orogen in southern Europe and northern Africa. *Tectonophysics,***398**,181-198.

Sláma, J., Kosler, J., Condon, D.J., Crowley, J.L., Gerdes, A., Hanchar, J.M., Horstwood, M.S.A., Morris, G.A., Nasdala, L., Norberg, N., Schaltegger, U., Schoene, B.,

Tubrett, M.N., Whitehouse, M.J. 2008. Plesovice zircon—a new natural reference material for U-Pb and Hf isotopic micro-analysis. *Chemical Geology*, **249**, 1–35

Solomon, M. and Quesada, C. 2003. Zn–Pb–Cu massive sulfide deposits: brine-pool types occur in collisional orogens, black smoker types occur in backarc and/or arc basins. *Geology,***31**, 1029–1032.

Soler, E. 1980. Spilites et métallogénie: La province pyrito-cuprifère de Huelva (SW Espagne). *Mem Sci Terre Nancy*, **39**, 1-461.

Soper, N.J., England, R.W., Snyder, D.B., Ryan, P.D. 1992. The Iapetussuture zone in England, Scotland and eastern Ireland: a reconciliation of geological and deep seismic data. *Journal of the Geological Society*, **149**, 697-700

Soriano, C. and Martí, J. 1999. Facies analysis of volcano-sedimentary successions hosting massive sulfide deposits in the Iberian pyrite belt, Spain. *Economic Geology*, **94**, 867-882.

Soriano, C. and Casas, J M. 2002.Variscan tectonics in the Iberian pyrite belt, South Portuguese Zone. *International Journal of Earth Sciences*, **91**, 882-896.

Stampfli, G.M. and Borel, G.D. 2002. A plate tectonic model for the Paleozoic and Mesozoic constrained by dynamic plate boundaries and restored synthetic oceanic isochrones. *Earth and Planetary Science Letters,***196**, 17-33.

Sun, S.S. and McDonough, W.F. 1989. Geochemical and isotopic systematics of oceanic basalts: Implications for mantle compositions and processes. *In* Magmatism in

ocean basins. (*Eds*)A.D. Saunders and M.J. Norrty. *Journal of the Geological Society, Special Publication*, **42**, 313–345.

Tapponnier, P. andMolnar, P. 1976. Slip-line field theory and large-scale continental tectonics.*Nature,***264**, 319-324.

Thorogood, E.J. 1990. Provenance of the pre-Devonian sediments of England and Wales: Sm–Nd evidence. *Journal of the Geological Society*, **147**, 591–594.

Timmermann, H., Parrish, R.R., Noble, S.R., Kryza, R. 2000. New U–Pb monazite and zircon data from the Sudetes Mountains in SW Poland: evidence for a single-cycle Variscan orogeny.*Journal of the Geological Society*,**157**, 265-268.

Twiss, R. J. and Moores, E. M. 2007. Structural Geology, New York, 2nd ed., 736 pp.

Ujiie, K. 2002. Evolution and kinematics of an ancient décollement zone, mélange in the Shimanto accretionary complex of Okinawa Island, Ryukyu Arc. *Journal of Structural Geology*, **24**, 937-952.

Van Achterbergh, E., Ryan, C.G., Jackson, S.E., Griffin, W.L. 2001. Data reduction software for LA-ICP-MS: appendix; *In* Sylvester, P.J. *(eds.)*, Laser Ablation –ICP-Mass Spectrometry in the Earth Sciences: *Principles and Applications, Mineralogical Association of Canada Short Course Series, Ottawa, Ontario, Canada*, **29**, 239-243.

van der Pluijm, B.A. and Marshak, S. 1997. Earth Structure - An Introduction to Structural Geology and Tectonics. *WCB-McGraw-Hill*, 495pp.

Van der Voo, R. 1979. Palaeozoic assembly of Pangea : a new plate tectonic model for the Taconic, Caledonian and Hercynian orogenies (abstract). EOS Trans. AGU 60, 241.

Van der Voo, R. 1982. Pre-Mesozoic paleomagnetism and plate-tectonics. *Annual Review of Earth and Planetary Sciences,* **10,** 191-220.

Van der Voo, R. 2004. Paleomagnetism, Oroclines, and Growth of the Continental Crust: Presidential Address. *GSA Today*, **14**, 4-9

van Staal, C.R., Dewey, J.F., Mac Niocaill, C., McKerrow, W.S. 1998. The Cambrian-Silurian tectonic evolution of the Northern Appalachians and British Caledonides: history of a complex, west and southwest Pacific-type segment of Iapetus. In D. Blundell and A.C. Scott, (Eds). Lyell: The Past is the Key to the Present. *Journal of the Geological Society, Special Publication*, **143**, 199-242.

van Staal, C.R., Whalen, J.B., Valverde-Vaquero, P., Zagorevski, A., Rogers, N. 2009. Pre-Carboniferous, episodic accretion-related, orogenesis along the Laurentian margin of the northern Appalachians. *Journal of the Geological Society, Special Publication*, **327**, 271-316.

Veevers, J.J., 1990. Tectonic–climatic supercycle in the billion-year plate-tectonic eon: Permian Pangean icehouse alternates with Cretaceous dispersed-continents greenhouse,
Sedimentary Geology, **68**, 1–16.

Wakabayashi, J. and Medley, E.W. 2004. Geological characterization of mélanges for practitioners. *Felsbau*, **22**, 10-18.

Waldron, J.W.F., Fyold, J.D., Simonetti, A. and Heaman,L.M. 2008. Ancient Laurentian detrital zircon in the closing Iapetus Ocean, Southern Uplands terrane, Scotland. *Geology,***36**, 527–530.

Waldron, J.W.F., White, C.E., Barr, S.M., Simonetti, A. and Heaman, L.M. 2009. Provenance of the Meguma terrane, Nova Scotia: rifted margin of early Paleozoic Gondwana. *Canadian Journal of Earth Sciences,* **46**, 1-8.

Waldron, J.W.F., Schofield, D., White, C.E., Barr, S.M. *in press.* Cambrian successions of the Meguma Terrane, Nova Scotia, and Harlech Dome, North Wales: dispersed fragments of a peri-Gondwanan basin? *Journal of the Geological Society*.

Wetherill, G.W., 1956. Discordant Uranium-Lead Ages. *I. Trans Am Geophys Union,***37**, 320–326.

Weil, A.B., Gutiérrez-Alonso, G., Conan, J. 2010. New time constrains on lithospheric-scale oroclinal bending of the Ibero-Armorican Arc: a paleomagnetic study of earliest Permian rocks from Iberia. *Journal of the Geological Society,* **167**, 127-173.

Weil, A.B**,** Van der Voo, R. 2002.Application of the paleomagnetic fold test to complex geologic environments: A case study from northern Spain. *Physics and Chemistry of the Earth*, **27**, 1223-1235.

Weil, A.B., Van der Voo, R., van der Pluijm, B. 2001. New paleomagnetic data from the southern Cantabria-Asturias Arc, northern Spain: Implications for true oroclinal rotation and the final amalgamation of Pangea. *Geology*, **29**, 991-994.

Whitmeyer, S.J., Nicoletti, J., De Paor, D.G. 2010. The digital revolution in geologic mapping. *GSA Today*, **20**, 1-10.

Williams, H., and Hiscott, R.N. 1987. Definition of the Iapetus rift-drift succession in western Newfoundland. *Geology*, **15**. 1044-1047.

Williams, H. and Hatcher, R.D. 1982. Suspect terranes and accretionary history of the Appalachian orogen. *Geology*, **10**, 530-536

Woodcock, N.H., Soper, N.J., Strachan, R.A. 2007. A Rheic cause for the Acadian deformation in Europe.*Journal of the Geological Society,***164**, 1023–1036.

Worsley, T.R., Nance, R.D., Moody, J.B. 1984. Global tectonic and eustasy for the past 2 billion years. *Marine Geology*, **58**, 373–400.

APPENDIX A

FIELD DATA

A.1. Google Earth

Geologic field data collection, analysis and map compilation are undergoing a revolution in methods, largely precipitated by global positioning system (GPS) and geographic information system (GIS) equipped mobile computers paired with virtual globe visualizations (e.g. Whitmeyer et al., 2010). Geologic data, maps and interpretations are beginning to be presented in a variety of formats on virtual globes, such as Google Earth. Google Earth–based interactive geologic maps communicate data and interpretations in a format that is more intuitive and easy to grasp than the traditional format of paper maps and cross sections. The virtual three-dimensional (3-D) interface removes much of the cognitive barrier of attempting to visualize 3-D features from a two-dimensional map or cross section (Whitmeyer et al., 2010).

In this thesis all field and analytical data has been imported into Google earth (i.e. field notes, images, U-Pb diagrams) See examples of screenshots in figures A.1, A.2, A.3, A.4, A.5. These images and data can also be accessed in the supplementary DVD attached to this thesis. The images and overlays are compiled in KML code, which can be opened with any Google earth application. Insert the DVD into your computer for more detailed instructions.

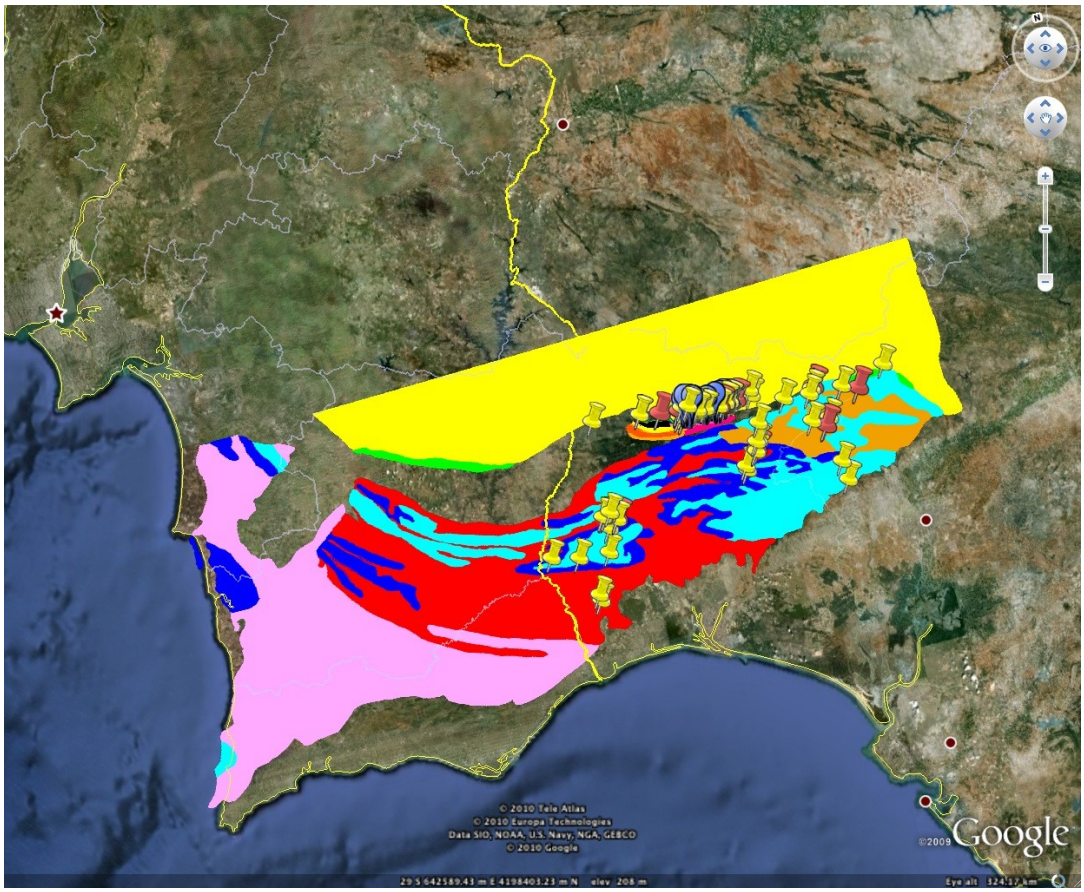

Fig. A.1 Google earth screen shot showing geologic map of southern Iberia overlay

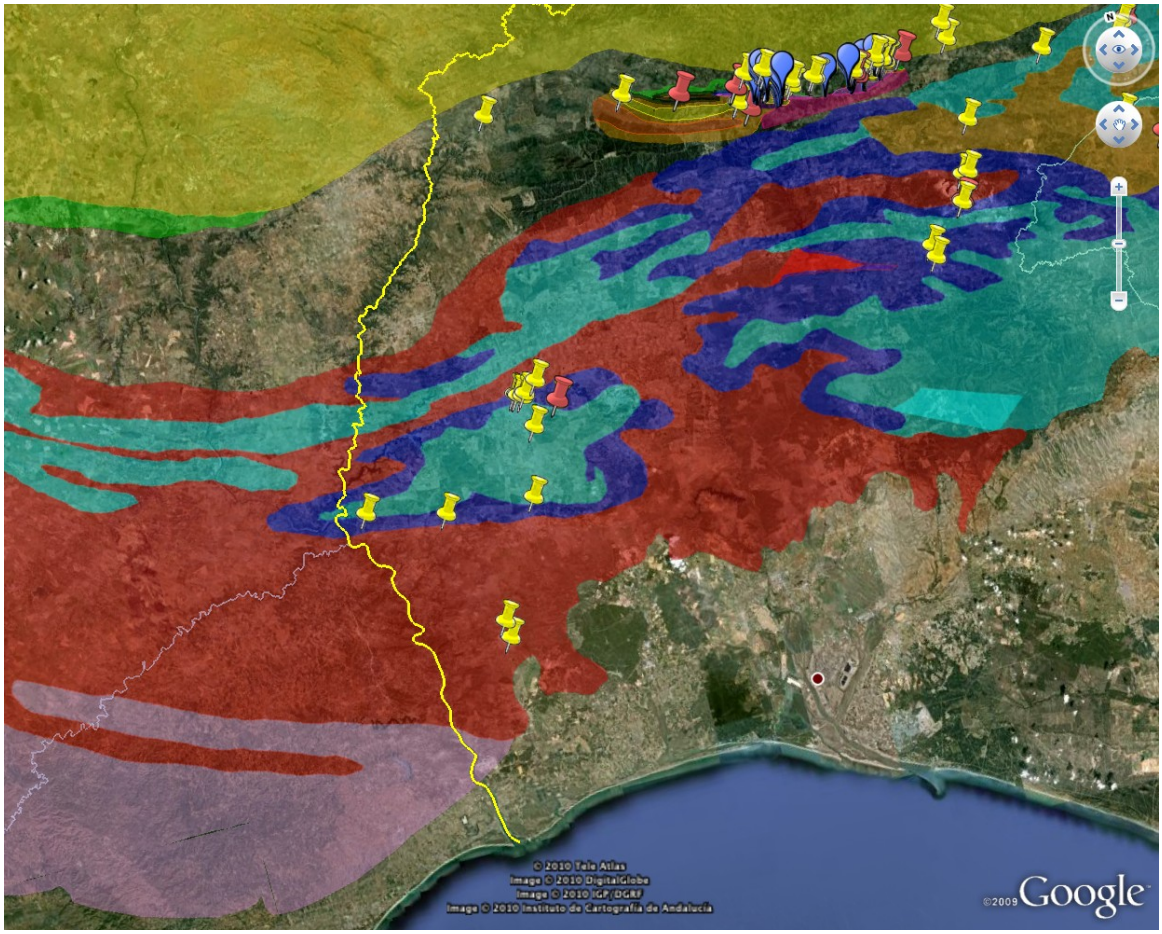

Fig. A.2 Google earth screen shot showing geologic overlays and placemarks for sample and outcrop locations.

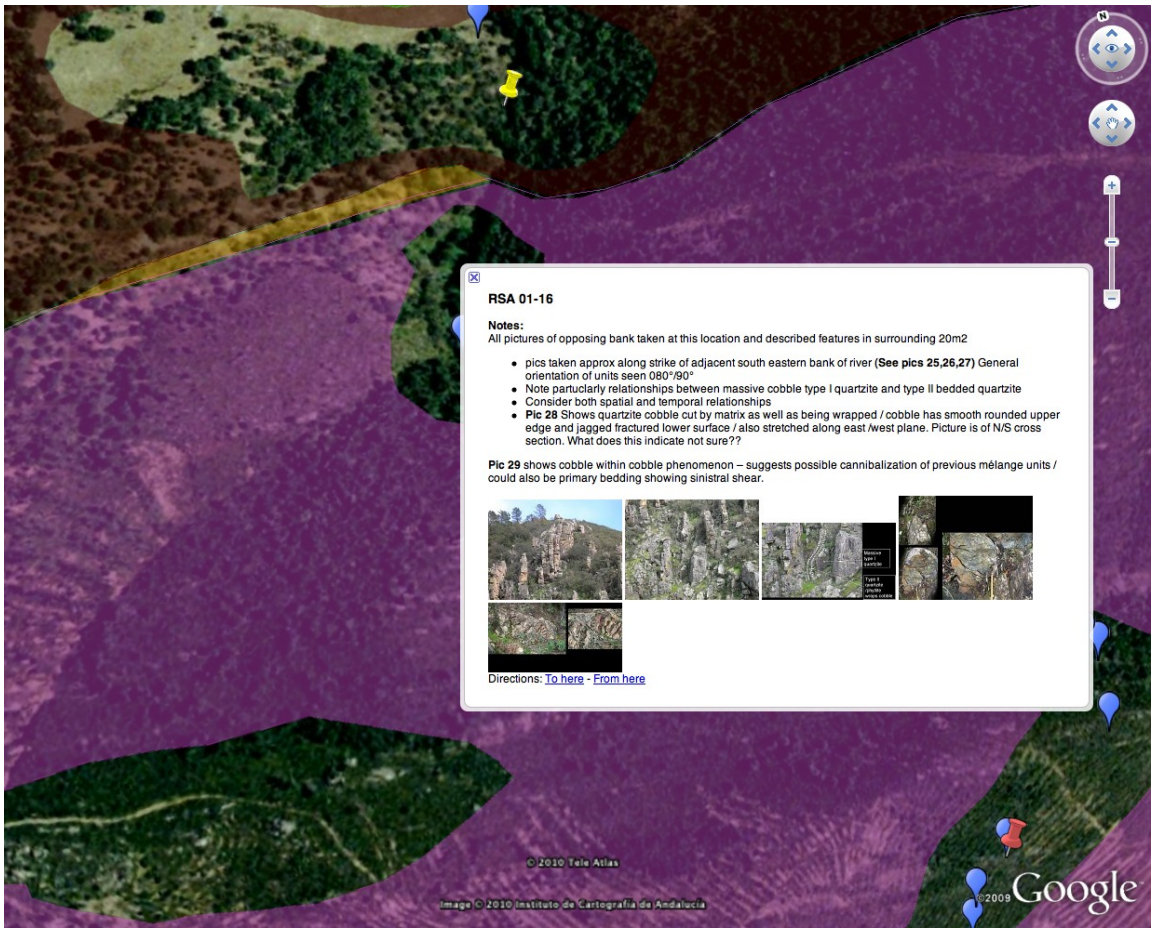

Fig. A.3 Google earth screen shot showing example of field note and field pictures linked to outcrop location.

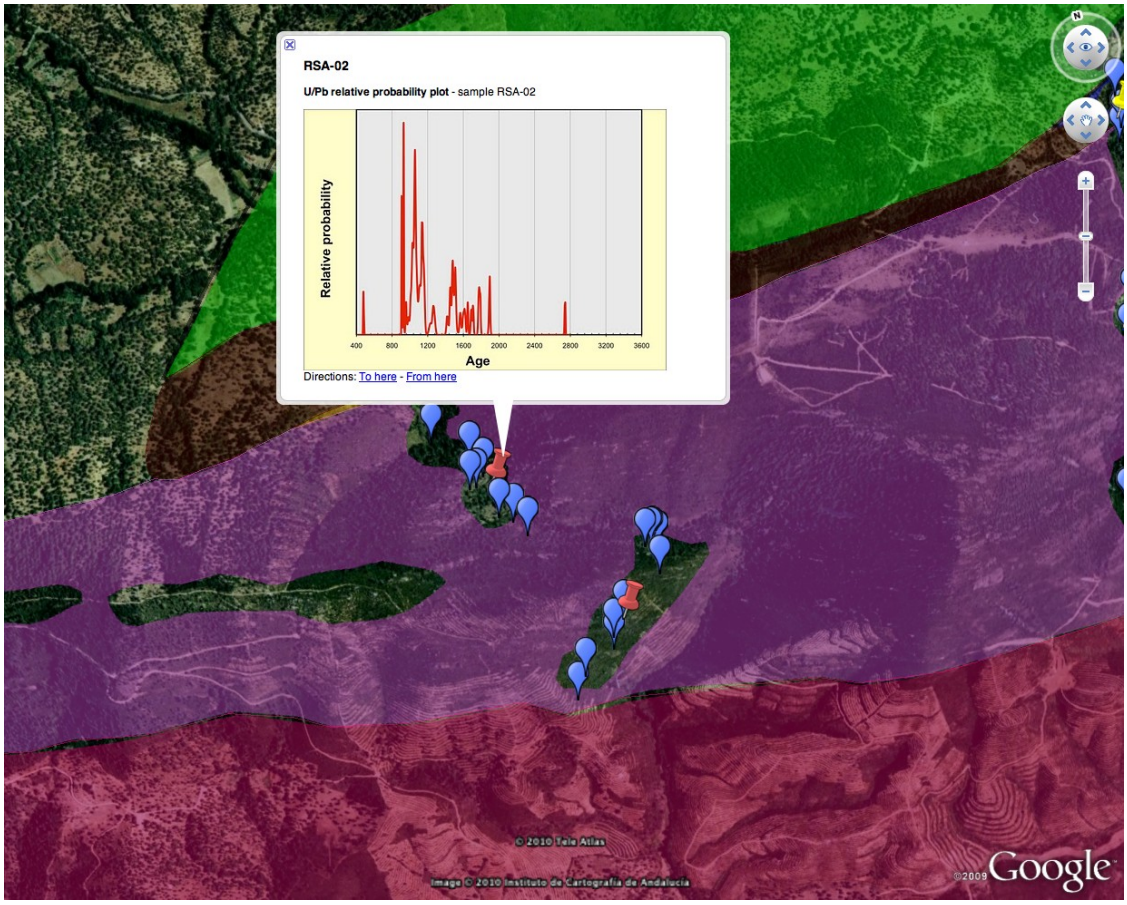

Fig. A.4 Google earth screen shot showing U-Pb probability plot link to sample and outcrop location.

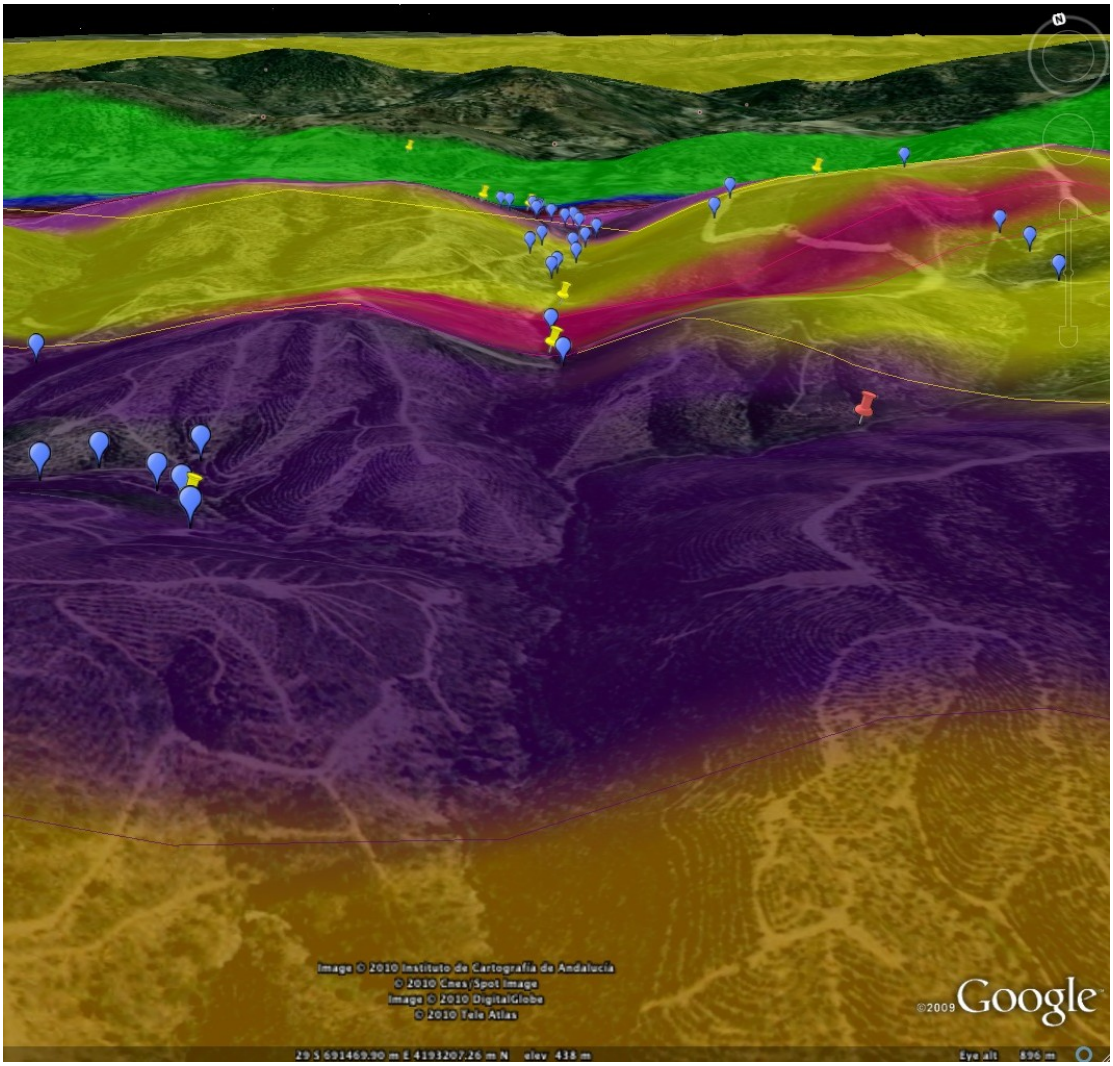

Fig. A.5 Google earth screen shot showing flyover of the PDLZ with sample and outcrop locations

APPENDIX B

GEOCHRONOLOGICAL DATA

B.1. Introduction

Uranium – lead(U-Pb) zircon dating of rocks described in chapters 3 and 4 constitutes the primary datasets for this thesis. All U-Pb dates (for both igneousand sedimentary rocks) were obtained from the mineral zircon using laser ablation inductively couple mass spectrometry (LA-ICPMS). The first part of this appendix briefly outlines the general principles behind U-Pb dating and the second part describes the sample preparation and analytical techniques.

B.2. Principles behind U-Pb dating

The U-Pb dating method relies on two separate decay chains, the uranium series from ^{238}U to ^{206}Pb, with a half-life of 4.47 billion years and the actinium series from ^{235}U to ^{207}Pb, with a half-life of 704 million years. The presence of these two independent decay processes of uranium results in two independent geochronometers and as a result is the most widely used geochronological tool. Some minerals, such as zircon, when formed incorporate ^{238}U and ^{235}U into their mineral structure and at the time of formation would have no initial radiogenic lead.

If a mineral remained closed, and therefore no lead loss has occurred, the age of the zircon can be calculated independently from the two equations:

$$^{206}Pb / ^{238}U = e^{\lambda_{238}t} - 1$$

And

$$^{207}Pb / ^{235}U = e^{\lambda_{235}t} - 1,$$

These are said to yield concordant ages. If these concordant ages are plotted over a series of time intervals, in a $^{206}Pb/^{238}U$ vs. $^{207}Pb/^{235}U$ diagram the resulting curve through time is generally called a 'concordia' line (Wetherill, 1956).

For example at the time of formation a mineral containing uranium with no initial lead will plot at the origin. The location of the point on concordia depends only on the age of the sample. If at some later date (e.g. 2.4 billion years after formation) the sample loses lead (i.e. system is opened), the point will move off of concordia along a straight line toward the origin (Fig. B.1). This lead loss can occur as the result of some geologic event (i.e. Mountain building and metamorphism) which causes the crystal system to become open.

At any time after the episodic lead loss (e.g 1.1 billion years later), various points will lie on a chord to concordia connecting the original age of the sample and the age of the lead loss episode, depending on the relative amounts of Pb loss. This chord is called a discordia. In this case the upper intercept of the discordia with concordia gives the original age of the rock, or 3.5 Ga in the example shown (Fig B.1c). There are several hypotheses for the interpretation of the lower intercept, but the most common

interpretation is that it indicates the age of the event that caused the lead loss (e.g. 1.1 Ga in example).

In addition, an "age" based on the $^{207}Pb/^{206}Pb$ ratio can be calculated because this ratio changes over time. If necessary, a correction can be made for the initial lead in these systems using ^{204}Pb as an index. Therefore if the three age calculations agree ($^{206}Pb/^{238}U$, $^{207}Pb/^{235}U$ and $^{207}Pb/^{206}Pb$), then the age represents the true age of the rock. Lead, however, is a volatile element, and so lead loss is commonly a problem. As a result, simple U-Pb ages are often discordant.

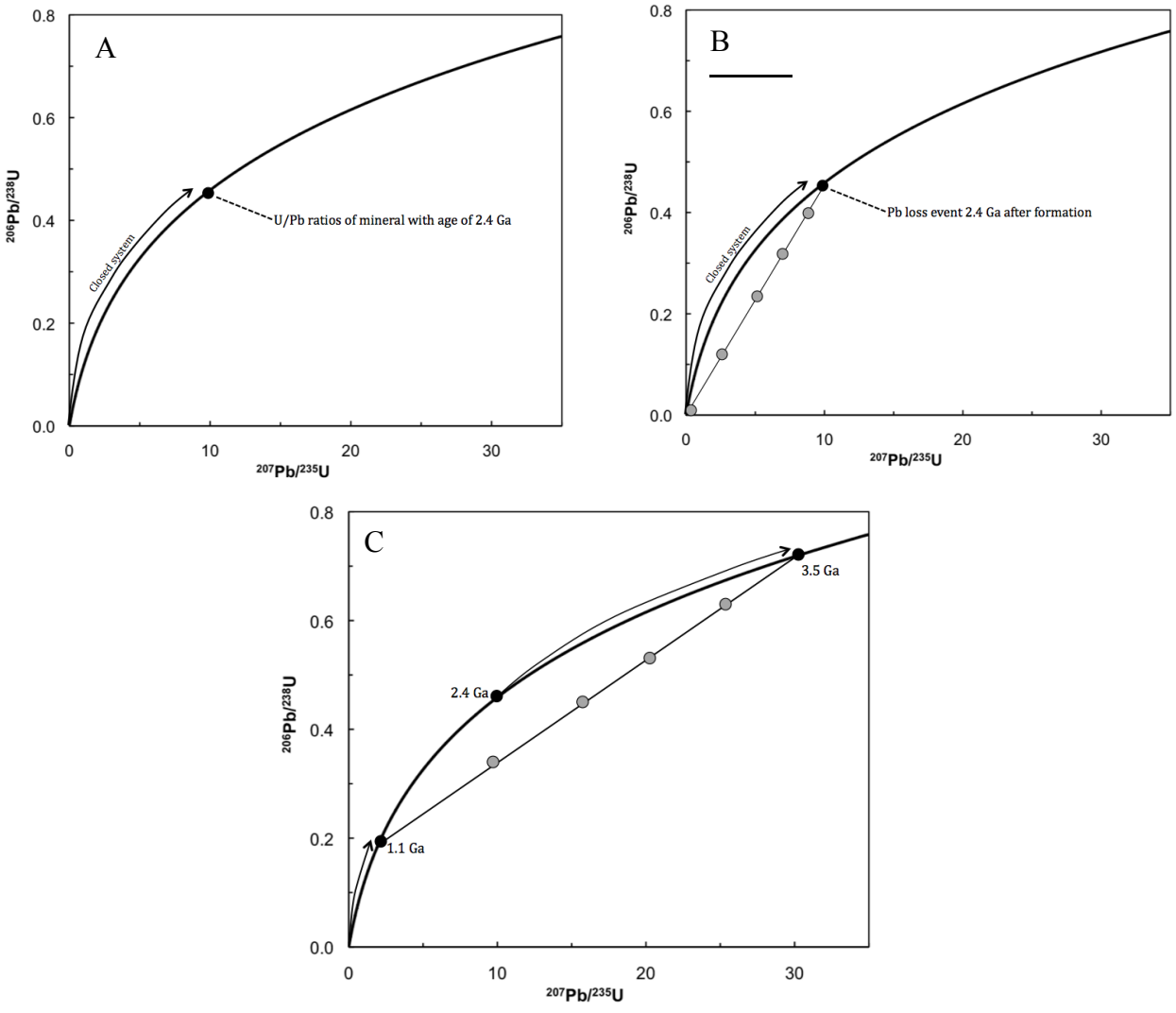

Fig. B.1 Principle behind the U-Pb concordia diagram (a) Concordant age (2.4 Ga) (b)Pb loss event 2.4 Ga after formation (c) 1.1 Ga after Pb loss

B.3. Laser Ablation Inductively Coupled Mass Spectrometry

B.3.1. Sample Selection and Preparation

Approximately 15-20 Kg of rocks were selected for each sample. Zircon grains were separated using conventional crushing, grinding and wet shaking table methods, followed by heavy liquid and magnetic separation at the Pacific Centre for Isotopic and Geochemical Research (PCIGR). Zircon grains were then hand-picked and mounted, together with zircon standards and in-house standards on an epoxy puck. The zircons were mounted in a grid format so individual zircon grains could be indentified. Following mounting in epoxy the pucks were polished to reveal central portions of the zircon grains. After polishing the mount was washed by soap and rinsed in deionized water.

B.3.2. Methodology

Zircon grains were dated using laser ablation LA-ICPMS methods, employing a New Wave UP-213 laser ablation system and a Thermo Finnigan Element 2 single collector, double-focusing, magnetic sector ICP-MS. Zircons were handpicked from the heavy mineral concentrate and mounted in an epoxy puck along with several grains of the Plešovice zircon standard (Sláma et al. 2008), together with a separate in-house, 197 Ma standard zircon, and brought to a very high polish. High quality portions of each grain free of alteration, inclusions, or possible inherited cores were selected for analysis. The

surface of the mount was washed for 10 minutes with dilute nitric acid and rinsed in ultraclean water prior to analysis. Line scans were employed in order to minimize elemental fractionation during the analyses. Backgrounds were measured with the laser shutter closed for ten seconds, followed by data collection with the laser firing for approximately 29 seconds. The time-integrated signals were analysed using GLITTER software (Van Achterbergh et al. 2001; Griffin et al. 2008), which automatically subtracts background measurements, propagates all analytical errors, and calculates isotopic ratios and ages. Time-resolveddata were carefully examined to identify and avoid portionsof the signal that reflected Pb loss and/or the presence ofolder inherited cores or altered zones in the zircon being analyzed. Corrections for mass and elemental fractionation were made by bracketing analyses of unknown grains with replicate analyses of the Plešovice zircon standard. A typical analytical session for dating zircons at the PCIGR consists of four analyses of the standard zircon, followed by four analyses of unknown zircons, two standard analyses, four unknown analyses, etc., and finally four standard analyses. The 197 Ma in-house zircon standard was analysed as an unknown in order to monitor the reproducibility of the age determinations on a run-to-run basis. Final interpretation and plotting of the analytical results employed the ISOPLOT software (Ludwig 2003). The final interpreted age for intrusive samples is based on a weighted average of the individually calculated $^{206}Pb/^{238}U$ ages. Analytical results for detrital zircon samples are filtered, with analyses that exhibit >5% reverse discordance or >10% normal discordance being rejected. Errors are quoted at the 2σ level. For samples yielding

isotopic ages >1Ga, the $^{207}Pb/^{206}Pb$ ages are reported, whereas for samples <1 Ga the $^{206}Pb/^{238}U$ ages are reported. Detrital zircon ages are presented as cumulative density plots.

Table B.1 U-Pb analytical data, detrital zircon sample JAB-08

Analysis	Isotopic ratios and 2σ (%) errors						Ages and 2σ absolute errors (Ma)						Reported Age		
number	$^{206}Pb/^{238}U$	±2σ	$^{207}Pb/^{235}U$	±2σ	$^{207}Pb/^{206}Pb$	±2σ	$^{206}Pb/^{238}U$	±2σ	$^{207}Pb/^{235}U$	±2σ	$^{207}Pb/^{206}Pb$	±2σ	Age (Ma)	±2σ	Disc. (%)
1	0.2657	1.28	3.5254	2.05	0.0970	1.41	1519	4	1533	5	1567	35	1567	35	-0.9
2	0.0921	1.54	0.7544	3.24	0.0582	2.78	568	4	571	5	538	36	568	4	-0.5
3	0.2120	1.55	2.3298	3.47	0.0799	2.38	1240	4	1221	5	1193	33	1193	33	1.5
4	0.2721	1.29	3.4689	2.07	0.0958	1.42	1551	4	1520	5	1544	34	1544	34	2.0
5	0.3768	1.23	6.8253	1.75	0.1361	1.20	2062	5	2089	13	2178	145	2178	145	-1.3
6	0.5021	1.21	12.1960	1.62	0.1768	1.14	2623	6	2620	15	2623	174	2623	174	0.1
7	0.2382	1.43	2.6724	2.88	0.0844	1.94	1377	4	1321	11	1302	130	1302	130	4.3
8	0.4068	1.25	7.4503	1.92	0.1380	1.25	2200	4	2167	5	2202	35	2202	35	1.5
9	0.5029	1.21	12.3892	1.56	0.1803	1.13	2626	17	2634	16	2656	26	2656	26	-0.3
10	0.4681	1.38	10.0874	2.98	0.1548	1.50	2475	8	2443	14	2400	60	2400	60	1.3
11	0.3633	1.24	6.3023	1.77	0.1273	1.22	1998	17	2019	25	2061	46	2061	46	-1.0
12	0.2487	1.27	3.0612	2.00	0.0889	1.42	1432	18	1423	16	1401	27	1401	27	0.6
13	0.3787	1.23	6.6830	1.70	0.1293	1.19	2070	22	2070	15	2088	21	2088	21	0.0
14	0.1622	1.40	1.6747	2.58	0.0766	1.94	969	4	999	5	1112	34	1112	34	-3.0
15	0.1995	1.66	2.4047	3.91	0.0858	2.65	1172	26	1244	15	1334	19	1334	19	-5.8
16	0.4085	1.38	8.2212	2.88	0.1416	1.55	2208	18	2256	21	2247	37	2247	37	-2.1
17	0.1015	1.41	0.8082	2.64	0.0587	2.23	623	23	602	17	556	22	623	23	3.6
18	0.0844	1.29	0.6736	1.99	0.0588	1.70	522	26	523	15	561	19	522	26	-0.1

Table B.1 (continued)U-Pb analytical data, detrital zircon sample JAB-08.

Analysis	Isotopic ratios and 2σ (%) errors						Ages and 2σ absolute errors (Ma)						Reported Age		
number	$^{206}Pb/^{238}U$	±2σ	$^{207}Pb/^{235}U$	±2σ	$^{207}Pb/^{206}Pb$	±2σ	$^{206}Pb/^{238}U$	±2σ	$^{207}Pb/^{235}U$	±2σ	$^{207}Pb/^{206}Pb$	±2σ	Age (Ma)	±2σ	Disc. (%)
37	0.0882	1.61	0.7124	3.52	0.0600	3.05	545	9	546	17	602	71	545	9	-0.3
38	0.0910	1.87	0.7088	4.63	0.0558	4.02	562	4	544	5	442	34	562	4	3.2
39	0.0650	2.25	0.5126	6.58	0.0552	6.06	406	31	420	26	422	22	406	31	-3.4
40	0.0589	1.24	0.4412	1.70	0.0541	1.48	369	11	371	23	377	92	369	11	-0.5
41	0.0986	1.31	0.8233	2.11	0.0611	1.77	606	7	610	9	643	35	606	7	-0.6
42	0.0580	1.55	0.4217	3.28	0.0533	3.02	363	8	357	15	341	88	363	8	1.7
43	0.0600	1.27	0.4404	1.83	0.0539	1.60	375	5	371	9	367	60	375	5	1.3
44	0.0591	1.44	0.4238	2.77	0.0530	2.53	370	4	359	5	327	35	370	4	3.1
45	0.0604	1.37	0.4321	2.46	0.0525	2.23	378	4	365	13	308	177	378	4	3.7
46	0.0977	1.83	0.8263	4.58	0.0613	3.91	601	6	612	16	651	184	601	6	-1.7
47	0.0663	1.30	0.5210	2.05	0.0564	1.79	414	5	426	16	467	205	414	5	-2.8
48	0.0922	1.74	0.7022	4.27	0.0559	3.74	568	4	540	5	448	36	568	4	5.2
49	0.1034	1.26	0.9034	1.82	0.0646	1.53	635	5	654	8	763	50	635	5	-2.9
50	0.3861	1.26	7.1213	2.06	0.1336	1.36	2105	5	2127	7	2146	43	2146	43	-1.0
51	0.0826	1.31	0.7490	2.05	0.0659	1.74	512	5	568	8	804	52	512	5	-9.9
52	0.0606	1.30	0.4361	2.04	0.0534	1.80	379	5	368	6	345	37	379	5	3.1
53	0.2863	1.32	4.1670	2.35	0.1077	1.58	1623	8	1668	10	1761	37	1761	37	-2.7
54	0.1023	1.68	0.9334	3.78	0.0655	3.15	628	4	669	5	790	36	628	4	-6.2

Table B.1 (continued)U-Pb analytical data, detrital zircon sample JAB-08.

Analysis	Isotopic ratios and 2σ (%) errors						Ages and 2σ absolute errors (Ma)						Reported Age		
number	$^{206}Pb/^{238}U$	±2σ	$^{207}Pb/^{235}U$	±2σ	$^{207}Pb/^{206}Pb$	±2σ	$^{206}Pb/^{238}U$	±2σ	$^{207}Pb/^{235}U$	±2σ	$^{207}Pb/^{206}Pb$	±2σ	Age (Ma)	±2σ	Disc. (%)
37	0.0882	1.61	0.7124	3.52	0.0600	3.05	545	9	546	17	602	71	545	9	-0.3
38	0.0910	1.87	0.7088	4.63	0.0558	4.02	562	4	544	5	442	34	562	4	3.2
39	0.0650	2.25	0.5126	6.58	0.0552	6.06	406	31	420	26	422	22	406	31	-3.4
40	0.0589	1.24	0.4412	1.70	0.0541	1.48	369	11	371	23	377	92	369	11	-0.5
41	0.0986	1.31	0.8233	2.11	0.0611	1.77	606	7	610	9	643	35	606	7	-0.6
42	0.0580	1.55	0.4217	3.28	0.0533	3.02	363	8	357	15	341	88	363	8	1.7
43	0.0600	1.27	0.4404	1.83	0.0539	1.60	375	5	371	9	367	60	375	5	1.3
44	0.0591	1.44	0.4238	2.77	0.0530	2.53	370	4	359	5	327	35	370	4	3.1
45	0.0604	1.37	0.4321	2.46	0.0525	2.23	378	4	365	13	308	177	378	4	3.7
46	0.0977	1.83	0.8263	4.58	0.0613	3.91	601	6	612	16	651	184	601	6	-1.7
47	0.0663	1.30	0.5210	2.05	0.0564	1.79	414	5	426	16	467	205	414	5	-2.8
48	0.0922	1.74	0.7022	4.27	0.0559	3.74	568	4	540	5	448	36	568	4	5.2
49	0.1034	1.26	0.9034	1.82	0.0646	1.53	635	5	654	8	763	50	635	5	-2.9
50	0.3861	1.26	7.1213	2.06	0.1336	1.36	2105	5	2127	7	2146	43	2146	43	-1.0
51	0.0826	1.31	0.7490	2.05	0.0659	1.74	512	5	568	8	804	52	512	5	-9.9
52	0.0606	1.30	0.4361	2.04	0.0534	1.80	379	5	368	6	345	37	379	5	3.1
53	0.2863	1.32	4.1670	2.35	0.1077	1.58	1623	8	1668	10	1761	37	1761	37	-2.7
54	0.1023	1.68	0.9334	3.78	0.0655	3.15	628	4	669	5	790	36	628	4	-6.2

Table B.1 (continued) U-Pb analytical data, detrital zircon sample JAB-08.

Analysis	Isotopic ratios and 2σ (%) errors						Ages and 2σ absolute errors (Ma)						Reported Age		
number	$^{206}Pb/^{238}U$	±2σ	$^{207}Pb/^{235}U$	±2σ	$^{207}Pb/^{206}Pb$	±2σ	$^{206}Pb/^{238}U$	±2σ	$^{207}Pb/^{235}U$	±2σ	$^{207}Pb/^{206}Pb$	±2σ	Age (Ma)	±2σ	Disc. (%)
55	0.0929	1.34	0.7448	2.24	0.0594	1.92	572	10	565	18	581	64	572	10	1.3
56	0.1172	1.29	0.9934	2.04	0.0619	1.68	714	8	701	15	669	65	714	8	2.0
57	0.0951	1.44	0.8165	2.73	0.0621	2.32	586	10	606	20	678	87	586	10	-3.4
58	0.0605	1.57	0.4466	3.48	0.0535	3.19	379	9	375	23	351	130	379	9	1.0
59	0.4729	1.54	9.8940	3.87	0.1554	1.89	2496	4	2425	5	2406	33	2406	33	2.9
60	0.0941	2.35	0.7338	6.61	0.0586	5.75	580	4	559	5	554	37	580	4	3.7
61	0.0591	1.40	0.4680	2.54	0.0559	2.29	370	8	390	10	449	38	370	8	-5.0
62	0.0553	2.04	0.4032	5.80	0.0546	5.50	347	5	344	10	394	67	347	5	0.9
63	0.3637	1.21	6.3187	1.62	0.1260	1.28	2000	5	2021	6	2043	36	2043	36	-1.1
64	0.3906	1.25	6.9182	1.98	0.1292	1.38	2125	5	2101	8	2087	56	2087	56	1.2
65	0.3901	1.33	7.2349	2.58	0.1307	1.56	2123	5	2141	8	2107	50	2107	50	-0.8

Table B.2 U-Pb analytical data, detrital zircon sample JAB-43

Analysis	Isotopic ratios and 2σ (%) errors						Ages and 2σ absolute errors (Ma)						Reported Age		
number	$^{206}Pb/^{238}U$	±2σ	$^{207}Pb/^{235}U$	±2σ	$^{207}Pb/^{206}Pb$	±2σ	$^{206}Pb/^{238}U$	±2σ	$^{207}Pb/^{235}U$	±2σ	$^{207}Pb/^{206}Pb$	±2σ	Age (Ma)	±2σ	Disc. (%)
1	0.2598	1.10	3.2549	2.15	0.0928	1.47	1489	15	1470	17	1483	28	1483	28	1.3
2	0.1925	1.03	2.0371	1.69	0.0772	1.31	1135	11	1128	11	1125	26	1125	26	0.6
3	0.0704	1.04	0.5734	1.61	0.0593	1.40	439	4	460	6	579	30	439	4	-4.7
4	0.2584	1.31	3.2065	3.18	0.0937	1.99	1482	17	1459	25	1503	37	1503	37	1.6
5	0.1842	1.05	1.9597	1.80	0.0773	1.37	1090	11	1102	12	1128	27	1128	27	-1.1
6	0.3141	1.08	4.6107	2.10	0.1052	1.37	1761	17	1751	17	1717	25	1717	25	0.5
7	0.0715	1.05	0.5517	1.71	0.0557	1.49	445	5	446	6	440	32	445	5	-0.2
8	0.1545	1.14	1.4485	2.24	0.0703	1.74	926	10	909	13	936	35	926	10	1.8
9	0.2796	1.13	3.7480	2.32	0.0986	1.52	1589	16	1582	19	1598	28	1598	28	0.5
10	0.1849	2.20	2.1173	6.52	0.0795	4.35	1094	22	1154	45	1183	84	1183	84	-5.3
11	0.1858	2.24	1.8078	6.89	0.0703	4.81	1099	23	1048	45	937	96	1099	23	4.8
12	0.2891	1.01	4.0338	1.60	0.1022	1.19	1637	15	1641	13	1664	22	1664	22	-0.2
13	0.1728	1.14	1.7519	2.26	0.0745	1.69	1028	11	1028	15	1054	34	1054	34	0.0
14	0.1581	1.30	1.5691	2.99	0.0727	2.26	946	11	958	19	1005	45	1005	45	-1.2
15	0.3314	1.09	5.1764	2.18	0.1120	1.38	1845	18	1849	19	1831	25	1831	25	-0.2
16	0.1765	1.00	1.8016	1.50	0.0742	1.21	1048	10	1046	10	1047	24	1047	24	0.2
17	0.2261	1.34	2.6412	3.29	0.0873	2.20	1314	16	1312	24	1368	42	1368	42	0.1
18	0.2394	1.05	2.9449	1.86	0.0892	1.35	1383	13	1394	14	1408	26	1408	26	-0.7

Table B.2 (continued). U-Pb analytical data, detrital zircon sample JAB-43

Analysis	Isotopic ratios and 2σ (%) errors						Ages and 2σ absolute errors (Ma)						Reported Age		
number	$^{206}Pb/^{238}U$	±2σ	$^{207}Pb/^{235}U$	±2σ	$^{207}Pb/^{206}Pb$	±2σ	$^{206}Pb/^{238}U$	±2σ	$^{207}Pb/^{235}U$	±2σ	$^{207}Pb/^{206}Pb$	±2σ	Age (Ma)	±2σ	Disc. (%)
19	0.1793	1.08	1.8504	1.99	0.0753	1.51	1063	11	1064	13	1077	30	1077	30	0.0
20	0.2278	1.08	2.7399	1.99	0.0858	1.43	1323	13	1339	15	1333	28	1333	28	-1.2
21	0.1825	1.28	1.9143	2.89	0.0780	2.09	1081	13	1086	19	1147	41	1147	41	-0.5
22	0.1945	1.13	2.0490	2.25	0.0769	1.66	1146	12	1132	15	1120	33	1120	33	1.2
23	0.1833	1.19	1.8668	2.60	0.0726	1.89	1085	12	1069	17	1003	38	1003	38	1.5
24	0.2485	1.03	3.1293	1.69	0.0939	1.26	1431	13	1440	13	1505	24	1505	24	-0.6
25	0.1553	1.34	1.5112	3.24	0.0714	2.47	931	12	935	20	968	50	931	12	-0.5
26	0.2976	1.02	4.2220	1.68	0.1036	1.23	1679	15	1678	14	1690	22	1690	22	0.1
27	0.5337	1.12	14.0483	2.55	0.1909	1.31	2757	25	2753	24	2750	21	2750	21	0.1
28	0.1850	1.53	1.8326	4.04	0.0730	2.89	1094	15	1057	27	1013	57	1013	57	3.5
29	0.2167	1.03	2.5275	1.71	0.0854	1.30	1264	12	1280	12	1323	25	1323	25	-1.2
30	0.3051	1.01	4.4682	1.64	0.1068	1.21	1717	15	1725	14	1745	22	1745	22	-0.5
31	0.1788	1.23	1.9465	2.80	0.0737	2.01	1060	12	1097	19	1034	40	1034	40	-3.4
32	0.1697	1.10	1.6747	2.06	0.0727	1.58	1010	10	999	13	1006	32	1006	32	1.1
33	0.2500	0.99	3.1284	1.51	0.0914	1.18	1438	13	1440	12	1456	22	1456	22	-0.1
34	0.3873	1.22	7.0837	2.92	0.1332	1.61	2110	22	2122	26	2141	28	2141	28	-0.6
35	0.1640	1.40	1.6703	3.40	0.0745	2.51	979	13	997	22	1056	50	1056	50	-1.9
36	0.1845	1.00	2.0403	1.54	0.0782	1.24	1091	10	1129	11	1152	24	1152	24	-3.3

Table B.2 (continued). U-Pb analytical data, detrital zircon sample JAB-43

Analysis	Isotopic ratios and 2σ (%) errors						Ages and 2σ absolute errors (Ma)						Reported Age		
number	$^{206}Pb/^{238}U$	±2σ	$^{207}Pb/^{235}U$	±2σ	$^{207}Pb/^{206}Pb$	±2σ	$^{206}Pb/^{238}U$	±2σ	$^{207}Pb/^{235}U$	±2σ	$^{207}Pb/^{206}Pb$	±2σ	Age (Ma)	±2σ	Disc. (%)
37	0.2729	1.08	3.7392	2.11	0.0981	1.44	1556	15	1580	17	1589	27	1589	27	-1.5
38	0.2444	1.15	3.0829	2.47	0.0907	1.65	1410	15	1428	19	1441	31	1441	31	-1.3
39	0.1627	1.21	1.6043	2.59	0.0721	1.97	972	11	972	16	988	40	972	11	0.0
40	0.2861	1.03	3.9765	1.79	0.1015	1.30	1622	15	1629	15	1652	24	1652	24	-0.5
41	0.2400	1.04	2.9851	1.83	0.0894	1.35	1387	13	1404	14	1413	26	1413	26	-1.2
42	0.2848	1.08	3.9122	2.07	0.1004	1.42	1616	15	1616	17	1632	26	1632	26	0.0
43	0.1570	1.94	1.4414	5.60	0.0664	4.20	940	17	906	34	818	85	940	17	3.7
44	0.2268	0.99	2.6560	1.48	0.0839	1.19	1318	12	1316	11	1290	23	1290	23	0.1
45	0.1922	1.12	2.0763	2.24	0.0784	1.66	1133	12	1141	15	1158	33	1158	33	-0.7
46	0.1755	1.07	1.8409	1.96	0.0744	1.51	1043	10	1060	13	1051	30	1051	30	-1.7
47	0.2039	1.04	2.1656	1.78	0.0788	1.37	1196	11	1170	12	1167	27	1167	27	2.2
48	0.3366	1.20	5.5090	2.77	0.1181	1.63	1870	19	1902	24	1927	29	1927	29	-1.7
49	0.1858	1.14	2.0759	2.31	0.0783	1.70	1099	12	1141	16	1155	33	1155	33	-3.7
50	0.1572	1.35	1.5563	3.21	0.0723	2.42	941	12	953	20	993	49	941	12	-1.2
51	0.2732	1.14	3.5135	2.45	0.0908	1.63	1557	16	1530	19	1443	31	1443	31	1.8
52	0.0715	1.11	0.5643	2.02	0.0568	1.76	445	5	454	7	484	39	445	5	-2.0
53	0.1560	1.06	1.5113	1.92	0.0698	1.52	935	9	935	12	923	31	935	9	-0.1
54	0.2010	1.08	2.1944	2.02	0.0810	1.52	1181	12	1179	14	1221	30	1221	30	0.1

Table B.2 (continued). U-Pb analytical data, detrital zircon sample JAB-43

Analysis	Isotopic ratios and 2σ (%) errors						Ages and 2σ absolute errors (Ma)						Reported Age		
number	$^{206}Pb/^{238}U$	±2σ	$^{207}Pb/^{235}U$	±2σ	$^{207}Pb/^{206}Pb$	±2σ	$^{206}Pb/^{238}U$	±2σ	$^{207}Pb/^{235}U$	±2σ	$^{207}Pb/^{206}Pb$	±2σ	Age (Ma)	±2σ	Disc. (%)
55	0.1929	1.15	2.0390	2.37	0.0777	1.74	1137	12	1129	16	1139	34	1139	34	0.7
56	0.1768	1.18	1.8177	2.49	0.0727	1.86	1050	11	1052	16	1005	37	1005	37	-0.2
57	0.1697	1.09	1.7149	2.08	0.0721	1.61	1011	10	1014	13	990	32	1011	10	-0.3
58	0.2779	1.05	3.6983	1.89	0.0964	1.37	1581	15	1571	15	1556	26	1556	26	0.6
59	0.1924	1.25	1.9668	2.83	0.0760	2.05	1134	13	1104	19	1096	41	1096	41	2.7
60	0.2003	1.02	2.1899	1.67	0.0791	1.33	1177	11	1178	12	1175	26	1175	26	-0.1
61	0.1886	1.21	1.9748	2.64	0.0757	1.94	1114	12	1107	18	1088	38	1088	38	0.6
62	0.2367	1.46	2.8744	3.79	0.0880	2.44	1369	18	1375	29	1382	46	1382	46	-0.4
63	0.2467	1.09	3.0869	2.14	0.0905	1.53	1421	14	1429	16	1435	29	1435	29	-0.6
64	0.2594	1.35	3.1268	3.41	0.0886	2.19	1487	18	1439	26	1395	41	1395	41	3.3
65	0.2827	1.31	4.0624	3.27	0.1027	1.99	1605	19	1647	27	1673	36	1673	36	-2.5

Table B.3. U-Pb analytical data, detrital zircon sample JB-17

Analysis	Isotopic ratios and 2σ (%) errors						Ages and 2σ absolute errors (Ma)						Reported Age		
number	$^{206}Pb/^{238}U$	±2σ	$^{207}Pb/^{235}U$	±2σ	$^{207}Pb/^{206}Pb$	±2σ	$^{206}Pb/^{238}U$	±2σ	$^{207}Pb/^{235}U$	±2σ	$^{207}Pb/^{206}Pb$	±2σ	Age (Ma)	±2σ	Disc. (%)
1a	0.3445	0.71	6.2255	2.55	0.1293	1.23	1908	12	2008	22	2088	21	2088	21	8.6
1b	0.0991	1.20	0.8232	3.90	0.0606	3.18	609	7	610	18	626	67	609	7	2.7
1c	0.0915	0.52	0.7533	1.53	0.0594	1.30	564	3	570	7	582	28	564	3	3.1
1d	0.3824	0.46	7.0583	1.50	0.1356	0.96	2087	8	2119	13	2172	17	2172	17	3.9
1e	0.1022	0.56	0.8455	1.65	0.0615	1.37	627	3	622	8	657	29	627	3	4.6
7a	0.3612	0.56	6.6021	1.85	0.1305	1.16	1988	10	2060	16	2104	20	2104	20	5.5
7b	0.3542	0.60	5.8050	2.01	0.1183	1.27	1955	10	1947	17	1931	22	1931	22	-1.2
7c	0.0864	0.80	0.7103	2.44	0.0587	2.08	534	4	545	10	556	45	534	4	4.0
7d	0.1068	1.01	0.9492	3.17	0.0627	2.55	654	6	678	16	698	54	654	6	6.3
7e	0.4782	0.65	11.3161	2.21	0.1695	1.37	2519	13	2550	21	2552	23	2552	23	1.3
1f	0.1000	0.63	0.8746	1.82	0.0622	1.59	614	4	638	9	681	34	614	4	9.8
1g	0.0969	0.64	0.8372	1.87	0.0612	1.65	596	4	618	9	645	35	596	4	7.6
1h	0.3097	0.73	5.0073	2.32	0.1131	1.70	1739	11	1821	20	1850	30	1850	30	6.0
1i	0.3436	0.74	5.7769	2.33	0.1222	1.74	1904	12	1943	20	1988	31	1988	31	4.3
1j	0.1016	0.75	0.8310	2.20	0.0601	1.93	624	4	614	10	607	41	624	4	-2.8
2a	0.3668	0.82	6.5101	2.56	0.1280	1.96	2014	14	2047	23	2070	34	2070	34	2.7
2b	0.1672	0.80	1.6775	2.35	0.0728	2.03	997	7	1000	15	1009	41	1009	41	1.2
2c	0.2581	0.95	4.2806	2.95	0.1156	2.24	1480	13	1690	24	1890	40	1890	40	21.7

Table B.3 (continued). U-Pb analytical data, detrital zircon sample JB-17

Analysis	Isotopic ratios and 2σ (%) errors						Ages and 2σ absolute errors (Ma)						Reported Age		
number	$^{206}Pb/^{238}U$	±2σ	$^{207}Pb/^{235}U$	±2σ	$^{207}Pb/^{206}Pb$	±2σ	$^{206}Pb/^{238}U$	±2σ	$^{207}Pb/^{235}U$	±2σ	$^{207}Pb/^{206}Pb$	±2σ	Age (Ma)	±2σ	Disc. (%)
2d	0.3518	0.93	6.0541	2.93	0.1219	2.25	1943	16	1984	26	1984	40	1984	40	2.0
2e	0.0962	1.07	0.8077	3.23	0.0603	2.80	592	6	601	15	615	59	592	6	3.8
2f	0.2075	0.95	2.3670	2.81	0.0818	2.46	1215	11	1233	20	1242	47	1242	47	2.1
2g	0.0976	1.73	0.7960	5.45	0.0593	4.59	600	10	595	25	579	97	600	10	-3.7
2h	0.0965	1.03	0.8032	3.02	0.0594	2.68	594	6	599	14	582	57	594	6	-2.1
2i	0.0861	1.31	0.7014	3.97	0.0586	3.46	532	7	540	17	553	74	532	7	3.7
2j	0.0993	1.12	0.8366	3.30	0.0602	2.92	610	7	617	15	612	62	610	7	0.2
3a	0.1040	1.46	0.8696	4.40	0.0609	3.81	638	9	635	21	635	80	638	9	-0.4
3b	0.0966	1.39	0.7791	4.13	0.0583	3.62	595	8	585	18	539	78	595	8	-10.4
3c	0.0981	1.40	0.8178	4.14	0.0594	3.64	603	8	607	19	580	77	603	8	-3.9
3d	0.3494	1.41	5.9663	4.18	0.1222	3.65	1932	24	1971	36	1989	63	1989	63	2.9
3e	0.3534	1.50	6.0394	4.51	0.1214	3.81	1951	25	1982	39	1978	66	1978	66	1.4
3f	0.4151	1.56	8.2699	4.66	0.1418	4.03	2238	30	2261	42	2249	68	2249	68	0.5
3g	0.2915	1.60	5.0399	4.71	0.1209	4.15	1649	23	1826	40	1969	72	1969	72	16.2
3h	0.3603	1.72	6.1806	5.20	0.1296	4.34	1984	29	2002	45	2092	74	2092	74	5.2
3i	0.0980	2.83	3.5654	7.18	0.2755	5.47	603	16	1542	57	3337	83	3337	83	81.9
3j	0.1045	1.86	0.8977	5.51	0.0613	4.79	641	11	651	26	651	100	641	11	1.5
4a	0.2522	1.51	3.2945	4.13	0.0922	3.51	1450	20	1480	32	1472	65	1472	65	1.5

Table B.3 (continued). U-Pb analytical data, detrital zircon sample JB-17

Analysis	Isotopic ratios and 2σ (%) errors						Ages and 2σ absolute errors (Ma)						Reported Age		
number	$^{206}Pb/^{238}U$	±2σ	$^{207}Pb/^{235}U$	±2σ	$^{207}Pb/^{206}Pb$	±2σ	$^{206}Pb/^{238}U$	±2σ	$^{207}Pb/^{235}U$	±2σ	$^{207}Pb/^{206}Pb$	±2σ	Age (Ma)	±2σ	Disc. (%)
4b	0.3675	1.49	6.4471	4.05	0.1272	3.48	2018	26	2039	36	2060	60	2060	60	2.0
4c	0.0969	1.58	0.7778	4.30	0.0592	3.85	596	9	584	19	575	81	596	9	-3.7
4d	0.0890	1.61	0.7760	4.34	0.0602	3.87	550	8	583	19	611	81	550	8	10.0
4e	0.2903	1.51	5.0879	4.00	0.1246	3.62	1643	22	1834	34	2023	63	2023	63	18.8
4f	0.5418	1.68	14.8327	4.74	0.2014	3.98	2791	38	2805	45	2838	63	2838	63	1.6
4g	0.1006	1.74	0.8514	4.79	0.0615	4.28	618	10	625	22	656	89	618	10	5.8
4h	0.3615	1.73	6.7714	4.85	0.1309	4.14	1989	30	2082	43	2109	71	2109	71	5.7
4i	0.0939	1.78	0.7850	4.90	0.0602	4.39	579	10	588	22	610	92	579	10	5.2
4j	0.1015	1.87	0.8724	5.30	0.0611	4.70	623	11	637	25	642	98	623	11	3.0
5a	0.0990	1.83	0.8300	5.06	0.0604	4.54	608	11	614	23	617	95	608	11	1.5
5b	0.3511	1.80	6.0420	4.98	0.1240	4.44	1940	30	1982	43	2015	77	2015	77	3.7
5c	0.1008	1.84	0.8537	5.07	0.0602	4.57	619	11	627	24	611	96	619	11	-1.3
5d	0.3881	1.85	7.3213	5.17	0.1330	4.59	2114	33	2151	46	2138	78	2138	78	1.1
5e	0.0960	2.02	0.8083	5.69	0.0602	5.05	591	11	602	26	610	105	591	11	3.2
5f	0.0995	2.06	0.8448	5.83	0.0608	5.16	611	12	622	27	632	108	611	12	3.3
5g	0.0971	2.03	0.7978	5.68	0.0605	5.07	597	12	596	26	622	106	597	12	3.9
5h	0.3666	2.03	6.4560	5.75	0.1281	5.00	2013	35	2040	51	2072	86	2072	86	2.8
5i	0.0951	2.02	0.7999	5.64	0.0601	5.07	585	11	597	25	607	106	585	11	3.6

Table B.3 (continued). U-Pb analytical data, detrital zircon sample JB-17

Analysis	Isotopic ratios and 2σ (%) errors						Ages and 2σ absolute errors (Ma)						Reported Age		
number	$^{206}Pb/^{238}U$	±2σ	$^{207}Pb/^{235}U$	±2σ	$^{207}Pb/^{206}Pb$	±2σ	$^{206}Pb/^{238}U$	±2σ	$^{207}Pb/^{235}U$	±2σ	$^{207}Pb/^{206}Pb$	±2σ	Age (Ma)	±2σ	Disc. (%)
5j	0.2583	2.04	3.4073	5.70	0.0951	5.12	1481	27	1506	45	1531	93	1531	93	3.2
6a	0.4002	2.17	7.5477	6.12	0.1389	5.44	2170	40	2179	55	2213	91	2213	91	2.0
6b	0.3277	2.20	5.0502	6.20	0.1123	5.52	1827	35	1828	53	1837	97	1837	97	0.5
6c	0.3653	2.24	6.2867	6.34	0.1237	5.61	2007	39	2017	56	2010	96	2010	96	0.2
6d	0.3361	2.48	5.8635	7.38	0.1270	5.91	1868	40	1956	64	2057	101	2057	101	9.2
6e	0.3503	2.32	6.0300	6.58	0.1227	5.79	1936	39	1980	57	1996	99	1996	99	3.0
6f	0.5188	2.40	15.0379	6.92	0.2076	5.96	2694	53	2818	66	2887	94	2887	94	6.7
6g	0.3742	2.43	6.9775	6.93	0.1321	6.06	2049	43	2109	62	2126	102	2126	102	3.6
6h	0.3358	2.48	5.7743	7.10	0.1250	6.16	1867	40	1943	61	2028	105	2028	105	8.0
6i	0.0983	2.49	0.8232	7.04	0.0597	6.30	605	14	610	32	593	130	605	14	-2.0
6j	0.0935	2.55	0.7517	7.21	0.0588	6.43	576	14	569	31	559	134	576	14	-3.0

Table B.4 U-Pb analytical data, detrital zircon sample RSA-01

Analysis	Isotopic ratios and 2σ (%) errors						Ages and 2σ absolute errors (Ma)						Reported Age		
number	$^{206}Pb/^{238}U$	±2σ	$^{207}Pb/^{235}U$	±2σ	$^{207}Pb/^{206}Pb$	±2σ	$^{206}Pb/^{238}U$	±2σ	$^{207}Pb/^{235}U$	±2σ	$^{207}Pb/^{206}Pb$	±2σ	Age (Ma)	±2σ	Disc. (%)
1a	0.1915	0.38	2.0961	1.11	0.0778	0.82	1129	4	1148	8	1141	16	1141	16	-0.6
1b	0.3097	0.46	4.5395	1.51	0.1053	0.91	1739	7	1738	13	1720	17	1720	17	-1.0
1c	0.5016	0.62	12.7093	2.28	0.1909	1.00	2621	13	2658	21	2750	16	2750	16	3.3
1d	0.4890	0.46	11.7479	1.56	0.1738	0.89	2566	10	2585	15	2594	15	2594	15	0.4
1e	0.2335	0.47	2.8829	1.42	0.0887	1.04	1353	6	1378	11	1398	20	1398	20	1.5
1f	0.0710	0.41	0.5558	1.10	0.0563	1.01	442	2	449	4	462	22	442	2	2.8
1g	0.1780	0.53	1.8820	1.61	0.0759	1.23	1056	5	1075	11	1092	24	1092	24	1.6
1h	0.4914	0.83	11.5197	3.14	0.1743	1.37	2577	18	2566	29	2599	23	2599	23	1.3
1i	0.1642	0.46	1.6433	1.33	0.0716	1.10	980	4	987	8	974	22	980	4	-1.3
1j	0.1852	0.51	2.0116	1.51	0.0786	1.18	1095	5	1119	10	1161	23	1161	23	3.6
1k	0.1998	0.50	2.2659	1.48	0.0788	1.17	1174	5	1202	10	1167	23	1167	23	-3.0
1l	0.2082	0.70	2.4832	2.21	0.0848	1.53	1220	8	1267	16	1312	30	1312	30	3.4
1m	0.2688	0.57	3.7157	1.80	0.0987	1.27	1535	8	1575	14	1599	24	1599	24	1.5
1n	0.1637	0.75	1.6031	2.35	0.0723	1.78	977	7	971	15	994	36	977	7	2.2
1o	0.1781	0.84	1.8934	2.74	0.0744	1.96	1057	8	1079	18	1052	39	1052	39	-2.5
2a	0.2634	0.67	3.5231	2.12	0.0981	1.46	1507	9	1532	17	1588	27	1588	27	3.5
2b	0.2548	0.67	3.1598	2.10	0.0907	1.48	1463	9	1447	16	1440	28	1440	28	-0.5
2c	0.2656	0.66	3.6754	2.08	0.0982	1.46	1518	9	1566	17	1590	27	1590	27	1.5

Table B.4 (continued). U-Pb analytical data, detrital zircon sample RSA-01

Analysis	Isotopic ratios and 2σ (%) errors						Ages and 2σ absolute errors (Ma)						Reported Age		
number	$^{206}Pb/^{238}U$	±2σ	$^{207}Pb/^{235}U$	±2σ	$^{207}Pb/^{206}Pb$	±2σ	$^{206}Pb/^{238}U$	±2σ	$^{207}Pb/^{235}U$	±2σ	$^{207}Pb/^{206}Pb$	±2σ	Age (Ma)	±2σ	Disc. (%)
2d	0.2824	0.60	3.9712	1.86	0.1009	1.39	1604	9	1628	15	1641	25	1641	25	0.8
2e	0.4799	0.72	11.9856	2.49	0.1782	1.43	2527	15	2603	23	2636	24	2636	24	1.2
2f	0.1754	1.12	1.8888	3.66	0.0742	2.57	1042	11	1077	24	1048	51	1048	51	-2.8
2g	0.1945	0.68	2.1350	2.05	0.0779	1.63	1146	7	1160	14	1145	32	1145	32	-1.4
2h	0.0729	0.84	0.5828	2.49	0.0563	2.20	453	4	466	9	461	48	453	4	-1.0
2i	0.1815	0.62	1.9755	1.81	0.0777	1.56	1075	6	1107	12	1139	31	1139	31	2.8
2j	0.1978	0.60	2.1965	1.72	0.0795	1.52	1163	6	1180	12	1184	30	1184	30	0.4
2k	0.5743	1.15	17.1938	4.72	0.2163	1.95	2926	27	2946	45	2954	31	2954	31	0.3
2l	0.2030	0.87	2.3070	2.67	0.0840	2.01	1192	9	1214	19	1293	39	1293	39	6.1
2m	0.1903	0.78	2.0483	2.37	0.0783	1.90	1123	8	1132	16	1154	37	1154	37	1.9
2n	0.2568	0.69	3.4092	2.01	0.0939	1.71	1473	9	1507	16	1506	32	1506	32	0.0
2o	0.2496	1.22	3.3026	4.14	0.0945	2.62	1437	16	1482	32	1519	49	1519	49	2.4
3a	0.1708	0.97	1.7477	3.01	0.0723	2.34	1017	9	1026	19	995	47	1017	9	-3.1
3b	0.1726	0.74	1.7735	2.14	0.0731	1.87	1026	7	1036	14	1018	37	1018	37	-1.8
3c	0.1694	0.86	1.7377	2.55	0.0746	2.10	1009	8	1023	16	1058	42	1058	42	3.4
3d	0.2852	0.79	4.0807	2.33	0.1028	1.95	1618	11	1650	19	1675	36	1675	36	1.5
3e	0.1966	0.89	2.1215	2.68	0.0776	2.17	1157	9	1156	19	1136	43	1136	43	-1.7
3f	0.3277	0.92	5.0744	2.79	0.1132	2.22	1827	15	1832	24	1852	40	1852	40	1.1

Table B.4 (continued). U-Pb analytical data, detrital zircon sample RSA-01

Analysis	Isotopic ratios and 2σ (%) errors						Ages and 2σ absolute errors (Ma)						Reported Age		
number	$^{206}Pb/^{238}U$	±2σ	$^{207}Pb/^{235}U$	±2σ	$^{207}Pb/^{206}Pb$	±2σ	$^{206}Pb/^{238}U$	±2σ	$^{207}Pb/^{235}U$	±2σ	$^{207}Pb/^{206}Pb$	±2σ	Age (Ma)	±2σ	Disc. (%)
3g	0.2514	0.85	3.2787	2.46	0.0950	2.17	1446	11	1476	19	1528	40	1528	40	3.4
3h	0.1712	2.06	1.7067	6.78	0.0744	4.96	1019	19	1011	43	1051	97	1051	97	3.8
3i	0.2535	0.90	3.2824	2.65	0.0927	2.29	1457	12	1477	21	1481	43	1481	43	0.3
3j	0.2945	0.93	4.2109	2.77	0.1029	2.33	1664	14	1676	23	1677	43	1677	43	0.1
3k	0.2688	1.04	3.5091	3.16	0.0962	2.54	1535	14	1529	25	1551	47	1551	47	1.4
3l	0.1621	1.24	1.6108	3.78	0.0737	3.04	968	11	974	24	1034	60	1034	60	5.7
3m	0.1675	1.03	1.7057	3.03	0.0742	2.60	998	10	1011	19	1048	52	1048	52	3.5
3n	0.2745	1.02	3.7628	3.01	0.0975	2.55	1564	14	1585	24	1576	47	1576	47	-0.5
3o	0.3026	1.12	4.5081	3.46	0.1076	2.69	1704	17	1733	29	1760	49	1760	49	1.5
4a	0.1940	1.05	2.0817	3.05	0.0770	2.67	1143	11	1143	21	1122	53	1122	53	-1.8
4b	0.2527	1.05	3.2095	3.06	0.0910	2.69	1452	14	1460	24	1447	51	1447	51	-0.9
4c	0.1969	1.22	2.1789	3.67	0.0819	3.00	1159	13	1174	26	1242	58	1242	58	5.5
4d	0.3259	1.16	4.9688	3.48	0.1105	2.86	1818	18	1814	29	1808	51	1808	51	-0.4
4e	0.2564	1.24	3.2650	3.76	0.0936	3.03	1472	16	1473	29	1501	56	1501	56	1.9
4f	0.1743	1.37	1.7502	4.12	0.0762	3.42	1036	13	1027	27	1101	67	1101	67	6.7
4g	0.1745	1.35	1.8031	4.05	0.0736	3.40	1037	13	1047	26	1029	67	1029	67	-1.7
4h	0.3119	1.21	4.7030	3.49	0.1096	3.10	1750	18	1768	29	1793	55	1793	55	1.4
4i	0.1951	1.65	2.0780	5.21	0.0790	4.04	1149	17	1142	36	1172	78	1172	78	2.6

Table B.4 (continued).U-Pb analytical data, detrital zircon sample RSA-01

Analysis	Isotopic ratios and 2σ (%) errors						Ages and 2σ absolute errors (Ma)						Reported Age		
number	$^{206}Pb/^{238}U$	±2σ	$^{207}Pb/^{235}U$	±2σ	$^{207}Pb/^{206}Pb$	±2σ	$^{206}Pb/^{238}U$	±2σ	$^{207}Pb/^{235}U$	±2σ	$^{207}Pb/^{206}Pb$	±2σ	Age (Ma)	±2σ	Disc. (%)
4j	0.2507	1.33	3.1669	3.96	0.0916	3.33	1442	17	1449	31	1458	62	1458	62	0.6
4k	0.2865	1.30	4.0313	3.79	0.1000	3.33	1624	19	1641	31	1624	61	1624	61	-1.0
4l	0.1769	1.42	1.8494	4.20	0.0741	3.59	1050	14	1063	28	1043	71	1043	71	-1.9
4m	0.1754	1.58	1.7679	4.72	0.0755	3.91	1042	15	1034	31	1081	76	1081	76	4.4
4n	0.2613	1.39	3.3027	4.09	0.0906	3.53	1497	19	1482	32	1439	66	1439	66	-3.0
4o	0.2581	1.38	3.3349	4.01	0.0929	3.54	1480	18	1489	31	1485	66	1485	66	-0.3
5a	0.2564	1.40	3.2973	4.04	0.0928	3.62	1471	18	1480	31	1483	67	1483	67	0.2
5b	0.1656	1.68	1.6155	5.06	0.0709	4.22	988	15	976	32	953	84	988	15	-2.4
5c	0.1724	1.46	1.7540	4.18	0.0726	3.76	1025	14	1029	27	1004	74	1004	74	-2.5
5d	0.2956	1.52	4.1196	4.45	0.1058	3.86	1670	22	1658	36	1728	69	1728	69	4.1
5e	0.2394	1.54	2.8486	4.47	0.0889	3.91	1384	19	1369	34	1402	73	1402	73	2.4

Table B.5 U-Pb analytical data, detrital zircon sample RSA-02

Analysis	Isotopic ratios and 2σ (%) errors						Ages and 2σ absolute errors (Ma)						Reported Age		
number	$^{206}Pb/^{238}U$	±2σ	$^{207}Pb/^{235}U$	±2σ	$^{207}Pb/^{206}Pb$	±2σ	$^{206}Pb/^{238}U$	±2σ	$^{207}Pb/^{235}U$	±2σ	$^{207}Pb/^{206}Pb$	±2σ	Age (Ma)	±2σ	Disc. (%)
1a	0.1555	0.46	1.4816	1.38	0.0702	0.98	931	4	923	8	933	20	931	4	0.2
1b	0.1776	0.33	1.7816	0.96	0.0736	0.67	1054	3	1039	6	1030	14	1030	14	-2.3
1c	0.1949	0.74	2.2441	2.48	0.0814	1.57	1148	8	1195	17	1231	31	1231	31	6.7
1d	0.1883	0.52	2.0391	1.64	0.0782	1.06	1112	5	1129	11	1153	21	1153	21	3.5
1e	0.1665	0.48	1.6766	1.45	0.0753	1.00	993	4	1000	9	1076	20	1076	20	7.7
1f	0.2541	0.46	3.2049	1.48	0.0943	0.85	1460	6	1458	11	1514	16	1514	16	3.5
1g	0.2204	0.47	2.4601	1.51	0.0826	0.93	1284	5	1260	11	1261	18	1261	18	-1.9
1h	0.5148	0.31	13.3748	1.04	0.1898	0.45	2677	7	2707	10	2740	7	2740	7	2.3
1i	0.2650	0.48	3.4525	1.58	0.0969	0.88	1515	6	1516	12	1565	16	1565	16	3.2
1j	0.1884	0.36	1.9845	1.06	0.0777	0.71	1113	4	1110	7	1139	14	1139	14	2.3
2a	0.1772	0.34	1.8287	1.01	0.0745	0.70	1052	3	1056	7	1055	14	1055	14	0.4
2b	0.1543	1.11	1.3870	3.54	0.0689	2.54	925	10	883	21	896	51	925	10	-3.2
2c	0.1888	0.47	2.0080	1.48	0.0780	0.97	1115	5	1118	10	1147	19	1147	19	2.7
2d	0.1820	0.42	1.9522	1.28	0.0786	0.85	1078	4	1099	9	1162	17	1162	17	7.2
2e	0.1886	0.51	2.0129	1.65	0.0773	1.07	1114	5	1120	11	1130	21	1130	21	1.4
2f	0.1627	0.32	1.6597	0.90	0.0746	0.64	972	3	993	6	1059	13	1059	13	8.2
2g	0.1802	0.77	1.8880	2.55	0.0752	1.69	1068	8	1077	17	1073	34	1073	34	0.5
2h	0.1538	0.46	1.5416	1.41	0.0719	1.00	922	4	947	9	983	20	983	20	6.2

Table B.5 (continued).U-Pb analytical data, detrital zircon sample RSA-02

Analysis	Isotopic ratios and 2σ (%) errors						Ages and 2σ absolute errors (Ma)						Reported Age		
number	$^{206}Pb/^{238}U$	±2σ	$^{207}Pb/^{235}U$	±2σ	$^{207}Pb/^{206}Pb$	±2σ	$^{206}Pb/^{238}U$	±2σ	$^{207}Pb/^{235}U$	±2σ	$^{207}Pb/^{206}Pb$	±2σ	Age (Ma)	±2σ	Disc. (%)
2i	0.1682	0.27	1.6948	0.71	0.0746	0.52	1002	2	1007	5	1057	11	1057	11	5.2
2j	0.2447	0.29	3.0210	0.83	0.0925	0.53	1411	4	1413	6	1477	10	1477	10	4.5
3a	0.1951	0.23	2.0580	0.57	0.0776	0.43	1149	2	1135	4	1137	9	1137	9	-1.1
3b	0.2994	0.32	4.4575	1.00	0.1094	0.56	1688	5	1723	8	1789	10	1789	10	5.6
3c	0.1656	0.48	1.6315	1.44	0.0751	1.00	988	4	982	9	1072	20	1072	20	7.8
3d	0.1842	0.68	1.9540	2.24	0.0766	1.48	1090	7	1100	15	1111	29	1111	29	1.8
3e	0.1869	0.44	1.9557	1.36	0.0765	0.90	1105	4	1100	9	1108	18	1108	18	0.3
3f	0.1701	0.45	1.7423	1.39	0.0744	0.95	1013	4	1024	9	1052	19	1052	19	3.7
3g	0.2477	0.75	3.1522	2.55	0.0926	1.44	1427	10	1446	20	1480	27	1480	27	3.6
3h	0.3283	0.31	5.1408	0.94	0.1160	0.52	1830	5	1843	8	1896	9	1896	9	3.4
3i	0.0773	1.35	0.5979	4.41	0.0568	3.89	480	6	476	17	483	84	480	6	0.7
3j	0.2594	0.52	3.3396	1.73	0.0927	0.97	1487	7	1490	14	1482	18	1482	18	-0.4
4a	0.1775	1.87	1.7822	6.67	0.0753	4.63	1053	18	1039	43	1078	90	1078	90	2.3
4b	0.1690	0.47	1.7135	1.45	0.0736	0.99	1007	4	1014	9	1030	20	1030	20	2.2
4c	0.1882	0.48	1.9903	1.49	0.0775	0.98	1112	5	1112	10	1135	19	1135	19	2.1
4d	0.2596	0.49	3.6033	1.61	0.0996	0.88	1488	7	1550	13	1616	16	1616	16	7.9
4e	0.1743	0.50	1.7512	1.56	0.0747	1.06	1036	5	1028	10	1060	21	1060	21	2.3
4f	0.1681	0.42	1.6746	1.27	0.0744	0.89	1002	4	999	8	1053	18	1053	18	4.9

Table B.5 (continued). U-Pb analytical data, detrital zircon sample RSA-02

Analysis	Isotopic ratios and 2σ (%) errors						Ages and 2σ absolute errors (Ma)						Reported Age		
number	$^{206}Pb/^{238}U$	±2σ	$^{207}Pb/^{235}U$	±2σ	$^{207}Pb/^{206}Pb$	±2σ	$^{206}Pb/^{238}U$	±2σ	$^{207}Pb/^{235}U$	±2σ	$^{207}Pb/^{206}Pb$	±2σ	Age (Ma)	±2σ	Disc. (%)
4g	0.1885	0.74	2.0311	2.47	0.0768	1.62	1114	8	1126	17	1116	32	1116	32	0.2
4h	0.2927	0.35	4.2293	1.10	0.1047	0.61	1655	5	1680	9	1709	11	1709	11	3.1
4i	0.1515	0.60	1.4778	1.89	0.0708	1.34	909	5	921	11	950	27	909	5	4.3
4j	0.1703	0.47	1.7286	1.45	0.0741	1.00	1014	4	1019	9	1044	20	1044	20	2.8
5a	0.3137	0.40	4.6771	1.31	0.1084	0.68	1759	6	1763	11	1772	13	1772	13	0.7
5b	0.1549	0.49	1.4896	1.50	0.0711	1.07	928	4	926	9	959	22	928	4	3.2
5d	0.3129	0.44	4.8187	1.52	0.1087	0.77	1755	7	1788	13	1778	14	1778	14	1.3
5e	0.1682	0.32	1.6662	0.90	0.0728	0.65	1002	3	996	6	1008	13	1008	13	0.6
5f	0.2664	1.37	3.4220	4.83	0.0937	2.59	1523	19	1510	38	1502	48	1502	48	-1.4
5g	0.2229	0.50	2.7082	1.60	0.0897	0.97	1297	6	1331	12	1420	18	1420	18	8.6
5h	0.1899	0.47	2.1084	1.49	0.0783	0.97	1121	5	1152	10	1155	19	1155	19	2.9
5i	0.1694	0.40	1.6881	1.18	0.0734	0.83	1009	4	1004	8	1026	17	1026	17	1.6
5j	0.2462	0.43	3.0441	1.34	0.0912	0.80	1419	5	1419	10	1451	15	1451	15	2.2
6a	0.1554	0.46	1.4955	1.38	0.0701	0.98	931	4	929	8	930	20	931	4	-0.1
6b	0.2591	0.67	3.3717	2.29	0.0934	1.26	1485	9	1498	18	1496	24	1496	24	0.7
6c	0.1678	0.58	1.6976	1.80	0.0735	1.22	1000	5	1008	12	1027	25	1027	25	2.6
6d	0.2894	0.32	3.9995	0.99	0.1013	0.58	1638	5	1634	8	1648	11	1648	11	0.6
6e	0.2616	0.32	3.4026	0.96	0.0940	0.58	1498	4	1505	8	1509	11	1509	11	0.7

Table B.5 (continued).U-Pb analytical data, detrital zircon sample RSA-02

Analysis	Isotopic ratios and 2σ (%) errors						Ages and 2σ absolute errors (Ma)						Reported Age		
number	$^{206}Pb/^{238}U$	±2σ	$^{207}Pb/^{235}U$	±2σ	$^{207}Pb/^{206}Pb$	±2σ	$^{206}Pb/^{238}U$	±2σ	$^{207}Pb/^{235}U$	±2σ	$^{207}Pb/^{206}Pb$	±2σ	Age (Ma)	±2σ	Disc. (%)
6f	0.3823	0.40	7.7579	1.31	0.1542	0.62	2087	7	2203	12	2393	10	2393	10	12.8
6g	0.2491	0.42	3.1155	1.34	0.0914	0.80	1434	5	1437	10	1455	15	1455	15	1.5
6h	0.2255	0.56	2.6105	1.86	0.0833	1.13	1311	7	1304	14	1275	22	1275	22	-2.8
6i	0.1801	0.45	1.8359	1.38	0.0746	0.94	1067	4	1058	9	1059	19	1059	19	-0.8
6j	0.1742	1.25	1.7471	4.16	0.0746	2.87	1035	12	1026	27	1057	57	1057	57	2.1
7a	0.3371	0.47	5.3014	1.58	0.1158	0.79	1873	8	1869	14	1892	14	1892	14	1.0
7b	0.1511	0.46	1.5014	1.40	0.0706	1.01	907	4	931	9	945	20	907	4	4.0
7c	0.1599	1.21	1.5402	3.95	0.0717	2.77	956	11	947	24	979	56	956	11	2.3
7d	0.2999	0.38	4.1903	1.20	0.1035	0.68	1691	6	1672	10	1688	12	1688	12	-0.1
7e	0.2770	0.55	3.8008	1.86	0.0987	1.00	1576	8	1593	15	1599	19	1599	19	1.4

Table B.6U-Pb analytical data, detrital zircon sample AC-03

Analysis	Isotopic ratios and 2σ (%) errors						Ages and 2σ absolute errors (Ma)						Reported Age		
number	$^{206}Pb/^{238}U$	±2σ	$^{207}Pb/^{235}U$	±2σ	$^{207}Pb/^{206}Pb$	±2σ	$^{206}Pb/^{238}U$	±2σ	$^{207}Pb/^{235}U$	±2σ	$^{207}Pb/^{206}Pb$	±2σ	Age (Ma)	±2σ	Disc. (%)
1a	0.1717	0.40	1.7432	1.18	0.0732	0.83	1021	4	1025	8	1021	17	1021	17	0.0
11a	0.1732	0.58	1.8041	1.84	0.0749	1.24	1030	6	1047	12	1066	25	1066	25	3.4
11b	0.2674	0.87	3.4926	3.21	0.0942	1.69	1528	12	1526	25	1512	32	1512	32	-1.1
11c	0.1966	0.38	2.1244	1.14	0.0771	0.77	1157	4	1157	8	1123	15	1123	15	-3.1
11d	0.2401	0.33	2.9099	0.99	0.0890	0.63	1387	4	1385	7	1403	12	1403	12	1.2
11e	0.1771	0.35	1.8154	1.02	0.0747	0.72	1051	3	1051	7	1059	15	1059	15	0.7
11f	0.2217	0.80	2.7142	2.73	0.0856	1.62	1291	9	1332	20	1330	31	1330	31	2.9
11g	0.4684	0.38	10.8110	1.31	0.1717	0.58	2477	8	2507	12	2574	10	2574	10	3.8
11h	0.1893	0.42	2.0244	1.25	0.0793	0.84	1118	4	1124	9	1180	17	1180	17	5.3
11i	0.2849	0.47	3.8955	1.56	0.0992	0.87	1616	7	1613	13	1610	16	1610	16	-0.4
11j	0.2570	0.79	3.3906	2.71	0.0939	1.50	1475	10	1502	21	1506	28	1506	28	2.1
11k	0.1585	0.68	1.5369	2.10	0.0719	1.49	948	6	945	13	984	30	948	6	3.6
11l	0.1962	0.36	2.1941	1.09	0.0786	0.74	1155	4	1179	8	1162	14	1162	14	0.6
11m	0.2609	0.34	3.3107	1.04	0.0951	0.64	1495	5	1484	8	1529	12	1529	12	2.2
11n	0.2238	0.60	2.6737	1.97	0.0858	1.20	1302	7	1321	15	1333	23	1333	23	2.3
11o	0.2856	0.41	4.0451	1.31	0.1049	0.74	1620	6	1643	11	1712	14	1712	14	5.4
22a	0.2591	2.54	3.0775	9.10	0.0942	5.23	1485	34	1427	70	1513	96	1513	96	1.8
22b	0.1909	0.29	2.0282	0.79	0.0771	0.57	1127	3	1125	5	1123	11	1123	11	-0.3

Table B.6 (continued). U-Pb analytical data, detrital zircon sample AC-03

Analysis	Isotopic ratios and 2σ (%) errors						Ages and 2σ absolute errors (Ma)						Reported Age		
number	$^{206}Pb/^{238}U$	±2σ	$^{207}Pb/^{235}U$	±2σ	$^{207}Pb/^{206}Pb$	±2σ	$^{206}Pb/^{238}U$	±2σ	$^{207}Pb/^{235}U$	±2σ	$^{207}Pb/^{206}Pb$	±2σ	Age (Ma)	±2σ	Disc. (%)
22c	0.1723	0.27	1.7677	0.70	0.0739	0.54	1025	3	1034	5	1038	11	1038	11	1.2
22d	0.1807	0.42	1.8377	1.25	0.0753	0.86	1071	4	1059	8	1077	17	1077	17	0.6
22e	0.1550	0.77	1.4933	2.55	0.0707	1.85	929	7	928	15	949	37	929	7	2.1
22f	0.1913	0.42	2.0800	1.27	0.0794	0.86	1128	4	1142	9	1182	17	1182	17	4.5
22g	0.1925	0.36	2.0247	1.05	0.0774	0.74	1135	4	1124	7	1132	15	1132	15	-0.2
22h	0.1681	1.10	1.6916	3.60	0.0727	2.52	1002	10	1005	23	1005	50	1005	50	0.3
22i	0.1825	1.10	2.0224	3.62	0.0782	2.37	1081	11	1123	25	1151	46	1151	46	6.1
22j	0.2346	0.43	2.8480	1.36	0.0891	0.84	1359	5	1368	10	1407	16	1407	16	3.4
22k	0.2516	0.39	3.2196	1.19	0.0907	0.74	1447	5	1462	9	1441	14	1441	14	-0.4
22l	0.1920	0.64	2.0911	2.02	0.0802	1.32	1132	7	1146	14	1202	26	1202	26	5.8
22m	0.1880	1.99	1.9286	7.39	0.0770	4.94	1111	20	1091	49	1121	95	1121	95	0.9
22n	0.1719	0.35	1.7602	0.99	0.0741	0.72	1022	3	1031	6	1044	14	1044	14	2.1
22o	0.1762	0.60	1.7760	1.88	0.0735	1.29	1046	6	1037	12	1028	25	1028	25	-1.7
33a	0.3190	0.38	4.8281	1.21	0.1105	0.68	1785	6	1790	10	1807	12	1807	12	1.2
33b	0.3360	0.59	5.2907	2.08	0.1140	1.02	1867	10	1867	18	1864	18	1864	18	-0.2
33c	0.1973	0.67	2.1026	2.18	0.0767	1.41	1161	7	1150	15	1114	28	1114	28	-4.3
33d	0.2034	0.70	2.2499	2.26	0.0816	1.43	1194	8	1197	16	1235	28	1235	28	3.3
33e	0.1659	0.93	1.5817	3.09	0.0713	2.20	989	9	963	19	965	44	989	9	-2.5

Table B.6 (continued). U-Pb analytical data, detrital zircon sample AC-03

Analysis	Isotopic ratios and 2σ (%) errors						Ages and 2σ absolute errors (Ma)						Reported Age		
number	$^{206}Pb/^{238}U$	±2σ	$^{207}Pb/^{235}U$	±2σ	$^{207}Pb/^{206}Pb$	±2σ	$^{206}Pb/^{238}U$	±2σ	$^{207}Pb/^{235}U$	±2σ	$^{207}Pb/^{206}Pb$	±2σ	Age (Ma)	±2σ	Disc. (%)
33f	0.4652	0.77	10.5619	2.91	0.1649	1.12	2462	16	2485	27	2507	19	2507	19	1.8
33g	0.2941	0.76	3.9757	2.60	0.1008	1.39	1662	11	1629	21	1639	25	1639	25	-1.4
33h	0.1584	0.49	1.5591	1.48	0.0713	1.07	948	4	954	9	965	22	948	4	1.8
33i	0.1578	0.68	1.4970	2.08	0.0728	1.48	944	6	929	13	1008	30	1008	30	6.3
33j	0.2765	0.49	3.6604	1.63	0.0953	0.92	1574	7	1563	13	1533	17	1533	17	-2.6
33k	0.1826	1.04	1.8292	3.43	0.0756	2.34	1081	10	1056	23	1084	46	1084	46	0.3
33l	0.1823	0.41	1.9120	1.21	0.0747	0.84	1080	4	1085	8	1061	17	1061	17	-1.8
33m	0.2841	0.48	3.9076	1.59	0.0995	0.89	1612	7	1615	13	1615	17	1615	17	0.2
33n	0.1737	0.97	1.7424	3.11	0.0757	2.13	1032	9	1024	20	1088	42	1088	42	5.1
33o	0.2499	0.40	3.0320	1.24	0.0908	0.78	1438	5	1416	9	1443	15	1443	15	0.3
44a	0.2240	0.59	2.6331	1.91	0.0863	1.18	1303	7	1310	14	1345	23	1345	23	3.2
44b	0.4600	0.36	10.1685	1.20	0.1592	0.60	2440	7	2450	11	2448	10	2448	10	0.3
44c	0.2711	0.34	3.6237	1.01	0.0951	0.65	1546	5	1555	8	1530	12	1530	12	-1.1
44d	0.3248	0.33	4.7587	0.98	0.1069	0.61	1813	5	1778	8	1748	11	1748	11	-3.7
44e	0.2709	0.40	3.6023	1.23	0.0978	0.76	1545	5	1550	10	1582	14	1582	14	2.3
44f	0.2557	0.59	3.4164	1.98	0.0932	1.13	1468	8	1508	16	1492	21	1492	21	1.6
44g	0.1810	0.53	1.8691	1.64	0.0734	1.12	1072	5	1070	11	1024	22	1024	22	-4.7
44h	0.2596	0.63	3.3364	2.10	0.0935	1.21	1488	8	1490	16	1497	23	1497	23	0.6

Table B.6 (continued). U-Pb analytical data, detrital zircon sample AC-03

Analysis	Isotopic ratios and 2σ (%) errors						Ages and 2σ absolute errors (Ma)						Reported Age		
number	$^{206}Pb/^{238}U$	±2σ	$^{207}Pb/^{235}U$	±2σ	$^{207}Pb/^{206}Pb$	±2σ	$^{206}Pb/^{238}U$	±2σ	$^{207}Pb/^{235}U$	±2σ	$^{207}Pb/^{206}Pb$	±2σ	Age (Ma)	±2σ	Disc. (%)
44i	0.2183	0.44	2.4836	1.35	0.0837	0.88	1273	5	1267	10	1287	17	1287	17	1.0
44j	0.2622	0.43	3.4130	1.39	0.0939	0.83	1501	6	1507	11	1506	16	1506	16	0.4
44k	0.1894	0.50	2.0233	1.56	0.0774	1.06	1118	5	1123	11	1132	21	1132	21	1.2
44l	0.2721	0.35	3.6947	1.02	0.0989	0.66	1552	5	1570	8	1603	12	1603	12	3.2
44m	0.5172	0.26	12.9430	0.71	0.1824	0.50	2687	6	2676	7	2675	8	2675	8	-0.4
44n	0.1732	0.63	1.7080	2.00	0.0731	1.42	1030	6	1012	13	1017	28	1017	28	-1.2
44o	0.2872	0.57	3.9130	1.92	0.0991	1.07	1628	8	1616	16	1606	20	1606	20	-1.3
55a	0.3380	0.68	5.3941	2.44	0.1154	1.19	1877	11	1884	21	1886	21	1886	21	0.5
55b	0.1939	0.51	2.0756	1.56	0.0781	1.05	1142	5	1141	11	1148	21	1148	21	0.5
55c	0.5059	0.53	12.8339	1.93	0.1891	0.79	2639	12	2668	18	2734	13	2734	13	3.5
55d	0.2936	0.56	4.1814	1.89	0.1028	1.03	1660	8	1670	15	1675	19	1675	19	0.9
55e	0.1762	0.47	1.8416	1.40	0.0747	0.98	1046	4	1060	9	1060	20	1060	20	1.3

Table B.7 U-Pb analytical data, igneous zircon sample JAB-09

Analysis	Isotopic ratios and 2σ (%) errors						Ages and 2σ absolute errors (Ma)						Reported Age		
number	$^{206}Pb/^{238}U$	±2σ	$^{207}Pb/^{235}U$	±2σ	$^{207}Pb/^{206}Pb$	±2σ	$^{206}Pb/^{238}U$	±2σ	$^{207}Pb/^{235}U$	±2σ	$^{207}Pb/^{206}Pb$	±2σ	Age (Ma)	±2σ	Disc. (%)
1	0.0617	2.61	0.4604	6.68	0.0573	6.18	386	10	385	21	501	131	386	10	0.4
2	0.0542	1.66	0.4081	3.51	0.0538	3.23	340	6	348	10	364	71	340	6	-2.0
3	0.0519	1.33	0.3883	2.04	0.0539	1.82	326	4	333	6	368	41	326	4	-2.1
4	0.0516	1.32	0.3825	1.99	0.0537	1.77	325	4	329	6	357	40	325	4	-1.3
5	0.0516	1.38	0.4375	2.23	0.0599	1.99	324	4	369	7	599	43	324	4	-12.0
6	0.0548	1.37	0.4096	2.32	0.0539	2.10	344	5	349	7	367	46	344	5	-1.4
7	0.0534	1.39	0.4121	2.31	0.0573	2.08	335	5	350	7	504	46	335	5	-4.3
8	0.0526	1.35	0.3845	2.16	0.0529	1.93	331	4	330	6	324	43	331	4	0.1
10	0.0536	1.49	0.4026	2.80	0.0545	2.57	337	5	344	8	391	56	337	5	-2.0
12	0.0534	1.35	0.3987	2.21	0.0545	1.98	335	4	341	6	393	44	335	4	-1.6
13	0.0526	1.45	0.3937	2.73	0.0534	2.49	330	5	337	8	344	56	330	5	-2.0
14	0.0540	1.37	0.3968	2.34	0.0536	2.11	339	5	339	7	353	48	339	5	-0.1
15	0.0537	1.53	0.3974	2.97	0.0534	2.72	337	5	340	9	345	60	337	5	-0.8
16	0.0572	1.38	0.4050	2.38	0.0523	2.16	359	5	345	7	297	48	359	5	3.8
17	0.0531	1.35	0.3924	2.24	0.0532	2.01	334	4	336	6	338	45	334	4	-0.7
18	0.0552	1.38	0.4350	2.29	0.0561	2.05	347	5	367	7	457	45	347	5	-5.5
19	0.0530	1.34	0.3850	2.21	0.0532	1.99	333	4	331	6	338	44	333	4	0.6
20	0.0541	1.44	0.3983	2.79	0.0533	2.57	340	5	340	8	341	57	340	5	-0.1

Table B.7. (continued).U-Pb analytical data, igneous zircon sample JAB-09

Analysis	Isotopic ratios and 2σ (%) errors						Ages and 2σ absolute errors (Ma)						Reported Age		
number	$^{206}Pb/^{238}U$	±2σ	$^{207}Pb/^{235}U$	±2σ	$^{207}Pb/^{206}Pb$	±2σ	$^{206}Pb/^{238}U$	±2σ	$^{207}Pb/^{235}U$	±2σ	$^{207}Pb/^{206}Pb$	±2σ	Age (Ma)	±2σ	Disc. (%)
21	0.0530	1.40	0.3811	2.47	0.0526	2.24	333	5	328	7	311	50	333	5	1.6
22	0.0530	1.47	0.3886	2.84	0.0523	2.60	333	5	333	8	298	58	333	5	-0.1
23	0.0531	1.32	0.3909	2.04	0.0540	1.81	333	4	335	6	371	41	333	4	-0.5
24	0.0539	1.47	0.3784	2.82	0.0518	2.59	339	5	326	8	277	58	339	5	3.9
25	0.0516	2.25	0.4305	5.30	0.0627	4.96	324	7	364	16	698	102	324	7	-10.8
26	0.0530	1.58	0.4006	3.17	0.0556	2.91	333	5	342	9	435	63	333	5	-2.7
28	0.0531	1.56	0.3905	3.23	0.0542	2.99	334	5	335	9	377	66	334	5	-0.3
29	0.0530	1.45	0.4140	2.67	0.0546	2.43	333	5	352	8	397	53	333	5	-5.3
30	0.0532	1.30	0.4106	1.93	0.0563	1.70	334	4	349	6	465	38	334	4	-4.4
Inherited core															
9	0.0515	1.30	0.5702	1.78	0.0795	1.55	324	4	458	7	1185	30	1185	30	-29.3
11	0.3304	1.99	5.4603	5.48	0.1258	2.88	1841	32	1894	47	2041	50	2041	50	-2.8
27	0.3855	1.50	6.7525	3.47	0.1282	1.89	2102	27	2080	31	2073	33	2073	33	1.1

Table B.8U-Pb analytical data, igneous zircon sample JAB-28

Analysis	Isotopic ratios and 2σ (%) errors						Ages and 2σ absolute errors (Ma)						Reported Age		
number	$^{206}Pb/^{238}U$	±2σ	$^{207}Pb/^{235}U$	±2σ	$^{207}Pb/^{206}Pb$	±2σ	$^{206}Pb/^{238}U$	±2σ	$^{207}Pb/^{235}U$	±2σ	$^{207}Pb/^{206}Pb$	±2σ	Age (Ma)	±2σ	Disc. (%)
2	0.0491	1.47	0.3512	4.53	0.0498	4.32	309	4	306	12	184	98	309	4	1.1
3	0.0499	1.30	0.3697	3.88	0.0528	3.71	314	4	319	11	322	82	314	4	-1.8
4	0.0519	1.16	0.3827	3.24	0.0539	3.06	326	4	329	9	366	67	326	4	-0.9
5	0.0577	3.54	0.4293	10.73	0.0531	10.04	362	12	363	33	334	213	362	12	-0.3
8	0.0538	1.71	0.3792	5.08	0.0550	4.84	338	6	326	14	410	105	338	6	3.5
9	0.0545	0.86	0.4009	2.46	0.0531	2.32	342	3	342	7	334	52	342	3	-0.1
11	0.0538	1.40	0.3721	4.15	0.0502	3.93	338	5	321	11	203	89	338	5	5.1
16	0.0525	1.07	0.4118	2.90	0.0555	2.72	330	3	350	9	430	59	330	3	-5.7
17	0.0531	3.32	0.3892	10.98	0.0523	10.50	333	11	334	31	297	223	333	11	-0.1
20	0.0517	0.60	0.4192	1.54	0.0595	1.45	325	2	356	5	586	31	325	2	-8.6
21	0.0505	1.39	0.3725	3.95	0.0534	3.75	317	4	322	11	345	82	317	4	-1.3
22	0.0539	1.24	0.3938	3.47	0.0548	3.27	339	4	337	10	402	71	339	4	0.4
23	0.0559	1.36	0.4038	3.91	0.0533	3.68	351	5	344	11	342	81	351	5	1.8
25	0.0549	2.35	0.3843	7.22	0.0506	6.82	345	8	330	20	221	151	345	8	4.4
29	0.0541	0.46	0.3939	1.13	0.0550	1.05	339	2	337	3	412	23	339	2	0.6

Table B.8 (continued). U-Pb analytical data, igneous zircon sample JAB-28

Analysis	Isotopic ratios and 2σ (%) errors						Ages and 2σ absolute errors (Ma)						Reported Age		
number	$^{206}Pb/^{238}U$	±2σ	$^{207}Pb/^{235}U$	±2σ	$^{207}Pb/^{206}Pb$	±2σ	$^{206}Pb/^{238}U$	±2σ	$^{207}Pb/^{235}U$	±2σ	$^{207}Pb/^{206}Pb$	±2σ	Age (Ma)	±2σ	Disc. (%)
Inherited core															
1	0.0910	1.41	0.7445	4.03	0.0626	3.51	561	8	565	17	696	73	561	8	-0.6
6	0.5319	0.89	13.9590	3.29	0.1919	1.28	2749	20	2747	31	2759	21	2759	21	0.1
7	0.1056	1.75	0.8861	5.44	0.0609	4.58	647	11	644	26	635	96	647	11	0.5
10	0.5521	0.65	15.6437	2.30	0.2106	0.95	2834	15	2855	22	2910	15	2910	15	-0.7
12	0.0975	0.52	0.8411	1.35	0.0621	1.16	600	3	620	6	677	25	600	3	-3.2
13	0.0948	0.78	0.7513	2.20	0.0575	1.90	584	4	569	10	510	42	584	4	2.6
14	0.0924	1.46	0.7670	4.21	0.0598	3.61	570	8	578	19	595	77	570	8	-1.4
15	0.1026	0.67	0.8485	1.88	0.0597	1.61	630	4	624	9	593	34	630	4	0.9
18	0.1028	1.60	0.8595	4.69	0.0602	3.94	631	10	630	22	611	83	631	10	0.1
19	0.5071	0.54	13.7588	1.71	0.2002	0.91	2644	12	2733	16	2828	15	2828	15	-3.2
24	0.1025	0.73	0.8456	2.02	0.0620	1.73	629	4	622	9	673	37	629	4	1.1
26	0.3514	0.77	5.8518	2.49	0.1222	1.41	1941	13	1954	22	1989	25	1989	25	-0.7
27	0.1009	1.04	0.8849	2.99	0.0623	2.54	620	6	644	14	683	53	620	6	-3.7
28	0.3672	0.53	6.0893	1.53	0.1233	1.05	2016	9	1989	13	2005	19	2005	19	1.4
30	0.0967	1.33	0.8153	3.86	0.0603	3.30	595	8	605	18	616	70	595	8	-1.7

Table B.9U-Pb analytical data, igneous zircon sample JB-26B

Analysis	Isotopic ratios and 2σ (%) errors						Ages and 2σ absolute errors (Ma)						Reported Age		
number	$^{206}Pb/^{238}U$	±2σ	$^{207}Pb/^{235}U$	±2σ	$^{207}Pb/^{206}Pb$	±2σ	$^{206}Pb/^{238}U$	±2σ	$^{207}Pb/^{235}U$	±2σ	$^{207}Pb/^{206}Pb$	±2σ	Age (Ma)	±2σ	Disc. (%)
6a	0.0523	0.78	0.1408	8.62	0.0198	8.56	329	3	134	11	0	0	329	3	145.7
6b	0.0522	0.82	0.3762	2.47	0.0531	2.28	328	3	324	7	331	51	328	3	1.1
6c	0.0524	0.88	0.3749	2.77	0.0517	2.57	329	3	323	8	270	58	329	3	1.8
6d	0.0529	0.89	0.3584	2.81	0.0494	2.61	332	3	311	8	167	60	332	3	6.8
6e	0.0531	0.92	0.4494	2.62	0.0628	2.41	334	3	377	8	701	50	334	3	-11.5
6f	0.0494	1.03	0.3654	3.13	0.0551	2.92	311	3	316	8	416	63	311	3	-1.7
6g	0.0490	1.00	0.3606	3.16	0.0536	2.97	308	3	313	9	353	66	308	3	-1.4
6h	0.0529	1.08	0.3851	3.28	0.0564	3.05	332	3	331	9	468	67	332	3	0.5
6i	0.0512	1.58	0.3637	5.39	0.0496	5.06	322	5	315	15	178	114	322	5	2.3
6j	0.0502	1.67	0.6041	4.20	0.0874	3.76	316	5	480	16	1370	71	316	5	-34.2
6k	0.0533	1.60	0.3904	4.70	0.0538	4.29	335	5	335	13	364	94	335	5	0.0
6l	0.0532	1.60	0.4205	4.77	0.0574	4.37	334	5	356	14	506	94	334	5	-6.3
6m	0.0529	1.10	0.3592	3.27	0.0522	3.03	332	4	312	9	292	68	332	4	6.6
6n	0.0526	0.67	0.3798	1.94	0.0542	1.79	330	2	327	5	380	40	330	2	1.0
6o	0.0526	1.20	0.3625	3.66	0.0512	3.40	331	4	314	10	251	76	331	4	5.2
6p	0.0529	0.94	0.3910	2.92	0.0541	2.70	333	3	335	8	374	59	333	3	-0.7

Table B.10U-Pb analytical data, igneous zircon sample ACR-04

Analysis	Isotopic ratios and 2σ (%) errors						Ages and 2σ absolute errors (Ma)						Reported Age		
number	$^{206}Pb/^{238}U$	±2σ	$^{207}Pb/^{235}U$	±2σ	$^{207}Pb/^{206}Pb$	±2σ	$^{206}Pb/^{238}U$	±2σ	$^{207}Pb/^{235}U$	±2σ	$^{207}Pb/^{206}Pb$	±2σ	Age (Ma)	±2σ	Disc. (%)
4a	0.0533	0.39	0.4071	0.97	0.0561	0.87	335	1	347	3	457	19	335	1	-3.4
4b	0.0535	0.45	0.3954	1.19	0.0532	1.07	336	1	338	3	335	24	336	1	-0.7
4c	0.0569	0.49	0.4279	1.33	0.0553	1.21	357	2	362	4	426	27	357	2	-1.3
4d	0.0529	0.49	0.3906	1.32	0.0535	1.20	332	2	335	4	349	27	332	2	-0.8
4e	0.0518	0.54	0.3602	1.51	0.0517	1.39	326	2	312	4	271	32	326	2	4.2
4i	0.0533	0.47	0.3910	1.23	0.0517	1.12	335	2	335	4	273	25	335	2	-0.1
4j	0.0526	1.04	0.6161	2.59	0.0823	2.29	331	3	487	10	1252	44	331	3	-32.2
4k	0.0533	0.62	0.4345	1.65	0.0582	1.50	335	2	366	5	536	33	335	2	-8.7
4l	0.0535	0.60	0.3894	1.64	0.0536	1.49	336	2	334	5	353	33	336	2	0.6
4m	0.0536	0.77	0.4291	2.10	0.0575	1.91	337	3	363	6	512	42	337	3	-7.2
4n	0.0532	0.71	0.4294	1.89	0.0599	1.72	334	2	363	6	601	37	334	2	-7.9
4o	0.0532	0.75	0.4313	2.05	0.0587	1.86	334	2	364	6	556	40	334	2	-8.3
4p	0.0531	1.04	0.4335	2.85	0.0611	2.60	333	3	366	9	643	55	333	3	-8.8
Inherited core															
4f	0.1715	0.65	1.7071	1.97	0.0753	1.38	1021	6	1011	13	1075	28	1075	28	0.9
4g	0.1675	0.50	1.7219	1.44	0.0752	1.05	998	5	1017	9	1075	21	1075	21	-1.8
4h	0.1709	0.60	1.7713	1.79	0.0768	1.26	1017	6	1035	12	1116	25	1116	25	-1.8

Table B.11U-Pb analytical data, igneous zircon sample JB-18

Analysis	Isotopic ratios and 2σ (%) errors						Ages and 2σ absolute errors (Ma)						Reported Age		
number	$^{206}Pb/^{238}U$	±2σ	$^{207}Pb/^{235}U$	±2σ	$^{207}Pb/^{206}Pb$	±2σ	$^{206}Pb/^{238}U$	±2σ	$^{207}Pb/^{235}U$	±2σ	$^{207}Pb/^{206}Pb$	±2σ	Age (Ma)	±2σ	Disc. (%)
8a	0.0552	0.62	0.4011	1.77	0.0536	1.62	346	2	342	5	352	36	346	2	1.2
8b	0.0550	0.49	0.3986	1.36	0.0521	1.25	345	2	341	4	288	28	345	2	1.4
8c	0.0550	1.13	0.3993	3.50	0.0551	3.25	345	4	341	10	416	71	345	4	1.1
8d	0.0543	0.88	0.4043	2.58	0.0530	2.36	341	3	345	8	328	52	341	3	-1.0
8e	0.0545	0.50	0.4058	1.35	0.0535	1.22	342	2	346	4	349	27	342	2	-1.0
8f	0.0547	0.42	0.4159	1.12	0.0550	1.02	343	1	353	3	413	22	343	1	-2.8
8g	0.0549	0.69	0.4004	1.96	0.0539	1.78	345	2	342	6	367	40	345	2	0.8
8h	0.0550	0.69	0.4112	1.97	0.0548	1.79	345	2	350	6	403	39	345	2	-1.3
8i	0.0547	0.73	0.4222	2.03	0.0562	1.85	343	2	358	6	459	41	343	2	-4.0
8j	0.0546	0.79	0.3934	2.23	0.0530	2.04	343	3	337	6	331	46	343	3	1.8
8k	0.0550	0.76	0.4018	2.18	0.0543	2.01	345	3	343	6	382	44	345	3	0.6
8l	0.0548	0.42	0.4083	1.09	0.0541	0.98	344	1	348	3	374	22	344	1	-1.1
8m	0.0552	0.47	0.4955	1.20	0.0640	1.08	346	2	409	4	741	23	346	2	-15.3
8n	0.0547	0.79	0.4286	2.18	0.0562	1.98	343	3	362	7	459	43	343	3	-5.3
8o	0.0548	0.69	0.3870	2.01	0.0528	1.84	344	2	332	6	319	41	344	2	3.5
8p	0.0548	0.69	0.4024	1.96	0.0544	1.78	344	2	343	6	389	39	344	2	0.1

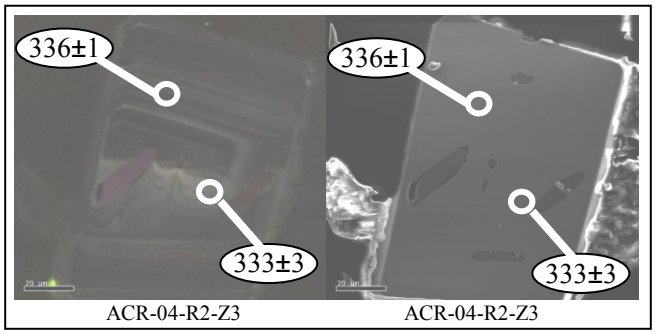

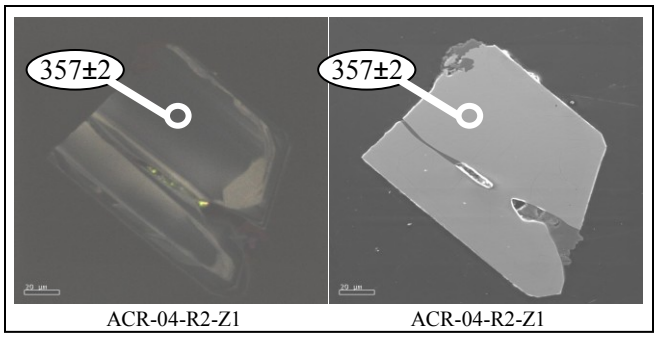

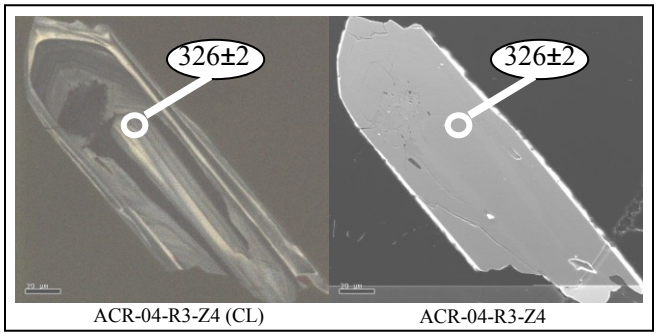

Fig. B.2 LA-ICPMS line scan locations for concordant $^{206}Pb/^{238}U$ ages for sample ACR-04.

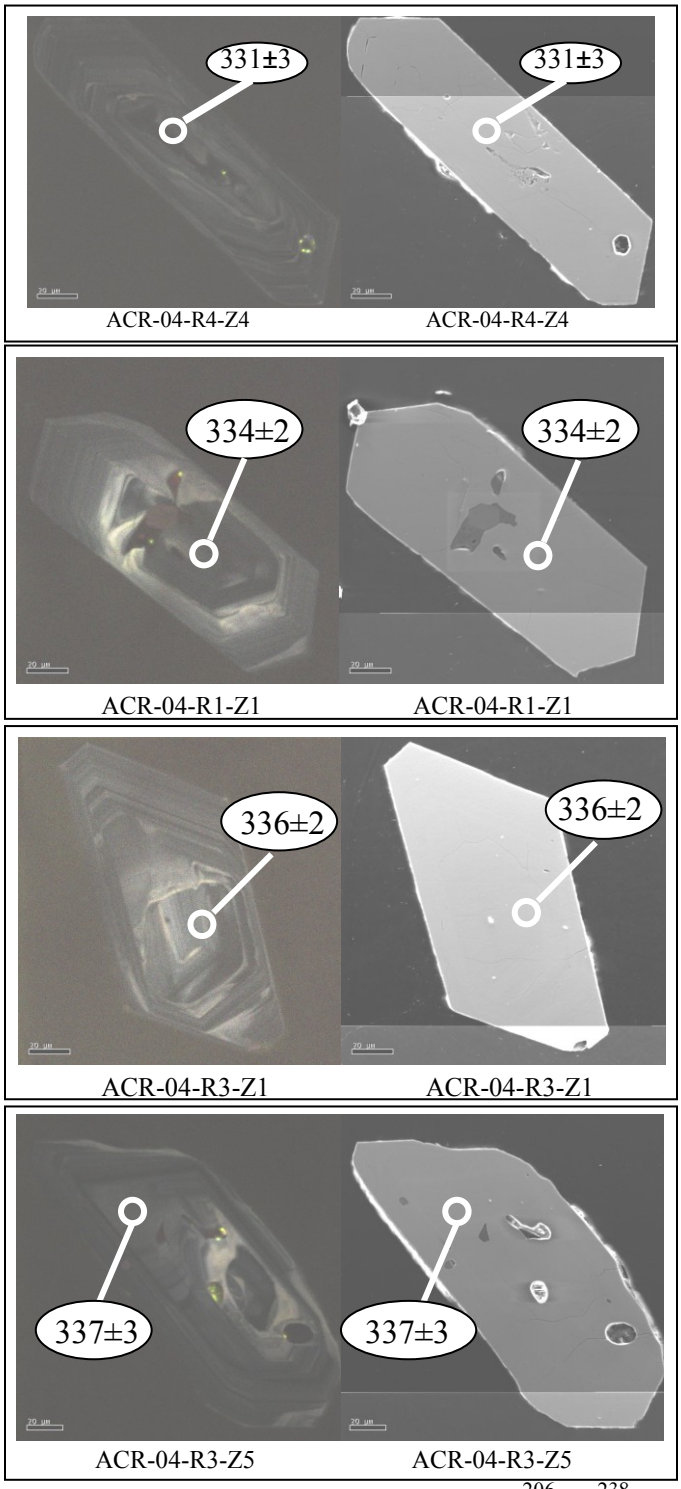

Fig. B.2 (cont.). LA-ICPMS line scan locations for concordant $^{206}Pb/^{238}U$ ages for sample ACR-04.

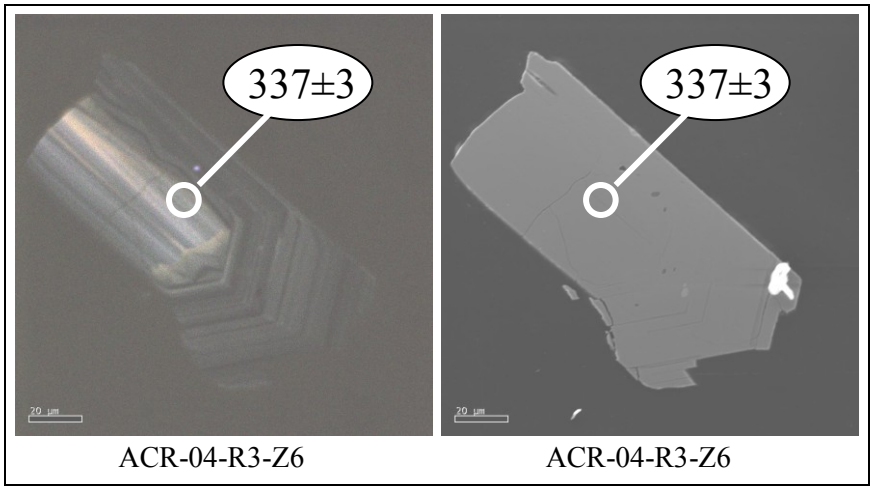

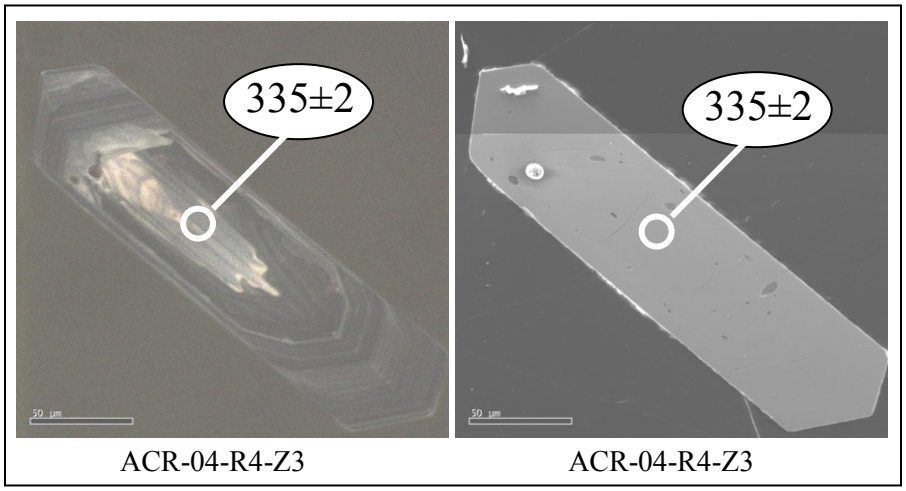

Fig. B.2 (cont.). LA-ICPMS line scan locations for concordant $^{206}Pb/^{238}U$ ages for sample ACR-04.

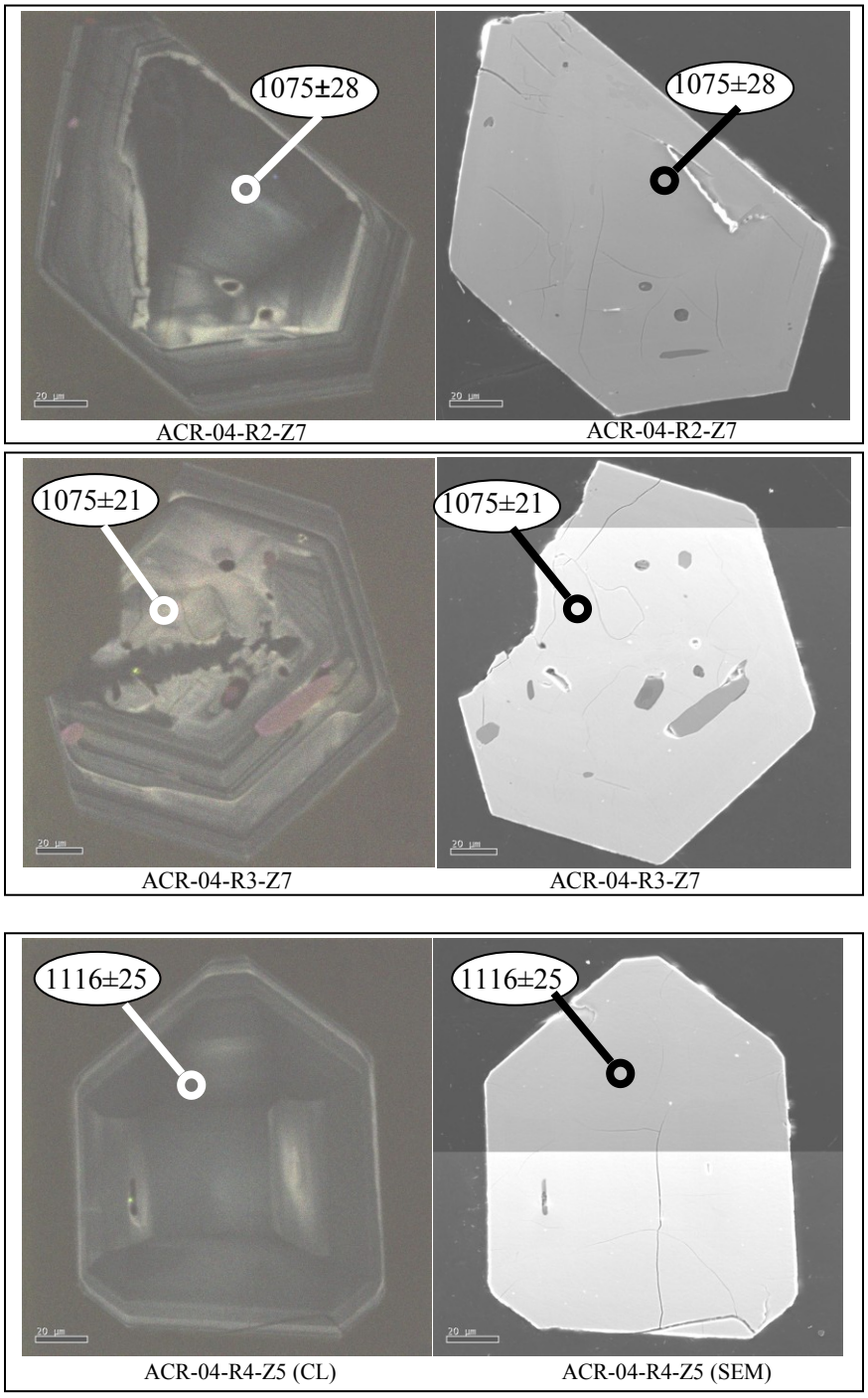

Fig. B.2(cont.). LA-ICPMS line scan locations for concordant $^{207}Pb/^{206}Pb$ ages for sample ACR-04 zircons with xenocrystic cores.

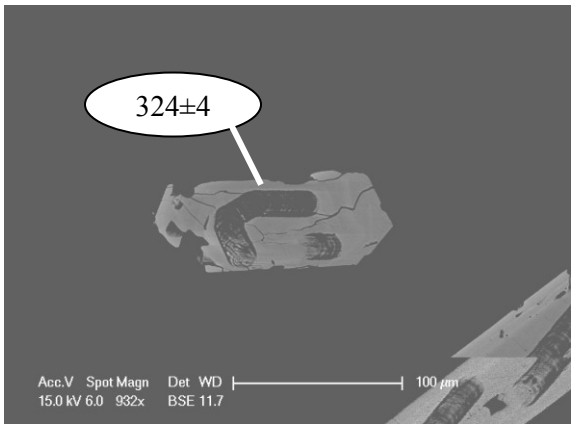

JAB09-5 (BSE)

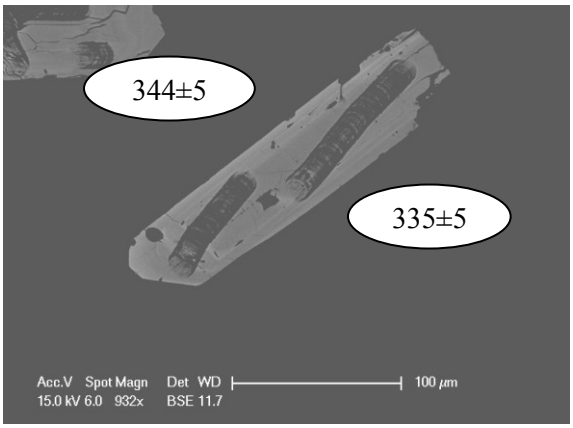

JAB09-6 & JAB09-7 (BSE)

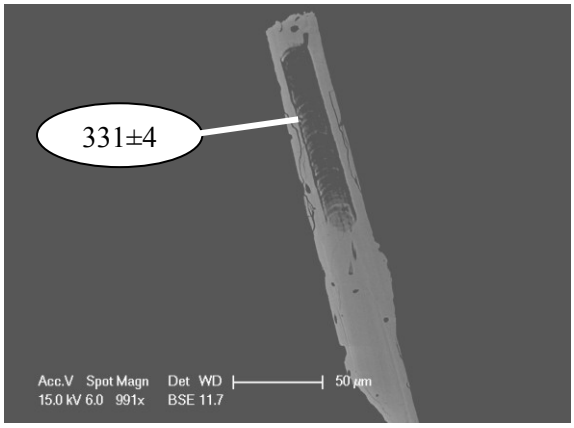

JAB09-8 (BSE)

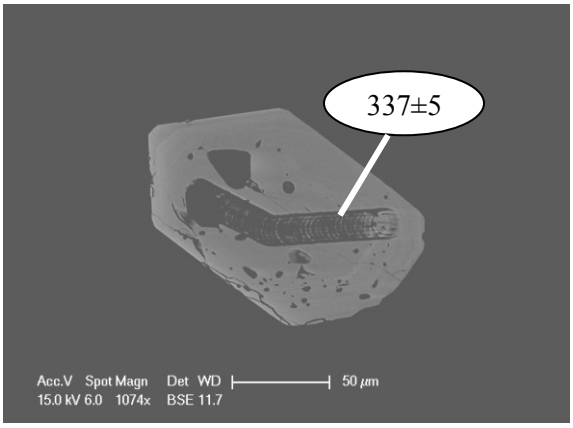

JAB09-10 (BSE)

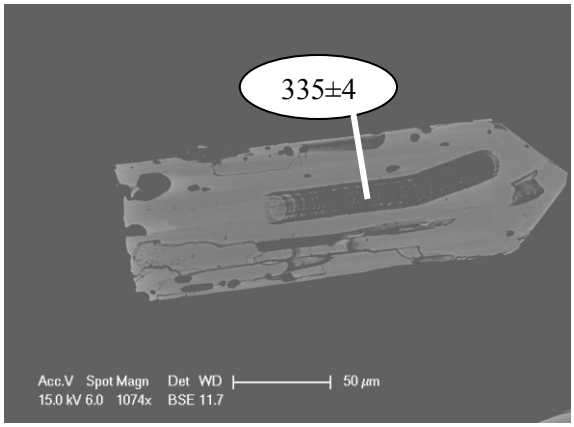

JAB09-12 (BSE)

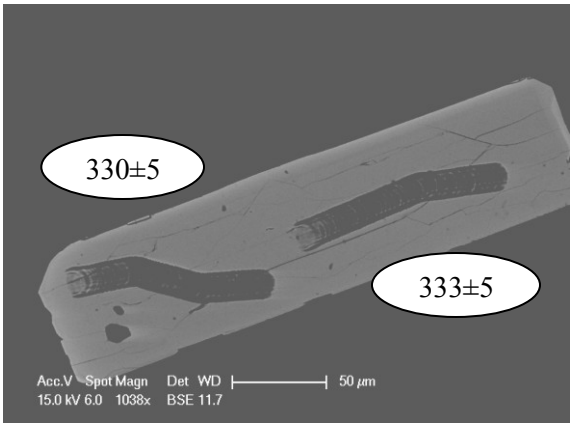

JAB09-13 & JAB09-21 (BSE)

Fig. B.3 LA-ICPMS line scan locations for concordant $^{206}Pb/^{238}U$ ages for sample JAB-09.

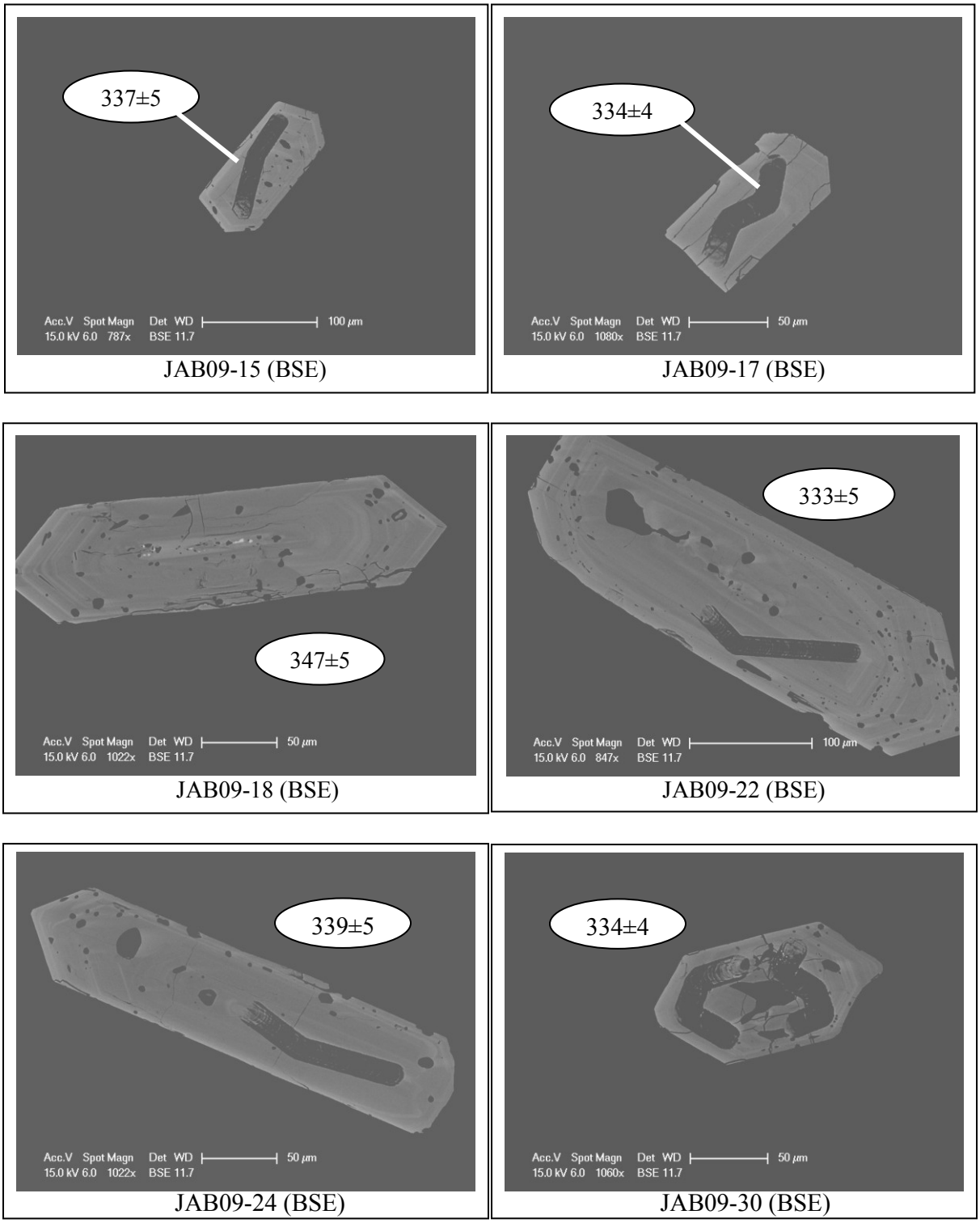

Fig. B.3 (cont). LA-ICPMS line scan locations for concordant $^{206}Pb/^{238}U$ ages for sample JAB-09.

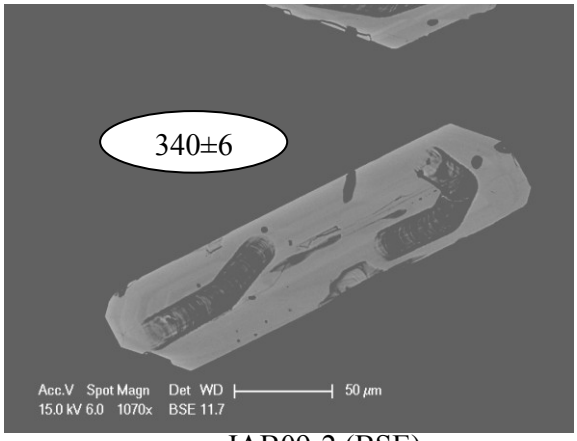

JAB09-2 (BSE)

JAB09-14 (BSE)

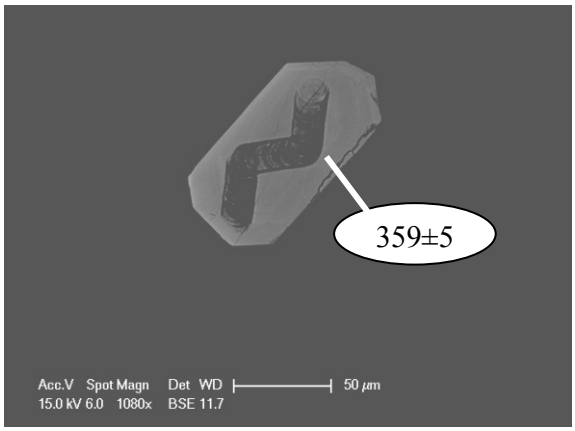

JAB09-16 (BSE)

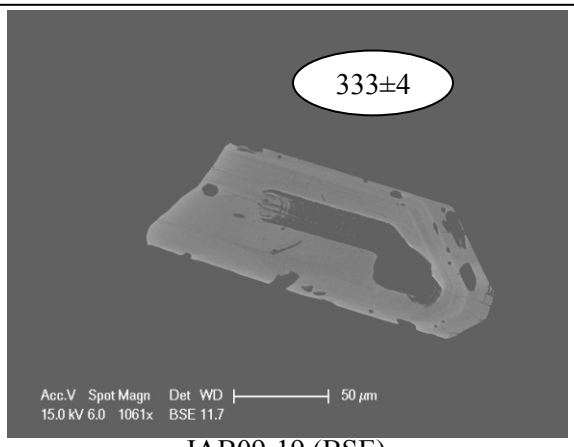

JAB09-19 (BSE)

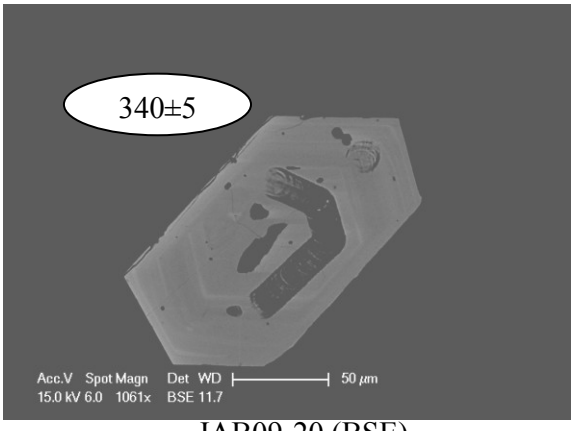

JAB09-20 (BSE)

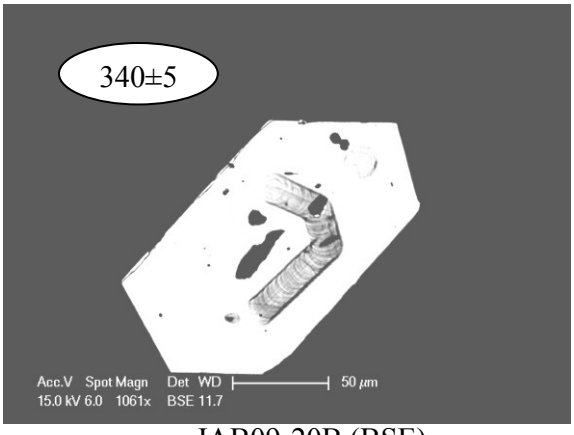

JAB09-20B (BSE)

Fig. B.3 (cont). LA-ICPMS line scan locations for concordant $^{206}Pb/^{238}U$ ages for sample JAB-09.

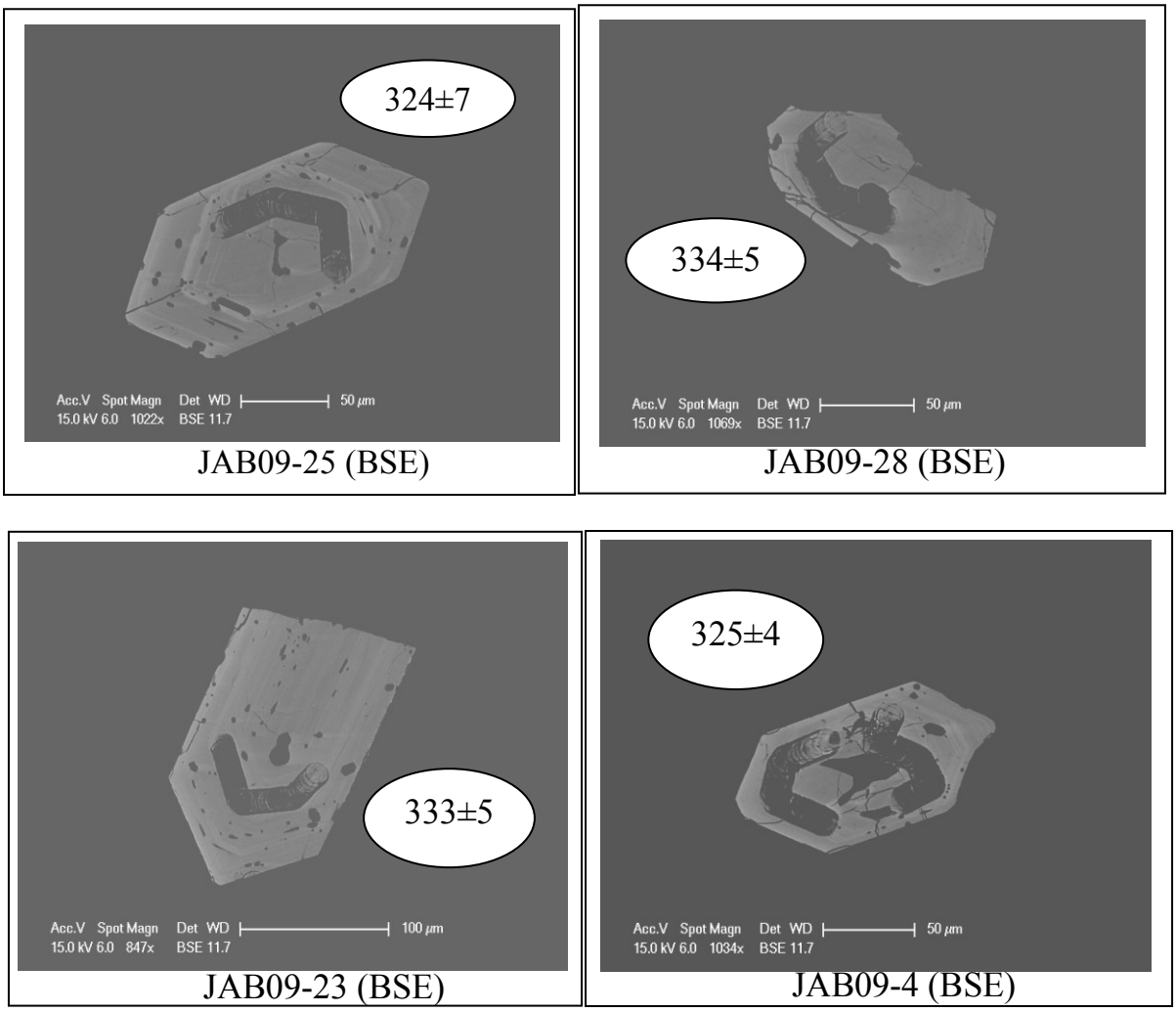

Fig. B.3 (cont). LA-ICPMS line scan locations for concordant $^{206}Pb/^{238}U$ ages for sample JAB-09.

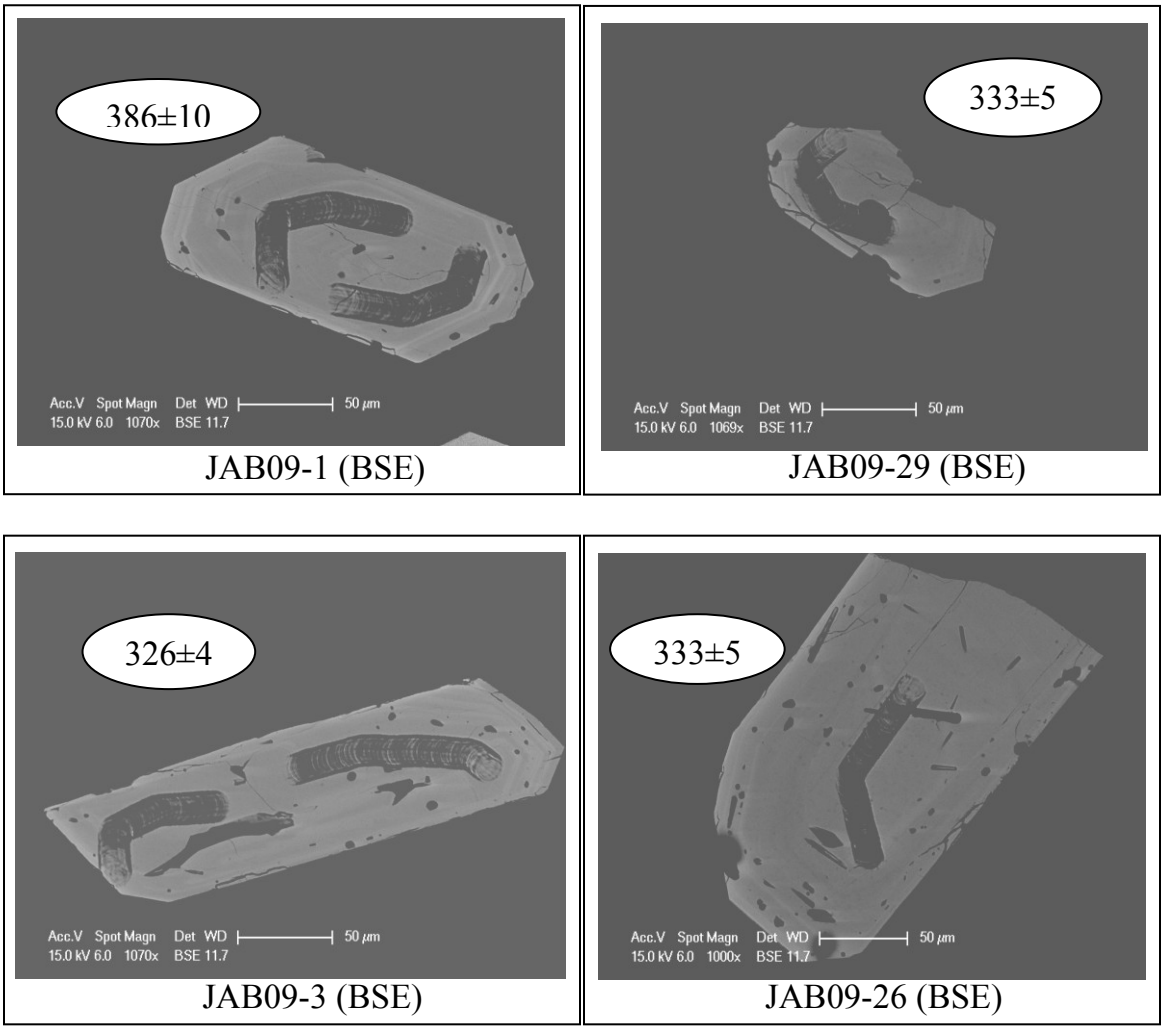

Fig. B.3 (cont). LA-ICPMS line scan locations for concordant $^{206}Pb/^{238}U$ ages for sample JAB-09.

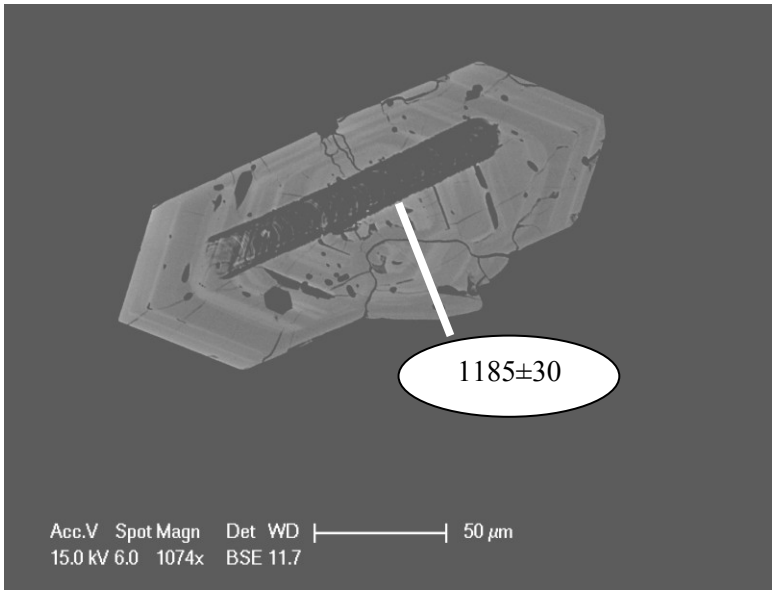

JAB09-9 (BSE)

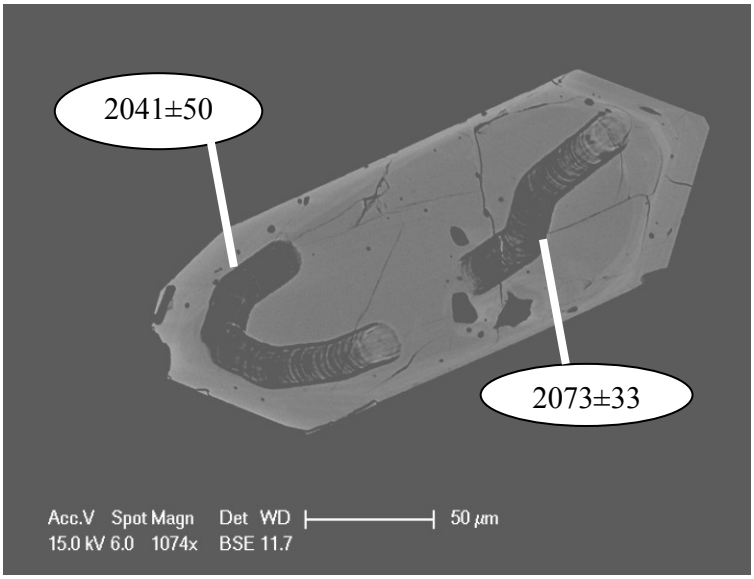

JAB09-11 & JAB09-27 (BSE)

Fig. B.3 (cont) LA-ICPMS line scan locations for concordant $^{207}Pb/^{206}Pb$ ages for sample JAB-09 zircons with xenocrystic cores.

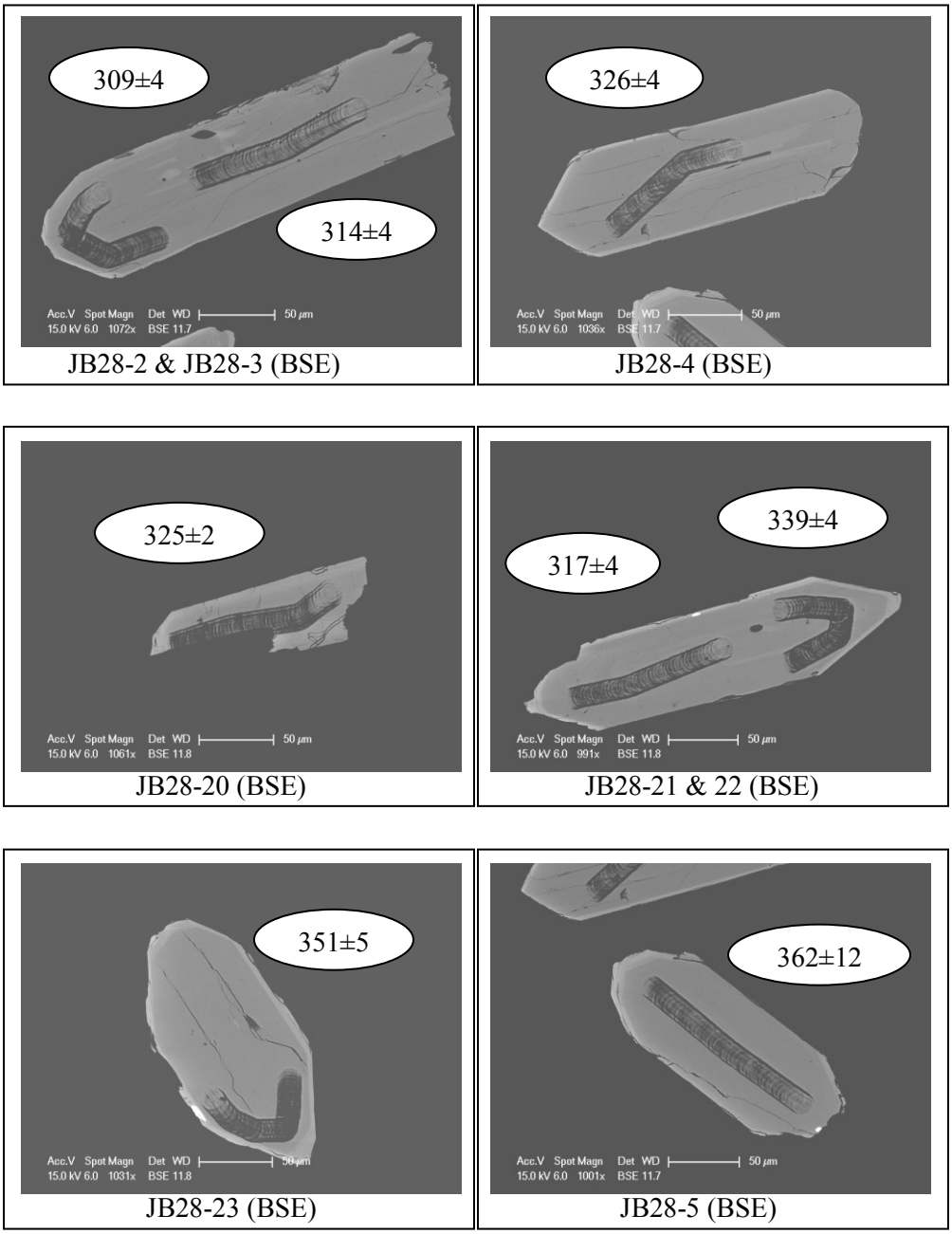

Fig. B.4 LA-ICPMS line scan locations for concordant $^{206}Pb/^{238}U$ ages for sample JB-28.

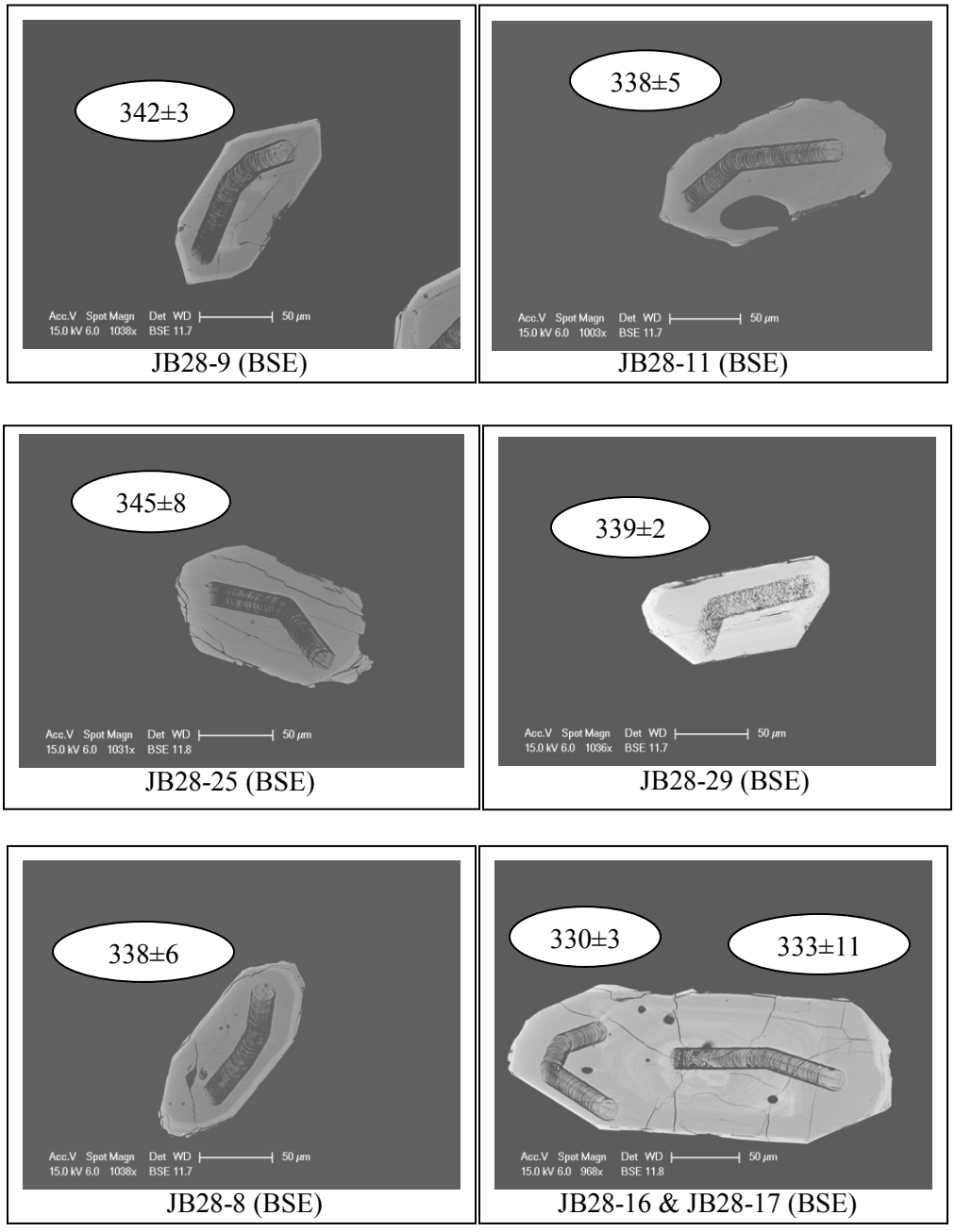

Fig. B.4 (cont) LA-ICPMS line scan locations for concordant $^{206}Pb/^{238}U$ ages for sample JB-28.

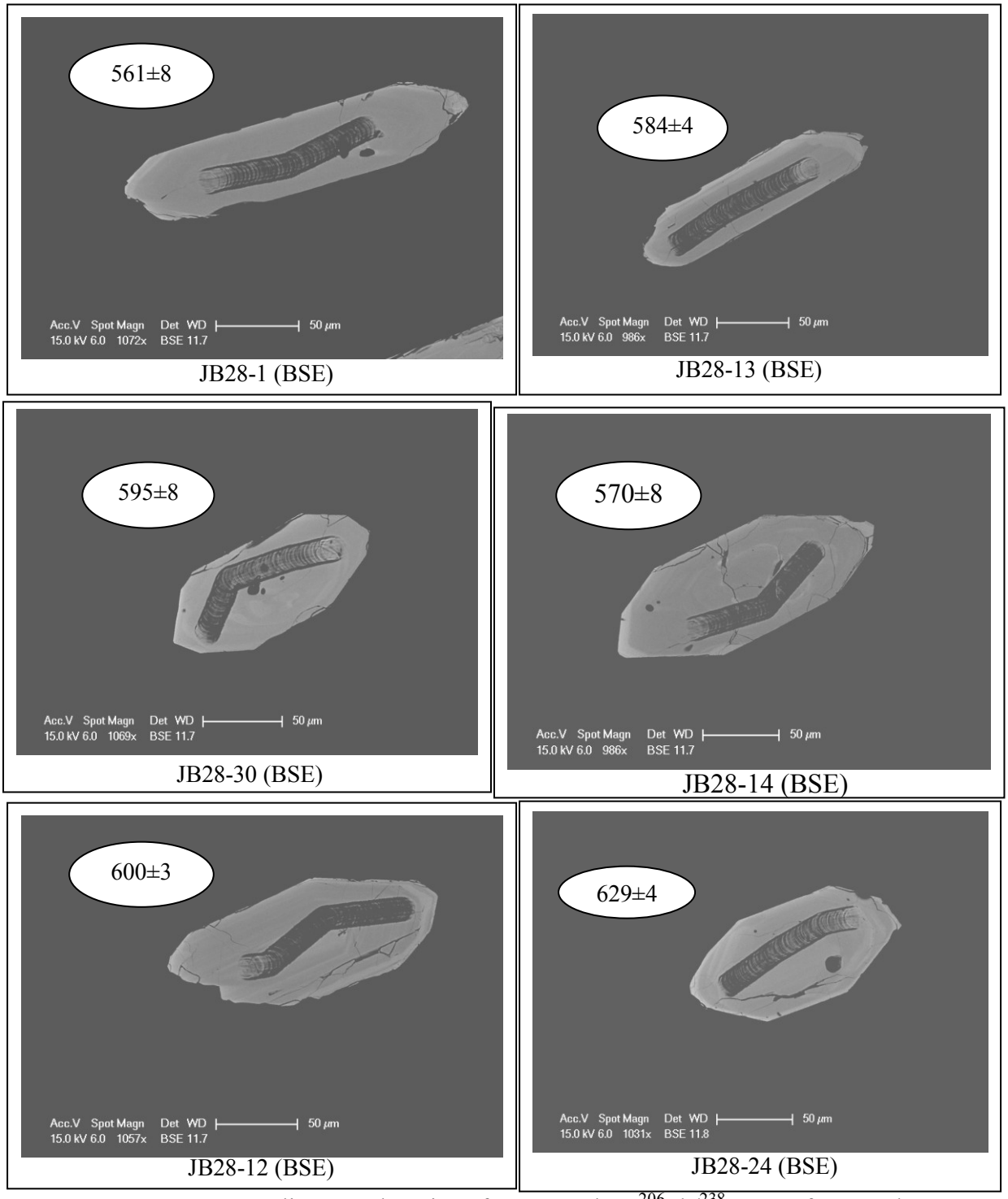

Fig. B.4 (cont) LA-ICPMS line scan locations for concordant $^{206}Pb/^{238}U$ ages for sample JB-28. Zirconswith xenocrystic cores.

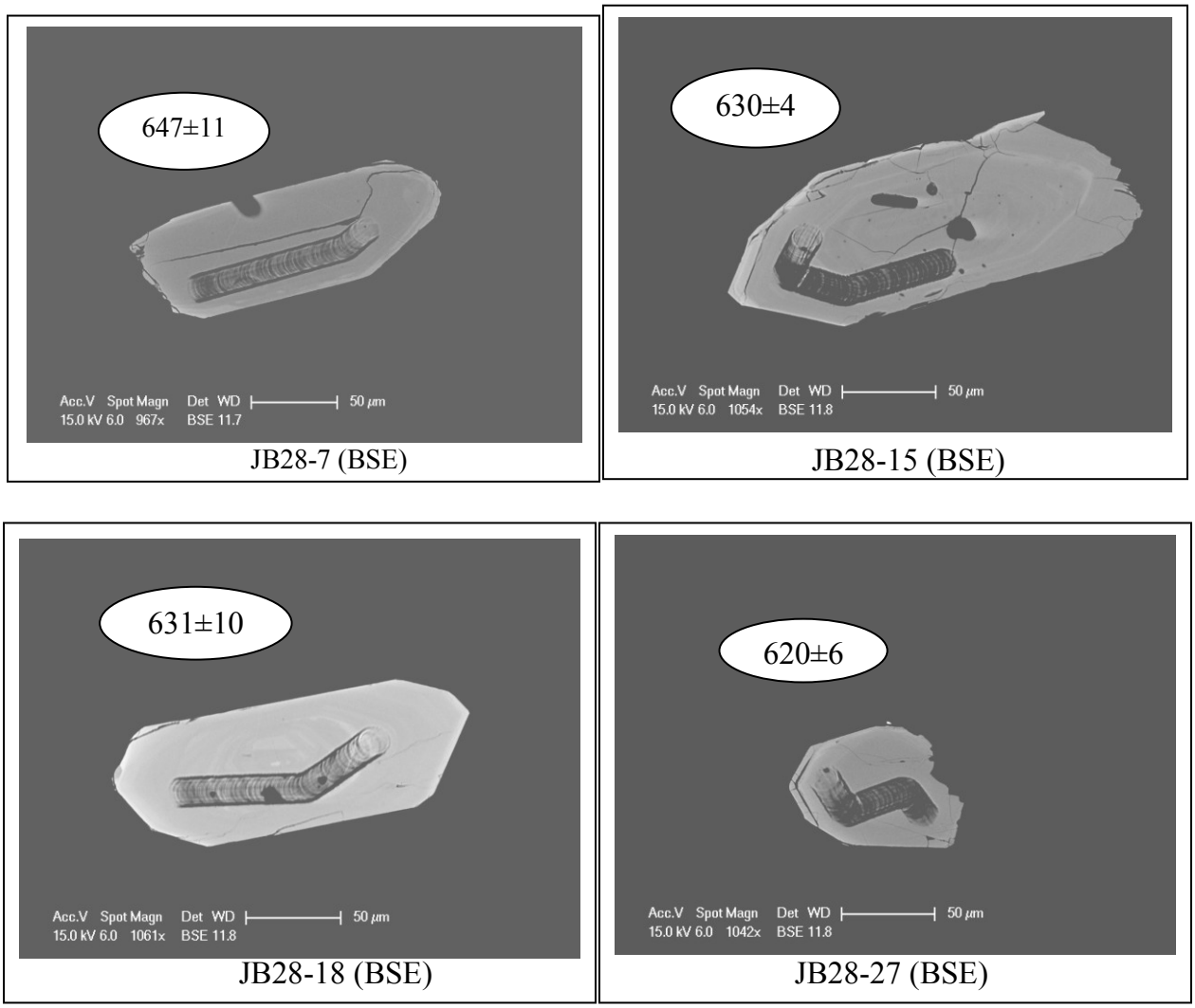

Fig. B.4 (cont) LA-ICPMS line scan locations for concordant $^{207}Pb/^{206}Pb$ ages for sample JB-28 zircons with xenocrystic cores.

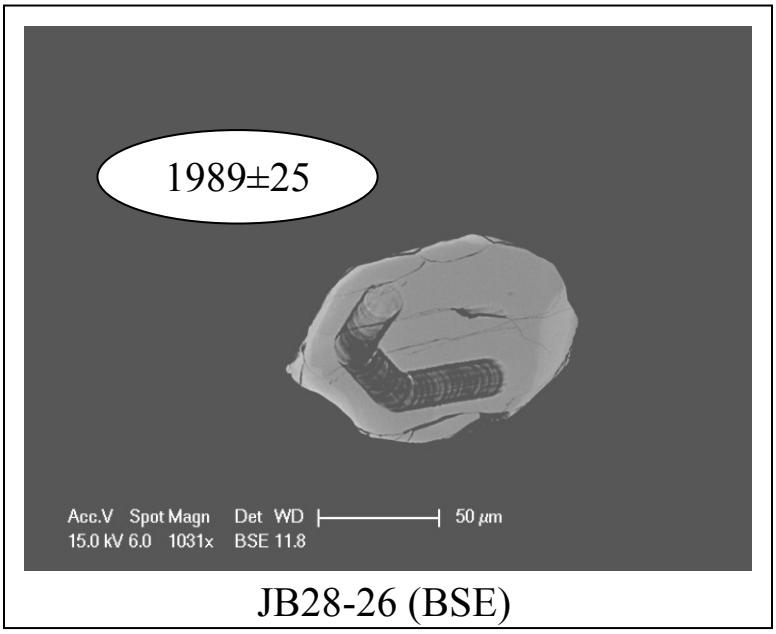

JB28-26 (BSE)

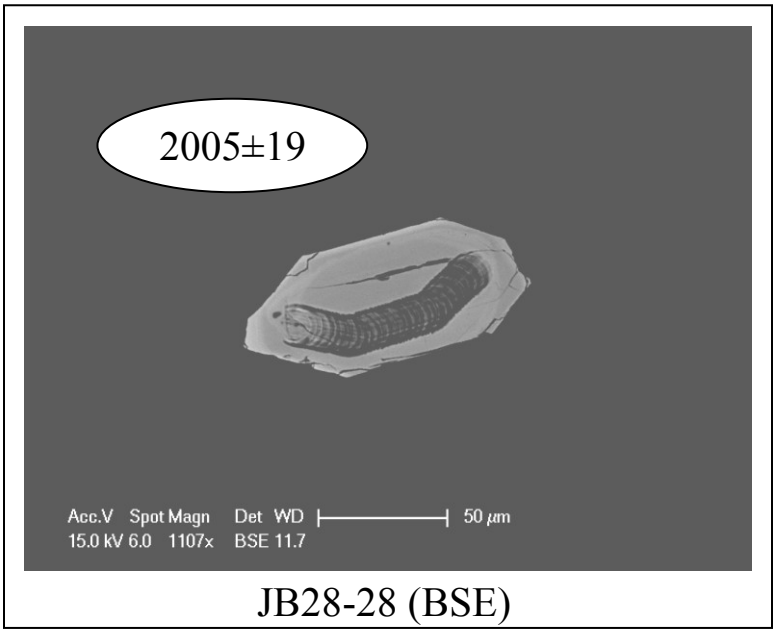

JB28-28 (BSE)

Fig. B.4 (cont) LA-ICPMS line scan locations for concordant $^{207}Pb/^{206}Pb$ ages for sample JB-28 zircons with xenocrystic cores.

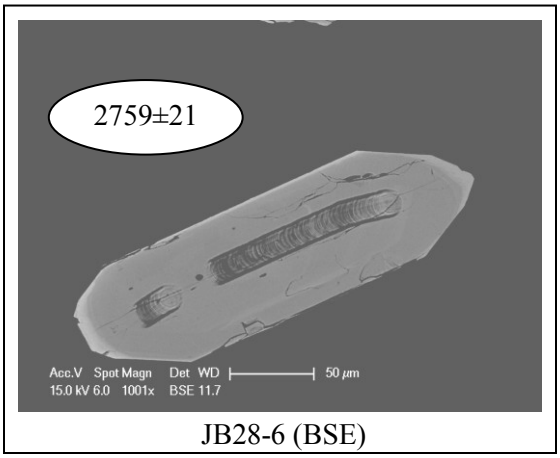

JB28-6 (BSE)

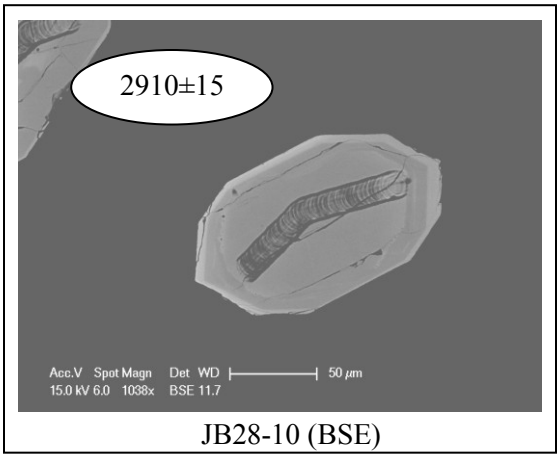

JB28-10 (BSE)

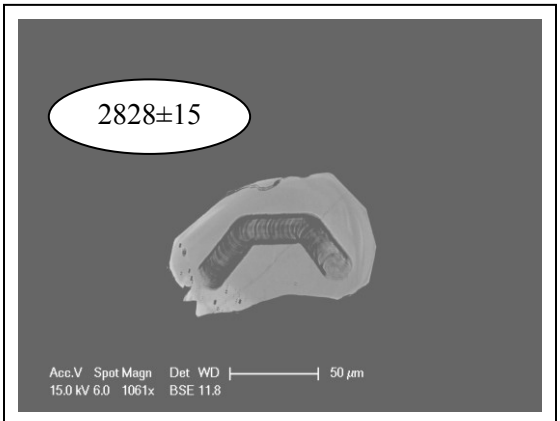

JB28-19 (BSE)

Fig. B.4 (cont). LA-ICPMS line scan locations for concordant $^{207}Pb/^{206}Pb$ ages for sample JB-28 zircons with xenocrystic cores.

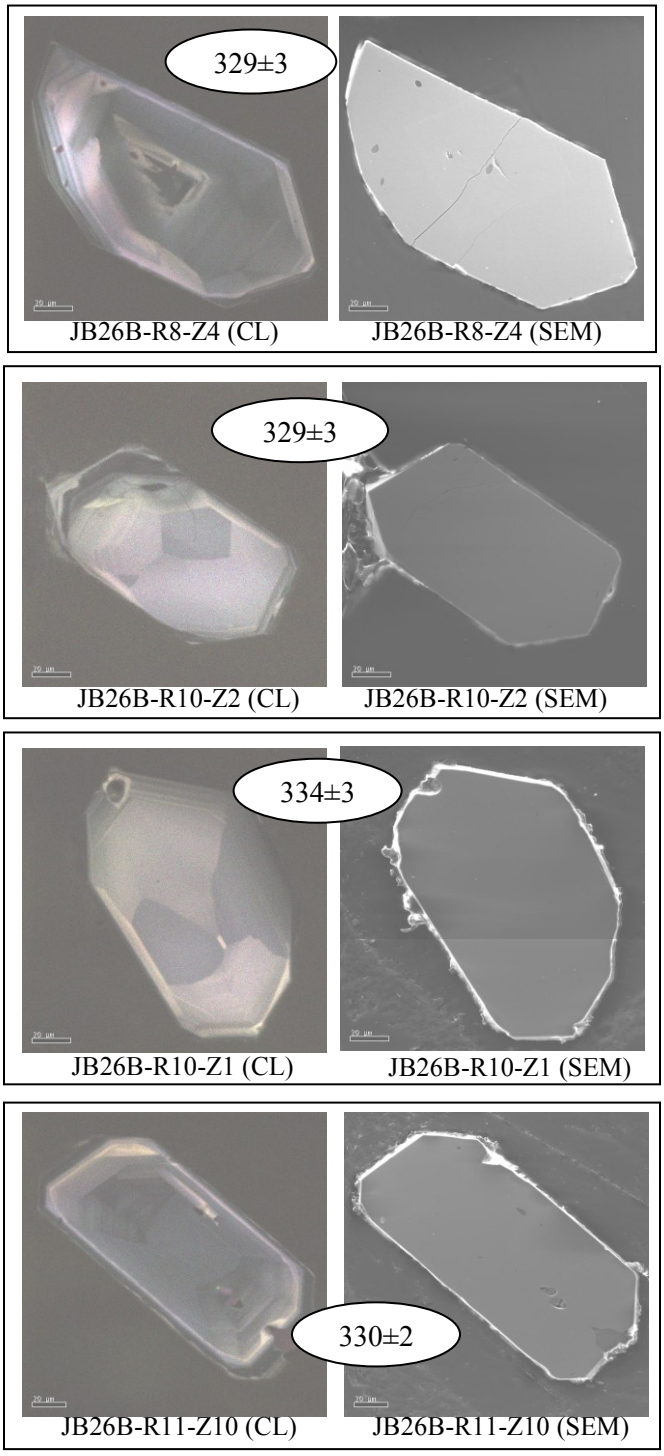

Fig. B.5LA-ICPMS line scan locations for concordant $^{206}Pb/^{238}U$ ages for sample JB-26B.

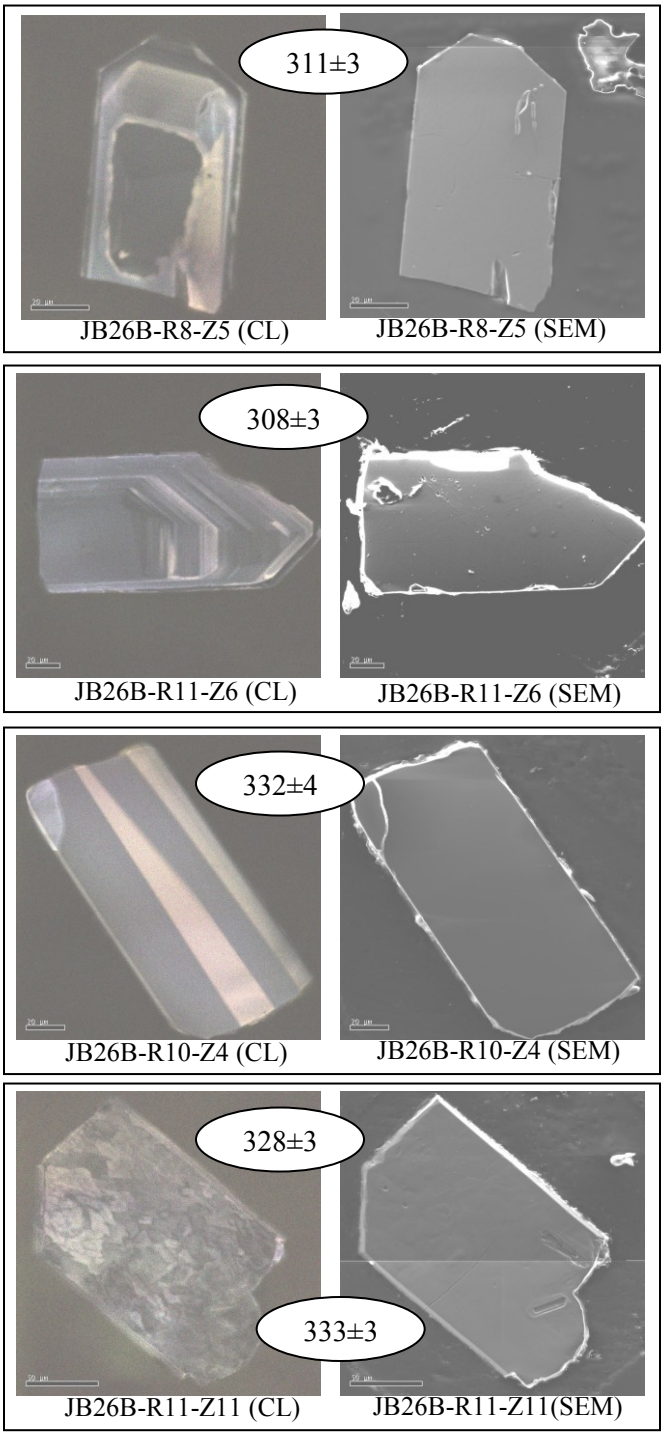

Fig. B.5 (cont) LA-ICPMS line scan locations for concordant $^{206}Pb/^{238}U$ ages for sample JB-26B.

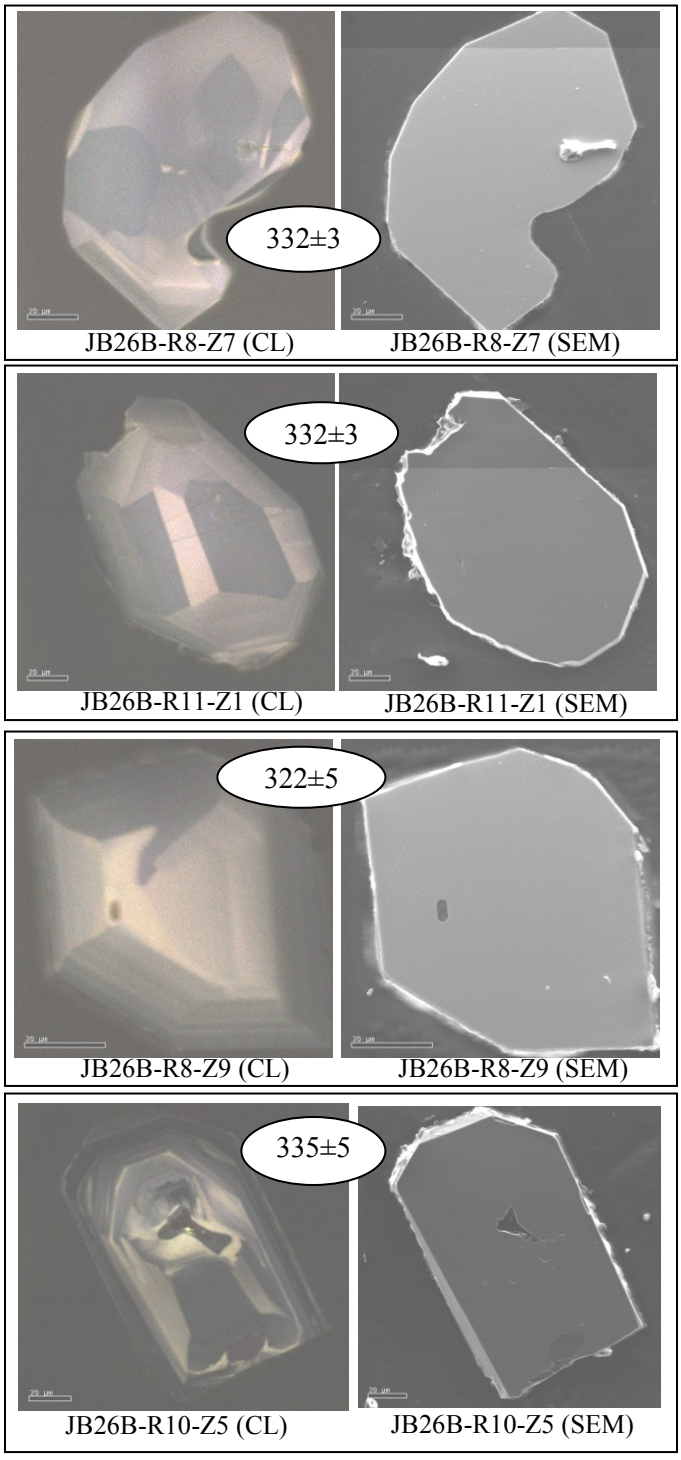

Fig. B.5 (cont) LA-ICPMS line scan locations for concordant $^{206}Pb/^{238}U$ ages for sample JB-26B.

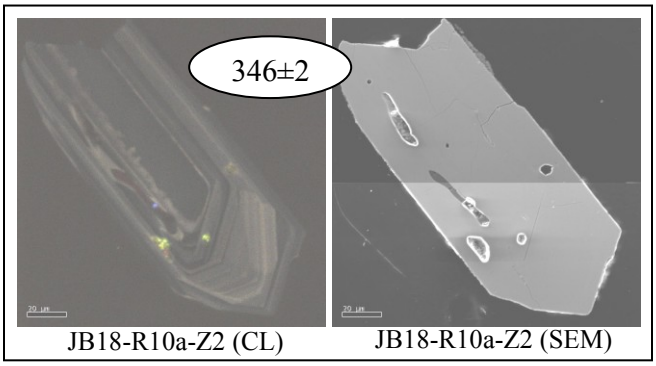

JB18-R10a-Z2 (CL) JB18-R10a-Z2 (SEM)

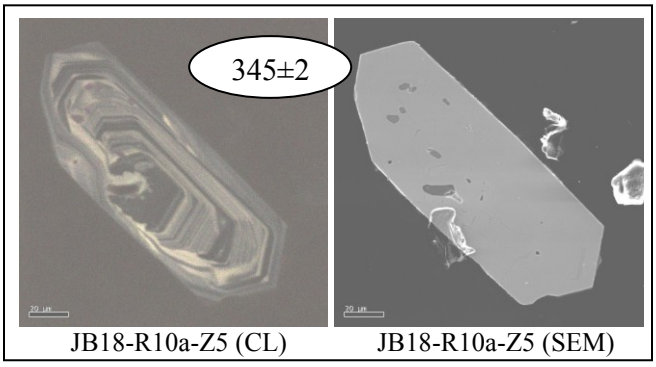

JB18-R10a-Z5 (CL) JB18-R10a-Z5 (SEM)

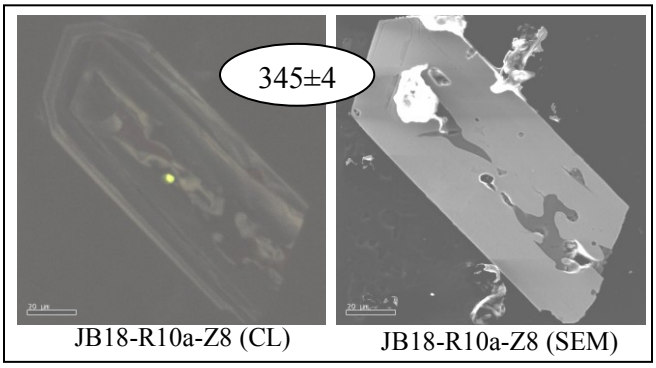

JB18-R10a-Z8 (CL) JB18-R10a-Z8 (SEM)

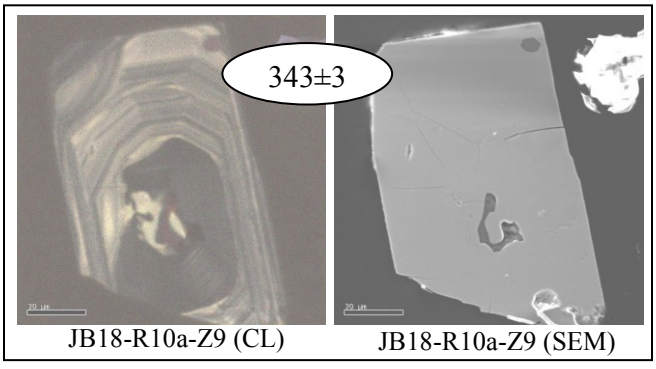

JB18-R10a-Z9 (CL) JB18-R10a-Z9 (SEM)

Fig. B.6LA-ICPMS line scan locations for concordant $^{206}Pb/^{238}U$ ages for sample JB-18.

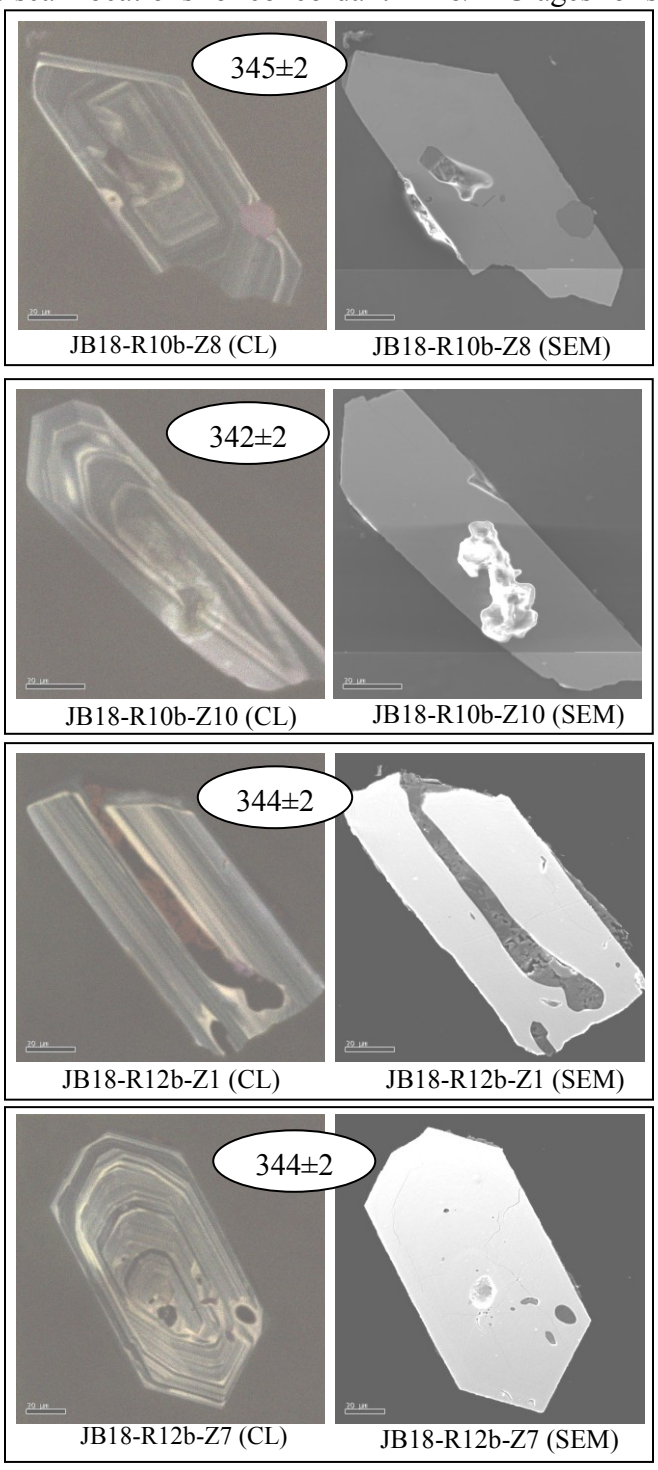

Fig. B.6 (cont) LA-ICPMS line scan locations for concordant $^{206}Pb/^{238}U$ ages for sample JB-18.

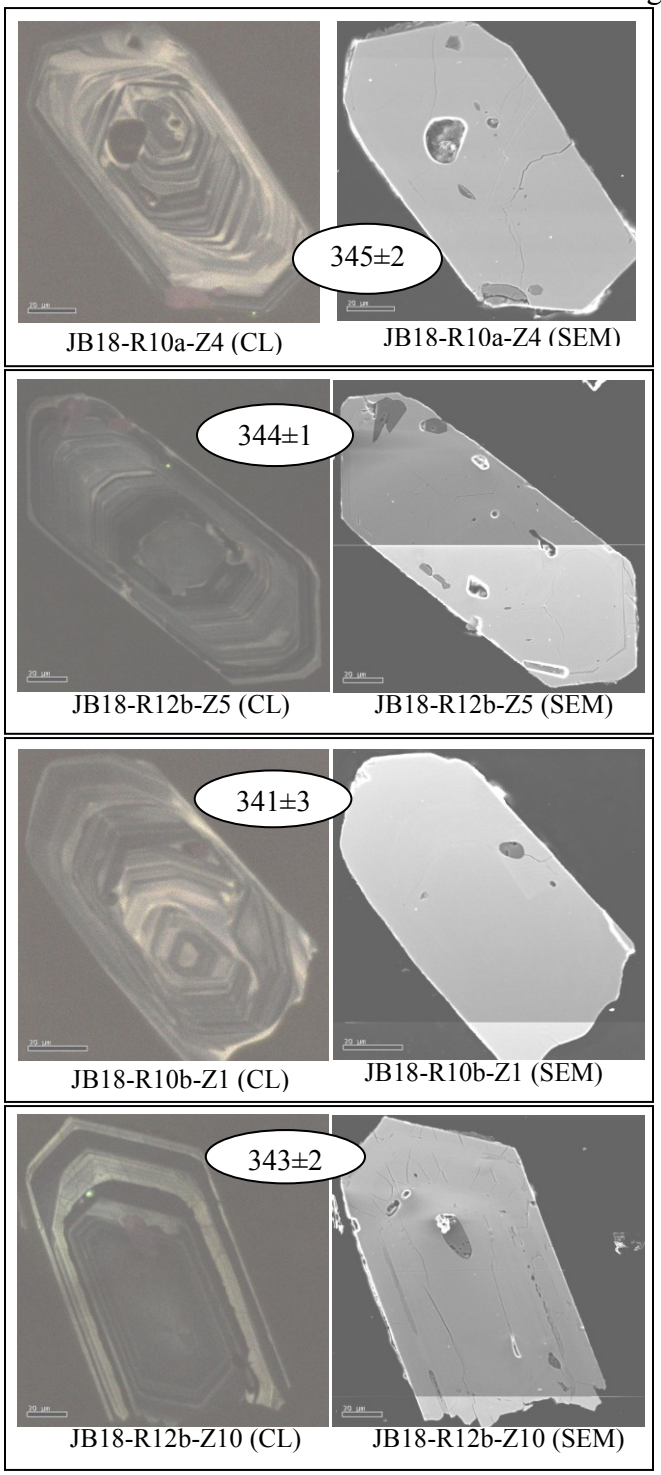

Fig. B.6 (cont) LA-ICPMS line scan locations for concordant $^{206}Pb/^{238}U$ ages for sample JB-18.

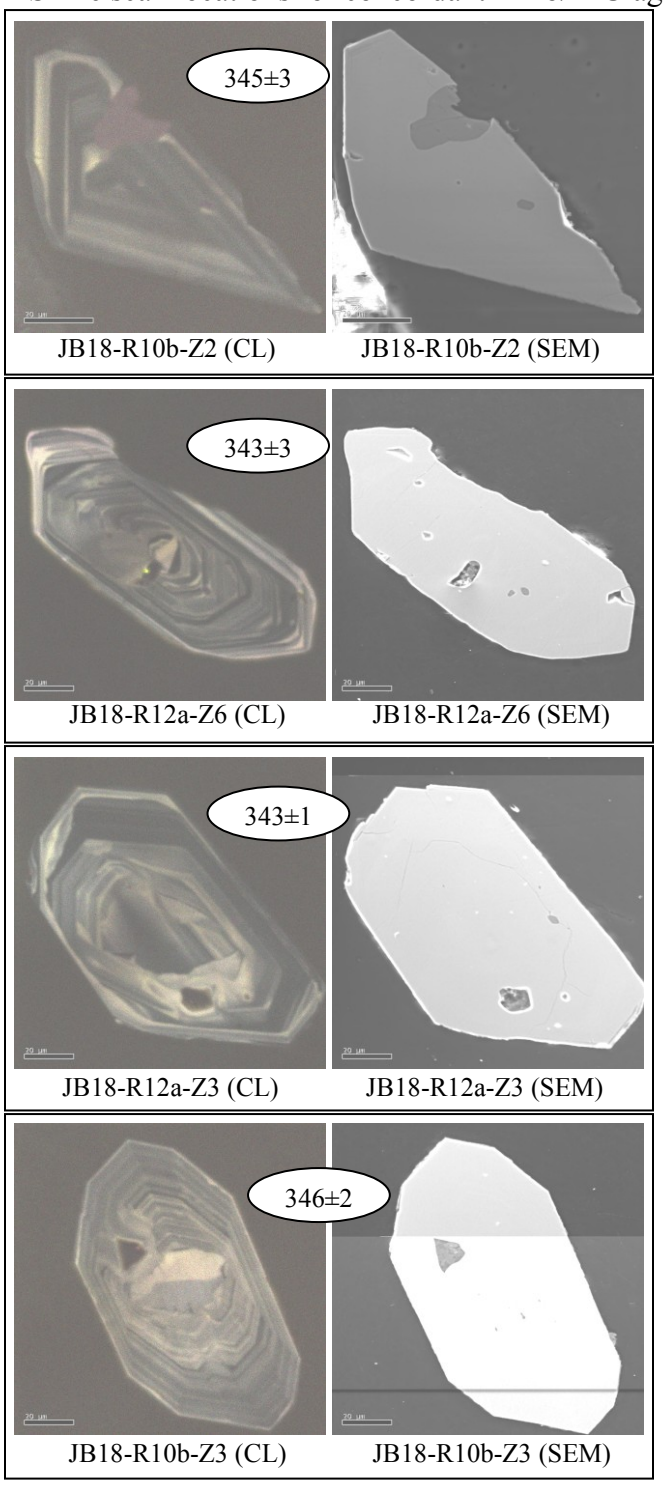

Fig. B.6 (cont) LA-ICPMS line scan locations for concordant $^{206}Pb/^{238}U$ ages for sample JB-18.

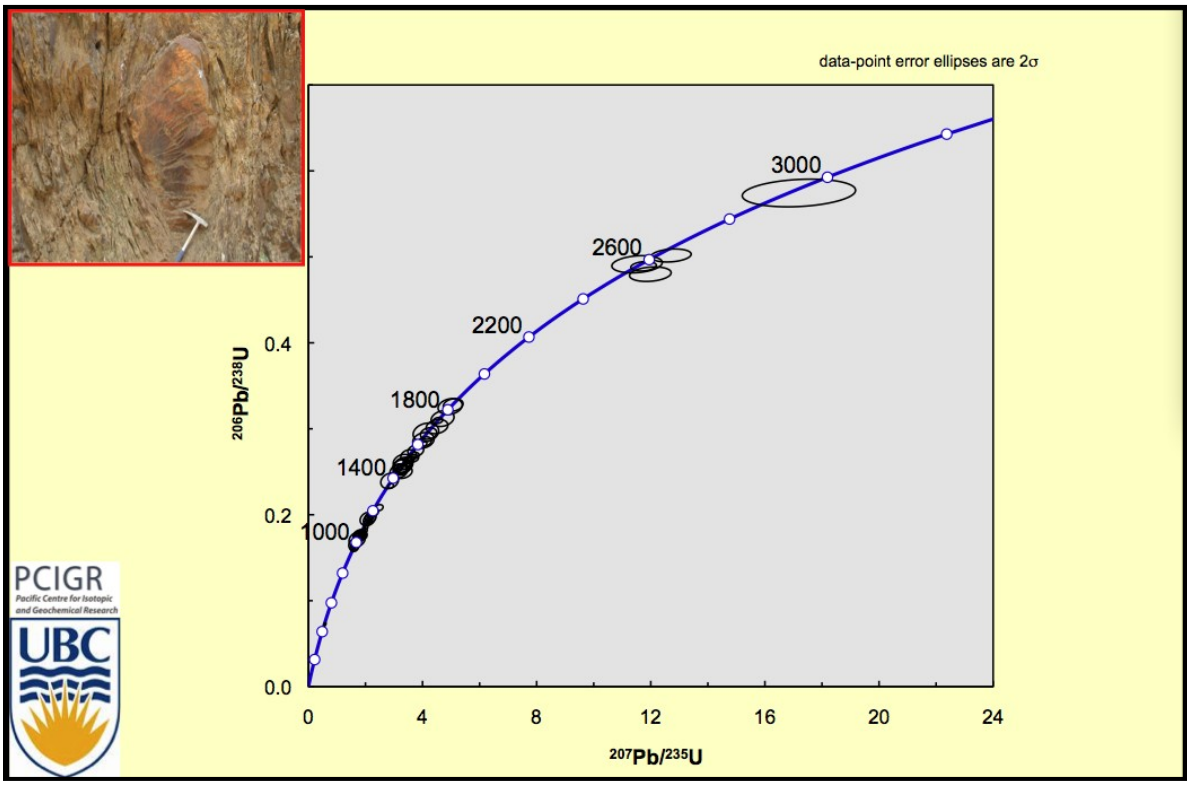

Fig. B.7 U-Pb concordia for sample RSA-01.

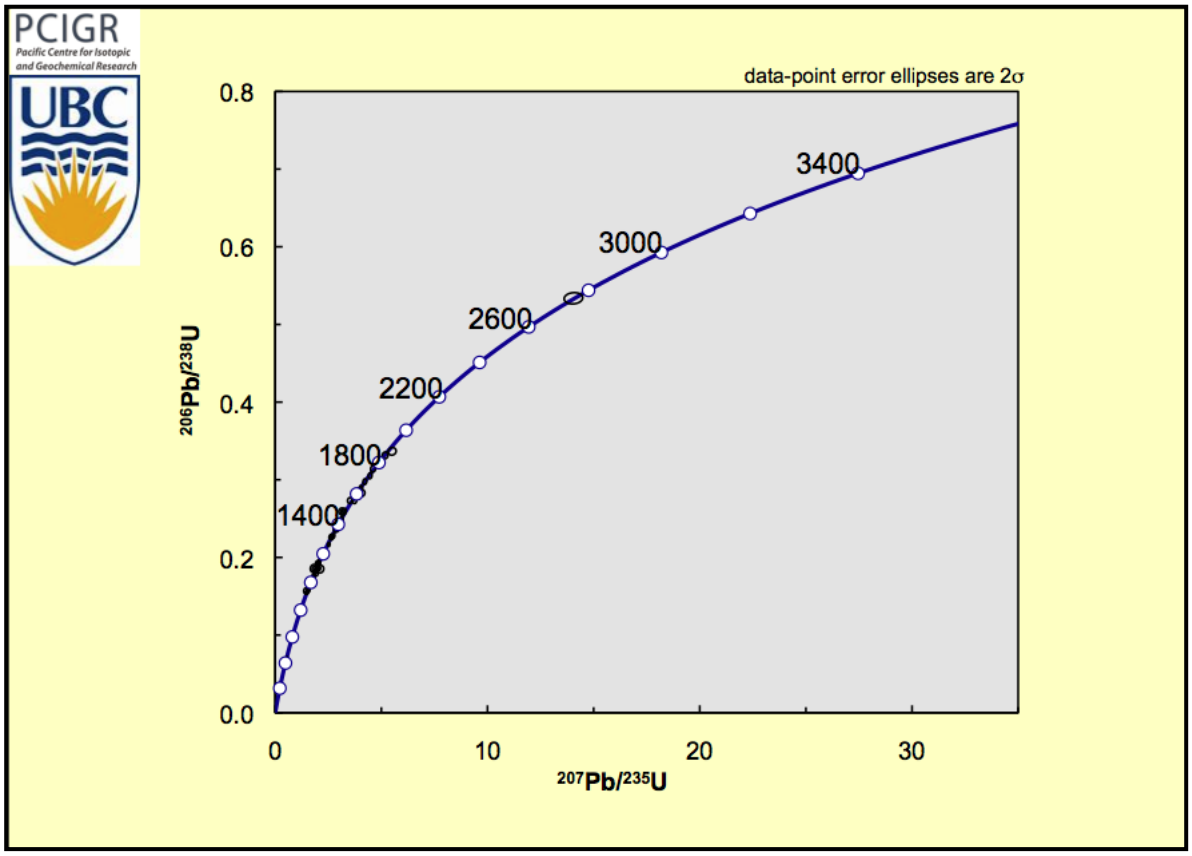

Fig. B.8 U-Pb concordia for sample JB-43.

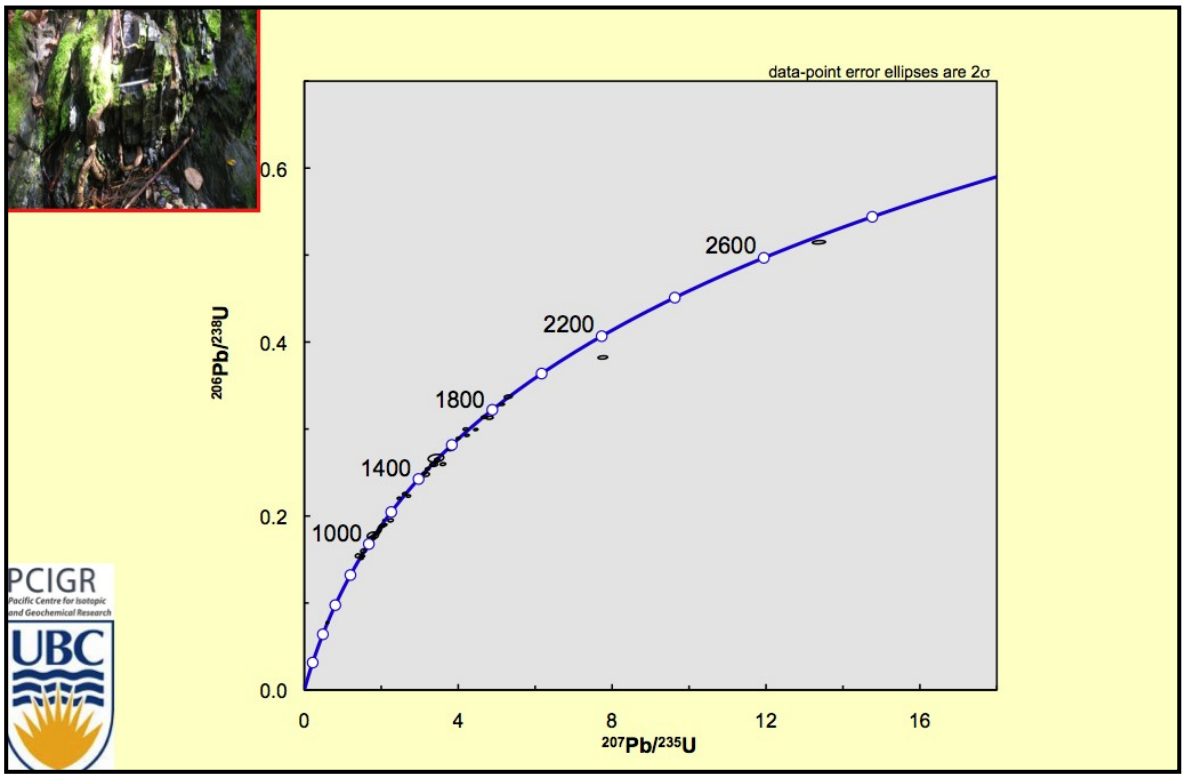

Fig. B.9 U-Pb concordia for sample RSA-02.

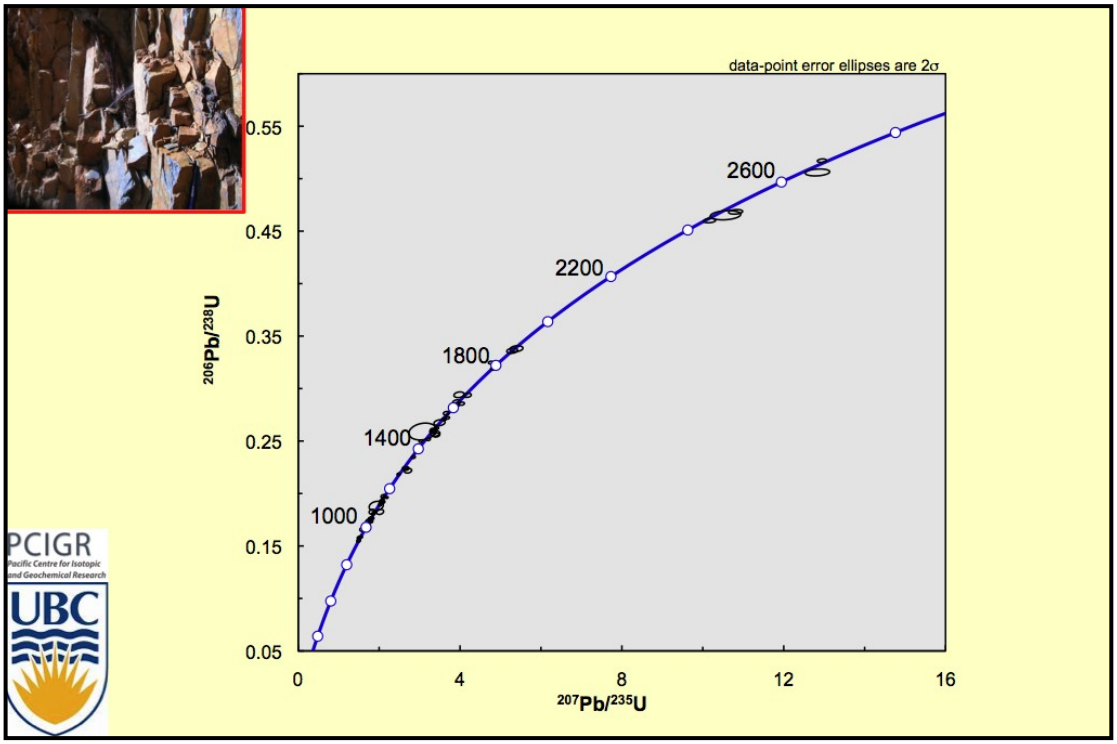

Fig. B.10 U-Pb concordia for sample AC-03

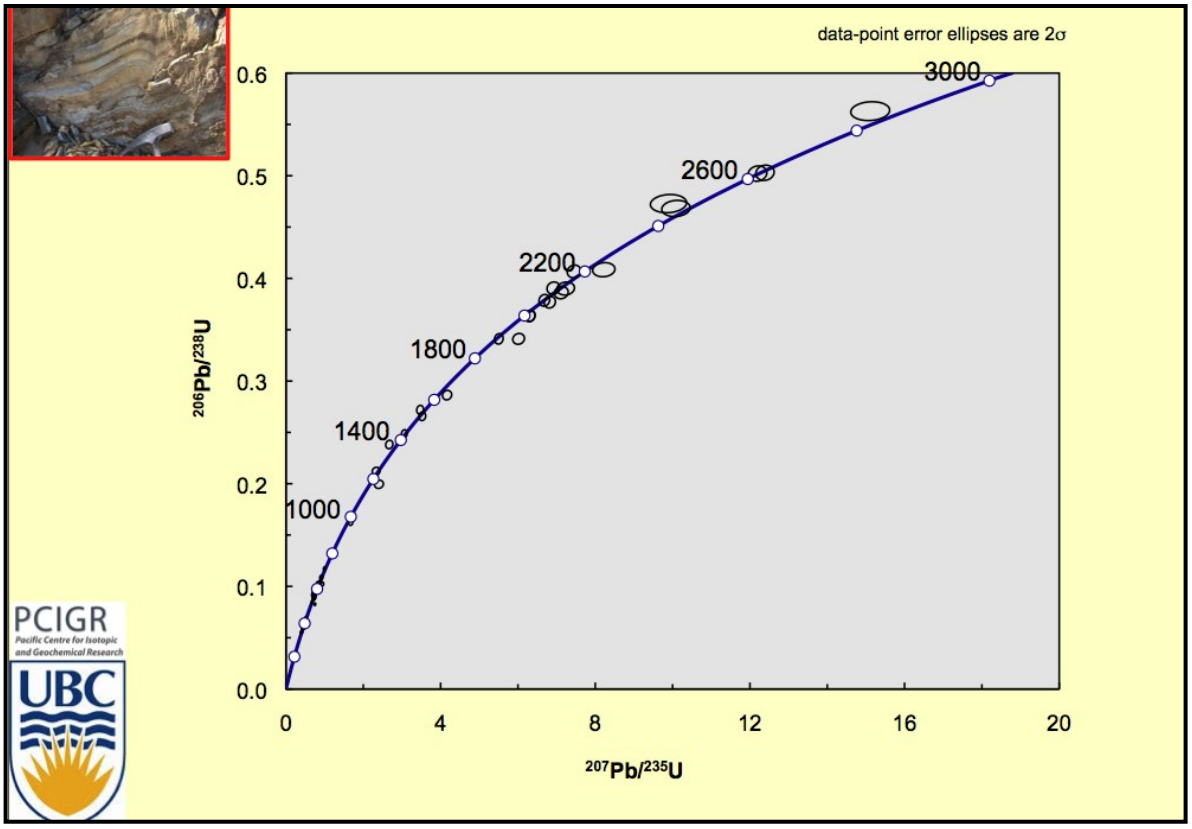

Fig. B.11 U-Pb concordia for sample JAB-08.

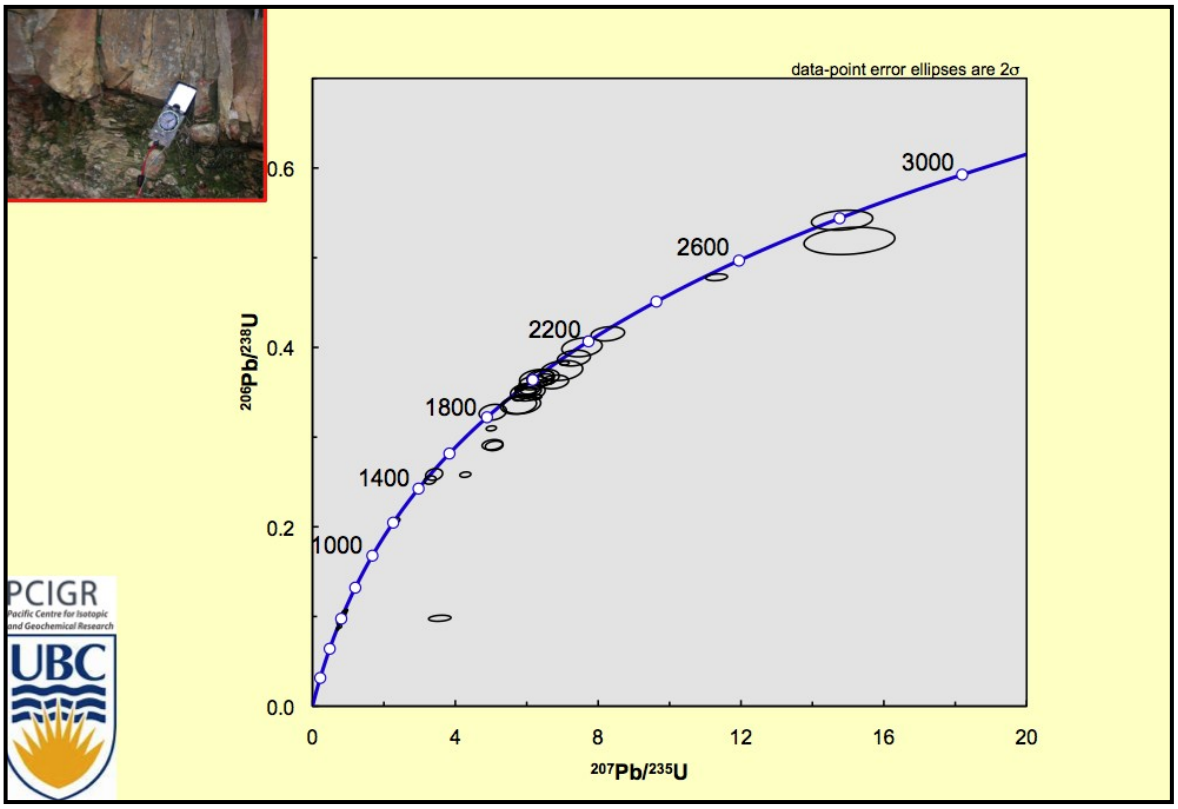

Fig. B.12 U-Pb concordia for sample JB-17

APPENDIX C

PRINCIPLES OF SM-ND ISOTOPIC ANALYSIS

C.1. Sm/Nd Systematics

Understanding the processes which occur during mountain building and the destruction of oceanic lithosphere rely heavily on determining the timing of important geologic events internal to these systems. While surface geology remains the foundation for any tectonic study, many steps in the history of an exposed rock cannot be determined by simple field methods. This is true particularly for igneous rocks, which often have long lived complex thermal histories recording processes deep within the earth's crust to eventual exposure at shallow levels. To understand these processes Sm Nd isotopic systems are extremely valuable. Samarium and neodymium are rare earth elements (REE) joined in a parent-daughter relationship by the alpha-decay of ^{147}Sm to ^{143}Nd with a half life of 1.06 x 1011 years. The isotopes also have both a similar ionic radii and valency, and consequently intra-crustal processes such as anatexis, fractionation and regional metamorphism rarely have little effect on the samarium neodymium ratio (Murphy and Nance, 2002). This ratio is controlled primarily by the depleted mantle, which preferentially retains samarium over neodymium (DePaolo, 1981). Consequently, the

samarium, neodymium ratio is about 40% lower in crustal rocks than it is in the depleted mantle.

This difference is the primary control on samarium neodymium systematics; resulting in differential isotopic signatures through time on both the crustal and depleted mantle reservoirs. Due to the radioactive decay of ^{147}Sm to ^{143}Nd and these varying initial concentrations the ratio of ^{143}Nd to ^{144}Nd (a stable isotope) will increase more rapidly in the depleted mantle than in the continental crust. The bulk earth (represented by CHUR; Chondritc Uniforn Reservoir) is a mixing of both depleted and enriched sources, subsequently the initial Sm/Nd ration increases more rapidly than continental rocks and less than the depleted mantle (See Fig. C.1). Differences between the $^{143}Nd/^{144}Nd$ initial ratios for each system can be expressed by epsilon neodymium (εNd). A given sample plotted for εNd at the time of crystallization can be extrapolated backward using the Sm/Nd ratio to the intersection with the depleted mantle. This intersection gives the depleted mantle model age (T_{dm}). This intersection is the potential age at which the crust was derived from the mantle. Model ages, however may be influenced by mixing of a relatively juvenile with a relatively ancient crust during its thermal evolution (Fig. C.1) and consequently T_{dm} ages must be interpreted with caution in conjunction with primary data indicative of the crustal evolution of the rock (e.g. Petrology, U/Pb geochronology).

The samarium neodymium ratio is not only preserved through crustal processes but also through most surface processes. This is due predominantly to the natural tendency for REE (rare earth elements) to concentrate in robust accessory mineral phases.

During melt evolution, minerals that crystallize early in the fractionation processes, (i.e. olivine clinopyroxene), generally contain low REE abundances and consequently total REE concentration in a melt tends to increase during fractionation processes. During eventual magma cooling, REE's ultimately become concentrated in accessory phases such as zircon, titanite and monazite.

The robust nature of some of these minerals (ie zircon) in most geologic environments allow for samarium and neodymium to remain intact during weathering processes, carried in solid detritus and deposited in various sedimentary systems. This characteristic enables Sm/Nd to be used as a tracer of the source materials of sedimentary rocks (e.g. McCulloch and Wasserburg, 1978). Sm-Nd isotopic ratios determine a weighted average of samarium neodymium ratios in the source material. However as noted by Murphy and Nance (2002), because REEs are concentrated in heavy minerals, sedimentary processes such as fractionation or accumulation of heavy minerals during sediment transport may exert a dominant control, so that the source of the dominant silicate phases is unconstrained.

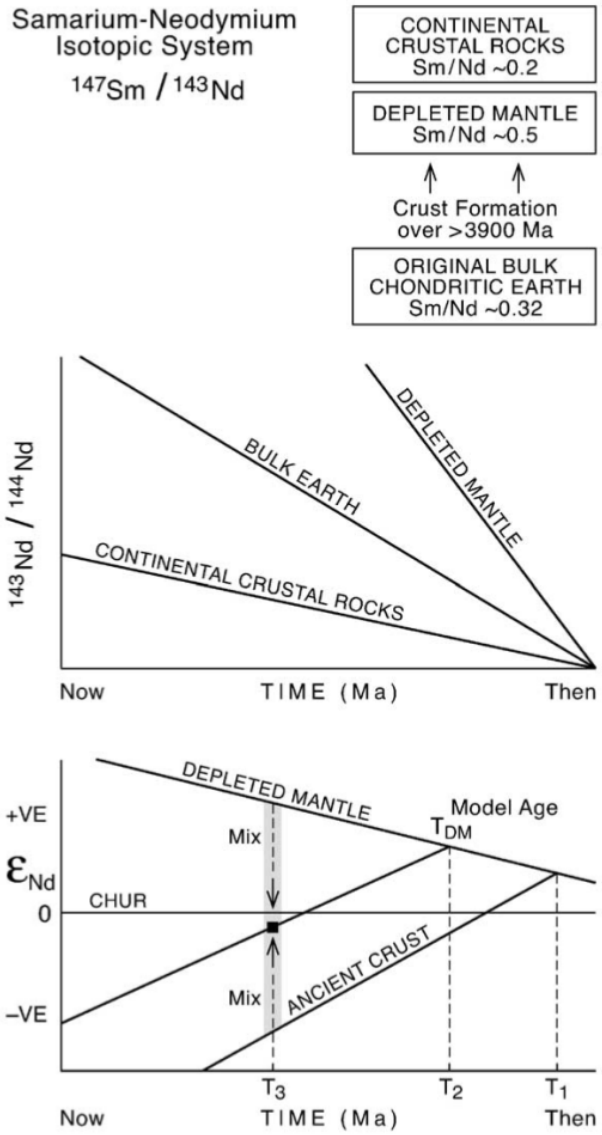

Fig. C.1 (from Murphy and Nance, 2002) Sm – Nd isotopic system. Upper panel: The depleted mantlepreferentially retains Sm over Nd so that its Sm/Nd ratio (f0.5) isgreater than that of bulk earth (CHUR) (~0.32) and the continentalcrust (~0.2). Center panel: As a result of the variations in Sm/Ndand the decay of ^{147}Sm to ^{143}Nd, the $^{143}Nd/^{144}Nd$ initial ratioincreases more rapidly in the depleted mantle than in CHUR and incontinental crustal source rocks. Lower panel: Differences betweenthe $^{143}Nd/^{144}Nd$ initial ratio of depleted mantle, CHUR, and crustalrocks expressed asepsilon Ndvalues relative to CHUR. The Sm/Nd ratioand theeNdvalue of a sample (calculated for the age of the rock) canbe used to produce a growth line that intersects the depleted mantlecurve. This intersection yields a depleted mantle (T_{DM})model age.This model age is open to various interpretations. It could reflect thetime (T_2)at which the crust was derived from the depleted mantle.Alternatively, the model age may reflect a mixing age of moreancient (e.g. with aTDMmodel age ofT_1)with more juvenile (with aT_{DM}model age ofT_3) crust (modified fromFryer et al., 1992).

Table C.1 Epsilon-Nd values and Samarium-Neodymium ratios for samples of the Pulo do Lobo Zone (PDLZ)

Sample	Formation	Nd (ppm)	Sm (ppm)	$^{147}Sm/^{144}Nd$	$^{143}Nd/^{144}Nd$	2s	$\varepsilon Nd_{(0)}$	$\varepsilon Nd_{(330)}$	$\varepsilon Nd_{(350)}$	$\varepsilon Nd_{(600)}$	T De Paolo	TDM2
RSA02	melange	8.039	1.441	0.1084	0.512085	7	-10.8	-7.1	-6.8	-4.0	1383	1540
AC03	melange	18.65	3.487	0.1130	0.511986	4	-12.7	-9.2	-9.0	-6.3	1595	1759
RSA01	melange	23.75	4.467	0.1137	0.512016	6	-12.1	-8.6	-8.4	-5.8	1562	1726
JAB-05	basalt	7.298	2.655	0.2199	0.513151	6	10.0	9.0	9.0	8.2	2520	-
JAB-06	mafic block	9.441	3.234	0.2071	0.513097	6	9.0	8.5	8.5	8.2	-	1242
JAB-07	mafic matrix	10.52	3.699	0.2126	0.513141	5	9.8	9.1	9.1	8.6	-	1370

Table C.2 Epsilon-Nd values and Samarium-Neodymium ratios for samples of the Sierra del Norte Batholith (SDNB)

Sample	Formation	Nd (ppm)	Sm (ppm)	$^{147}Sm/^{144}Nd$	$^{143}Nd/^{144}Nd$	2s	$\varepsilon Nd_{(0)}$	$\varepsilon Nd_{(330)}$	$\varepsilon Nd_{(350)}$	$\varepsilon Nd_{(600)}$	T De Paolo	TDM2
JAB-09	SDNB	33.41	7.646	0.1383	0.512559	7	-1.5	0.9	1.1	2.9	983	1195
JAB-02	SDNB	18.44	4.105	0.1346	0.512419	10	-4.3	-1.7	-1.5	0.5	1201	1408
JAB 24	SDNB	54.64	13.50	0.1494	0.512610	8	-0.5	1.4	1.6	3.1	1029	1281
JAB 26	SDNB	27.24	5.628	0.1249	0.512329	6	-6.0	-3.0	-2.8	-0.5	1224	1409
JAB 27	SDNB	6.077	2.529	0.2516	0.512373	6	-5.2	-7.5	-7.6	-9.4	-	-
JAB 10	SDNB	17.19	4.039	0.142	0.512459	7	-3.5	-1.2	-1.0	0.7	1239	1469
JAB 28	SDNB	25.32	5.246	0.1252	0.51199	9	-12.6	-9.6	-9.5	-7.2	1810	1993
JAB 25	SDNB	11.6	2.136	0.1113	0.512371	7	-5.2	-1.6	-1.4	1.3	1003	1160
JB-26B	SDNB	94.38	15.77	0.101	0.512483	4	-3.0	1.0	1.3	4.3	766	903

Table C.3 Epsilon-Nd values and Samarium-Neodymium ratios for samples of the South Portuguese Zone (SPZ)

Sample	Formation	Nd (ppm)	Sm (ppm)	$^{147}Sm/^{144}Nd$	$^{143}Nd/^{144}Nd$	2s	$\varepsilon Nd_{(0)}$	$\varepsilon Nd_{(330)}$	$\varepsilon Nd_{(350)}$	$\varepsilon Nd_{(600)}$	T De Paolo	TDM2
JAB-12	VSC	27.19	5.846	0.1300	0.512182	7	-8.9	-6.1	-5.9	-3.8	1563	1760
JAB-13	VSC	18.92	4.315	0.1379	0.512319	5	-6.2	-3.7	-3.6	-1.7	1450	1669
JAB-14	VSC	38.46	7.125	0.1120	0.512016	7	-12.1	-8.6	-8.4	-5.6	1535	1697
JAB-15	VSC	30.98	5.598	0.1092	0.511864	7	-15.1	-11.4	-11.2	-8.4	1716	1872
JB-11	VSC	58.25	12.48	0.1295	0.512446	7	-3.7	-0.9	-0.7	1.4	1082	1275
JB-13	VSC	39.29	7.476	0.1150	0.512086	5	-10.8	-7.3	-7.1	-4.5	1475	1641
JB-14	VSC	20.90	4.812	0.1392	0.512424	5	-4.2	-1.8	-1.6	0.2	1264	1485
JB-16	VSC	16.27	3.201	0.1189	0.511931	4	-13.8	-10.5	-10.3	-7.8	1785	1956
JAB 19	VSC	44.63	8.389	0.1136	0.512118	6	-10.1	-6.6	-6.4	-3.8	1406	1570
JAB 17	VSC	45.69	8.714	0.1153	0.511947	6	-13.5	-10.1	-9.8	-7.2	1694	1860
JAB 18	VSC	41.05	7.466	0.1099	0.511923	7	-13.9	-10.3	-10.1	-7.3	1642	1799
JB-17	PQ	14.93	3.749	0.1518	0.512038	5	-11.7	-9.8	-9.7	-8.3	2498	2727
JB-25	PQ	41.03	7.631	0.1124	0.511912	5	-14.2	-10.6	-10.4	-7.7	1698	1859
JB-24	PQ	22.47	4.379	0.1178	0.512071	5	-11.1	-7.7	-7.5	-5.0	1542	1713

APPENDIX D

GEOCHEMISTRY

Table D.1 Geochemistry of granite samples from Sierra del Norte Batholith (SDNB)

Sample	JAB-02	JAB-09	JAB-10	JAB-24	JAB-25	JAB-26	JAB-27	JAB-28	JB-26B
Formation	SDNB	SDNB	SDNB	SDNB	SDNB	SDNB	SDNB	SDNB	SDNB
SiO2	75.32	68.07	76.63	76.18	76.31	71.69	76.72	71.44	60.28
TiO2	0.183	0.542	0.257	0.139	0.051	0.375	0.028	0.209	0.74
Al2O3	13.61	15.45	13.1	12.69	13.02	14.08	14.21	14.97	12.11
Fe2O3	1.57	4.75	0.99	1.1	0.61	2.55	0.98	1.18	7.45
MnO	0.021	0.086	0.004	0.009	0.003	0.034	0.029	0.008	0.16
MgO	0.19	0.69	0.31	0.09	0.01	0.76	0.19	0.69	2.94
CaO	0.78	2.85	2.71	0.24	0.83	1.63	0.83	1.77	4.35
Na2O	3.39	4.17	5.2	3.46	3.64	3.26	0.51	3.38	3.39
K2O	5.04	3.34	0.26	5.05	4.7	4.26	3.63	5.27	0.77
P2O5	0.055	0.182	0.05	0.028	0.021	0.132	0.164	0.174	0.14
L.O.I.	0.79	0.10	1.18	0.53	0.20	1.55	2.89	0.26	
Total	100.949	100.23	100.691	99.516	99.395	100.321	100.181	99.351	94.89
V	13	42	24	205	186	309	4	120	101
Cr	0	9	3	488	115	75	0	37	197
Co	1	5	2	37	21	31	1	16	
Ni	3	4	3	133	68	23	4	37	10
Cu	2	7	1	69	28	35	3	88	155
Zn	23	76	6	87	96	85	13	85	34
Ga	16	23	14	15	26	19	24	21	9
Rb	167	117	6	91	189	22	283	155	32
Sr	81	141	164	1097	81	159	58	2973	136
Y	24	48	41	24	30	42	29	25	51
Zr	107	267	119	241	188	153	47	611	1126
Nb	6	11	7	28	20	7	18	75	11
Ba	333	420	82	1099	445	42	140	2887	113
La	32	48	32	47	36	7	19	185	
Pb	26	20	8	5	14	14	8	-1	39
Th	16	11	18	5	20	6	5	48	32
U	4	2	2	0	5	4	10	6	<LD
Ce	41	83	55	82	65	28	15	304	292
Nd	19	44	21	50	30	23	4	130	
Cs	2	4	2	0	7	3	9	0	

Table D.2. Rare Earth Elements granite samples from Sierra del Norte Batholith(SDNB)

Sample	JAB-02	JAB-09	JAB-10	JAB-24	JAB-25	JAB-26	JAB-27	JAB-28	JB-26B
Formation	SDNB	SDNB	SDNB	SDNB	SDNB	SDNB	SDNB	SDNB	SDNB
Y	17.52	42.10	31.81	81.74	19.47	19.82	28.94	17.82	
Zr	130.42	361.92	150.35	242.20	81.49	172.89	66.01	105.23	
Nb	4.40	12.34	4.93	4.41	2.01	7.62	9.54	10.01	
Ba	342.16	523.24	71.87	165.64	231.70	514.97	101.52	579.22	
La	19.59	39.43	20.39	45.12	20.14	32.23	5.79	27.95	
Ce	36.15	81.75	47.06	76.91	31.78	61.97	12.76	55.27	
Pr	4.67	9.79	4.73	12.34	3.88	7.31	1.60	6.28	
Nd	17.62	37.88	18.38	50.61	13.14	26.78	5.65	23.48	
Sm	3.79	8.01	3.92	12.40	2.28	5.76	2.27	4.82	
Eu	0.56	1.71	0.69	0.66	0.27	0.92	0.25	1.09	
Gd	3.21	7.10	4.07	11.58	2.21	4.24	2.97	3.41	
Tb	0.54	1.31	0.80	2.28	0.41	0.67	0.74	0.61	
Dy	3.29	8.26	5.62	15.00	3.09	4.12	5.09	3.51	
Ho	0.65	1.58	1.23	3.08	0.64	0.76	1.02	0.66	
Er	1.94	4.54	3.59	9.47	2.01	2.04	3.27	1.85	
Tm	0.25	0.69	0.57	1.36	0.35	0.32	0.52	0.27	
Yb	1.88	4.45	3.93	8.62	2.47	1.94	3.29	1.68	
Lu	0.28	0.64	0.56	1.25	0.37	0.28	0.48	0.22	
Hf	3.29	7.06	4.14	6.54	3.59	4.50	2.42	2.69	
Ta	0.28	0.42	0.35	0.41	0.23	0.71	1.45	1.04	
Th	10.22	7.71	11.69	12.34	15.18	15.67	5.18	11.57	

Table D.3. Geochemistry of samples from the South Portuguese Zone (SPZ)

Sample	JB-24	JB-25	JB-17	JAB-19	JAB-14	JAB-12	JAB-13	JB-13
Formation	PQ	PQ	PQ	VSC	VSC	VSC	VSC	VSC
SiO2	74.10	53.85	54.99	64.54	64.08	76.9	75.32	64.91
TiO2	0.65	0.96	0.23	0.729	0.741	0.402	0.321	0.81
Al2O3	12.32	24.80	1.57	16.7	18.33	10.8	10.75	21.20
Fe2O3	5.63	9.29	36.48	7.65	7.3	4.57	4.69	7.30
MnO	0.10	0.11	0.09	0.436	0.209	0.11	0.169	0.18
MgO	2.00	2.02	0.06	1.68	1.33	1.17	1.3	1.82
CaO	0.12	0.05	0.04	0.18	0.09	0.05	0.16	0.17
Na2O	0.78	0.71	<LD	0.95	0.32	0.01	-0.01	0.18
K2O	1.38	3.70	0.18	3.11	4.78	3.8	3.62	4.61
P2O5	0.08	0.07	0.32	0.068	0.087	0.068	0.124	0.07
L.O.I.				3.74	3.15	2.59	3.31	
Total	97.33	95.84	93.99	99.783	100.417	100.47	99.754	101.52
V	62	147	47	200	7	84	188	138
Cr	65	137	49	114	0	39	112	96
Co				27	2	12	13	
Ni	26	61	44	78	4	37	57	59
Cu	5	51	19	33	3	95	29	259
Zn	17	51	21	123	39	52	104	41
Ga	8	31	<LD	28	25	17	27	23
Rb	40	174	6	179	172	155	188	193
Sr	34	103	18	100	18	16	95	88
Y	20	28	16	33	106	29	30	28
Zr	228	165	404	173	181	77	193	154
Nb	13	21	6	22	23	9	23	18
Ba	267	726	52	446	184	568	447	495
La				53	61	30	48	
Pb	8	14	17	15	26	9	11	19
Th	8	14	<LD	22	14	13	19	13
U	<LD	<LD	6	8	7	3	4	<LD
Ce	72	166	62	97	86	45	86	125
Nd				51	56	21	40	
Cs				6	5	8	8	

Table D.3 (continued). Geochemistry of samples from the South Portuguese Zone (SPZ)

Sample	JB-14	JB-10	JB-11	JB-16	JAB-15	JAB-17	JAB-18
Formation	VSC	VSC	VSC	VSC	VSC	VSC	VSC
SiO2	72.45	103.53	68.92	86.68	62.01	57.24	59.15
TiO2	0.91	<LD	0.63	0.49	1.066	1.073	1.09
Al2O3	13.69	<LD	16.20	11.19	19.78	19.61	19.56
Fe2O3	7.19	7.48	5.03	4.22	6.43	10.06	8.2
MnO	0.44	0.18	0.16	0.04	0.068	0.112	0.072
MgO	4.05	<LD	1.55	1.17	1.27	1.53	1.39
CaO	0.30	0.03	0.24	0.06	0.05	0.08	0.13
Na2O	1.22	<LD	4.83	0.33	0.36	0.33	0.27
K2O	2.04	0.01	1.57	1.40	3.93	3.7	3.9
P2O5	0.07	0.00	0.06	0.05	0.108	0.129	0.117
L.O.I.					4.93	5.95	5.75
Total	102.55	110.73	99.37	105.77	100.002	99.814	99.629
V	157	28	78	72	71	151	151
Cr	39	<LD	9	41	54	301	626
Co					8	27	35
Ni	23	<LD	15	21	20	114	150
Cu	47	81	12	19	19	49	63
Zn	32	<LD	5	6	59	72	71
Ga	20	<LD	23	8	20	19	15
Rb	81	<LD	46	51	162	177	209
Sr	53	2	84	41	1115	1245	896
Y	27	<LD	70	16	16	23	12
Zr	143	<LD	348	219	334	354	244
Nb	8	<LD	20	11	56	38	10
Ba	263	<LD	282	142	1495	2113	1534
La					60	69	31
Pb	<LD	5	7	7	15	9	13
Th	5	<LD	13	6	15	6	11
U	<LD	<LD	<LD	<LD	-1	2	2
Ce	57	<LD	153	45	93	121	62
Nd					35	56	31
Cs					2	0	4

Table D.4 Rare Earth Elements from the South Portuguese Zone (SPZ)

Sample	JB-24	JB-25	JB-17	JAB-19	JAB-14	JAB-12	JAB-13	JB-13
Formation	PQ	PQ	PQ	VSC	VSC	VSC	VSC	VSC
Y	19.72			34.88	24.59	21.67	20.68	
Zr	199.91			137.62	135.25	88.37	66.30	
Nb	12.27			16.52	17.92	9.53	7.74	
Ba	220.94			656.20	563.07	681.20	476.75	
La	23.77			51.39	44.66	19.05	26.67	
Ce	48.46			57.26	84.29	38.17	50.31	
Pr	5.60			11.25	10.24	4.69	6.07	
Nd	21.53			43.50	38.26	18.52	24.43	
Sm	4.32			7.73	6.84	3.82	4.84	
Eu	0.94			1.57	1.40	0.95	0.99	
Gd	4.50			6.76	4.75	3.33	4.30	
Tb	0.69			1.08	0.83	0.63	0.70	
Dy	4.23			6.60	5.20	4.12	4.28	
Ho	0.84			1.38	0.96	0.84	0.75	
Er	2.29			3.65	2.87	2.40	2.00	
Tm	0.38			0.51	0.42	0.35	0.27	
Yb	2.35			3.25	2.82	2.30	1.80	
Lu	0.34			0.49	0.41	0.34	0.27	
Hf	3.98			2.87	2.89	1.71	1.41	
Ta	0.50			0.69	0.68	0.36	0.25	
Th	7.00			10.40	11.72	7.43	5.13	

Table D.4 Continued. Rare Earth Elements from the South Portuguese Zone(SPZ)

Sample	JB-14	JB-10	JB-11	JB-16	JAB-15	JAB-17	JAB-18
Formation	VSC	VSC	VSC	VSC	VSC	VSC	VSC
Y			62.72	13.19	23.71	26.35	25.41
Zr			293.79	163.64	195.95	175.88	201.53
Nb			18.33	8.70	23.68	23.81	24.80
Ba			297.25	130.93	522.70	497.25	532.56
La			47.97	15.55	47.41	48.29	47.13
Ce			100.72	31.55	95.07	96.02	95.04
Pr			13.89	3.68	10.86	11.20	10.74
Nd			57.84	14.42	40.29	41.89	40.89
Sm			12.02	2.82	7.42	7.71	7.50
Eu			1.89	0.66	1.37	1.61	1.51
Gd			10.56	2.72	4.23	5.21	4.58
Tb			1.74	0.44	0.81	0.92	0.81
Dy			11.34	2.78	4.75	5.61	5.27
Ho			2.43	0.50	0.97	1.07	1.00
Er			7.32	1.61	2.91	3.32	3.07
Tm			1.09	0.21	0.42	0.44	0.46
Yb			6.82	1.52	2.79	3.02	2.77
Lu			1.02	0.22	0.46	0.42	0.43
Hf			6.79	3.39	4.41	4.10	4.30
Ta			0.82	0.50	0.97	0.95	0.98
Th			14.67	5.14	13.64	13.84	14.49

Table D.5 Geochemistry of samples from the Pulo do Lobo Zone (PDLZ)

Sample	JAB-01	JAB-03	JAB-08	RSA01	RSA02	AC03
Formation	SIF	SIF	SIF	melange	melange	melange
SiO2	75.16	76.33	72.26	90.12	88.91	83.98
TiO2	0.792	0.889	0.92	0.58	0.21	0.51
Al2O3	11.95	11.74	13.37	6.07	3.36	10.68
Fe2O3	6.24	4.57	6.69	3.50	2.49	3.21
MnO	0.09	0.126	0.031	0.02	0.02	0.05
MgO	0.48	0.36	0.7	0.87	0.78	1.26
CaO	0.02	0.04	0.02	0.04	0.03	0.13
Na2O	0.14	0.05	0.17	<LD	<LD	0.33
K2O	2.45	2.08	2.03	0.54	0.26	1.56
P2O5	0.11	0.069	0.113	0.06	0.02	0.06
L.O.I.	2.86	3.29	3.87			
Total	100.292	99.544	100.174	101.82	96.04	101.95
V	87	94	104	28	10	44
Cr	58	68	80	47	97	62
Co	4	9	11			
Ni	25	37	50	17	6	18
Cu	30	18	27	4	<LD	10
Zn	55	64	84	13	9	15
Ga	16	16	18	-1	<LD	8
Rb	118	96	100	14	6	42
Sr	49	16	43	16	4	22
Y	18	35	27	21	5	17
Zr	247	272	262	463	115	271
Nb	16	15	16	16	11	14
Ba	316	444	404	47	39	221
La	20	57	42			
Pb	24	14	15	6	<LD	12
Th	12	17	15	8	<LD	7
U	8	7	3	<LD	<LD	<LD
Ce	29	49	69	63	<LD	70
Nd	6	51	40			
Cs	1	6	4			

Table D.5 Continued. Geochemistry of samples from the Pulo do Lobo Zone

Sample	JAB-07	JAB-06	JAB-23	JAB-05	JAB-21	JAB-22
Formation	mafic matrix	mafic block	mafic block	basalt	basalt	basalt
SiO2	48.24	44.65	48.55	47.32	49.24	50.7
TiO2	1.633	1.359	1.806	1.161	1.406	2.289
Al2O3	14.41	15	13.46	15.01	16.71	15.37
Fe2O3	12.5	11.49	12.56	10.89	10.19	13.1
MnO	0.204	0.169	0.2	0.177	0.19	0.262
MgO	8.56	7.41	6.46	8.63	7.85	5.6
CaO	9.13	16.55	11.35	13.02	11.31	9.85
Na2O	3.25	0.62	2.94	1.83	1.58	1.71
K2O	0.21	0.32	0.32	0.16	0.61	0.35
P2O5	0.154	0.121	0.197	0.095	0.163	0.283
L.O.I.	2.00	1.97	2.00	1.88	0.93	0.69
Total	100.291	99.659	99.843	100.173	100.179	100.204
V	305	286	98	269	331	22
Cr	212	361	9	460	273	23
Co	41	41	12	38	38	3
Ni	64	107	20	101	66	9
Cu	34	37	68	47	59	2
Zn	90	76	76	76	91	8
Ga	14	21	21	15	16	12
Rb	4	7	107	2	6	136
Sr	111	203	4527	122	199	202
Y	35	33	20	27	39	25
Zr	88	79	855	61	129	93
Nb	3	4	104	2	5	11
Ba	21	26	4083	26	71	595
La	2	3	201	6	2	40
Pb	6	5	0	10	5	32
Th	2	0	52	0	6	15
U	2	3	0	3	2	6
Ce	10	11	327	11	21	59
Nd	6	13	132	12	12	21
Cs	0	2	0	4	0	2

Table D.6 Rare earth elements of samples from the Pulo do Lobo Zone (PDLZ)

Sample	JAB-01	JAB-03	JAB-08	RSA01	RSA02	AC03
Formation	SIF	SIF	SIF	melange	melange	melange
Y				20.86	5.08	14.91
Zr				351.59	108.57	252.24
Nb				15.25	10.03	12.66
Ba				72.33	29.94	191.78
La				25.44	8.34	20.26
Ce				48.46	15.87	37.03
Pr				5.80	1.87	4.71
Nd				22.90	7.62	18.99
Sm				4.27	1.46	3.74
Eu				0.87	0.17	0.69
Gd				3.67	0.90	3.02
Tb				0.62	0.13	0.48
Dy				3.80	0.95	2.90
Ho				0.83	0.20	0.57
Er				2.58	0.56	1.70
Tm				0.39	0.10	0.25
Yb				2.47	0.66	1.66
Lu				0.40	0.10	0.26
Hf				7.08	2.23	4.87
Ta				0.66	0.36	0.50
Th				7.58	1.80	5.61